Investigating the structure and function of HSV-1 tegument proteins: UL7 and UL51

Danielle Jane Owen

Gonville and Caius College

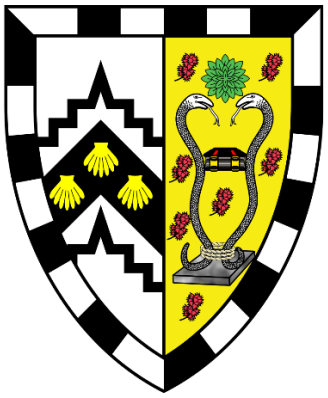

Supervisor: Dr Stephen Graham

Division of Virology

Department of Pathology

September 2017

This dissertation is submitted for the degree of Doctor of Philosophy

Summary

Danielle Jane Owen

Investigating the structure and function of HSV-1 tegument proteins: UL7 and UL51

Herpes simplex virus-1 (HSV-1) has a large double-stranded DNA genome encased within an icosahedral capsid. The capsid is surrounded by a protein-rich layer, termed tegument, and a membranous envelope containing viral glycoproteins. HSV-1 genome replication and encapsidation occurs in the nucleus, after which, DNA-loaded capsids enter the cytoplasm where they undergo tegumentation and assembly. This thesis presents a structural and functional investigation of two HSV-1 tegument proteins, UL7 and UL51 that are conserved across all herpesviruses. Deletion of UL7 or UL51 results in impaired viral replication, a small plaque phenotype and an accumulation of unenveloped capsids in the cytoplasm, the latter of which is indicative of a defect in tegumentation and/or secondary envelopment. Similar phenotypes have been observed upon deletion of homologous proteins in pseudorabies virus and human cytomegalovirus, suggesting a conserved role for these proteins.

This thesis presents evidence for the formation of a UL7-UL51 complex in transfected and infected cells. Pull-down experiments using recombinant UL7 and UL51 protein purified from *E. coli* demonstrated that the interaction is direct, and mapped the UL7-binding region within UL51. The interaction was shown to be conserved between UL7 and UL51 homologues from murid herpesvirus, ORF42 and ORF55, respectively. The UL7-UL51 complex was purified from *E.coli* and, after optimisation of the purification protocol and the UL51 construct, a pure protein sample was obtained that was suitable for crystallisation trials. Two conditions were identified that produced reproducible crystals. These crystals proved to be thin and fragile, preventing their analysis by X-ray diffraction. Optimisation of the crystallisation conditions to produce more robust crystals and/or *in situ* diffraction measurements may yet yield X-ray diffraction data for the complex.

Host-cell binding partners for UL7 and UL51 were identified by yeast-two-hybrid screen and quantitative proteomics (SILAC). An interaction between UL51 and the G-Box domain of the centriole protein CPAP was identified by Y2H screen, and validated by immunoprecipitation from transfected cells and in pull-down experiments using recombinant proteins purified from *E. coli*. The CPAP-binding region within UL51 was mapped and shown to resemble a motif present in the cellular protein STIL that mediates an interaction between STIL and CPAP. Two UL51 point-mutations within the putative CPAP-binding motif blocked the interaction between UL51 and the CPAP G-box domain. A mutant HSV-1 virus carrying these UL51 mutations was generated, but no difference was evident between single-step growth curves of wild-type HSV-1 and the UL51 mutant. Host-cell proteins pontin and reptin were identified as putative UL7/UL51 interaction partners in two SILAC screens. Purified GST-tagged UL7-UL51 complex was able to interact with pontin and reptin. However, it is likely that the interaction is non-specific since pontin and reptin were also found to bind a misfolded protein in a similar manner.

Declaration

This dissertation is the result of my own work and includes nothing which is the outcome of work done in collaboration except as declared in the text. It is not substantially the same as any that I have submitted, or, is being concurrently submitted for a degree or diploma or other qualification at the University of Cambridge or any other University or similar institution. I further state that no substantial part of my dissertation has already been submitted, or, is being concurrently submitted for any such degree, diploma or other qualification at the University of Cambridge or any other University or similar institution. In accordance with the Biology Degree Committee guidelines this thesis does not exceed 60,000 words excluding figure legends, tables, appendices and bibliography.

Signed:

Danielle Owen

Acknowledgements

First and foremost, I would like to express my sincere gratitude to my supervisor Dr Stephen Graham for the opportunity to work on this project. Stephen has been generous with his time, advice and support during the last four years, even during sick leave and whilst on holiday. His knowledge and enthusiasm for science is inspiring and his mentorship was invaluable during this PhD project. I have learnt a lot, thank you!

Special thanks goes to my friends and colleagues in Stephen's lab and numerous members of the Division of Virology, past and present. It has been a delight to work and socialise with so many friendly, funny and extremely helpful people. In particular, fellow PhD student Julia for being a true friend and always being prepared to offer her assistance, and occasionally cake. Thank you to post docs Morag, Chen and Lyudmila for answering my many lab-based questions and conundrums. Thanks are also due to Susanna Colaco (another source of delicious cake), Dr Heather Coleman and Deb Walsh for all they do to support the work in the Division. I am also grateful to Dr Janet Dean for critiquing my first year report, her advice and humour during lab meetings and assistance with SEC-MALS experiments.

Thank you to my mentor Dr Colin Crump and members of his lab, especially Viv Conner for generating the mutant viruses used in this work, also Dr Tim Soh and Firoz Ahmed for their friendship and help all things herpes. I am grateful to Dr Edward Emmott for his assistance with the SILAC experiments and Giles Lewis for running the crystallisation facility in CIMR.

To my parents, Harry and Julia, without your encouragement and support I simply would not have been able to do any of this, thank you. And to my family at home and in Australia who have always been on hand for advice and a giggle. Last but by no means least, to my wonderful partner Mark for making me happy. It's mad that you've spent the last four years driving between Manchester and Cambridge on the weekends but I'm extremely glad you did.

Abbreviations

AH – amphipathic helix
CCS – cell-to-cell spread
Cryo-EM - cryo-electron microscopy
CVSC – capsid vertex-specific component
DMEM – Dulbecco's Modified Eagle Medium
DSF – differential scanning fluorimetry
DTT – dithiothreitol
E genes – early genes
EBV – Epstein-Barr virus
EDTA – ethylenediaminetetraacetic acid
ELISA – enzyme-linked immunosorbent assay
EYFP – enhanced yellow fluorescent protein
FAB – UL7-UL51 complex
FITC – fluorescein isothiocyanate
FPLC – fast protein liquid chromatography
GAB – ORF42-ORF55 complex
GFP – green fluorescent protein
GSH – glutathione
GST – glutathione S-transferase
h – hour(s)
h.p.i. – hours post infection
HCMV – human cytomegalovirus
HSV – herpes simplex virus
HVEM – herpesvirus entry mediator
IE genes – immediate early genes
INM – inner nuclear membrane
IP – immunoprecipitation
IPTG – isopropyl β-D-1 thiogalactopyranoside
kpsi – kilopound per square inch
KSHV – Kaposi sarcoma-associated herpesvirus
L genes – late genes
LC-MS/MS – liquid chromatography-mass spectrometry
m – minute(s)
MALS – multi-angle light scattering
MHV – murid herpesvirus
MOI – multiplicity of infection
MQW – Milli-Q® water
MTOC – microtubule organising centre
Mw – molecular weight
NEC – nuclear egress complex (UL31-UL34)
NPC – nuclear pore complex
ONM – outer nuclear membrane
PAGE – polyacrylamide gel electrophoresis
PBS – phosphate-buffered saline
PBS-T – phosphate-buffered saline with 0.1% Tween-20
PCR – polymerase chain reaction
PDB – Protein Data Bank
PFU – plaque forming unit
PM – plasma membrane
PNPP - p-Nitrophenyl phosphate

Abbreviations

PrV – pseudorabies virus
rpm – rotation per minute
RPMI – Roswell Park Memorial Institute
s – second(s)
SAXS – small-angle X-ray scattering
SDS – sodium dodecyl sulphate
SEC – size exclusion chromatography
SILAC – stable isotope labelling with amino acids in cell culture
TGN - trans-Golgi network
UL – unique long
US – unique short
VAC – virus assembly compartment
VZV – varicella-zoster virus
Y2H – yeast two-hybrid screen

Table of contents

List of figures

List of figures

1 Introduction

Parts of this introduction have been adapted from:

Owen, D.J.; Crump, C.M.; Graham, S.C. Tegument assembly and secondary envelopment of alphaherpesviruses. *Viruses* **2015**, *7*, 5084-5114.

1.1 History and taxonomy

Ancient Greek scholars are said to have coined the term 'herpes' (derived from the Greek 'herpein' meaning 'to creep or crawl') in reference to lesions that appear to creep and crawl across the skin. The taxonomy of herpesviruses was first addressed in 1971 by the International Committee on the Taxonomy of Viruses (ICTV; www.ictvonline.org) [1]. Since then, herpesvirus classification and nomenclature has been refined and expanded with the aid of genome sequencing. An overview of the order *Herpesvirales* is presented in Table 1-1. Briefly, the order *Herpesvirales* is divided into three families: the *Herpesviridae* family, which includes mammalian, bird and reptile viruses; the *Alloherpesviridae* family, which includes fish and frog viruses; and the *Malacoherpesviridae* family, which contains a single bivalve virus (ostreid herpesvirus-1). The *Herpesviridae* family is further divided into three subfamilies: *Alphaherpesvirinae*, *Betaherpesvirinae* and *Gammaherpesvirinae* [1]. Molecular phylogenetic analysis suggests that the *Herpesviridae* subfamilies diverged from a common ancestor around 400 million years ago, and evolution over this time has given rise to at least 135 species [1,2]. The herpesviruses occupy a diverse range of biological niches, both in terms of host cell type and length of replicative cycle.

Members of the *Herpesviridae* family were originally classified based on virus structure and biological properties (Table 1-2) [3]. Subsequent genome sequencing has proven the accuracy of the original classification in predicting the relatedness of the viruses, with only a few members requiring reclassification. The *Herpesviridae* share a common virion morphology and a group of approximately 40 conserved genes that have key functions during viral replication [4,5]. Mature virions range in diameter from 120 to 300 nm, and are organised into four morphologically distinct structures: 1) a linear double-stranded DNA genome (120 to 250 kb); 2) an icosahedral capsid with T=16 symmetry, that contains the genome; 3) a protein-rich layer, termed 'tegument', that surrounds the capsid; 4) and an outer envelope derived from host-cell membrane structures, studded with viral envelope proteins and membrane proteins from the host cell [5,6].

The course of herpesvirus infection can be divided into three stages, starting with primary acute infection, followed by the establishment of latency and then periodic reactivation from latency, leading to productive infection that may be symptomatic or asymptomatic. Once established, a latent infection persists throughout the life of the host.

Table 1-1 Taxonomy of the order *Herpesvirales* [1]

Taxon	Name		
Order	*Herpesvirales*		
Family	*Herpesviridae*		
Subfamily	*Alphaherpesvirinae*	*Betaherpesvirinae*	*Gammaherpesvirinae*
Genus	*Simplexvirus*	*Cytomegalovirus*	*Lymphocryptovirus*
Genus	*Varicellovirus*	*Muromegalovirus*	*Rhadinovirus*
Genus	*Mardivirus*	*Roseolovirus*	*Macavirus*
Genus	*Iltovirus*	*Proboscivirus*	*Percavirus*
Family	*Alloherpesviridae*		
Genus	*Ictalurivirus*		
Family	*Malacoherpesviridae*		
Genus	*Osteavirus*		

Table 1-2 The *Herpesviridae* subfamilies are characterised by common biological properties

Table compiled from [7]

Subfamily	Biological properties
Alphaherpesvirinae	Infect a wide range of hosts. Establish latency in sensory and cranial nerve ganglia. Relatively short reproductive cycle associated with rapid spread in tissue culture and the destruction of host cells.
Betaherpesvirinae	More restricted host range compared to the alphaherpesviruses, with the ability to establish latency in monocyte progenitor cells, kidney and salivary epithelial cells, and macrophages. Relatively long reproductive cycle and slow spread in tissue culture with cells becoming enlarged upon infection.
Gammaherpesvirinae	Restricted host range, will replicate in lymphoblastoid cells *in vitro*. Latency is usually established in lymphoid tissue with viruses being specific for either T or B lymphocytes.

1.2 Human herpesviruses

Eight human herpesviruses have been identified and are officially named human herpesviruses (HHV) 1-8. However, they are often referred to by the common names presented in Table 1-3. Human herpesviruses are among the most prevalent human pathogens and are subsequently the best characterised viruses of the *Herpesviridae* family. Human *Alphaherpesvirinae* include: the herpes simplex viruses HSV-1 and HSV-2, which are widespread in most populations and cause recurrent orofacial or genital lesions and herpetic keratitis (infection of the corneal epithelium); and varicella-zoster virus (VZV), the etiological agent of varicella (chickenpox) and herpes zoster (shingles). Human *Betaherpesvirinae* include: human cytomegalovirus (HCMV), which causes malaise and fatigue during

productive infection, congenital birth defects, severe disease in immunocompromised hosts and is a leading cause of transplant rejection; and the closely related *roseoloviruses* (HHV-6 and HHV-7) that are often acquired before two years of age and are associated with fever, diarrhoea and a roseola rash. Human *Gammaherpesvirinae* include Epstein-Barr virus (EBV), the etiological agent of infectious mononucleosis (glandular fever); and Kaposi sarcoma-associated herpesvirus (KSHV), an oncovirus that gives its name to the cutaneous lesions of Kaposi sarcoma, and is also linked to Castleman's disease. Herpesviruses have evolved mechanisms to modulate the host immune response, enabling them to establish long-term latent infections. The viral genome is maintained in the nucleus of host cells during latency, genes associated with lytic infection are suppressed while latency associated transcripts (LATs) and transcripts expressed in latency (TELs) are induced [8]. Despite a lack of clinical symptoms, there is evidence for the occurrence of low-level viral reactivation events in latently infected cells that are thought to constantly stimulate the immune system [9]. A pool of T cells directed against HCMV and EBV is maintained during clinical latency, with approximately 10-20% and 5-10% of circulating T cells being specific for HCMV and EBV antigens, respectively [10-13]. Similarly, a high proportion of $CD8^+$ cells are maintained and exhibit an active phenotype in association with HSV-1 infected trigeminal ganglia, the site of latency for this virus [14-17]. The interplay between latent herpesviruses and the immune system helps to keep resurgent viral reactivation at bay and may also modulate the host immune response to other antigens [9,18,19]. For example, EBV and HCMV-specific $CD8^+$ T cells may be activated in response to infection with hepatitis B virus and contribute to the heterologous anti-viral T cell response [18].

Table 1-3 Human herpesviruses
Eight human herpesviruses have been identified and are officially named human herpesviruses (HHV) 1-8. However, they are frequently referred to by their common names: herpes simplex virus (HSV-1 and 2); varicella zoster virus (VZV), Epstein-Barr virus (EBV); human cytomegalovirus (HCMV); Kaposi sarcoma-associated virus (KSHV). [7]

Virus	Common name	Subfamily	Genome (kb)	Seroprevalence (% adults worldwide)*
HHV-1	HSV-1	Alpha	152 (~90 genes)	50-90
HHV-2	HSV-2	Alpha	152 (~90 genes)	20-60
HHV-3	VZV	Alpha	125 (>70 genes)	50-95
HHV-4	EBV	Gamma	172 (~85 genes)	80-100
HHV-5	HCMV	Beta	248 (~213 genes)	40-80
HHV-6A/B	Roseolovirus	Beta	159-170 (~97 genes)	60-100
HHV-7	Roseolovirus	Beta	145 (~97 genes)	40-100
HHV-8	KSHV	Gamma	170-210 (>87 genes)	3-50**

* Large differences occur between different socioeconomic populations and geographical areas. ** No approved assays currently available.

Herpes simplex virus-1 is routinely used as a model to study the *Herpesviridae* family, partly due to its prevalence within human populations, but also because it replicates well in tissue culture and

there are well established techniques for manipulating its genome. Similarly, the swine virus pseudorabies virus (PrV), which can also infect other mammals including monkeys but not higher primates or man, has been extensively studied as a model alphaherpesvirus [20]. HSV-1 was the model system selected for this study and serves as the focus for the remaining sections of this introductory chapter.

1.3 Herpes simplex virus (HSV)-1

Primary HSV-1 infection typically occurs within orofacial mucoepithelial cells and is frequently asymptomatic. More recently, there has been increasing evidence for HSV-1 primary infection at the genital mucosal epithelium, a site most commonly linked with HSV-2 infection [21]. Following primary infection in epithelial cells, HSV-1 spreads to adjacent sensory neurones where DNA-loaded capsids are trafficked along microtubules to the cell body (schematic presented in Figure 1.1) [22]. Life-long latent infection is established in the maxillary branch of the trigeminal ganglion, part of the peripheral nervous system [8,23]. Upon reactivation, new virions are assembled in neuronal cells and are transported along axons towards synaptic junctions with target epithelial cells (anterograde transport) [22]. Secondary productive infection is established in epithelial cells and may be asymptomatic or manifest as labial lesions commonly referred to as cold sores [8]. While most productive HSV-1 infections will be cleared by the immune system, serious complications can arise in infants and immunocompromised individuals. Trans-neuronal spread to the central nervous system occurs infrequently but is associated with severe encephalitis even in immune competent individuals, and may be fatal [24]. Two frequently studied HSV-1 strains are KOS (JQ673480.1) and strain 17 (NC_001806.1). Investigation of the spatial and temporal progression of HSV-1 infection in live mice has been made possible with the generation of transgenic mice carrying a firefly luciferase gene under the control of the HSV-1 thymidine kinase promoter – enabling HSV-1 infected cells to be visualised [25]. These mice have been used to investigate the pathogenicity of the different HSV-1 strains after corneal scarification and suggest that strain 17 is more pathogenic than KOS based on the amount of bioluminescence measured over the course of infection, bioluminescence was shown to be proportional to the titre of the input virus [25].

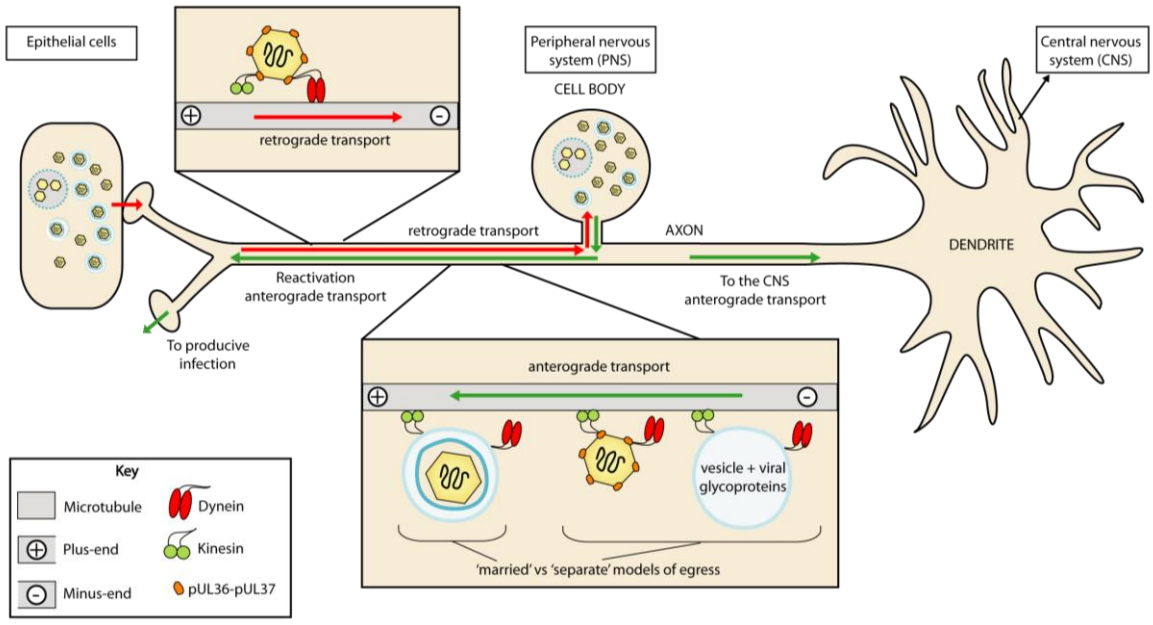

Figure 1.1 Neuronal trafficking of HSV-1: establishing latency and reactivation leading to secondary infection
HSV-1 establishes latency in nuclei within the cell bodies of trigeminal ganglia following retrograde (minus-end directed) transport of capsids along axonal microtubules. Reactivation results in the production of new virions that undergo anterograde (plus-end directed) trafficking back to mucosal epithelial cells. The assembly state of the virus particles prior to anterograde trafficking is disputed and two models have been proposed: the 'married model' predicts that complete virions are assembled in the cell body and are transported as such, while the 'separate model' predicts that the viral envelope and assembled capsids are separately transported from the cell body to virus assembly sites nearer the site of egress. Directional transport along microtubules is mediated by motor proteins: dynein (retrograde) and kinesin (anterograde). There is evidence that both class of motor protein can bind the tegument proteins UL36 and UL37 (discussed in section 1.3.3.2, page 11) to facilitate transport along microtubules, but it is unknown how the net direction of transport during entry and egress is determined. [23,26-30]

1.3.1 Herpes simplex virus-1 genome organisation

The HSV-1 viral genome consists of a single segment of linear double-stranded DNA approximately 152 kb in length, with approximately 68% G+C composition. There are at least 80 open-reading frames encoding viral proteins required for DNA replication and packaging, host-cell immune evasion, entry and egress, along with the major structural proteins that form the capsid. The genome consists of two covalently linked segments referred to as Long (L) and Short (S), within which are the unique long (UL; 108 kb) and unique short (US; 13 kb) coding sequence regions [7,31,32]. The unique regions are flanked by inverted DNA repeat sequences, two internal and one at each termini (referred to at R_L and R_S for repeats flanking the UL and US segments, respectively), such that the overall genome organisation is: R_L-UL-R_L--R_S-US-R_S [32]. The majority of HSV-1 genes are encoded as single copies within the UL and US sequencing regions and are named accordingly, e.g. UL51 and US8. HSV-1 genes

RL1, RL2 and RS1 are located within repeat regions and each genome carries two copies [32]. Many genes also have common names that are linked to the function of the encoded protein, e.g. portal protein (UL6), glycoprotein L (UL1) and thymidine kinase (UL23).

Herpesvirus genes are classified as immediate early (IE or α), early (E or β) or late (L or γ) depending on the stage at which they are expressed during infection. Despite being classified according to these three groups, herpesvirus genes are expressed in a continuous cascade fashion without clear boundaries, and the products of earlier gene groups can influence the expression of later groups. IE gene expression occurs prior to de novo viral protein synthesis and is activated by virus-delivered UL48 (a.k.a. VP16) in complex with cellular proteins [32-35]. The levels of IE gene products (ICP4/gene RS1, ICP0, ICP22/US1 and ICP27/UL54) peak at around 3-4 hours post infection (h.p.i.) in HEp-2 cells [36], and are required for the transcription of E genes [37]. E gene expression rates are highest between 5-7 h.p.i. in HEp-2 cells and include genes necessary for viral DNA synthesis [36]. The L genes encode major structural proteins including tegument and glycoproteins, and are expressed at increasing rates up until 12 h.p.i. Expression of the IE and E proteins along with efficient DNA replication are prerequisite for efficient L gene transcription [36].

1.3.2 HSV-1 virion structure

1.3.2.1 Capsid and DNA packaging

The HSV-1 genome is replicated and packaged into capsids in the cell nucleus, the protein-rich tegument layer is then acquired in the cytoplasm. Mature capsids are 125 nm in diameter and have a wall thickness of approximately 15 nm [38]. The major HSV-1 capsid protein UL19/VP5 forms 162 surface capsomeres that are subdivided into 150 hexamers (termed hexons) and 11 pentamers (termed pentons). Hexons form the faces and edges of the icosahedron, while the pentons are located at 11 of the 12 vertices (Figure 1.2) [38-41]. In addition, the maturational protease UL26 and the scaffold protein UL26.5 (consisting of a C-terminal segment of UL26) are essential for capsid formation but are not incorporated into the final structure [5]. Six copies of UL35/VP26 form a cap over the hexons by interacting with UL19/VP5, and triplexes formed from UL38/VP19C and UL18/VP23 sit between the pentons and hexons [38,41]. Each capsid has a unique portal vertex through which DNA enters and leaves the capsid, which is formed from a dodecameric ring of UL6 [42]. Finally, a heterotrimeric complex of UL17, UL25 and the major tegument protein UL36 forms part of the so-called capsid vertex-specific component (CVSC) that forms over the penton-proximal UL38-UL18 (VP19C-VP23) triplexes [43-46]. Assembly of the CVCS is thought to promote the egress of DNA-filled capsids from the nucleus [43]. Analysis of DNA-loaded capsids *in vitro* shows the genomic DNA to be densely packaged within the capsid, existing in a liquid-crystalline state [47]. During infection, the temperature of the human body (37°C) is likely to induce a solid-to-fluid-like transition, resulting in

regions of the packaged genome having increased mobility, which may facilitate genome release through the portal vertex [48,49].

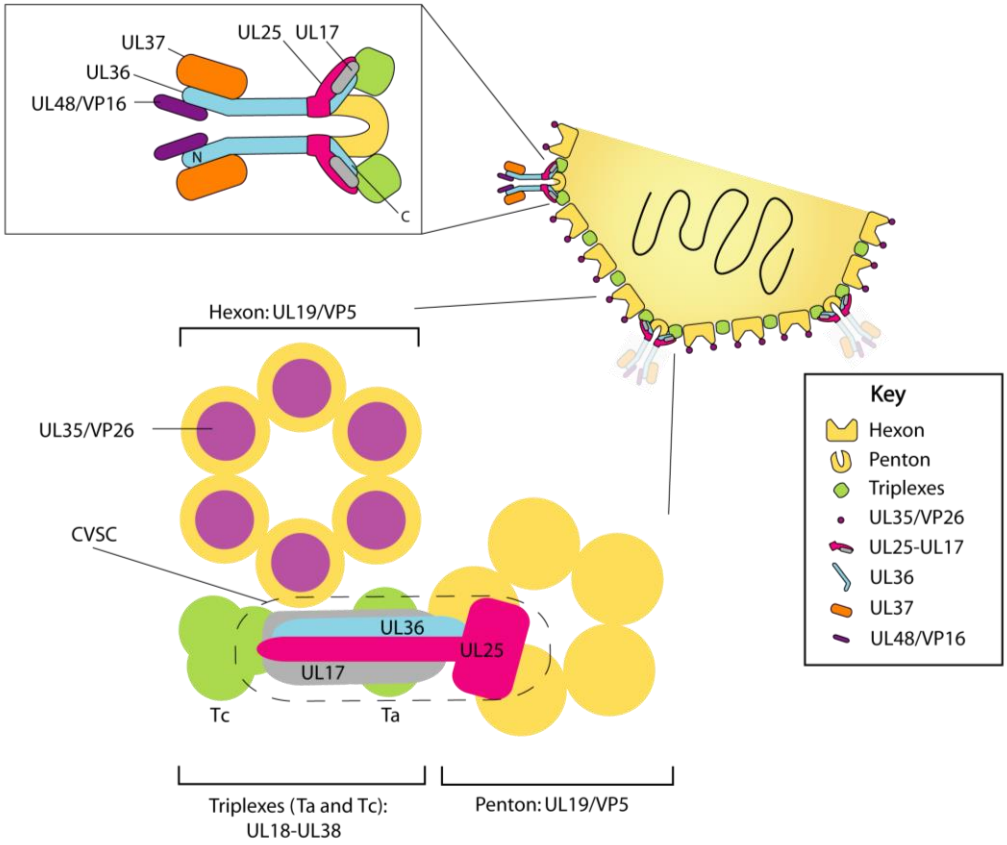

Figure 1.2 Schematic of the HSV-1 capsid
The faces and edges of the icosahedral capsid are formed from hexamers of the major capsid protein UL19/VP5, pentamers of UL19 also form the vertices. Triplexes comprising UL38/VP19C and UL18/VP23 sit between the pentons and hexons. Studies of HSV, PrV and KSHV [39,50,51] suggest that CVSC component UL25 lies over the penton vertex, UL17 lies above the penton proximal UL38-UL18 triplex, and a C-terminal region of UL36 contributes to the CVSC [38,40,41,44,46,52-55].

1.3.2.2 Tegument

The tegument is a densely-packaged proteinaceous layer positioned between the capsid and the outer viral envelope that accounts for 40% or more of the total virion mass [56]. Many tegument proteins are conserved across the *Herpesviridae* family and are thought to have conserved roles during infection (Table 1-4). Numerous protein-protein interactions support the tegument structure, such that it remains largely intact following the removal of the outer membrane from capsid-less HSV L-particles [57]. Analysis of extracellular virions by mass spectrometry identified 26 virally-encoded tegument proteins, which range in size (the smallest, UL11, is 10.5 kDa and the largest, UL36, is 336 kDa) and abundance [58]. The most abundant tegument proteins, UL47, UL48 and UL49, are present at between 600 and 1300 copies per virion [56]. Mass spectrometry of mature virions also identified

host-cell enzymes, chaperones and structural proteins, which are likely to be incorporated in the tegument layer [58]. Tegument proteins are generally described as belonging to either the 'inner' or 'outer' tegument depending on their preferential association with either the capsid or viral membranes [5,59,60]. While the outer tegument appears to be amorphous, the inner layer has partial icosahedral order due to its close association with capsids [53,54,61]. More recently, super-resolution microscopy and single-particle fluorescence imaging techniques have been employed to locate specific tegument proteins within the tegument layer [62,63]. Cryo-EM analysis shows the tegument to be asymmetrically arranged around the capsid, ranging in thickness from 35 nm at the 'distal pole', to 5 nm at the 'proximal pole' [61]. This asymmetry is reflected in the distribution of glycoproteins in the mature virion, with glycoprotein clusters more likely to be associated with the tegument-rich distal pole [61].

Aside from contributing to the structural integrity of herpes virions, tegument proteins perform diverse functions within the cell (reviewed in [64]), such as preparing an environment that is conducive to viral replication. For example, the HSV-1 protein UL41/vhs is an mRNA-specific RNase that rapidly suppresses host-cell protein synthesis by degrading host mRNA early during infection [65,66], in doing so UL41 is thought to contribute to immune evasion (reviewed in [67]). Tegument assembly is mediated through conserved protein-protein interactions between tegument proteins and with the capsid, interactions between tegument and glycoproteins are likely to facilitate envelopment. Table 1-4 lists the HSV-1/2 tegument proteins and their homologues from VZV, PrV, HCMV, EBV and KSHV, they are classified according to whether there is evidence for them having a role in tegumentation and envelopment.

Table 1-4 HSV-1 tegument genes and their homologues
Virus subfamily [*Alpha-, Beta- or Gamma-herpesvirinae*] and alternative protein names (in parentheses) are shown.

HSV-1/-2 [α]	Mass of HSV Protein, kDa	VZV [α]	PrV [α]	HCMV [β]	EBV [γ]	KSHV [γ]
UL7	33	ORF53	UL7	UL103	BBRF2	ORF42
UL11	10	ORF49	UL11	UL99	BBLF1	ORF38
UL13 (VP18.8)	57	ORF47	UL13 (VP18.8)	UL97	BGLF4	ORF36
UL14	24	ORF46	UL14	UL95	BGLF3	ORF34
UL16	40	ORF44	UL16	UL94	BGLF2	ORF33
UL21	58	ORF38	UL21	UL87	BcRF1	ORF24
UL23 (thymidine kinase)	41	ORF36	TK	-	BXLF2	ORF21
UL36 (VP1-2)	336	ORF22 (p22)	UL36	UL48	BPLF1	ORF64
UL37	121	ORF21	UL37	UL47	BOLF1	ORF63
UL41 (vhs)	55	ORF17	UL41	-	-	-
UL46 (VP11-12)	78	ORF12	UL46	-	-	-
UL47 (VP13-14)	74	ORF11	UL47	-	-	-
UL48 (VP16)	54	ORF10	UL48	-	-	-
UL49 (VP22)	32	ORF9	UL49	-	-	-
UL50 (dUTPase)	39	ORF8	UL50	-	-	-
UL51	25	ORF7	UL51	UL71	BSRF1	ORF55
UL55	20	ORF3	-	-	-	-
US2	32	-	-	-	-	-
US3	53	ORF66	US3	-	-	-
US10	34	ORF64/69	-	-	-	-
US11	18	-	-	-	-	-
RL1 (ICP34.5)	26	-	-	-	-	-
RL2 (ICP0)	78	ORF61	EP0 (ICP0)	-	-	-
RS1 (ICP4)	133	ORF62/71 (IE62)	IE180 (ICP4)	-	-	-

1.3.2.3 Outer envelope and glycoproteins

The final step in herpesvirus maturation is the wrapping of tegumented capsids in a double membrane in a process referred to as secondary envelopment. To achieve this, capsids bud into specialised vesicles containing the surface glycoproteins of the mature virion [5]. This process simultaneously provides the viral envelope and also packages HSV-1 into transport vesicles that can later fuse with the plasma membrane [68]. Glycoproteins contribute to the overall diameter of the virion and are visualised by cryo-EM as surface spikes that range from 10 to 25 nm in length, with each virion possessing in the region of 550 to 750 spikes [61]. The HSV-1 genome is known to encode 11 glycoproteins (gB, gC, gD, gE, gG, gH, gI, gJ, gK, gL, gM) [7].

1.3.3 HSV-1 life cycle

Productive HSV-1 infection occurs in mucosal epithelial cells and progresses in several stages, commencing with entry at the plasma membrane followed by capsid trafficking to the nucleus where the viral genome is deposited. Genome replication and capsid assembly occurs in the nucleus, after which assembled capsids must traverse the nuclear envelope to reach the cytoplasm. In the cytoplasm capsids acquire a tegument layer and outer membranous envelope in processes referred to as tegumentation and secondary envelopment, respectively (see Figure 1.3, page 14). The following sections outline the steps involved in HSV-1 replication and highlight key viral proteins involved at each stage.

1.3.3.1 Fusion at the plasma membrane during entry

Prior to replication a virus must first gain access to the cellular environment by crossing the plasma membrane. HSV-1 can enter cells by fusion with the plasma membrane at neutral pH, or via fusion with an endocytic membrane following endocytosis in a pH-dependent or pH-independent manner [69]. HSV-1 entry into cells proceeds via three stages: (1) attachment of the virion to the cell surface; (2) interaction with cellular receptors; and (3) fusion of the viral envelope with the plasma or endosomal membrane. The core herpesvirus fusion machinery comprises glycoprotein gB, and a complex of gH-gL [70]; in HSV-1 an additional non-conserved accessory glycoprotein gD is also required during entry and determines cell tropism by recognising specific cell receptors [71]. When transiently expressed in cells gB, gD and gH-gL are sufficient to stimulate membrane fusion between neighbouring cells [72]. Initial cellular attachment is mediated by an interaction between heparan sulphate and gB or gC, which serves to concentrate the virus at the cell membrane but does not trigger fusion. Glycoprotein gB is a conserved herpesvirus fusion protein [73,74] that is essential for membrane fusion, though its heparan sulphate-binding activity is not [75]. Following initial attachment, gD interacts with one or more potential entry receptors: nectin-1 and 2 [76]; HVEM (herpesvirus entry mediator) [77,78]; and 3-O-sulphated heparan sulphate [78,79], which triggers an activating conformational change in gD [69,80]. It has been proposed that the activated form of gD binds and then converts the gH-gL complex to a form that can interact with the herpesvirus fusogen gB [69]. Recent cryo-EM models highlight conformational changes in gB embedded in exosomes that may promote membrane fusion [70]. Thus, the gH-gL complex likely acts as a regulator of the gB viral fusion protein, and the complex is activated when gD interacts with a suitable receptor. As mentioned in section 1.3.2.2, the HSV-1 virion is asymmetric and has two distinct poles: the distal pole is tegument and glycoprotein-rich compared to the proximal pole. During membrane fusion, the proximal pole appears to preferentially form the fusion pore with cell membranes. It has been proposed that reduced steric hindrance of the entry-associated glycoproteins at the proximal pole might give rise to the increased frequency of fusion at the less-crowded proximal pole [81].

1.3.3.2 In the cytoplasm: transport to the nucleus and injection of DNA

Following fusion at the plasma membrane DNA-loaded capsids enter the cytoplasm and are transported along microtubules at a rate of 30 μm/s, reaching the nucleus within 1 h post entry [82]. Movement of capsids along microtubules is salutatory and bidirectional with the net direction of travel being towards the microtubule organising centre (MTOC) and nucleus [27,29,82]. Trafficking along microtubules is mediated by two types of motor protein: dynein and kinesin, which promote retrograde (towards the nucleus) or anterograde (towards the plasma membrane) transport, respectively. Thus, the bidirectional movement of capsids during entry suggests that both motor proteins are recruited to incoming capsids possibly by interacting with capsid-associated tegument proteins. Cryo-electron tomography of HSV-1 infected adherent cells lines (HFF, PtK_2 and Vero) and synaptosomes has shown that the majority of tegument proteins remain associated with the cytoplasmic face of the plasma membrane early during entry, while incoming capsids appear to lack tegument-associated density [81]. However, the inner tegument proteins UL36 and UL37 have been show to co-transport with capsids along axons of primary sensory neurons infected with HSV-1, whereas UL47, UL48 and UL49 did not [83]. Ultrastructural investigation of HSV-1 capsids during entry and axonal transport in human foetal dorsal root ganglia, using transmission immunoelectron microscopy, demonstrated the loss of UL48, UL49 and most of the inner tegument protein UL37 as well as some UL36 [84]. Purified HSV-1 capsids can recruit dynein, dynactin and kinesin-1 *in vitro*, and these interactions are increased when the capsids are washed with a high salt buffer, which removes all tegument proteins besides UL36, UL37, ICP0, UL14,UL21 and US3 [59]. Deletion of tegument proteins US3, UL14 and UL21 from the virus does not block retrograde transport [85], while deletion of the C-terminal 167 residues of UL36 was sufficient to block capsid transport towards the nucleus [86]. Based on current evidence UL36 and UL37 are considered to be the most likely candidates for the recruitment of motor protein complexes for retrograde transport. Additionally, the UL36 protein is also thought to mediate capsid docking at nuclear pore complexes (NPCs) since antibodies targeted against UL36, but not UL37, UL19/VP5 or UL18/VP23 are able to impair capsid attachment at NPCs [87]. Furthermore, the release of DNA into the nucleus is contingent on functional UL36 protein being present, as demonstrated by the use of a temperature sensitive UL36 mutant HSV-1 virus (tsB7): at non-permissive temperatures (39°C) capsids accumulate at NCPs but fail to release their DNA, within 30 m of shifting to the permissive temperature (33.5°C) viral DNA is released [88-90]. The nuclear pore complex protein CAN/Nup214 has also been shown to interact with viral protein UL25 (a component of the CSVC) and is thought to stimulate the release of viral DNA into the nucleus [91]. After uncoating, the viral DNA circularises by ligating head to tail in the cell nucleus to become ready to serve as a template for transcription and genome replication [92,93].

1.3.3.3 Inside the nucleus: DNA replication and nucleocapsid assembly

HSV-1 genome replication and packaging into capsids (encapsidation) occurs in the nucleus, following an assembly pathway resembling that established for dsDNA bacteriophage such as P22 and HK97 [94]. Proteins required for capsid formation are synthesised in the cytoplasm and transported to the nucleus where they are assembled. The minimum protein requirement for the formation of morphologically typical capsids are: UL19/VP5, UL38/VP19C, UL18/VP23, UL26/VP24 and UL26.5/VP22A [95-98]. A recent model for capsid assembly proposes the formation of a protomer complex comprising one triplex (UL18-UL38) surrounded by three copies of the major capsid protein (UL19), and that each procapsid shell is formed from 320 copies of the protomer [99,100], supported by the scaffold protein UL26.5. Once assembled, the scaffold protein is cleaved and expelled from the interior of the procapsid resulting in the mature icosahedral capsid form [95,100-102]. The CSVC proteins UL17 and UL25 have been detected on procapsids prior to DNA encapsidation and are thought to stabilise the maturing capsid [103,104], later forming the CVSC with UL36 (Figure 1.2) [43,50,55,105]. UL17 is required for the recruitment of both UL25 and UL36 to the capsid and has been proposed to bridge capsid triplexes [100,104].

Replication of the viral genome is initiated after the expression of IE genes and before the onset of L gene expression. Viral DNA is synthesised by a 'rolling-circle' mechanism that results in the formation of long concatemeric strands of progeny DNA [106,107]. Cleavage of the concatemeric DNA into individual genomes and encapsidation requires seven conserved viral proteins that are encoded by the genes UL6, UL15, UL17, UL25, UL28, UL32 and UL33. Although UL32 is required for cleavage and encapsidation, its exact role remains to be determined [100]. The so-called terminase complex, formed from UL15, UL28 and UL33, is at the crux of concatemer cleavage and encapsidation. The interaction between UL28 and UL15 is enhanced by UL33 [108,109], and UL15 contains a NLS that is required for its own nuclear import and that of UL28 and UL33 [110]. The cleavage and encapsidation process is initiated when the terminase complex binds viral concatemeric DNA and docks at the portal vertex. It has been hypothesised that UL17 may be bound to triplexes surrounding the portal vertex and may contribute to the assembly of the portal/terminase packaging complex, since the phenotype for UL17 null-mutants resembles that of mutants lacking either of the terminase components [100]. When docked with a capsid, the terminase complex is oriented such that UL15 is close to the opening at the portal vertex. The UL28 component binds and scans the concatemeric DNA for specific signal sequences that, once encountered, stimulate UL15 endonuclease activity. Activated UL15 cleaves the DNA, creating a free terminus, and begins translocating the cleaved end into the associated capsid in an ATP-dependent manner [100].

1.3.3.4 Nuclear egress: envelopment-de-envelopment model

Once assembled, nucleocapsids must negotiate several obstacles during their journey from the nucleus to the plasma membrane, including nuclear egress. Assembled capsids are too large (125 nm) to exit via nuclear pore complexes, subsequently alternative means for capsids to translocate across the nuclear membrane have evolved. According to the widely accepted envelopment-development model, capsids bud into the inner nuclear membrane (INM) forming an enveloped virion within the perinuclear space in a process referred to as primary envelopment (to distinguish it from the envelopment of tegumented capsids that occurs in the cytoplasm, Figure 1.3). Perinuclear viral particles fuse with the outer nuclear membrane (ONM) and undergo a de-envelopment process that releases naked capsids in the cytoplasm ready for tegumentation. Two proteins UL31 and UL34, which are conserved across the *Herpesviridae* are essential for budding at the INM and membrane scission [111-114]. These proteins form the nuclear egress complex (NEC), which has been shown to vesiculate membranes *in vitro* in the absence of other proteins or chemical energy [115,116]. Oligomerisation of the NEC on the INM results in a honeycomb lattice that may drive INM budding in the presence of a capsid [115,117-119]. Each perinuclear virion is estimated to have between 2,500-3,000 copies of the NEC complex, all of which are lost upon fusion with the ONM and no UL31 or UL34 protein is detected in mature virions [120]. In addition to the NEC, tegument protein US3 is also associated with primary virus particles in the perinuclear space. During budding at the INM, the phosphorylation of UL31 by the US3 kinase may regulate NEC-mediated membrane budding [121]. Furthermore, deletion of US3 results in the accumulation of primary virions in the perinuclear compartment [120,122,123], suggesting that US3 may play a role during fusion and egress at the ONM. It has been hypothesised that US3-mediated phosphorylation of UL31 protein associated with the primary virus particle might lead to disassembly of the NEC lattice during de-envelopment [119]. Glycoproteins gB and gH are also likely to be involved in the process of de-envelopment at the ONM, since simultaneous mutation of both gB and gH leads to the accumulation of primary virus particles in the perinuclear space, a similar phenotype to that of the US3 deletion virus [123]. Interestingly, mutations in either gB or gH alone did not significantly affect the de-envelopment stage, suggesting that this process is distinct from membrane fusion during cellular entry where functional gB and gH(-gL) are both required [123]. Furthermore, HSV-1 capsids are still detected in the cytoplasm in the absence of gB and gH(-gL) and so they are not essential for nuclear egress, implying that other herpesvirus proteins could also be involved [123]. Phosphorylation of gB by US3 may contribute to gB-mediated fusion at the ONM; gB is phosphorylated by US3 at residue T887 in the context of infection, and US3 was shown to directly phosphorylate GST-tagged gB *in vitro* [124,125]. HSV-1 virus carrying an alanine substitution at T887 in gB, in conjunction with the deletion of gH, is defective for nuclear egress compared to wild-type [124]. Nuclear egress was measured as the ratio of perinuclear virus particles to cell-surface virus particles for HaCAT cells, this ratio for WT HSV-1 was 0.06 such that there were more virions at the cell

surface compared to the perinuclear compartment. For the ΔgB-ΔgH and the gB T887A + ΔgH mutant viruses the ratio of perinuclear to cell surface virus particles was 2.9 and 1.7, respectively [124], thus suggesting that phosphorylation of gB at T887A may contribute to the efficient fusion of perinuclear virus particles with the ONM [124].

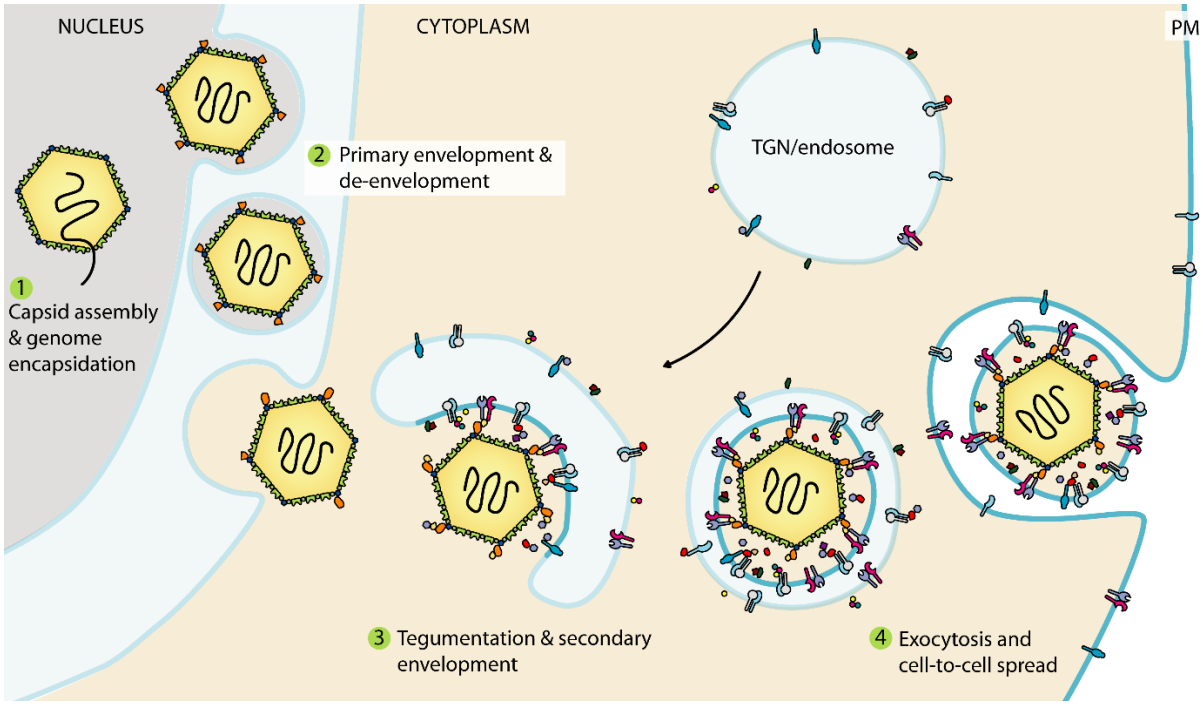

Figure 1.3 Herpesvirus maturation and egress
Replication of the viral genome and encapsidation occurs in the nucleus. Assembled capsids then interact with the inner nuclear membrane and bud into the perinuclear space where they form primary enveloped virions. The primary envelope is lost upon fusion with the outer nuclear membrane, releasing naked capsids into the cytoplasm. Cytoplasmic capsids undergo tegumentation and bud into specialised vesicles in a process referred to as secondary envelopment. The vesicles are studded with viral glycoproteins and outer tegument proteins. Secondary envelopment simultaneously provides the outer viral envelope and a transport vesicle that can fuse with the plasma membrane (PM) to release a mature virion from the cell. [5,126-132]

1.3.3.5 Tegumentation occurs in the cytoplasm

HSV-1 undergoes viral maturation in the cytoplasm through the intrinsically linked processes of tegumentation and secondary envelopment. The acquisition of outer tegument is likely to be coordinated with secondary envelopment via a complex network of protein-proteins interactions between tegument proteins, membrane-associated tegument proteins and viral glycoproteins (Figure 1.4) [64,133-135]. A high degree of redundancy is built into the network of tegument protein-protein interactions, which enables HSV-1 to adapt to the deletion of some 'non-essential' tegument proteins, in some instances by increasing the incorporation of other tegument and cellular proteins, such as actin, into the virion [136-138]. This redundancy makes it difficult to elucidate the precise

contribution(s) of specific tegument proteins to viral maturation. However, recent studies have begun to elucidate how specific tegument proteins may contribute to tegumentation and secondary envelopment by identifying tegument-capsid, tegument-tegument and tegument-glycoprotein complexes (listed in Table 1-5, page 21). Several HSV-1 tegument proteins have been identified that may promote tegumentation and secondary envelopment, of these proteins: UL7, UL11, UL16, UL21, UL36, UL37, UL51 are conserved in all three *Herpesviridae* subfamilies while others, UL46, UL47, UL48 and UL49, are unique to the *Alphaherpesvirinae* [64]. The following sub-sections describe the complexes formed by the tegument proteins listed above and how they may contribute to viral maturation.

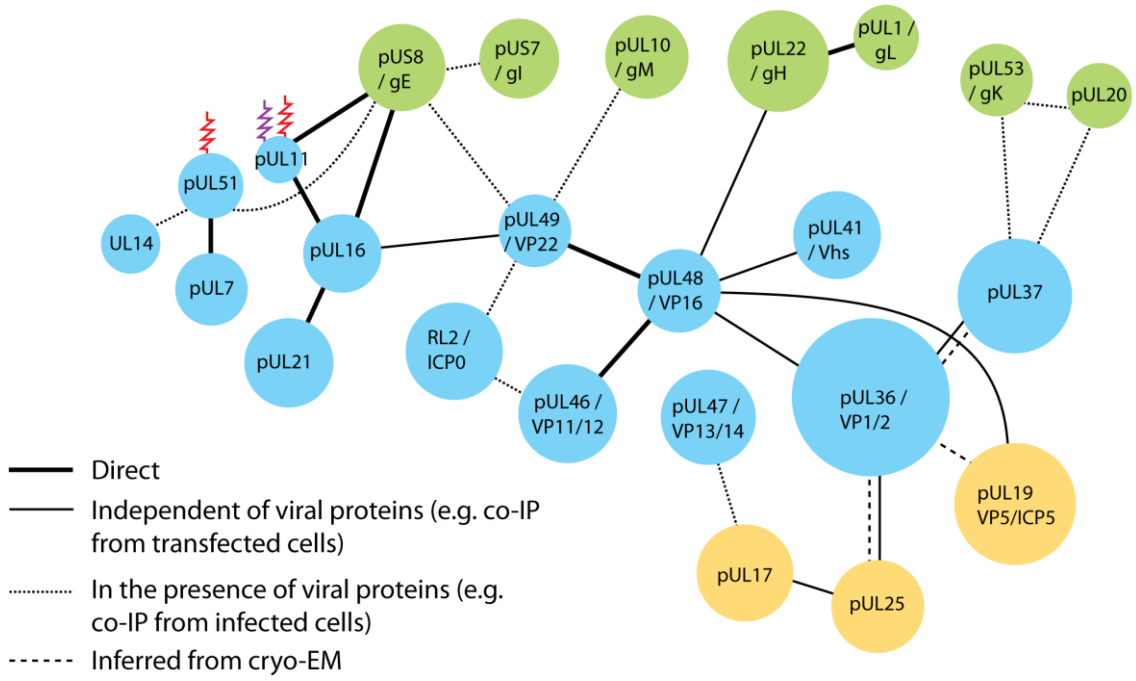

Figure 1.4 Schematic overview of HSV-1 tegument protein interactions
Schematic overview of experimentally determined tegument-tegument, tegument-capsid and tegument-glycoprotein interactions, this is not to say that all of these interactions occur simultaneously or within virions. Bold solid lines depict interactions that have been shown to be direct using recombinantly expressed protein/protein fragments purified from *E.coli*. Evidence for the interactions depicted with thin solid lines and dotted lines largely comes from immunoprecipitation experiments, where there is potential for cellular and/or other viral proteins to mediate the interaction. In all instances, interactions that are shown to be direct have also been confirmed in co-immunoprecipitation experiments. Tegument and capsid proteins are coloured blue and yellow, respectively; glycoproteins and envelope proteins are coloured green. Palmitoyl and myristoyl groups are depicted with red and purple lines, respectively [50,54,86,91,135,139-173].

UL36/VP1-2 interacts with the major capsid protein VP5/UL19 and UL25, a component of the CSVC:

The major tegument protein UL36 acts as a foundation stone for tegument assembly by providing a pivotal link between the capsid and tegument structures. UL36 is the largest tegument protein at 336 kDa and is essential for viral replication; deletion of UL36 in HSV-1 prevents tegumentation and secondary envelopment resulting in the accumulation of naked capsids in the cytoplasm [86,174-176]. Cryo-electron microscopic analysis of DNA-filled capsids from purified mature virions suggests that UL36 interacts with the major capsid protein UL19/VP5 at capsid vertices and is a component of the CVSC [53,54,146]. This is supported by evidence that UL36 and UL25 (a component of the CVSC) co-immunoprecipitate when transiently expressed in cells [91,147], and recruitment of UL36 to PrV (another alphaherpesvirus) capsids in infected cells was shown to be dependent on expression of UL25 [147]. Additionally, the UL25-UL36 interaction in HSV-1 is mediated by a C-terminal region within UL36 (encompassing residues 2430-2893) that is sufficient for UL36 recruitment to cytosolic capsids [86]. Although UL36 is not essential for nuclear egress, recent data for PrV suggests that a nuclear specific isoform comprising the C-terminal region of UL36 is recruited to capsids in the nucleus, where it functions to enhance nuclear egress, a function that may also be conserved in HSV-1 [46]. Full-length UL36 is then likely to replace the C-terminal fragment in the cytoplasm since full-length protein is the major species present in the mature virion [46].

UL36 interacts with UL37 and UL48/VP16 to form a scaffold for tegument assembly:

UL37 is the second largest tegument protein (≈120 kDa) and is essential for HSV-1 replication [177].The N-terminal region of UL36 (via residues F593 and E596) interacts with UL37, and this interaction is conserved between homologues in PrV, HCMV and KSHV, belonging to the *Alphaherpesvirinae, Betaherpesvirinae* and *Gammaherpesvirinae* subfamilies, respectively [148,178-181]. Recruitment of UL37 to HSV-1 capsids is dependent on UL36 expression and this interaction is essential for secondary envelopment [149,177,182,183]. The UL37-null phenotype of HSV-1 can be partially rescued by transfecting cells with a C-terminal fragment of UL37 (encompassing residues 568-1123) prior to infection [149]. Unlike most other tegument proteins, UL36 and UL37 are incorporated into virions with a fixed stoichiometry and overexpression of UL37 in infected cells does not increase its incorporation into virions [146,184,185]. Furthermore, UL36-UL37 stoichiometry is maintained in capsid-less L-particles, suggesting that it is determined by something intrinsic to the tegument structure or viral membrane in the absence of capsid [57,184].

The UL36-UL37 complex has been assigned to filamentous structures that project from capsid vertices in cryo-EM reconstructions of capsids lacking all tegument proteins except UL36 and UL37. These structures extend from the capsid and into the vicinity of the outer tegument and glycoprotein tails [54,62]. The crystal structure of a central portion of UL36 (1600-1733) shows the region to possess an elongated alpha-helical conformation, which might be consistent with filament formation [186].

Additionally, a dimer consisting of the UL36-UL37 homologues from HCMV (UL48-UL47) exhibits hydrodynamic properties consistent with the formation of a rod or a filamentous shape [187]. Recently, an interaction has been identified between UL37, and glycoprotein gK and its membrane-associated binding partner UL20 based on immunoprecipitation experiments from infected cells [154]. Deletion of UL20 from HSV-1 results in the accumulation of enveloped and non-enveloped capsids in the cytoplasm and a 100-fold reduction in viral titre (Vero and HEp-2 cells); similar growth defects are also apparent in PrV virus lacking UL20 [188-192]. It has been proposed that the interaction between UL37 and the gK-UL20 complex might contribute to secondary envelopment by linking capsid-associated UL36-UL37 complex with the viral envelope [154]. Interestingly, HSV-1 UL36 and UL37 also co-localise with Golgi markers independently of capsids [193]. How UL36 and UL37 are recruited to these membranes is unknown, but recruitment of UL37 depends on UL36 expression [193]. Direct or indirect interactions with outer tegument proteins, for example UL36 with UL48 [135,151,152], or glycoprotein tails may be involved [154].

Major tegument proteins: UL46, UL47, UL48 and UL49:

The UL46, UL47, UL48 and UL49 proteins are the most abundant tegument proteins in the mature virion and are unique to the *Alphaherpesvirinae* [56,58]. These proteins may have the capacity to bridge the tegument layer by forming interactions with inner and outer tegument proteins along with membrane embedded viral glycoproteins [56,58]. Of the four, only UL48 is essential for HSV-1 replication in tissue culture [157,194-197]. Mutants lacking UL48 exhibit major defects in viral egress and accumulate unenveloped capsids in the cytoplasm [194,195,198]. Tolerance to the deletion of UL46, UL47 and UL49 may arise from the redundancy in the protein-proteins interactions that form the tegument and/or through compensatory increases in the incorporation of other tegument proteins, for example, packaging of UL46 is enhanced in the absence of UL47 [196]. While UL46, UL47, UL48 and UL49 are unique to alphaherpesviruses, a recent crystal structure of a domain from UL47/VP22 shows unexpected structural homology with ORF52 from MHV, a protein that is conserved amongst gammaherpesviruses and is essential for tegumentation and egress of infectious MHV particles [199,200].

The HSV-1 tegument proteins UL48 and UL49 form numerous interactions that may bridge the capsid and viral envelope. For example, UL48 has been reported to interact with the major tegument protein UL36 [135,151,152], outer tegument proteins UL41, UL46, UL49 [135,155,158,161], and the cytoplasmic tail of gH *in vitro* [162,201]. Glycoproteins gB and gD were also highlighted as potential UL48 binding partners in a cross-linking experiment [202]. The UL36-UL48 interaction may provide a link between the capsid and the outer tegument proteins, which could extend to the viral envelope via interactions with glycoproteins, either directly or indirectly. While both UL36 and UL48 are essential for viral maturation the interaction between them is not, a HSV-1 mutant virus carrying a UL48 (K343A)

mutation that blocks the interaction with UL36 is replication competent, though it exhibits delayed growth kinetics and a 4-fold reduction in final viral titre in HaCAT cells [151,152]. Furthermore, packaging of UL48 into HSV-1 virions was not decreased when its interaction with UL36 was abolished [151].

The UL49 protein is not required for tegument assembly, though it may contribute to this process and secondary envelopment through the formation of tegument-glycoprotein complexes. HSV-1 lacking UL49 exhibits no decrease in plaque size and little defect in viral replication in Vero cells when compared to wild-type virus. However, a cell-type specific defect was reported for ΔUL49 HSV-1 in MDBK cells, resulting in a 50-fold reduction in viral titre [165,197]. There is a notable reduction of gE-gI complex and a moderate reduction of gD (~ 2-3 fold less) in mature ΔUL49 virions, and an absence of immediate early proteins ICP0 and ICP4, suggesting that UL49 is required for the efficient packaging of these proteins into virions [165,203]. It has been proposed that UL49 may contribute to tegument assembly and secondary envelopment through the formation of a tegument-glycoprotein complex comprising UL49, gE-gI, gM and ICP0, whereby the C terminus of UL49 bridges the cytoplasmic tails of gE and gM and the N terminus recruits ICP0 [163]. Glycoproteins gM and gE from HSV-1 have been shown to mediate the recruitment of UL49 to trans-Golgi network (TGN) membranes in infected cells and simultaneous deletion of both glycoproteins blocks UL49 packaging into virions, but not if gM or gE are deleted individually [163,204]. An additional complex comprising UL48, UL49 and UL41 has also been proposed; UL48 and UL49 expression is required to stabilise UL41 in transfected cells, and UL41 is required to stabilise the interaction between UL48 and UL49 [205]. The formation of this complex may contribute to secondary envelopment by associating with membranes via the UL49-gE-gI complex, or by associating with the capsid via the UL36-UL48 complex, but this hypothesis remains to be tested.

The precise contributions of UL46 and UL47 to virus assembly are yet to be fully explored. HSV-1 deletion viruses lacking UL46 or UL47, either separately or in combination, exhibit a 10-fold defect in plaque formation compared to wild-type [157]. A PrV UL47 deletion mutant accumulates partially tegumented capsids in the cytoplasm, but no assembly defect was evident for a UL46 deletion mutant [206]. Several capsid (UL19/VP5, UL18/VP23, UL38/VP19C and UL25), tegument (UL21, UL37, UL48, US3 and US10) and membrane proteins (UL45, gK and gM) have been identified as putative UL46 binding partners by Y2H screen [133,135,207]. Interactions between UL46 and UL21, US3, US10, ICP0 and gM were also identified by mass spectrometry following immunoprecipitation from cells infected with HSV-1 expressing GFP-tagged UL46 [156]. The interaction between UL46 and UL48 was confirmed by *in vitro* GST pull-down experiments [135], and the proteins were shown to co-localised in and co-purify from cells infected with HSV-2 [155]. The range of putative UL46 interaction partners, which includes capsid, tegument and viral glycoproteins, suggests that the UL46 protein could provide a link between the capsid and outer membrane. Similarly, Y2H screens have yielded several putative interaction partners for UL47 including UL14, UL21, UL48, UL49, US11 [207]. Co-immunoprecipitation

of UL47 and UL48 from infected cells has been reported [151]. Interestingly, the capsid protein UL17 (a component of the CVSC) has been shown to co-localise with UL47 in HSV-1-infected cells and both proteins co-immunoprecipitate from infected cell lysates, suggesting another possible link between the capsid and tegument layer [208].

UL11, UL16 and UL21 form a tripartite complex:

In addition to membrane-embedded glycoproteins, HSV-1 virions also contain membrane-associated tegument proteins such as UL11 and UL51 [7]. Membrane association is facilitated by the addition of lipid groups to tegument proteins. Membrane-associated tegument proteins may then recruit other tegument proteins and also interact with glycoprotein tails. For example, UL11 localises to Golgi membranes in infected cells via myristoyl and palmitoyl anchors, with the latter modification determining membrane specificity [209-211]. An interaction between UL11 and the cytoplasmic tail of gE has been demonstrated *in vitro*, which may also assist in UL11 recruitment to Golgi membranes [144,145,212]. This is supported by evidence that UL11 packaging into virions is substantially reduced upon deletion of the cytoplasmic tail of gE and *vice versa* [212]. Deletion of the HSV-1 UL11 gene or its homologues from PrV and HCMV results in the accumulation of unenveloped cytoplasmic capsids, suggesting a conserved role for UL11 in secondary envelopment [213-218]. HSV-1 lacking UL11 exhibits delayed replication and a >1000-fold decrease in the amount of infectious extracellular virus at 24 h.p.i. compared to the wild-type [213]. However, these growth defects can be partially rescued when UL11 is expressed without acyl modifications, demonstrating that some UL11 function is retained when the protein may not be membrane-associated [219].

A tripartite complex comprising HSV-1 tegument proteins UL11, UL16 and UL21 has been proposed based on evidence that UL16 interacts with UL11 [141,220], gE [140,145] and UL21 [142,145]. Purified GST-UL11 is able to capture UL16 and UL21 from lysates of cells infected with wild-type HSV-1, but cannot capture UL21 from lysates of cells infected with a UL16 deletion virus, placing UL16 at the heart of the complex [142]. Furthermore, packaging of UL11 and UL21 into HSV-1 virions is severely reduced in a virus lacking UL16, similarly there is a serious reduction in the amount of UL16 packaged in virions when either UL11 or UL21 is absent [143,221]. A model has been proposed whereby the tripartite UL11-UL16-UL21 complex assembles on the cytoplasmic tail of gE via UL11 and UL16, with direct binding of UL11 to gE promoting the interaction of gE with UL16, thus providing a link between the tegument and viral envelope that may mediate secondary envelopment [145]. Interestingly, UL16 has been shown to associate with HSV-1 capsids in the cytoplasm independently of the major capsid protein UL36 and UL37 [221,222]. These observations lead to the simple hypothesis that membrane-associated UL11 could interact with capsid-bound UL16 (and UL21) forming a link between the outer envelope and the capsid [223]. If this were the case then UL11 and UL16 deletion viruses might be expected to produce similar phenotypes. However, the two deletion viruses are

phenotypically distinct, with UL11 deletion leading to the accumulation of partially tegumented, non-enveloped capsids in the cytoplasm [213,214,218,224], whereas the UL16 deletion virus results in clusters of membrane-associated capsids in the cytoplasm and an increased propensity for multi-capsid virion formation [143]. Furthermore, UL11 is the smallest tegument protein thus it is questionable whether a complex of UL11 (10 kDa) with UL16 (40kDa) or UL21 (58 kDa) would be able to span the tegument layer. An interaction between UL16 and UL49 may also contribute to virus assembly, since a fragment (aa. 1-155) of HSV-1 UL16 has been shown to co-localise with UL49 in the absence of other viral proteins, and the incorporation of UL49 in to ΔUL16 virions is reduced [143].

UL7 and UL51 may promote secondary envelopment:

The final two conserved tegument proteins that have been implicated in tegumentation and secondary envelopment are UL7 and UL51. These proteins are the subject of the work presented in this thesis, which aimed to elucidate the precise role of these proteins during viral maturation. As such, UL7 and UL51 will be discussed in detail in section 1.3.4.

Table 1-5 Alphaherpesvirus tegument protein interactions
This table is mostly reproduced from [225]

Protein	Other Names	Interaction Partners	Function	Ref.
UL7	-	UL51 [HSV-1]	Putative role in CCS and secondary envelopment.	[139]
UL11	-	UL16 [HSV-1]	Role in secondary envelopment, also enhances interaction of UL16 with gE. A tripartite complex of UL11, UL16 and UL21 is proposed to play a role in cell fusion during syncytia formation, possibly through the interaction with gE.	[141,142,220]
		gE [HSV-1]	CCS and cell fusion during syncytia formation. Glycoprotein E accumulates at the plasma membrane in the presence of UL11, UL16 and UL21, in a cell-type dependent manner. Possible role in secondary envelopment.	[144,145,212]
UL16	-	UL11	(See UL11)	
		UL21 [HSV-1 & PrV]	UL21 enhances the interaction between UL16 and UL11 in triple-transfected cells. Putative role in CCS, syncitia formation and secondary envelopment when in complex with UL11 and gE.	[142,145,226]
		gE [HSV-1]	Putative roles in CCS, cell fusion and secondary envelopment. The interaction is enhanced in the presence of UL11 in transfected cells.	[140,145]
		UL49 [HSV-1]	Putative role in secondary envelopment.	[143]
UL21	-	UL16	(See UL16)	
UL36	VP1-2	UL19/VP5 [HSV-1]	Links the capsid and tegument, essential for tegumentation and secondary envelopment.	[53,54,146]
		UL25 [HSV-1 & PrV]	Links the capsid and tegument. May be required for stabilisation of the CVSC of nuclear and cytoplasmic capsids. Enhances dynein-mediated transport during PrV entry.	[50,86,91,147,227]
		UL37 [HSV-1 & PrV]	Provides a scaffold for tegumentation and secondary envelopment. Implicated in enhancing microtubule-based transport during entry and egress.	[135,148,150,181]
		UL48 [HSV-1]	Contributes to virus assembly. Both proteins are essential in HSV-1 but this is not an essential interaction.	[135,151,152]
UL37	ICP32	UL36	(See UL36)	
		UL35/VP26 [HSV-1]	Minor role in recruiting UL37 to capsids.	[133,153]
		gK [HSV-1]	Putative role in secondary envelopment by linking capsid associated UL37 with the membrane associated complex gK-UL20.	[154]

		UL20 [HSV-1]	Putative role in secondary envelopment by linking capsid associated pUL37 with the membrane associated complex gK-UL20.	[154]
UL46	VP11-12	UL48 [HSV-1 & HSV-2]	May regulate UL48-dependent transcription of immediate-early genes.	[135,155]
		ICP0 [HSV-1]	E3 ligase activity of ICP0 mediates the partial degradation of UL46 during infection, which may potentiate a shift from IE (α) to E (β) and L (γ) viral gene expression.	[156]
		Many identified in Y2H screens	Unknown.	[133,135,207]
UL47	VP13-14	UL48 [HSV-1]	Regulation of UL48-dependent transcription of IE genes.	[151,157]
		UL17 [HSV-1]	May provide a link between the capsid and tegument.	[208]
		Many identified by Y2H screen	Unknown.	[207]
UL48	VP16/ICP25	UL36	(See UL36)	
		UL41/vhs [HSV-1]	UL48 inhibits pUL41 during late stage of infection to spare viral mRNAs from degradation by pUL41.	[65,151,158-160]
		UL46	(See UL46)	
		UL47	(see UL47)	
		UL49 [HSV-1]	Contributes to tegument assembly.	[151,161]
		gH [HSV-1]	May contribute to secondary envelopment.	[162,201,202]
		gD [HSV-1]	Unknown.	[202]
		gB [HSV-1]	Unknown.	[202]
UL49	VP22	UL16	(See UL16)	
		UL48	(See UL48)	
		ICP0 [HSV-1]	Packaging of ICP0 into virions.	[165,166]
		gE [HSV-1 & PrV]	Contributes to secondary envelopment.	[144,163,204,228]
		gM [HSV-1 & PrV]	Contributes to secondary envelopment.	[163,228]
UL51	-	UL7	(See UL7)	
		UL14	Contributes to secondary envelopment.	[229]
		gE	Co-immunoprecipitates with UL51 from infected cells. Plays a role in CCS.	[168]

1.3.3.6 Secondary envelopment

The final stage of viral maturation is secondary envelopment, which involves the wrapping of tegumented capsids in a double membrane. To achieve this, tegumented capsids bud into specialised vesicles containing the surface glycoproteins of the mature virion. This process simultaneously provides the viral envelope and also packages HSV-1 into transport vesicles that can later fuse at virus-modified sites in the plasma membrane [68]. The acquisition of outer tegument is likely to be coordinated with secondary envelopment via interactions between tegument proteins and membrane bound viral glycoproteins and membrane-associated tegument proteins, as outlined in the previous sections. Finally, a membrane-scission event fuses the tips of the enveloping vesicle, thereby sealing the capsid within the viral membrane whilst also generating the transport vesicle. Interestingly, HSV-1 infection also results in the synthesis and release of L-particles, these are enveloped structures that contain tegument but lack capsids, indicating that tegumentation and envelopment can proceed in the absence of a capsid [230,231].

The outer membrane of mature HSV-1 virions are thought to contain 16 virally encoded membrane proteins (gB, gC, gD, gE, gG, gH, gI, gJ, gK, gM, gN, UL20, UL43, UL45, UL56 and US9), some of which are important for secondary envelopment and viral entry. The glycoproteins are trafficked to sites of secondary envelopment either independently or in sub-complexes. Tyrosine-based clathrin adaptor motifs have been identified in the cytoplasmic tails of gE and gB, which have been shown to be important for endocytosis and the intracellular localisation of these glycoproteins [232-235]. Viral membrane proteins lacking canonical transport motifs may rely on the formation of sub-complexes with other viral proteins for their localisation to secondary envelopment sites, for example, the localisation of the gE-gI heterodimer is dependent on trafficking motifs within gE [236], and the localisation of the essential viral entry proteins gD and gH-gL to secondary envelopment sites is dependent on the trafficking activity of gM and/or gK-UL20 [192,237,238].

The source of the secondary envelope remains disputed, with evidence in support of a TGN [239,240], late endosome and plasma membrane origin [241]. The prevailing view in the literature is that the vesicles originate from the TGN, which was inferred from studies showing the co-localisation of nascent capsids, viral glycoproteins and TGN markers (reviewed in [223]). However, it has been argued that co-localisation of capsids with TGN markers may not actually correlate with the production of infectious virions [241]. A more recent model proposes the PM as the source of the viral envelope with envelopment occurring in tubular endocytic membranes [241]. According to this model, viral glycoproteins are first transported from the TGN to the PM via the default secretory pathway, and are then endocytosed to form vesicles suitable for capsid envelopment. Inhibition of the endocytic pathway by treating cells with a dynein inhibitor or deletion of Rab5 resulted in the retention of viral glycoproteins at the PM and the accumulation of unenveloped capsids in the cytoplasm [241]. Furthermore, combined deletion of Rab5 and Rab11, which are associated with the PM/early

endosomes and recycling endosomes respectively, resulted in a substantial reduction in virus yield, whereas deletion of late endosome associated proteins Rab7 and Rab9 had little effect. Similar observations were made upon deletion of Rab6 and its effector ERC1, which is involved in Golgi to PM trafficking, and was accompanied with inhibition of capsid envelopment, suggesting that glycoprotein trafficking to the PM may be prerequisite for viral maturation [241,242]. It is important to bear in mind the complex and dynamic nature of membrane trafficking, and that there is scope for exchange between compartments. Therefore, assigning the origin of membranes to specific membranous compartments is not straightforward. Furthermore, the cytoskeleton undergoes considerable re-arrangement in infected cells, which may result in the alteration/breakdown of typical membranous compartments present in uninfected cells.

The final stage in secondary envelopment is membrane-scission, which seals the capsid within an envelope and generates the transport vesicle. Intriguingly, there is a topological similarity between HSV-1 secondary envelopment and the formation of intraluminal vesicles (ILV) within multivesicular bodies (MVBs). ESCRT (endosomal sorting complexes required for transport) machinery drives membrane invagination during MVB formation and plays a role in abscission at the end of cytokinesis (reviewed in [243]). It is well documented that HIV and several other RNA viruses are able to usurp host cell ESCRT machinery to drive budding of progeny virions at the plasma membrane (reviewed in [244,245]). Specifically, HIV Gag protein localises at the plasma membrane and recruits ESCRT complexes to HIV budding sites [246,247]. Furthermore, evidence exists to suggest that HSV-1 requires ESCRT function during envelopment and egress [248-250]. Expression of dominant-negative ESCRT components VPS4 and CHMP4A/B/C inhibits HSV-1 replication during secondary envelopment, resulting in an increase in unenveloped capsids in the cytoplasm and virtually no extracellular virions [249,250]. ESCRT function is also important for the assembly of PrV and HCMV [251,252]. Tegument and glycoproteins are likely candidates to recruit ESCRT machinery to secondary envelopment sites. Interestingly, UL36 from HSV-1 has been shown to interact with TSG101, a component of the ESCRT-1 complex, though what contribution this interaction makes to secondary envelopment has not been fully investigated [253].

Once packaged within a transport vesicle mature herpesvirions are likely to utilise the host-cell secretory pathway to facilitate their transport to egress sites. It is currently unknown how herpesviruses regulate and recruit host-cell trafficking proteins, though viral glycoproteins and membrane-associated tegument proteins are good candidates since they are predicted to be present on the cytoplasmic surface of viral transport vesicles. Kinesin-1, the motor protein involved in anterograde transport, and membrane trafficking proteins: Rab3A, Rab6A, Rab8A, Rab11A and SNAP-25 have been shown to traffic with HSV-1 and PrV viral particles to egress sites [254,255].

1.3.3.7 Exocytosis and cell-to-cell spread

Secondary envelopment simultaneously provides the viral envelope and packages the virion into a vesicle that can undergo microtubule-mediated transport to egress sites (Figure 1.3) at the PM or cell-cell junctions. Egress in non-polarised cells was shown to occur at patches in the PM that are heavily enriched in viral glycoproteins [68]. The formation of these patches is independent of virus trafficking to the PM as demonstrated during infection of cells with a UL25 deletion virus that is defective for nuclear egress. This suggests that HSV-1 is able to modify the PM to facilitate its own egress. Cortical actin is likely involved in the formation of these patches since actin de-polymerisation led to the dispersal of viral glycoproteins and PM-associated virions [68]. Interestingly, expression of a dominant negative isoform of the actin motor protein myosin Va was shown to reduce HSV-1 secretion by 50-75% while increasing intracellular virus infectivity levels, which is consistent with a defect in viral egress [256]. Levels of gB, gM and gD at the plasma membrane were also reduced in the presence of dominant negative myosin Va [256]. In cells, myosin Va is responsible for the transport of secretory granules along cortical actin, promoting membrane fusion at the PM and contributing to the stability of the fusion pore [257,258]. It has been suggested that HSV-1 may hijack this pathway to transport virions or glycoprotein-laden vesicles to the PM and/or assist in the formation of a fusion pore [256].

While viral egress can occur at apical cell membranes, HSV-1 remains largely cell-associated during infection and has evolved mechanisms for direct CCS, which enables the virus to evade immune effectors present in the extracellular environment. CCS is achieved either by syncytia formation, i.e. the fusion of an infected cell with a neighbouring (uninfected) cell, or by traveling via cell junctions. The process of membrane fusion during syncytia formation is thought to resemble the membrane fusion mechanism that occurs during viral entry (discussed in section 1.3.3.1), whereby viral glycoproteins expressed on the surface of the infected cell (i.e. gB, gD, gH-gL) mediate membrane fusion with a neighbouring cell [259,260]. Syndecan-1 has been shown to contribute to HSV-1 CSS via syncytia formation; increased expression of syndecan-1 in target cells leads to enhanced cell fusion while decreased expression in target cells reduces cell fusion and virus spread [260]. Sorting of mature virions to epithelial cell junctions for CCS is closely linked to the gE-gI complex [261,262]. The gE-gI complex accumulates at cell junctions at late stages of infection, the extracellular domain of gE is sufficient for localisation to cell junctions, but not for CCS [236,261,263]. When gE is deleted, virions traffic to apical surfaces rather than cell junctions [261]. Once concentrated at cell junctions virions can spread to neighbouring cells through interactions with cellular receptors that also accumulate at cell junctions [264,265].

1.3.4 HSV-1 tegument proteins: UL7 and UL51

This study focuses on two HSV-1 tegument proteins: UL7 and UL51, which are conserved across the *Herpesviridae* family. Deletion of either UL7 or UL51 results in impaired viral maturation and a

small plaque phenotype [266-268]. UL7 or UL51 knockout viruses are replication competent but exhibit substantially delayed and inefficient secondary envelopment, with electron micrographs of infected cells showing an accumulation of unenveloped capsids in the cytoplasm compared to wild-type. Similar phenotypes have been observed upon deletion of homologous proteins in PrV [269,270], VZV [271] and HCMV [272-274], suggesting a conserved role for these proteins. Preliminary work from the laboratory of Dr Colin Crump showed that single (ΔUL7 or ΔUL51) and double (ΔUL7+ΔUL51) deletion viruses exhibit comparable growth kinetics, and that UL7 was able to interact with UL51 in a Y2H screen. Thus, it was hypothesised that the UL7 and UL51 proteins may function as a complex during virus assembly and egress. The latter stages of herpesvirus assembly and egress remain unclear despite a wealth of research. This study aimed to elucidate the function of UL7 and UL51 during infection in the hope that it may provide some insight into HSV-1 assembly and egress at the molecular level, which may then be extended to other herpesviruses given that both UL7 and UL51 are conserved.

1.3.4.1 The UL7 protein

Deletion of UL7 from HSV-1 and PrV results in a 10 to 100-fold reduction in viral titre, a small plaque phenotype and the accumulation of unenveloped capsids in the cytoplasm [270,275]. The HSV-2 UL7 protein is expressed late during infection, being first detected by immunofluorescence in the nucleus at 6 h.p.i. and later shown to localise in the cytoplasm in the vicinity of the nucleus [268]. UL7 is a 33 kDa protein and possesses a conserved herpesvirus UL7-like domain (1-223 in HSV-1) of unknown function (Figure 3.6). An interaction between UL7 and the mitochondrial protein adenine nucleotide translocator 2 (ANT2) has been proposed, but not extensively studied [275].

1.3.4.2 The UL51 protein

UL51 is characterised as a late gene, being first detected by immunoblot at 6 h.p.i. in lysates of HSV-1 infected cells [276]. Overlap between the UL51 coding sequence and UL52 promoter region has prevented the generation of a complete UL51 deletion virus. Therefore, studies have been conducted using viruses that still encode N-terminal fragments of the UL51 gene: deletion of all but the N-terminal 42 residues of UL51 results in a 100-fold single-step growth defect, a small plaque phenotype and the accumulation of unenveloped cytoplasmic capsids in Vero cells [266]. A less severe 10-fold defect was reported when all but the N-terminal 73 residues of UL51 were deleted, measured in Vero cells [168]. Similarly, a 10-fold single-step growth defect was shown in this study (Figure 5.19) for HSV-1 virus lacking all but the first 20 amino acids of UL51, measured in HaCAT cells, this same virus exhibited a 100-fold reduction in Vero and HFF-Tert cells [277]. It is unknown what effect, if any, UL51 deletion has on pathogenicity *in vivo*.

The molecular mass of HSV-1 UL51 varies as a result of phosphorylation and acylation with species corresponding to 27, 29 and 30 kDa detected in mammalian cell lysates, with the latter two

species being first detected at 9 h.p.i. [276]. UL51 localises at the Golgi in transfected cells but predominantly localises in the juxtanuclear region during infection [139,277,278]. UL51 is also present at the perinuclear compartment during infection, which is interesting given that deletion of UL51 is also associated with delayed nuclear egress [278]. Localisation to the Golgi in transfected cells depends on palmitoylation of a conserved cysteine residue in position 9 [278]. Palmitoylation is the reversible attachment of a fatty acid moiety (palmitate) to a cysteine via a thioester bond, which enhances hydrophobicity and facilitates protein association with the inner face of phospholipid membranes [279]. Additionally, palmitoylation can alter protein conformation, trafficking, enzymatic activity, and interactions with other proteins [279]. It has been proposed that UL51 can exist in membrane-bound and soluble forms depending on its palmitoylation state [278]. In its membrane-bound state UL51 is likely to be displayed on the cytosolic surface of cytoplasmic membranes, where it could feasibly participate in secondary envelopment and/or vesicular trafficking (Figure 1.3, page 14). An interaction between UL51 and UL14 may play a role in secondary envelopment, since point mutations in UL51 (L111A, I119A, Y123A) that abolish the interaction result in a phenotype suggestive of defective secondary envelopment and comparable to that of the UL51 deletion virus, though the authors could not rule out possible wide-ranging structural changes in UL51 as a result of these mutations [229].

The small plaque phenotype and the accumulation of unenveloped and partially enveloped cytoplasmic capsids observed upon deletion of UL51 is indicative of a defect in virus assembly, particularly secondary envelopment. Such a defect could result from the inefficient budding of capsids into vesicles during secondary envelopment or possibly due to inefficient trafficking of vesicles to sites for secondary envelopment. Interestingly, it has been proposed that UL51 may have a role in mediating CCS, which would also contribute to the small plaque phenotype reported for ΔUL51 virus [168]. A point-mutation (Y19A) in UL51 has been linked to a cell-type specific defect in CCS, with no detectable defect in single-step growth or the efficiency with which virions are released into the medium [168]. This point-mutation occurs within a putative YXXϕ motif (ϕ means bulky hydrophobic residue) that is conserved across UL51 homologues in all subfamilies with the exception of PrV [168]. The YXXϕ motif resembles sorting signals within mammalian cell cargo proteins that interact with clathrin assembly polypeptide complexes (AP1-5) to mediate clathrin-coated vesicle formation [280,281]. It has been suggested that UL51, present on the surface of transport vesicles, might recruit cellular cargo adaptor proteins via this motif [168]. Furthermore, UL51 has been shown to interact with gE in infected cells, raising the possibility that UL51 may influence CCS in conjunction with the gE-gI complex (section 1.3.3.7). However, the CCS defect observed in the presence of the UL51-Y19A mutation was specific to HEp-2 cells with no defect apparent in Vero cells.

1.4 Objective and aims of this study

This study aimed to elucidate the function of two conserved HSV-1 tegument proteins: UL7 and UL51. Based on evidence published in the literature and unpublished work from the laboratory of Dr Colin Crump, it was hypothesised that UL7 and UL51 could form a complex during infection that contributes to virus assembly and egress. Given the potential for UL51 to associate with cellular membranes, via palmitoylation, it was postulated that UL51 could be displayed on the cytosolic surface of cytoplasmic membranes i.e. on the capsid facing surface during envelopment or on the outer envelope of mature vesicles (Figure 1.3, page 14). UL7 might also be recruited to these surfaces via an interaction with UL51. Thus, it would be feasible for membrane-associated UL51 (and UL7) to participate in secondary envelopment and/or vesicular trafficking by interacting with other viral or cellular proteins, which might explain why their deletion results in an accumulation of unenveloped capsids. One aim of this study was to screen for host-cell proteins that interact with UL7 and UL51, it was hypothesised that proteins involved in membrane trafficking and egress may be identified from such screens. Another aim was to characterise the putative UL7-UL51 complex by providing evidence for the formation of said complex in the context of infection, and by mapping the interaction using recombinantly expressed proteins from *E.coli*. Tied to this was the aim to solve the crystal structure of the UL7 and UL51 proteins either independently or in complex, solving the structure of a protein/complex can give an indication of function if there is similarity to protein folds of known function. The crystal structure of a UL7-UL51 complex would reveal the binding interface thus allowing specific point-mutations to be designed that abolish the interaction, such mutations could then be introduced into HSV-1 to further investigate the precise role of a UL7-UL51 complex during infection. While UL7 and UL51 proteins from HSV-1 were the focus of this study, attempts were also made to purify their homologues from a selection of viruses belonging to other *Herpesviridae* subfamilies: HCMV (β), EBV (γ), KSHV (γ) and murid herpesvirus (MHV, γ). It is useful from a biophysical and crystallographic perspective to trial multiple proteins to maximise the chance of obtaining soluble recombinant protein suitable for X-ray crystallography.

Objectives:

1) To characterise the putative UL7-UL51 complex in the context of infection and by using recombinantly expressed protein from *E.coli*.
2) Gain an insight into the function of UL7 and UL51 by identifying host-cell interaction partners using Y2H screening and quantitative proteomics, and by solving the crystal structure of the proteins independently or as part of a complex.

2 Materials and methods

2.1 Molecular Biology

2.1.1 Polymerase chain reaction (PCR)

2.1.1.1 Amplification from plasmid DNA

PCR reagents were combined as shown in Table 2-1. DNA amplification was performed using a thermocycler, programmed as follows: i) initial denaturation for 2 min at 95°C; ii) 20 cycles of denaturation for 20 s at 95°C, annealing for 10 s at 60°C and extension for 15 s/kb at 70°C; iii) final extension for 5 min at 70°C. Methylated template DNA was digested by incubating the PCR with 20 U of DpnI (New England Biolabs) for 2 h at 37°C. PCR products were visualised by agarose gel electrophoresis (section 2.1.2), and purified using EconoSpin™ All-in-One Mini Spin Columns (Epoch), according to the manufacturer's instructions. Template DNA was kindly provided by Prof. John Sinclair (HCMV Toledo), Dr Colin Crump (HSV-1 KOS) and Dr Mike Gill (EBV B95-6, MHV-68 and KSHV JSC-1). The UL7 sequence was amplified from a synthetic gene that had been codon optimised for expression in *E. coli* (purchased from Life Technologies). Primers are listed in Table 2-9, page 52).

2.1.1.2 Amplification from HeLa cDNA

Putative UL51 interaction partners identified by the Y2H screen were amplified using cDNA prepared from HeLa cells and the primers listed in (Table 2-10, page 53). The component for one PCR are shown in Table 2-1. Once compiled the 50 µl PCR mix was split into 5× 10 µl aliquots and placed across the PCR block, which was set-up with a temperature gradient so that each reaction experienced a different annealing temperatures. The thermocycler was programmed as follows: i) initial denaturation for 2 min at 95°C; ii) 35 cycles of denaturation for 20 s at 95°C, annealing for 10 s at 60°C with a 10°C gradient across the PCR block, and extension for 15 s/kb at 70°C; iii) final extension for 5 min at 70°C. HeLa cDNA was kindly provided by Dr Yvonne Hackmann.

Table 2-1 PCR components for amplification from plasmid DNA
Regents for a single polymerase chain reaction

Reagent	**Volume (µl)**
10× KOD Hot Start DNA Polymerase Buffer (Merck)	5.0
25 mM $MgSO_4$	3.0
25 mM dNTP mix	0.5
10 ng/µl DNA template (plasmid or HeLa cDNA)	1.0
10 µM forward primer	1.5
10 µM reverse primer	1.5
Nuclease-free water	37.5
KOD Hot Start DNA Polymerase (Merck)	1.0
Total	**50.0**

2.1.2 DNA analysis by agarose gel electrophoresis

1.0% Agarose gels were prepared using 0.5 g of molecular biology grade agarose powder (Sigma) and 50 ml 0.5× Tris-Borate EDTA (TBE) buffer (Appendix 1, page 196). The agarose was dissolved by microwave heating and 5 µl of 10,000x SYBR Safe™ DNA stain (ThermoFisher) was added. 10× DNA loading buffer (Appendix 1, page 196) was added to the DNA samples, DNA bands were resolved by electrophoresis in 0.5× TBE buffer (100 V, 100 mA) and visualised with visible blue light.

2.1.3 DNA digestion

2.1.3.1 His_6-tagged and GST-tagged human CPAP, UL7, UL51 and their homologues

The pOPTH, pOPTnH pOPT3G and pOPTn3G vectors (Table 2-7) were digested sequentially with NdeI then BamHI. The UL7 and UL51 insert DNA, along with their homologues, were digested in the same way, as was human CPAP G-box domain. For each reaction 1 µg of insert or vector DNA was combined with 20 U of NdeI enzyme (New England Biolabs) and 5 µl 10× New England Biolabs buffer 4, the reaction volume was adjusted to 50 µl using nuclease-free water. The reaction was incubated for 1 h at 37°C. DNA was purified using EconoSpin™ All-in-One Mini Spin Columns (Epoch) following the manufacturer's PCR clean-up instructions, and eluted into 30 µl nuclease-free water. The purified NdeI-digested DNA was digested with BamHI as follows: 1 µl BamHI (Roche) and 3.5 µl Roche buffer B were added to 30 µl of purified NdeI-digested vector or insert DNA, then incubated for 1 h at 37°C. Digested insert DNA was purified using EconoSpin™ All-in-One Mini Spin Columns (Epoch) following the manufacturer's PCR clean-up instructions, and eluted into 20 µl nuclease-free water. Digested vector DNA was incubated with 5 U Antarctic phosphatase (New England Biolabs) for 1 h at 37°C. NdeI/BamHI digested insert and vector DNA was resolved by agarose gel electrophoresis (section 2.1.2) and purified using EconoSpin™ All-in-One Mini Spin Columns (Epoch), according to the manufacturer's gel extraction instructions. Ligation was performed as described in section 2.1.4.

2.1.3.2 Myc-tagged constructs for mammalian cell and wheat germ cell-free expression

Constructs for expression using the wheat germ cell-free expression system were cloned into either *pF3A WG* or *pF3A Myc WG* (Table 2-7, page 50). DNA amplification was performed as described in section 2.1.1.2 from a HeLa cDNA library. *pF3A WG* vector and insert DNA were digested as follows: 1 µg of DNA was combined with 1 µl of SgfI/PmeI Flexi® Enzyme Blend (Promega) and 10 µl of 5× Flexi® Digest buffer, and diluted to 50 µl with nuclease-free water. The reaction was incubated for 1 h at 37°C. *pF3A Myc WG* vector and insert DNA were digested as follows: 1 µg of DNA was combined with 0.5 µl HindIII HF™, 0.5 µl PmeI and 5 µl CutSmart® buffer (enzymes and buffer: New England Biolabs), and diluted to 50 µl with nuclease-free water. The reaction was incubated for 1 h at 37°C. Digested

insert DNA was purified using EconoSpin™ All-in-One Mini Spin Columns (Epoch) following the manufacturer's PCR clean-up instructions, and eluted into 20 µl nuclease-free water. Ligation was performed as described in section 2.1.4.

2.1.3.3 Cloning FAB (UL7-UL51) and GAB (ORF42-ORF55) complexes into pOPC

The FAB and GAB complexes were expressed from the polycistronic expression plasmid pOPC (Table 2-7, page 50) [282]. *The FAB complex:* full-length UL51 C9S was first cloned into pOPTH and codon optimised UL7 was cloned into pOPT3nG (section 2.1.3.1), these were then sub-cloned into pOPC cassettes 1 (XbaI/BamHI) and 2 (EcoRI/HindIII), respectively. Site-directed mutagenesis was used to introduce His_6-UL51 truncations (section 2.1.8). *The GAB complex:* OFR55 C3S+C4S 1-163 was first cloned into pOPTH and ORF42 was cloned into pOPT3G, these were then respectively sub-cloned into cassettes 3 (SacI/KpnI) and 4 (BspEI/MluI) of a separate pOPC plasmid. Ligation was performed as described in section 2.1.4.

2.1.4 DNA ligation

Digested insert and vector DNA were combined in a 3:1 molar ratio and incubated with 0.5 µl of T4 ligase and 1.0 µl of 10× T4 ligase buffer, the volume was diluted to 10 µl with nuclease-free water (enzyme and buffer: New England Biolabs). Ligation reactions were incubated at 16°C overnight. Competent DH5α™ *E. coli* cells were transformed as described in (section 2.1.6), cells were also transformed with digested insert or digested vector only as negative controls.

2.1.5 Preparation of competent *E. coli* cells

All competent *E. coli* cell strains, except ArcticExpress™, were prepared in house. 100 ml cultures were grown in lysogeny broth (LB) supplemented with antibiotic as required: 25 µg/ml chloramphenicol was used for BL21 (DE3) pLysS and Rosetta2™ (DE3) pLysS cells, no antibiotic was used for DH5α™ and B834 (DE3) cells. The cultures were grown to OD_{600} ≈0.3 and chilled on ice for 15 min. Cells were pelleted by centrifugation at 4,000 ×g for 10 min at 4°C, then re-suspended in ice-cold, sterile 0.1 M $CaCl_2$ and incubated on ice for 30 min. The cells were pelleted again and re-suspended in 5 ml ice-cold, sterile 0.1 M $CaCl_2$ supplemented with 15% v/v glycerol. Cells were divided into 50 µl aliquots and stored at -80°C.

2.1.6 Transformation of competent *E. coli* cells

Either 0.5 µl of purified plasmid DNA or 3.0 µl of ligation reaction was added to 50 µl of competent *E. coli* cells and incubated on ice for 30 min. The cells were then heat-pulsed for 30 s at 42°C (20 seconds for ArcticExpress™ cells), then allowed to recover for 2 min on ice. 200 µl of 2xTY medium per transformation was added, and the cells were incubated at 37°C for 1 h on a shaking platform. 100 µl of transformation mix was spread on 2xTY agar plates containing the appropriate antibiotic: ampicillin (100 µg/ml), kanamycin (30 µg/ml) or ampicillin (100 µg/ml) + chloramphenicol (25 µg/ml). The plates were incubated overnight at 37°C. Ampicillin selects for pOPTH, pOPTnH pOPT3G, pOPTn3G, pF3A WG and pF5A vectors; kanamycin selects for pEGFP-C1; chloramphenicol selects for pLysS.

2.1.7 Purification of plasmid DNA

Plasmid DNA was amplified using DH5α™ cells that were transformed as described in section 2.1.6. Two or more colonies were selected for each construct and cultured overnight in 4 mL 2xTY medium with appropriate antibiotic (section 2.1.6) at 37°C on a shaking platform. For small-scale preparations (<20 µg DNA) the cultures were harvested by centrifugation at 11,000 ×g for 1 min and plasmid DNA was extracted using EconoSpin™ All-in-One Mini Spin Columns (Epoch) as directed by the manufacturer. For larger preparations (500-1000 µg DNA), 200 µl of the 4 ml overnight culture was used to inoculate 100 ml 2xTY medium supplemented with appropriate antibiotic (see section 2.1.6) and cultures were incubated overnight at 37°C on a shaking platform. The cells were harvested by centrifugation at 4,000 ×g for 15 min. DNA was purified using a PureLinK™ HiPure Plasmid Midiprep kit (ThermoFisher) according to the manufacturer's instructions. All plasmids were Sanger sequenced to ensure the sequence was correct and in frame (sequencing primers listed in Table 2-12, page 54). Purified plasmid DNA was stored at -20°C.

2.1.8 Site-directed mutagenesis

Site-directed mutagenesis was used to generate truncations and point mutations in UL51 and ORF55 plasmids. The PrimerX sever (http://www.bioinformatics.org/primerx/ - last updated 14/08/2006) was used to design the primers, which are listed in Table 2-11, page 53. Components for a single mutagenesis reaction are shown in Table 2-2. The thermocycler was programmed as follows: i) initial denaturation for 30 s at 98°C; ii) 5 cycles of denaturation for 30 s at 98°C, annealing for 60 s at 52°C, and extension at 68°C for 1.5 min/kb; iii) step ii was repeated for a further 7 cycles with the annealing temperature increased to 55°C; iv) final extension for 5 min at 68°C. Methylated template DNA was digested with 20 U of DpnI (New England Biolabs) for 2 h at 37°C. 1 µl of reaction mix was

used to transform DH5α™ cells as described in section 2.1.6. All plasmids were Sanger sequenced to ensure sequence was correct and in frame (sequencing primers listed in Table 2-12, page 54).

Table 2-2 Reaction components for site-directed mutagenesis of Plasmid DNA

Reagent	Volume (µl)
10× Pfu Turbo® DNA polymerase buffer (Agilent)	5.0
50 mM $MgCl_2$	2.0
2 mM dNTPs	5.0
10 ng/µl DNA template (plasmid)	2.0
10 µM forward primer	1.5
10 µM reverse primer	1.5
Nuclease-free water	32
Pfu Turbo® DNA polymerase (Agilent)	1.0
Total	**50.0**

2.2 Protein Chemistry

2.2.1 Small-scale protein expression and purification

Transformed BL21 (DE3) pLysS, Rosetta2™ (DE3) pLysS and B834 (DE3) cells were cultured overnight in 4 ml of 2xTY + appropriate antibiotic (see section 2.1.6) at 37°C on a platform shaking at 220 rpm. The overnight starter culture was used to inoculate 3.5 ml of fresh 2xTY + antibiotic (1:100 dilution of inoculum), which was cultured at 37°C until OD_{600} 0.6-0.8 was reached. Protein expression was induced with the addition of 0.2 mM IPTG (isopropyl 1-thiol-β-D-galactopyranoside), and allowed to continue at 37°C for 4 h or at 22°C for 20 h, with 220 rpm shaking. The cells were harvested by centrifugation at 2,000 ×g for 30 m, cell pellets were frozen at -20°C. For all steps, the cells were cultured in 24-well blocks with air-permeable seals. Buffers for small-scale protein purification are presented in Table 2-3. Cell pellets were lysed in the appropriate lysis buffer for 30 min at room temperature on a shaking platform, then centrifuged at 4,000 ×g for 30 min. Magnetic Ni-NTA or magnetic GSH beads were dispensed in a 96-well microtitre plate and pre-equilibrated with wash buffer. Supernatants were incubated with the beads for 30 min at room temperature on a shaking platform. The beads were washed three times with wash buffer and bound protein was eluted in 50 µl elution buffer.

Table 2-3 Buffers for small-scale protein purification

	His_6-tagged (Ni-NTA beads)	**GST-tagged (GSH beads)**
Lysis buffer	50 mM NaN_2PO_4 pH 8.0 300 mM NaCl 10 mM imidazole pH 7.5 1% Tween-20 15 U/ml DNAseI 1% EDTA-free protease inhibitors (Sigma) 30 mg/ml hen egg white lysozyme.	125 mM Tris pH 7.4 300 mM NaCl 1% Tween-20 1.4 mM β-mercaptoethanol 15 U/ml DNAseI 1% EDTA-free protease inhibitors (Sigma) 30 mg/ml hen egg white lysozyme.
Wash buffer	50 mM NaN_2PO_4 pH 8.0 300 mM NaCl 20 mM imidazole pH 7.5 0.05% Tween-20	125 mM Tris pH 7.4 300 mM NaCl 0.05% Tween-20
Elution buffer	50 mM NaN_2PO_4 pH 8.0 300 mM NaCl 250 mM imidazole pH 7.5 0.05% Tween-20	125 mM Tris pH 7.4 300 mM NaCl 0.05% Tween-20 50 mM reduced glutathione

2.2.2 Large-scale protein expression using BL21 (DE3) pLysS and Rosetta2™ (DE3) pLysS

The UL51, ORF55 and CPAP constructs and the FAB and GAB complexes were expressed in BL21 (DE3) pLysS *E. coli* cells. UL7 was expressed in Rosetta2™ (DE3) pLysS cells. Freshly-transformed colonies (section 2.1.6) were used to inoculate 5 ml of 2xTY medium supplemented with ampicillin (100 µg/ml) and chloramphenicol (25 µg/ml) and cultured overnight at 37°C with 220 rpm shaking. For large-scale protein expression bacterial cultures were grown in 1 L volumes of fresh 2xTY medium supplemented with ampicillin (50 µg/ml) and chloramphenicol (12.5 µg/ml), these were inoculated with the overnight starter culture in a 1:500 ratio then cultured at 37°C on a platform shaking at 220 rpm. Once OD_{600} 0.8-1.0 was reached, protein expression was induced with the addition of 0.2 mM IPTG and allowed to continue at 22°C for ≈20 h on a platform shaking at 220 rpm. Following expression, bacterial pellets were harvested by centrifugation at 5,000 ×g for 15 m. Bacterial pellets were immediately frozen and stored at -80°C.

2.2.3 Large-scale protein expression in ArcticExpress™ (DE3) Cells

ArcticExpress™ (DE3) Competent Cells (Agilent) were used for the expression of His_6-tagged UL7. The expression protocol used was similar to that described in section 2.2.2 but with the following exceptions: i) the overnight starter culture contained gentamycin (20 µg/ml) and ampicillin (100 µg/ml); ii) the 1 L culture was grown at 30°C and in the absence of any antibiotic selection; iii) once OD_{600} 0.8-1.0 was reached the temperature was dropped to 12°C for 30 m before expression was induced with IPTG; iv) expression continued at 12°C for 24 h.

2.2.4 Wheat-germ cell-free expression

Constructs for expression in wheat-germ cell-free expression system were cloned into either pF3A WG or pF3A myc WG (section 2.1.3.2). For each construct, 2-4 µg of DNA in a volume of 20 µl was combined with 30 µl of TNT® SP6 High Yield Wheat Germ reaction mix (Promega), then incubated at 25°C for 2 h.

2.2.5 Purification of UL51, UL7, ORF42, ORF55 and human CPAP protein

Recombinant proteins were purified using an appropriate affinity chromatography step followed by size-exclusion chromatography (SEC). The following method applies to the purification of wild-type and mutant proteins unless otherwise stated. Bacterial pellets were thawed on ice and re-suspended in 90 ml of chilled *lysis buffer* (20 mM Tris pH 7.5, 500 mM NaCl, 0.5 mM $MgCl_2$, 1.4 mM β -mercaptoethanol, 0.05% Tween-20, supplemented with 200 µl EDTA-free protease inhibitor cocktail (Sigma) and 400 U DNAse per 2 L of culture). Cells were lysed at 24 kpsi using a Constant Systems Cell Disrupter, the lysate was centrifuged at 40,000 ×g for 30 m to separate insoluble components. Cleared lysate was subjected to Ni-NTA affinity chromatography to capture His_6-tagged proteins or GSH-affinity chromatography to capture GST-tagged proteins.

2.2.5.1 Ni-NTA affinity chromatography

For each 2 L *E. coli* culture, 4 ml of Ni-NTA beads (Qiagen) were equilibrated with 2 column volumes of chilled *His-wash buffer* (20 mM Tris pH 7.5, 500 mM NaCl, 20 mM imidazole). Equilibrated beads were removed from the column and incubated with the cleared lysate at 4°C on a rolling bed for 1 hour. The beads were re-applied to the column and washed with ≈150 ml His-wash buffer. Bound-protein was eluted in *His-elution buffer* (20 mM Tris pH 7.5, 500 mM NaCl, 250 mM imidazole) and collected in 2 ml fractions at room temperature. Bradford reagent was used to identify fractions likely to contain the target protein; these fractions were then concentrated using a 10 kDa cut-off concentrator (Millipore) to ≈4 ml before performing size-exclusion chromatography. Concentrated wild-type UL51 and ORF55 protein was incubated with 50 mM DTT prior to loading on the SEC column.

2.2.5.2 GSH-affinity chromatography

For each 2 L *E. coli* culture, 3 ml of glutathione sepharose 4B beads (GE Healthcare) were used. The protocol for GST-affinity chromatography was the same as that for Ni-NTA (section 2.2.5.1) with the buffers adapted accordingly: *GST-wash buffer* (20 mM Tris pH 7.5, 300 mM NaCl, 1 mM DTT) and *GST-elution buffer* (GST-wash buffer + 25 mM reduced L-glutathione). Fractions containing GST-tagged protein were concentrated using a 30 kDa cut-off concentrator (Millipore).

2.2.5.3 Size-exclusion chromatography (SEC)

SEC was performed using either S75 16/600 (< 30 kDa), S200 16/600 (> 30 kDa) or analytical S200 10/300 Superdex^{TM} columns (GE Healthcare) connected to a FPLC ÄKTA purifier (GE Healthcare). Columns were equilibrated with 1.5 column volumes of 0.2 µm filtered *gel filtration buffer* (20 mM Tris pH 7.5, 200 mM NaCl, 1 mM DTT - 5% v/v glycerol was also included for the FAB and GAB complexes). All protein samples were centrifuged (20,000 ×g for 5 min) to pellet any precipitated protein before injection. Isocratic elution was performed and 1 ml fractions (0.5 ml for analytical column) were collected. The A_{280} chromatogram was used to select fractions for analysis by SDS-PAGE. Fractions containing the protein of interest were pooled, concentrated and plunge-frozen in liquid nitrogen then stored at -80°C.

2.2.6 Purification of FAB (UL7-UL51) and GAB (ORF42-ORF55) complexes

The FAB and GAB complexes were expressed as described in section 2.2.2. Figure 2.1 presents a schematic overview of the steps involved in purifying the complexes. Initial purification attempts used Tris buffers throughout. Once DNA contamination was detected, phosphate buffers were used for steps (1-3) and two additional steps (3a and 3b) were introduced, the final SEC step (8) was always performed in Tris buffer.

2.2.6.1 Purification with Tris buffers

Step 1: Bacterial pellets were thawed on ice and re-suspended in 90 ml of chilled *lysis buffer* (20 mM Tris pH 7.5, 500 mM NaCl, 0.5 mM $MgCl_2$, 1.4 mM β-mercaptoethanol, 0.05% Tween-20, 400U DNAse and 1% EDTA-free protease inhibitor cocktail (Sigma)). Cells were lysed at 24 kpsi using a Constant Systems Cell Disrupter, and the lysate centrifuged at 40,000 ×g for 30 min to remove insoluble components. **Step 2:** For each 2 L *E. coli* culture, 3 ml of glutathione sepharose 4B beads (GE Healthcare) were equilibrated in *GST-wash buffer* (20 mM Tris pH 7.5, 300 mM NaCl, 1 mM DTT). The cleared lysate was incubated with GSH beads at 4°C with gentle rotation for 1 h. **Step 3:** The beads and bound protein were washed with 90 ml of chilled GST-wash buffer in a re-usable column. **Step 4:** Bound-protein was eluted in chilled *GST-elution buffer* (GST-wash buffer + 25 mM reduced L-glutathione) and collected in 2 ml fractions. Bradford reagent was used to identify fractions likely to contain the target protein. **Step 5:** The fractions were pooled and SEC was performed to remove glutathione from the protein sample, an S200 16/600 column equilibrated in *gel filtration buffer* (20 mM Tris pH 7.5, 200 mM NaCl , 1 mM DTT) was used. **Step 6:** SEC fractions corresponding to the A_{280} peak were pooled and supplemented with 0.5 mM EDTA, then incubated with human rhinovirus 3C protease (10 µg protease per 1 L of *E. coli* culture) overnight at 4°C. **Step 7:** The protein sample was incubated with GSH beads, equilibrated in gel filtration buffer, for 1 h at 4°C on a rolling bed to capture

free GST, uncleaved GST-UL7 / ORF42 and GST-tagged 3C protease. **Step 8:** The flow-through from step 7 was concentrated using a 10 kDa cut-off concentrator (Millipore) to ≈4 ml and injected for SEC (section 2.2.5.3).

2.2.6.2 Purification with phosphate buffers

The protocol described above was followed for **steps 1-3** but replacing the buffers with: *lysis buffer* (50 mM sodium phosphate pH 7.5, 500 mM NaCl, 0.5 mM $MgCl_2$, 1.4 mM β-mercaptoethanol, 0.05% Tween-20, 400U DNAse and 1% EDTA-free protease inhibitor cocktail (Sigma)); *GST-wash buffer* (50 mM sodium phosphate pH 7.5, 300 mM NaCl, 1 mM DTT). For **step 3** the beads were washed with 20 ml chilled GST-wash buffer instead of 90 ml. **Step 3a:** The sample-loaded beads were re-suspended in 40 ml chilled *benzonase buffer* (25 mM sodium phosphate pH 7.5, 150 mM NaCl, 0.5 mM $MgCl_2$) then incubated with 50 U/ml benzonase (Sigma) for 30 min at room temperature on a roller bed. **Step 3b:** The sample-loaded beads were re-applied to the re-usable column and washed using 30 ml *high salt buffer* (50 mM sodium phosphate pH 7.5, 1 M NaCl, 1 mM DTT), followed by a 20 ml wash with GST-wash buffer. The **following steps (4 to 8)** were performed as described in section 2.2.6.1, using Tris buffers.

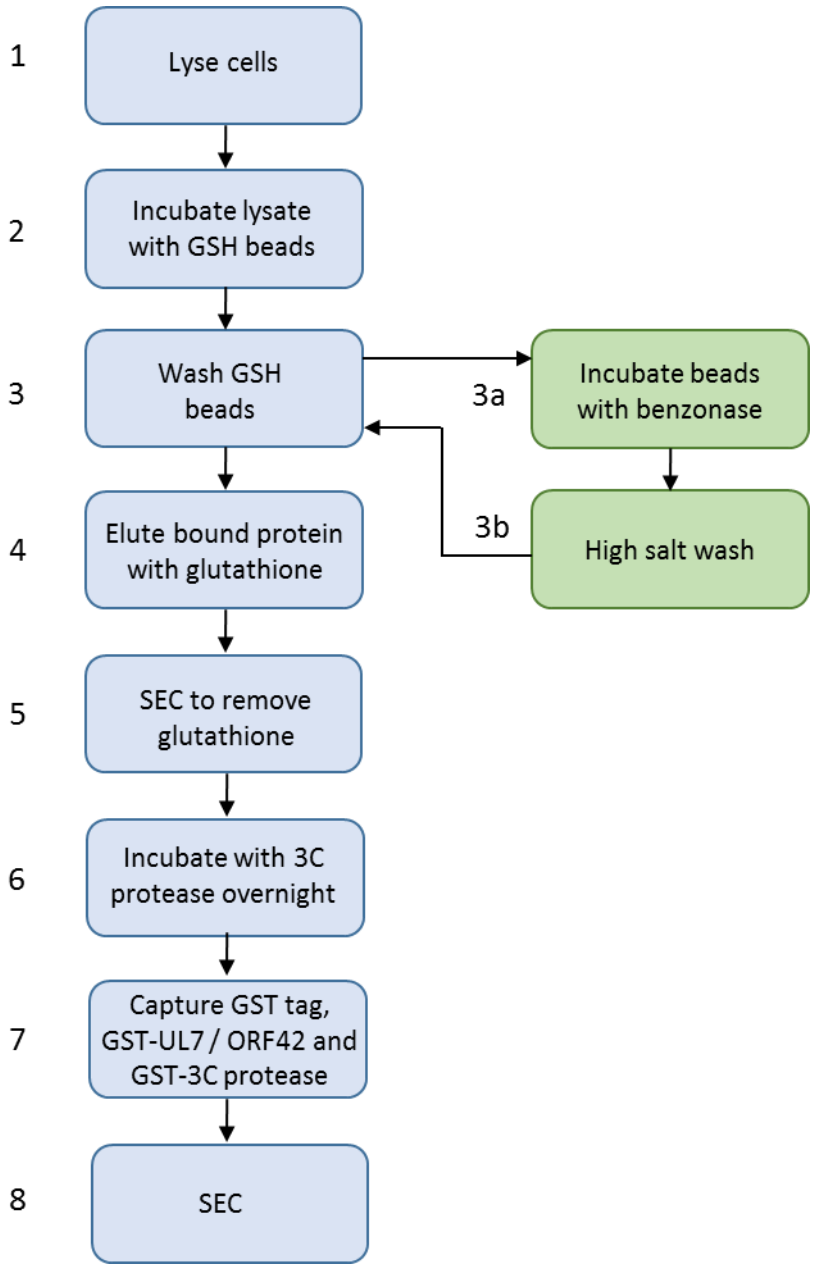

Figure 2.1 Schematic overview of the purification protocol for FAB and GAB complexes
Initially, steps 1-8 were performed using Tris-based buffers. The protocol was modified to remove nucleic acid contamination, this involved two additional steps, 3a and 3b, and switching to phosphate based buffers for steps 1-3.

2.2.7 Screening hybridoma supernatants by ELISA

Purified full-length His_6-UL51 or His_6-UL51 1-170 was used as the antigen to screen hybridoma supernatants for antibodies against UL51, and to distinguish between those that recognise epitopes in the N- or C-terminal regions of UL51. Antigens were prepared to a final concentration of 2.0 µg/ml in PBS and 100 µl volumes were dispensed into the wells of a CORNING 96-well Costar Assay plate. Plates were incubated with antigen overnight at room temperature on a shaking platform. The antigen solution was discarded and the wells were washed three times with PBS-T (PBS + 0.1% Tween-20).

200 µl of *blocking buffer* (2% BSA in PBS-T) was added to each well and incubated at room temperature for 30 min on a shaking platform. Blocking buffer was discarded and the wells were washed three times with PBS-T. To each well was added 50 µl of hybridoma supernatant diluted 1/50 with blocking buffer, followed by incubated at room temperature for a minimum of 2 h on a shaking platform. The wells were washed four times with PBS-T, then incubated with 200 µl blocking buffer for 10 min at room temperature before a further two washes with PBS-T. Anti-mouse alkaline phosphatase (Sigma AO162) was diluted 1/10,000 in blocking buffer and 100 µl was added to each well. Plates were further incubated for 2 h at 37°C on a shaking platform, followed by 11 washes with PBS-T. Plates were developed by adding 75 µl of NPP substrate (SIGMAFAST p-Nitrophenyl phosphate tablets, prepared according to the manufacturer's instructions) to each well. After incubating for 1 h at room temperature 25 µl of 3 M NaOH was added to the well to stop the hydrolysis reaction. PNPP hydrolysis was detected by the appearance of a yellow colour in the wells. The plates were wrapped in foil during all incubation steps.

2.2.8 Monoclonal antibody (IgG) purification

Hybridoma supernatant was spun at 10,000 ×g for 15 min and 0.45 µm filtered to remove cellular debris. If necessary, the supernatant was diluted with *binding buffer* (20 mM sodium phosphate pH 7.0) to adjust the pH to 7.0 before injection onto a HiTrap™ Protein G HP column (GE Healthcare), equilibrated in binding buffer. The column was washed with binding buffer and bound protein was eluted with *elution buffer* (0.1 M glycine, pH 2.7). 0.5 ml fractions were collected in tubes pre-loaded with enough *neutralising buffer* (1 M Tris pH 9.0) to adjust the pH to 7.0 (approximately 25-40 µl). Fractions corresponding to the elution peak in the A_{280} chromatogram were pooled and dialysed twice against 1 L of PBS supplemented with 0.02 % sodium azide before being stored at 4°C.

2.2.9 Analysis of protein samples by SDS-PAGE

Proteins sample were denatured and reduced in SDS-PAGE loading buffer (Appendix 1, page 196) at 95°C for 5 min. Protein bands were resolved by PAGE using standard protocols. PreScission Plus Protein™ dual colour standards (Bio-Rad) were used for all gels. Protein bands were visualised using InstantBlue™ Coomassie Stain (Expedion), unless the gel was to be used for an immunoblot.

2.2.10 Electrophoretic transfer of proteins for immunoblotting

Protein bands were transferred from polyacrylamide gels to 0.45 µm Protran® nitrocellulose membranes (Perkin Elmer) in transfer buffer (Appendix 1, page 196) by submerged tank transfer (Bio-Rad). Transfers were performed at 100 V for 1 h or at 20 V overnight at 4°C. An overnight transfer was always performed when probing for CPAP. Membranes were stained with ponceau stain (Appendix 1,

page 196) for 2 m to determine whether the transfer had been successful. The membrane was de-stained by washing with PBS buffer.

2.2.11 Immunoblotting

Protran® nitrocellulose membranes (Perkin Elmer) were blocked in *5% milk PBS buffer* (5% w/v dried Marvel™ skim milk powder in PBS) at room temperature for 2 h or overnight at 4°C on a rocking platform. When the anti-Penta-His (Qiagen) antibody was used, nitrocellulose membranes were blocked with 3% w/v BSA in PBS. Primary antibody was diluted in *5% milk PBS-T buffer* (5% w/v dried Marvel™ skim milk powder in PBS + 0.1% Tween-20) as shown in Table 2-4. Blocked membranes were incubated with primary antibody at room temperature for 2 h or overnight at 4°C on a rocking platform. When probing with αUL7 or αCPAP the incubation was always performed overnight. Three washes were performed using 5% milk PBS-T buffer, each for ≥ 5 min. Membranes were incubated for 1 h at room temperature with the appropriate secondary antibody, listed in Table 2-5, diluted in 5% milk PBS-Tween buffer. This was followed by three further ≥ 5 min washes in 5% milk PBS-T buffer, a 15 min wash in PBS-T buffer and three brief washes in PBS. Antibody fluorescence was visualised using an Odyssey CLx infrared imager and Image Studio™ Lite software (LI-COR).

Table 2-4 Primary antibodies

Antigen	Clone/ Cat. #	Species	Carrier	Dilution (IB)	Source
His_5	34660	mouse	BSA	1:1000	Qiagen
Myc	4A6 / 05-724	mouse	Skim milk	1:3000	Millipore
GFP	G1544	rabbit	Skim milk	1:5000	Sigma
GAPDH	AM4300	mouse	Skim milk	1:500,000	Ambion
CPAP	11517-1-AP	rabbit	Skim milk	1:1000	Proteintech™
NIPSNAP4	10751-1-AP	rabbit	Skim milk	1:1000	Proteintech™
NIPSNAP1/2	SC-393201	mouse	Skim milk	1:1000	Santa Cruz
NIPSNAP 1	SC-515197	mouse	Skim milk	1:1000	Santa Cruz
UL51	3D3	mouse	Skim milk	1:1000	In-house
UL51	2B3	mouse	Skim milk	1:1000	In-house
UL7	B1134	mouse	Skim milk	1:200	In-house
β-Actin	A5541	mouse	Skim milk	1:2000	Sigma
Pontin	5G3-11	mouse	Skim milk	1:1000	Sigma
Reptin	2E9-5	Mouse	Skim milk	1:1000	Sigma

Table 2-5 Secondary antibodies

Host/target IgG	Clone/Cat.#	Dilution	Source
IRDye® 680RD Goat-anti-Rabbit	926-32221	1:10,000	LI-COR Biosciences
IRDye® 800CW Goat-anti-Rabbit	925-32221	1:10,000	LI-COR Biosciences
IRDye® 800CW Goat-anti-Mouse	925-32210	1:10,000	LI-COR Biosciences

2.2.12 GST pull-down experiments

2.2.12.1 Purified GST-bait with wheat-germ expressed prey

All affinity capture ("pull-down") steps were performed at 4°C. For each pull-down experiment 20 µl of Pierce® Glutathione Magnetic Beads (ThermoScientific) was dispensed into flat-bottomed 96-well microtitre plates. The beads were prepared by washing twice with *wash buffer* (20 mM Tris pH 7.5, 200 mM NaCl, 0.1% NP-40, 1 mM DTT and 1 mM EDTA). GST-tagged bait protein or GST (2.5 µM) was incubated with the magnetic beads for 30 min on a shaking platform at 4°C. This was followed by 3× 1 min washes with wash buffer. The beads were then captured using a magnetic block and the buffer was removed. The wheat-germ cell-free reaction mix was diluted to 200 µl with wash buffer then divided 50:50 and added to the beads bound with GST-tagged bait protein or GST only control protein, 100 µl of wash buffer was then added to each well to make a final volume of 200 µl per well and incubated for 1 h on a shaking platform at 4°C. Unbound protein was removed and 4× 30 s washes were performed with wash buffer. The beads were then incubated with 48 µl of *elution buffe*r (wash buffer + 50 mM reduced L-glutathione) for 1 min. The eluate was combined with 12 µl 5× SDS-PAGE loading buffer and analysed by SDS-PAGE (section 2.2.9)

2.2.12.2 Purified GST-bait protein with purified prey protein

For pull-down assays using purified proteins, magnetic glutathione beads (Pierce) were equilibrated in *pull-down buffer* (20 mM Tris pH 7.5, 200 mM NaCl, 0.1% Nonidet P-40, 1 mM DTT, 1 mM EDTA) and then incubated with 0.5 nmol GST-tagged bait protein (e.g. UL7-GST or GST) for 30 min at 4°C. Beads were washed with pull-down buffer and incubated with 2.5 nmol prey protein (e.g. His_6-UL51 C9S, His_6-UL51 29–170, or N1-His_6. The vaccinia virus protein N1 was purified as described in [283]) for 1 h at 4°C. Unbound protein was removed and the beads were washed four times with pull-down buffer. Bound protein was eluted in *elution buffer* (pull-down buffer supplemented with 50 mM reduced glutathione). Samples were resolved by SDS-PAGE and visualized using Coomassie stain.

2.2.13 Protein quantification by bicinchoninic acid (BCA) assay

Whole cell lysate protein concentration was determined by BCA assay using reagents supplied with the Pierce™ BCA Protein Assay Kit (ThermoFisher), and according to the manufacturer's microplate procedure. Protein standards were prepared by 2-fold serial dilution of bovine serum albumin from 2 mg/ml to 62.5 mg/ml. Absorbance at A_{562} nm was measured using a SpectraMax i3 plate reader and accompanying software.

2.3 Biophysics

2.3.1 Multi-angle light scattering (SEC-MALS)

Molecular masses for the UL7-UL51 (1-170 C9S, 29-170 and 8-142 C9S) complexes were determined by SEC on a 1260 Infinity FPLC (Agilent) with in-line measurement of light scattering (Dawn 8+; Wyatt Technology), differential refractive index (Optilab T-rEX; Wyatt Technology), and UV absorbance at 280 nm (Agilent). 100 µl of protein sample was injected onto an analytical Superdex 200 Increase 10/300 gel filtration column (GE Healthcare) equilibrated in *SEC-MALS buffer* (20 mM Tris pH 7.5, 200 mM NaCl, 3 mM DTT, 5% v/v glycerol) at a flow rate of 0.4 ml/min. Molecular masses were calculated using the ASTRA6.1 software package (Wyatt Technology, using a protein dn/dc value of 0.186). To investigate the interaction between the UL7-UL51 complex and DrCPAP$^{943\text{-}1121}$ G-box domain, the SEC column was first equilibrated in SEC-MALS buffer, then 100 µl of UL7-UL51 complex was injected at 1.0 mg/ml. DrCPAP$^{943\text{-}1121}$ was combined with UL7-UL51 complex in a 1:1 molar ratio for 20 m, then 100 µl of the UL7-UL51+DrCPAP sample was injected at 1.0 mg/ml.

2.3.2 Differential Scanning Fluorimetry (DSF)

DSF experiments were performed in 96-well PCR plates using 2 µg of purified UL7-UL51 complex combined with 1× Protein Thermal Shift Dye (Applied Biosystems) and different additives in a final volume of 20 µl. The assay was performed using a Viia7 quantitative PCR machine (Applied Biosystems). Samples were heated from 25°C to 95°C in 1°C steps with 20 s equilibration per step and fluorescence was monitored at 1°C increments. The data were plotted and fitted to a Boltzmann-sigmoidal model using DSF analysis scripts (written by Dr Stephen Graham) and GraphPad Prism version 6.0, the melting temperature (T_m) was taken as the inflection point of the sigmoid [284].

2.3.3 Fluorescence polarisation

Fluorescence polarisation was measured using a SprectaMax i3 plate reader (Molecular Devices) set with 485/20 nm excitation and 535/25 nm emission filters and equilibrated to 30°C, with a 100 µl sample volume. The UL51$^{217\text{-}237}$ (RVSVPRPTASPTAPRPGPSRA) peptide was labelled with an N-terminal FITC fluorophore (fluorescein isothiocyanate) linked via an aminohexanoyl group (NH_2-CH_2-CH_2-CH_2-CH_2-CH_2-COOH), purchased from Genscript. For binding experiments, fluorescent UL51$^{217\text{-}237}$ peptide at a final concentration of 10 nM was titrated against triplicate 2-fold serial dilutions of DrCPAP$^{943\text{-}1121}$ prepared with a maximum concentration of 1 mM. GST protein was used as a negative control and was prepared in the same way. Protein and peptide dilutions were made in FP sample buffer (20 mM Tris pH 8.0, 200 mM NaCl, 3 mM DTT). Black polystyrene low bind half-area 96 well plates (Corning) were

used for measurement. Binding constants (k_d) were calculated by fitting the data to a one-site equilibrium binding model in GraphPad Prism version 6.0.

2.4 X-ray crystallography

2.4.1 Sparse-matrix screening

Commercial sparse-matrix crystallisation screens were pre-dispensed in 96-well MRC sitting drop plates (SwissSci) (see Table 2-6). For initial screening, 200 nl of protein sample was mixed with 200 nl reservoir solution and equilibrated against a 95 µl reservoir at 20°C, using the sitting drop vapour diffusion technique. The specific sparse-matrix screens and protein concentrations used for each sample are specified in the results chapter text. Drops were dispensed by either an Innovadyne Screenmaker or a TTP Labtech Mosquito nanolitre dispensing robot, as specified in the results chapter text. All plates were stored at 20°C within a Formulatrix imaging robot.

Table 2-6 Commercial sparse-matrix screens

Screen Name	Commercial Screen Name	Manufacturer
CIMR1	Structure Screen I Structure Screen II	Molecular Dimensions
CIMR2	Wizard Screen I Wizard Screen II	Emerald Biosystems
CIMR3	Wizard Screen III Wizard Screen IV	Emerald Biosystems
CIMR4	Cryo I Cryo II	Emerald Biosystems
CIMR5	PEG/Ion Screen PEG/Ion Screen 2	Hampton Research
CIMR6	Index Screen	Hampton Research
CIMR7	PACT premier™ Screen	Molecular Dimensions
CIMR8	JCSG-*plus*™	Molecular Dimensions
CIMR9	$(NH_4)_2SO_4$ Grid Screen PEG 6000 Grid Screen PEG/LiCl Grid Screen MPD Grid Screen	Hampton Research
CIMR10	MemStart™ MemSys™	Molecular Dimensions
CIMR11	Morpheus®	Molecular Dimensions
CIMR12	Stura Screen Macrosol™ Screen	Molecular Dimensions
CIMR13	ProPlex™ Screen	Molecular Dimensions
CIMR15	PEG/Ion Screen diluted 7:3 in H_2O PEG/Ion Screen diluted 1:1 in H_2O	Hampton Research

2.4.2 4-row/column optimisation

4-row/column optimisation screens were prepared in 96-well MRC sitting drop plates (SwissSci). A stock solution of the crystallisation condition of interest was made using commercially available buffer components, then diluted with MQW in 5% increments from 100% to 45 % for a 4-row screen, or diluted with MQW in 7.5% increments from 100% to 47.5% for a 4-column screen. Each reservoir dilution was screened against four different drop ratios: 100 nl protein (P):100 nl reservoir (R), 100P:200R, 200P:100R and 200P:200R. Drops were dispensed by either an Innovadyne Screenmaker or a TTP Labtech Mosquito nanolitre dispensing robot as specified in the results chapter text. All plates were stored at 20°C within a Formulatrix imaging robot.

2.4.3 Additive screening

Additive screens were prepared in 96-well MRC sitting drop plates (SwissSci). A stock solution of the crystallisation condition of interest (i.e. CIMR13 H8 diluted to 85% of the original condition using MQW) was made using commercially available buffer components. Each well contained 80 µl of reservoir solution. The JB Screen Plus™ HTS (C5-507L; Jenna Bioscience) additive screen was used, diluted 1:4 in MQW. A TTP Labtech Mosquito nanolitre dispensing robot was used to dispense 100 nl protein, 200 nl reservoir and 100 nl additive (diluted) on to the crystallisation stage. Plates were stored at 20°C within a Formulatrix imaging robot.

2.4.4 Harvesting CPAP crystals

Crystals were harvested in nylon loops mounted on SPINE pins. To prevent ice formation the crystals were cryoprotected using the reservoir solution supplemented with 25% glycerol. A separate cryoprotectant drop was made and the loop containing the crystal was swept through this before rapid cryo-cooling by plunging into liquid nitrogen. Crystal harvesting was performed by Dr Stephen Graham with assistance from Danielle Owen.

2.4.5 Data collection and structure solution

Diffraction data were recorded for cryo-cooled (100K) crystals at The Diamond Light Source beamline IO4 using a Pilatus 6M-F detector. Data were processed using the xia2 auto processing pipeline [285]. The structure was solved by molecular replacement using Refmac5 to perform ridged-body refinement and generate electron density maps. The structure of DrCPAP (PDB: 4LD1 [286]) with solvent atoms removed was used as a starting model. Data collection and structure solution was performed by Dr Stephen Graham with assistance from Danielle Owen.

2.5 Mammalian cell culture and virus work

2.5.1 Mammalian cells lines

HEK 293T (ATCC), Vero (ATCC), HFF-Tert (immortalised human foreskin fibroblasts) [287] and HaCAT [288] cells were grown in DMEM supplemented with 10% heat-treated foetal bovine serum, 2 mM glutamine, 100 U/ml penicillin and 100 µg/ml streptomycin. HeLa M cells were cultured in RPMI medium with the supplements listed above. Cells were maintained in a humidified incubator at 37°C with 5 % CO_2.

2.5.2 Immunoprecipitation of GFP-tagged bait protein from transfected cells

2.5.2.1 GFP-UL7 and untagged UL51

5×10^6 HEK 293T cells were seeded into 10 cm dishes and co-transfected the following day with pEGFP-C1-UL7 or pEGFP-C1 and pcDNA3.1-UL51 (full-length, 1-207 or 1-170) using Lipofectamine 2000 (Invitrogen) according to the manufacturer's protocol. A total of 10 µg of DNA was used in each transfection: GFP-UL7 and untagged UL51 were transfected in a 1:4 ratio. After 24 h the cells were harvested and lysed in *lysis buffer* (10 mM Tris pH 7.5, 150 mM NaCl, 0.5 mM EDTA, 0.5% NP-40, 1% EDTA-free protease inhibitor cocktail (Sigma)) at 4°C for 40 m. Cell lysates were cleared by spinning at 20,000 ×g for 10 min at 4°C, then normalised based on protein concentrations determined by BCA assay (section 2.2.13). GFP-Trap™ beads (ChromoTek) were equilibrated in *wash buffer* (10 mM Tris pH 7.5, 150 mM NaCl, 0.5 mM EDTA) and re-suspended in lysis buffer, 20 µl of bead slurry was used per experiment. The GFP-Trap™ beads were added and incubated with the lysates for 1 h at 4°C on a shaking platform. Samples were spun at 2,500 ×g at for 2 min at 4°C, after which the supernatant was removed. Beads were washed twice with wash buffer, then mixed with 45µl 2× SDS loading buffer.

2.5.2.2 GFP-UL7 and myc-tagged human CPAP$^{998\text{-}1338}$

5×10^6 HEK 293T cells were seeded into 10 cm dishes and co-transfected with 5 µg pEGFP-C1-UL51 and 5 µg pF5A-CPAP$^{998\text{-}1338}$ using Lipofectamine 2000 (Invitrogen) as per the manufacturer's instructions. After 26 h the cells were harvested and washed three times with cold PBS. The immunoprecipitation was performed as described in section 2.5.2.1.

2.5.2.3 GFP-UL7/UL51 and endogenous pontin-reptin

5.0×10^6 HEK 293T cells were seeded into 10 cm dishes and transfected with pEGFP-C1-UL7, pEGFP-C1-UL51, pEGFP-C1-UL56 or pEGFP-C1, or co-transfected with pEGFP-C1-UL7 and pcDNA3.1-UL51 using Lipofectamine 2000 (Invitrogen). A total of 9 µg of DNA was used in each transfection: GFP-UL7 and untagged UL51 were transfected at a ratio of 1:8. After 20 h the cells were harvested and washed three times with cold PBS. The GFP-Trap™ immunoprecipitation was performed as described

in section 2.5.2.1, using the following buffers: *lysis buffer* (50 mM sodium phosphate pH 7.5, 150 mM NaCl, 0.5 mM EDTA, 0.5% NP-40, 1% EDTA-free protease inhibitor cocktail (Sigma), plus 50 U/ml benzonase (Sigma)); *wash buffer* (50 mM sodium phosphate pH 7.5, 150 mM NaCl, 0.5 mM EDTA).

2.5.3 Generating wild-type and mutant HSV-1 stocks

Wild-type HSV-1 KOS strain was derived from a cloned bacterial artificial chromosome (Dr Colin Crump). The UL7, UL51 deletion viruses (ΔUL7 and ΔUL51) and EYFP (A206K)-UL7 virus were constructed using the bacterial artificial chromosome KOS strain HSV-1 (by Viv Connor) as described in [277]. The UL51$^{P221D+R222D}$ mutant virus was constructed in the same way (by Viv Connor).

2.5.4 Growth curves and plaque assays

For single-step growth curves, HaCaT cells were grown in 24-well plates and infected with wild-type HSV-1, ΔUL51 HSV-1 or the UL51$^{P221D+R22D}$ mutant virus at MOI 5.0. After 1 h of infection, unabsorbed virus was inactivated with an *acid wash* (40 mM citric acid, 135 mM NaCl, 10 mM KCl pH 3.0) for 1 min at room temperature. Cells were then washed three times with PBS and cultured in 0.5 ml medium (section 2.5.1). Cells were harvested at 2, 4, 6, 8, 12 and 24 h.p.i. by freezing at −70°C. Freeze-thawing was repeated twice, the cells were then scraped into the medium and ten-fold serial dilutions in 0.5 ml medium were prepared. To determine the virus titre by plaque assay, 5×10^5 Vero cells were seeded in 6-well dishes and grown to produce a monolayer. The 0.5 ml virus dilutions were added to the monolayer and incubated for 1 h. The wells were then overlaid with medium containing 0.6% carboxymethyl cellulose and 2% v/v foetal bovine serum. After 72 h, cells were fixed with formal saline and then stained with 0.1% toluidine blue solution.

2.5.5 Immunoprecipitation from infected cells

5×10^6 HaCaT cells were infected with either wild-type HSV-1 or ΔUL51 HSV-1 at MOI 5.0 or mock infected in 10 cm dishes. After 16 h (or 7 h for SILAC) the cells were washed three times with ice-cold PBS and lysed in ice-cold *lysis buffer* (10 mM Tris pH 7.5, 150 mM NaCl, 0.5% NP-40, 1% EDTA-free protease inhibitor cocktail (Sigma)), then centrifuged at 15,000 ×g at 4°C to remove the insoluble fraction. Cell lysates were precleared by incubation with 25 µl protein A/G-plus agarose beads (SantaCruz) for 30 min at 4°C. The samples were centrifuged at 2,000 ×g for 2 min, the supernatant was removed and incubated with 3 µg of anti-UL51 antibody (either 3D3 or 2B3) for 2 h at 4°C. 25 µl of protein A/G beads were added and incubated for a further 1 h. The beads were washed three times with ice-cold *wash buffer* (10 mM Tris pH 7.5, 150 mM NaCl, 0.5 mM EDTA), and then boiled in 45 µl of 2× SDS-PAGE loading buffer to elute protein for SDS-PAGE and immunoblotting.

2.5.5.1 Immunoprecipitation of EYFP-UL7 from infected cells

5×10^6 HaCaT cells were infected with either wild-type HSV-1 or ΔUL51 at MOI 5.0, or mock infected in 10 cm dishes. After 16 h, cells were washed with ice-cold PBS and lysed in ice-cold *lysis buffer* (10 mM Tris pH 7.5, 150 mM NaCl, 0.5% NP-40, 1% EDTA-free protease inhibitor cocktail (Sigma)) at 4°C for 40 min. Immunoprecipitation of EYFP-UL7 with GFP-Trap™ beads was performed as described in section 2.5.2.1.

2.5.6 Fluorescence microscopy

Glass cover slips were seeded with HFF-Tert cells in 24-well plates (≈2.5×10^5 cells per well). Cells were infected with HSV-1 expressing C-terminally tagged UL7-mCherry and UL51-EYFP (A206K), or mock infected at MOI 5.0. After 15 h, the cells were washed three times with PBS, fixed with 4% v/v EM-grade formaldehyde (Polysciences) for 20 min, and then permeabilised with 0.1% Triton for 5 min. The fixed slides were blocked for 90 min in *blocking buffer* (10% v/v foetal bovine serum in PBS) at room temperature. Mouse αreptin and αpontin antibodies were diluted in blocking buffer (1:100) and incubated with the fixed slides for 60 min at room temperature. The slides were washed three times in PBS then incubated for 30 min with anti-mouse Alexa-Fluor 633 secondary antibody (diluted 1:200 in blocking buffer). The cover slips were mounted using ProLong Gold anti-fade reagent containing DAPI (ThermoFisher). Images were captured using by Leica SP5 confocal microscope.

2.6 Screening for host-cell interaction partners

2.6.1 Yeast two-hybrid screen

Y2H screens were performed using the Clonetech Mate & Plate™ Library Screen system. Matchmaker™ Gold yeast were transformed with pGBKT7-UL7 and pGBKT7-UL51 plasmids (provided by Dr Colin Crump) according to the manufacturer's instructions. Transformed cells were cultured in 65 ml Trp-drop-out medium at 30°C overnight. The cells were then harvested and mated with 1 ml of human Clonetech Mate & Plate™ Library (Universal Human Normalised) in 2×TY medium + 50 µg/ml kanamycin at 30°C for 24 h on a platform shaking at 40 rpm. Mated cells were cultivated on nutrient selection plates (quadruple drop-out plates, QDO) lacking tryptophan, leucine, histidine and adenine (Formedium agar, Formedium yeast nitrogen base, Kaiser drop-out supplements). Colonies were picked from the QDO plates and streaked onto QDO/X/A plates (QDO medium supplemented with 40 µg/ml X-α-Gal (Clonetech) and 0.125 µg/ml Aureobasidin A (Clonetech)). Positive clones on the QDO/X/A plates appeared blue due to the degradation of the X-α-Gal by yeast galactosidase (MEL1), these were picked and re-streaked on fresh QDO/X/A plates to select for single clones. Blue colonies from the second streak were picked for colony PCR using Taq DNA polymerase (Invitrogen) and the following PCR program: initial denaturation 5 min at 95°C followed by 30 cycles of: i) denaturation for

30 s at 95°C; ii) annealing for 15 s at 67°C; iii) extension for 3.5 min at 72°C. PCR clean-up was performed using EconoSpin™ All-in-One Mini Spin Columns (Epoch) according to the manufacturer's instructions. PCR products were Sanger sequenced (primers Table 2-12, page 54) and BLASTn searches were performed to identify putative interaction partners.

2.6.2 SILAC

2.6.2.1 SILAC cell lines and immunoprecipitation

SILAC experiments were performed with either SILAC-labelled HEK 293T or HaCAT cell lines that were generated and maintained by Susanna Colaco. Cells were grown in DMEM containing stable-isotope labelled forms of arginine and lysine for a minimum of five passages before use. For each cell line, three cell populations were generated: 'Light' grown with unlabelled amino acids in the medium, 'Medium' grown with arginine R6 ($^{13}C_6$) and deuterated lysine K4 (D_4) medium, and 'Heavy' containing arginine R10 ($^{13}C_6$, $^{15}N_4$) and lysine K8 ($^{13}C_6$, $^{15}N_2$) in the medium.

2.6.2.2 SILAC-Immunoprecipitation of GFP-tagged bait protein

The SILAC screen was performed in triplicate, to do this 10 cm dishes were seeded with 5×10^6 SILAC-labelled HEK 293T cells, three dishes of each cell population (i.e. light, medium and heavy) were required (i.e. nine dishes in total). The cells were transfected with 10 µg of either pEGFP-C1-UL7, pEGFP-C1-UL51 or pEGFP-C1 using Lipofectamine 2000 (Invitrogen) as per the manufacturer's instructions. After 26 h, the cells were harvested and washed three times with cold PBS. The GFP-Trap™ immunoprecipitation was performed as described in section 2.5.2.1 using low-bind Eppendorf tubes (Costar).

2.6.2.3 SILAC-Immunoprecipitation of UL51 from infected cells

The SILAC screen was performed in triplicate, to do this 10 cm dishes were seeded with 5×10^6 SILAC-labelled HEK 293T cells, three dishes of each cell population (i.e. light, medium and heavy) were required (i.e. nine dishes in total). The cells were infected with wild-type HSV-1, ΔUL51 HSV-1 or mock-infected at MOI 5.0. After 16 h (SILAC screen 2) or 7 h (SILAC screen 3), the cells were harvested and washed three times with cold PBS. The immunoprecipitation was performed as described in section 2.5.5 using the αUL51 2B3 antibody. The virus stocks were generated using cells grown in 'light' medium.

2.6.2.4 Mass spectrometry measurements

SILAC-immunoprecipitation samples were analysed by LC-MS/MS on an Orbitrap Velos instrument as a service at The University of Bristol Proteomics Facility.

2.6.2.5 SILAC data processing using MaxQuant

Raw mass spectrometry data were processed using MaxQuant (v. 1.5.6.0) and searched against the Uniprot Human database (UP000005640, dated 9th March, 2017) and a custom file containing the HSV-1 KOS strain (JQ673480.1) protein sequences. Trypsin/P digestion, standard modifications (oxidation, N-terminal acetylation) were set as group-specific parameters in MaxQuant and SILAC quantification was performed using light (Arg0, Lys0), medium (Arg6, Lys6) and heavy (Arg10, Lys8) labels. Re-quantification, razor protein false discovery rate, and second peptide options were enabled. Minimum peptides was set to 1, minimum peptide length was set to 7, and the maximum false discovery rate was set to 0.1. The normalised SILAC ratios generated by MaxQuant were analysed in Perseus (v. 1.5.6.0). Common contaminant e.g. keratin (specified in the MaxQuant contaminants file) were removed, as were proteins identified by site or against the reverse database. The SILAC ratios were grouped by biological repeat and only proteins detected in two of the three repeats were considered for further analysis. A two-sided, one-sample t-test against a $\log_2$ ratio of 0 (no change in abundance) was performed with a threshold p-value of 0.05 to identify significantly enriched proteins. Proteins with a greater than two-fold increase in abundance (i.e. > $\log_2$ fold-change = 1) in the WT/mock and WT/ΔUL51 samples were considered genuine hits.

2.6.3 Primer and plasmid tables

Table 2-7 Expression plasmids

Name	Description	Antibiotic selection	Sequencing primers
pOPTH	N-terminal non-cleavable His_6 tag	Amp	T7 fwd
			T7 terminator
pOPTnH	C-terminal non-cleavable His_6 tag	Amp	T7 fwd
			T7 terminator
pOPT3G	N-terminal 3C-cleavable GST tag	Amp	Pgex5
			T7 terminator
pOPTn3G	C-terminal 3C-cleavable site followed by GST	Amp	T7 fwd
			GST rev
pOPC	Polycistronic expression vector [282]	Amp	T7 fwd
			Popc rev
PF3A WG (BYDV)	Wheat-germ SP6 cell-free expression vector (SgfI/PmeI). Myc tag encoded by primer.	Amp	SP6
			T7 terminator
PF3A Myc WG (BYDV)	Wheat-germ SP6 cell-free vector with N-terminal Myc tag (HindIII/PmeI)	Amp	SP6
			T7 terminator
PFf5A CMV-neo Flexi-vector	Mammalian expression vector (with neomycin cassette for making G-418 stables). Carries lethal barnase gene.	Amp	Pf5A fwd
			T7 terminator
pEGFP-C1	N-terminal EGFP tag for mammalian expression	Kan	EGFP-C
			SV40pA-R
pGBKT7	Yeast 2-hybrid bait vector	Kan	Pgbkt7 fwd
			Pgbkt7 rev
pGADT7	Yeast 2-hybrid prey vector	Amp	Pgadt7 fwd
			Pgadt7 rev
pcDNA3.1	Mammalian expression, no tag	Amp	CMV fwd
			BGH rev

Table 2-8 Expression constructs

Construct name	Description
Expression in yeast:	
UL7_GBKT7	GAL4BD.UL7 (full-length)
UL7_pGADT7	GAL4AD.UL7 (full-length)
UL51_GBKT7	GAL4BD.UL51 (full-length)
UL51_pGADT7	GAL4AD. UL51 (full-length)
Expression in E. coli:	
UL7_pOPTH	His6 tag.UL7 (full-length)
UL7_pOPTnH	UL7.His6 tag (full-length)
UL7syn_pOPTH	His6 tag.UL7 synthetic gene (full-length)
UL7syn_pOPTnH	UL7 synthetic gene (full-length).His6 tag
UL7syn_pOPT3G	GST.3C protease cleavage site.UL7 synthetic gene (full-length)
UL7syn_pOPT3nG	UL7 synthetic gene (full-length).3C protease cleavage site.GST
UL51_pOPTH	His6 tag.UL51 (full-length)
UL51 _pOPTnH	UL51.His6 tag (full-length)
UL51_1-170_ pOPTH	His6 tag.UL51 (aa. 1-170)
UL51_1-170_ pOPTnH	UL51 (aa. 1-170).His6 tag
UL51_29-170_ pOPTH	His6 tag.UL51 (aa. 29-170)

UL51_C9S_pOPTH	His6 tag.UL51 (full-length; C9S mutant)
UL51_170_C9S_pOPTH	His6 tag.UL51 (aa. 1-170; C9S mutant)
UL51_pOPT3G	GST tag.3C protease cleavage site.UL51 (full-length)
UL103_pOPTH	His6 tag.UL103 (full-length)
UL103_pOPTnH	UL103 (full-length).His6 tag
BSRF1_pOPTH	His6 tag.BSRF1 (full-length)
BSRF1_pOPTnH	BSRF1 (full-length).His6 tag
BSRF1_1-174_pOPTH	His6 tag.BSRF1 (aa. 1-174)
BBRF2_pOPTH	His6 tag.BBRF2 (full-length)
BBRF2_pOPTnH	BBRF2 (full-length).His6 tag
ORF42M_pOPTH	His6 tag.ORF42 (MHV) (full-length)
ORF42M_pOPTnH	ORF42 (MHV) (full-length).His6 tag
ORF42M_pOPT3G	GST tag.3C protease cleavage site.ORF42 (MHV) (full-length)
ORF55M_pOPTH	His6 tag.ORF55 (MHV) (full-length)
ORF55M _pOPTnH	ORF55 (MHV) (full-length).His6 tag
ORF55M _1-163_pOPTH	His6 tag.ORF55 (MHV) (aa. 1-163)
ORF55M _ C3S+C4S _pOPTH	His6 tag.ORF55 (MHV) (full-length; C3S+C4S mutant)
ORF55M_1-163_ C3S+C4S_pOPTH	His6 tag.ORF55 (MHV) (aa. 1-163; C3S+C4S mutant)
ORF55M _22-154_ pOPTH	His6 tag.ORF55 (MHV) (aa. 22-154)
ORF55M_22-163_ pOPTH	His6 tag.ORF55 (MHV) (aa. 22-163)
ORF55M_pOPT3G	GST tag.3C protease cleavage site.ORF55 (MHV) (full-length)
ORF55K_pOPTH	His6 tag.ORF55 (KSHV) (full-length)
ORF55K_pOPTnH	ORF55 (KSHV) (full-length).His6 tag
ORF55K_170_pOPTH	His6 tag.ORF55 (KSHV) (aa. 1-170)
ORF55K_170_pOPTnH	ORF55 (KSHV) (aa. 1-170).His6 tag
ORF42K_pOPTH	His6 tag.ORF42 (KSHV) (full-length)
ORF42K_pOPTnH	ORF42 (KSHV) (full-length).His6 tag
HsCPAP_1152-1338_ pOPTH	His6 tag.HsCPAP (aa. 1152-1338)
HsCPAP_1152-1338_ pOPTH	His6 tag.HsCPAP (aa. 1152-1338)
HsCPAP_1152-1338_pOPT3G	GST tag.3C protease cleavage site.HsCPAP (aa. 1152-1338)
DrCPAP_944-1121_pOPT3G	GST tag.3C protease cleavage site.DrCPAP (aa. 944-1121)
UL51 1-170 + UL7syn_pOPC	Untagged UL51 (aa. 1-170; C9S mutant) + UL7 synthetic gene.3C protease cleavage site.GST tag
UL51 + UL7syn_pOPC	His6 tag.UL51 (full-length; C9S mutant) + UL7 synthetic gene.3C protease cleavage site.GST tag
ORF55M 1-163 + ORF42M_pOPC	His6 tag.ORF55 (MHV) (aa. 1-163; C3S+C4S) + ORF42 (MHV).3C protease cleavage site.GST tag
UL51 8-142 + UL7_pOPC	Untagged UL51 (aa. 8-142; C9S mutant) + UL7 (full-length).3C protease cleavage site.GST tag
Expression in mammalian cells:	
UL7_pEGFP-C1	EGFP tag.UL7 (full-length)
UL51_pEGFP-C1	EGFP tag.UL51 (full-length)
UL51 FL_pCDNA3.1	Untagged UL51 (full-length)
UL51 1-207_pCDNA3.1	Untagged UL51 (aa. 1-207)
UL51 1-170_pCDNA3.1	Untagged UL51 (aa. 1-170)
CPAP_988-1338_pF5A	Myc tag.HsCPAP (aa. 988-1338)
NIPSNAP4_ pF5A	Myc tag.NIPSNAP4 (full-length)
Peroxiredoxin3_ pF5A	Myc tag.Peroxiredoxin3 (full-length)
Wheat germ cell-free expression:	
UL51_pF3A	Myc tag.UL51 (full-length)
UL51_1-170_pF3A	Myc tag.UL51 (aa. 1-170)

UL51_1-220_pF3A	Myc tag.UL51 (aa. 1-220)
UL51_1-227_pF3A	Myc tag.UL51 (aa. 1-227)
UL51_1-236_pF3A	Myc tag.UL51 (aa. 1-236)
UL51 P221D+R222D_pF3A	Myc tag.UL51 (full-length; P221D+R222D mutant)
UL51 A225E+P227D_pF3A	Myc tag.UL51 (full-length; A225E+P227D mutant)
UL51 176-244_pF3A	Myc tag.UL51 (176-244; wild-type)
STMN2_pF3A	Myc tag.Stathmin2 (full-length)
HsCPAP_pF3A	Myc tag.HsCPAP (aa. 988-1338)
PXRDX3_pF3A	Myc tag.PXRDX3 (full-length)
NIPSNAP1_pF3A	Myc tag.NIPSNAP1 (full-length)
NIPSNAP3A/4_pF3A	Myc tag.NIPSNAP3A/4 (full-length)
Pontin_pF3A	Myc tag.Pontin/RUVBL1 (full-length)
Reptin_pF3A	Myc tag.Reptin/RUVBL2 (full-length)

Table 2-9 Primers used to clone into pOPTH, pOPTnH, pOPT3G and pOPT3nG vectors

Name	Sequence (5'-3'; with restriction site underlined)	Enzyme
pOPTH _UL7syn_fwd	GGAAGTCATATGGCAGCAGCAACCGCAGATG	NdeI
pOPTnH_UL7syn_rev	GGAAGTGGATCCGCAAAACTGATAAAACAGACTG	BamHI
pOPTH _UL51_fwd	GGAAGTCATATGGCTTCTCTTCTCGGGGC	NdeI
pOPTH _UL51_rev	GGAAGTGGATCCTTATTGACCCAAAACACACGG	BamHI
pOPTnH_UL51_rev	GGAAGTGGATCCTTGACCCAAAACACACGG	BamHI
UL51_C9S_8-142_fwd	GGAAGTCATATGATAAGTGGCTGGGGAGC	NdeI
UL51_C9S_8-142_rev	GGAAGTGGATCCTCACCGAATAGCCTGGG	BamHI
pOPTH _BBRF2_fwd	GGAAGTCATATGGCATCCGGCAAGCAC	NdeI
pOPTH _BBRF2_rev	GGAAGTGGATCCTCAGGGAATTATTTTTGAGACCG	BamHI
pOPTnH_BBRF2_rev	GGAAGTGGATCCGGGAATTATTTTTGAGACCG	BamHI
pOPTH _BSRF1_fwd	GGAAGTCATATGGCCTTCTATCTCCCAG	NdeI
pOPTH _BSRF1_rev	GGAAGTGGATCCTCACGTTAACGCGAGCTCCG	BamHI
pOPTnH_BSRF1_rev	GGAAGTGGATCCCGTTAACGCGAGCTCCGTG	BamHI
pOPTH _ORF55M_fwd	GGAAGTCATATGAATTGCTGTGGTATCTGGC	NdeI
pOPTH _ORF55M_rev	GGAAGTGGATCCTCAATAAACAGCATTTGAAAGTTGTG	BamHI
pOPTnH_ORF55M_rev	GGAAGTGGATCCATAAACAGCATTTGAAAGTTGTGTG	BamHI
pOPTH _ORF42M_fwd	GGAAGTCATATGATCTCTTCAAACATTAGAGAAGC	NdeI
pOPTH _ORF42M_rev	GGAAGTGGATCCTCATAAAATAATGTTGTCTATGGC	BamHI
pOPTnH_ORF42M_rev	GGAAGTGGATCCTAAAATAATGTTGTCTATGGCCTC	BamHI
pOPTH _UL71_fwd	GGAAGTCATATGCAGCTAGCCCAGCG	NdeI
pOPTH _UL71_rev	GGAAGTGGATCCTCACGCGGAGGACAGCAAG	BamHI
pOPTnH_UL71_rev	GGAAGTGGATCCCGCGGAGGACAGCAAG	BamHI
pOPTH _UL103_fwd	GGAAGTCATATGGAGGCCCTGATGATC	NdeI
pOPTH _UL103_rev	GGAAGTGGATCCTCACTCTTCCTCTCCTCGTTC	BamHI
pOPTnH_UL103_rev	GGAAGTGGATCCCTCTTCCTCTCCTCGTTCCCAG	BamHI
pOPTH _ORF55K_fwd	GGAAGTCATATGTCGTCTCCATGGTACACCTG	NdeI
pOPTH _ORF55K_rev	GGAAGTGGATCCTCATGTCGAACCTATCGCGCTTTC	BamHI
pOPTnH_ORF55K_rev	GGAAGTGGATCCTGTCGAACCTATCGCGCTTTC	BamHI
pOPTH _ORF42K_fwd	GGAAGTCATATGTCCCTGGAAAGGGCCCTG	NdeI
pOPTH _ORF42K_rev	GGAAGTGGATCCTTATTTTGAAAAAAGGGAAACAATG	BamHI
pOPTnH_ORF42K_rev	GGAAGTGGATCCTTTTGAAAAAAGGGAAACAATGG	BamHI
pOPTH _BSRF1_174_rev	GGAAGTGGATCCTCACGATGAGACAACGGCCGAG	BamHI
pOPTnH_BSRF1_174_rev	GGAAGTGGATCCCGATGAGACAACGGCCGAG	BamHI
pOPTH _ORF55_163_rev	GGAAGTGGATCCTCAGCTAGATACAATACCAGCAATGTCAG	BamHI
pOPTnH_ORF55_163_rev	GGAAGTGGATCCGCTAGATACAATACCAGCAATGTCAG	BamHI

pOPTH _ORF55K_170_rev	GGAAGTGGATCCTCACAAGGAGTGGCTGATCTCAG	BamHI
pOPTnH_ORF55K_170_rev	GGAAGTGGATCCCAAGGAGTGGCTGATCTCAG	BamHI
pOPTH _UL71_173_rev	GGAAGTGGATCCTCACCGGCCTCGAGCATGTAC	BamHI
pOPTnH_UL71_173_rev	GGAAGTGGATCCCCGGCCTCGAGCATGTAC	BamHI
pOPTH _UL51_1-170_rev	GGAAGTGGATCCTCACCCGGCAACCCCGAAG	BamHI
pOPTnH_UL51_1-170_rev	GGAAGTGGATCCCCCGGCAACCCCGAAG	BamHI
pOPTH _CPAP_988_fw	GGAAGTCATATGAAAAAGGAACGTGAAGAAATACAGAC	NdeI
pOPTH _CPAP_1152_fw	GGAAGTCATATGGAAATCAGTCATCCTGATGG	NdeI
pOPTH _CPAP_1338_rev	GGAAGTGGATCCTCACAGCTCCGTGTCCATTAG	BamHI
pOPTnH_CPAP_1338_rev	GGAAGTGGATCCCAGCTCCGTGTCCATTAG	BamHI

Table 2-10 Primers for cloning into pF3A WG and pF3A myc WG vectors

Name	Sequence (5'-3'; with restriction site underlined)	enzyme
pF3A_CENPJ_990_fwd	GGAAGCGATCGCCATGGAGCAAAAGCTCATTTCTGAAGAGGACTT GAATAAAAAGGAACGTGAAGAAATACAGAC	SgfI
pF3A_CENPJ_1338_rev	GGAAGTTTAAACTCACAGCTCCGTGTCCATTAGC	PmeI
pF3A_ANEX7_189_fwd	GGAAGCGATCGCCATGGAGCAAAAGCTCATTTCTGAAGAGGACTT GAATGATGCAGAAATTCTTCGTAAGGCAATG	SgfI
pF3A_ANEX7_266_fwd	GGAAGCGATCGCCATGGAGCAAAAGCTCATTTCTGAAGAGGACTT GAATTTACGGAAAGCAATGCAGGGAG	SgfI
pF3A_ANEX7_488_rev	GGAAGTTTAAACTCACTGGCCCACAATAGCCAGAAG	PmeI
pF3Amyc_NIPS1_fwd	GGAAGCGATCGCCATGGAGCAAAAGCTCATTTCTGAAGAGGACTTGAATATGGCTCCGCGGCTGTG-	sgfI
pF3Amyc_NIPS1_rev	GGAAGTTTAAACTCACTGCAGAGGCGAGATC	PmeI
pF3Amyc_NIPS2_fwd	GGAAGAAGCTTCCATGGCGGCGCGAGTGC	HindIII
pF3Amyc_NIPS2_rev	GGAAGTTTAAACTCACTGGAGGGGCGAGGTC	PmeI
pF3Amyc_NIPS4_fwd	GGAAGAAGCTTCCATGCTCGTCCTCAGAAGCGC	HindIII
pF3Amyc_NIPS4_rev	GGAAGTTTAAACTCACTATTTCAGTGGTGAAAACGATG	PmeI
pF3Amyc_PXRD3_fwd	GGAAGAAGCTTCCATGGCGGCTGCTGTAGGAC	HindIII
pF3Amyc_PXRD3_rev	GGAAGTTTAAACTCACTGATTTACCTTCTGAAAGTACTC	PmeI
pF3Amyc_UL51_fwd	GGAAGAAGCTTCCATGGCTTCTCTTCTCGGGGC	HindIII
pF3Amyc_UL51_rev	GGAAGTTTAAACTCATTGACCCAAAACACACGG	PmeI
pF3Amyc_UL51 176_fwd	GGAAGAAGCTTCCGGGCTTGGGGTGACCG	HindIII
pF3Amyc_STMN2_fwd	GGAAGAAGCTTCCATGGCTAAAACAGCAATGGC-	HindIII
pF3Amyc_STMN2_29_fwd	GGAAGAAGCTTCCCCGGAACCTCGCAACATC	HindIII
pF3Amyc_STMN2_rev	GGAAGTTTAAACTCAGCCAGACAGTTCAAC	PmeI

Table 2-11 Primer used for site-directed mutagenesis

Name	Sequence (5'-3')	
pOPTH _UL51_C9S	fwd:	CTCGGGGCTATAAGTGGCTGGGGAG
	rev:	CTCCCCAGCCACTTATAGCCCCGAG
pOPTH _ORF55M_CC3&4SS	fwd:	CACCATCACCATATGAATTCCAGTGGTATCTGGCCATTTG
	rev:	CAAATGGCCAGATACCACTGGAATTCATATGGTGATGGTG
UL51 1-236/STOP	fwd:	GGCCCATCTCGAGCATGACCGTGTGTTTTGGG
	rev:	CCCAAAACACACGGTCATGCTCGAGATGGGCC
UL51 1-227/STOP	fwd:	CTACAGCCTCCCCATGAGCACCTCGCCCTG
	rev:	CAGGGCGAGGTGCTCATGGGGAGGCTGTAG
UL51 1-220/STOP	fwd:	GCGTGTCCGTTTGAAGACCTACAGCCTCCCCAAC
	rev:	GTTGGGGAGGCTGTAGGTCTTCAAACGGACACGC

UL51 1-170/STOP	fwd:	CGGGGTTGCCGGGTGAACCCGCTCG
	rev:	CGAGCGGGTTCACCCGGCAACCCCG
ORF55 1-154/STOP	fwd:	GACGGCCGCATGGGCCTGAGACATTGCTGGTATTG
	rev:	CAATACCAGCAATGTCTCAGGCCCATGCGGCCGTC
pOPTH_UL51_1-28del	fwd:	CACCATTCGGAGGCGGAGCCGCGGCTGCAGGAG
	rev:	CGCCTCCGAATGGTGATGGTGATGATGAGCCATATTTATATCTCCTTC
pOPTH_ORF55 1-21del	fwd:	CACCATGTAGAAACAGATGAGAGAATGGAGATGGAGATCAG
	rev:	CTGTTTCTACATGGTGATGGTGATGATGAGCCATATTTATATC
pOPC_UL51_-His_6 tag	fwd:	GAGATATAAATATGGCTTCTCTTCTCGGGGCTATAAGTG
	rev:	CACTTATAGCCCCGAGAAGAGAAGCCATATTTATATCTC
UL7 E269A_E270A	fwd:	GCTGGGCGTCGGCAGCAGTGCGCGCGCCTCTG
	rev:	CAGAGGCGCGCGCACTGCTGCCGACGCCCAGC
UL51 E16A_E17A	fwd:	CTGGGGAGCGCGCCCCGCAGCACAATATGAGATGATCCGC
	rev:	GCGGATCATCTCATATTGTGCTGCGGGGCGCGCTCCCCAG
UL51 P221D_R222D	fwd:	GTCCCCGCGTGTCCGTTGATGATCCTACAGCCTCCCCAAC
	rev:	GTTGGGGAGGCTGTAGGATCATCAACGGACACGCGGGGAC
UL51 A224E_ P227D	fwd:	GTTCCCAGACCTACAGAATCCGACACCGCACCTCGC
	rev:	GCGAGGTGCGGTGTCGGATTCTGTAGGTCTGGGAAC
UL51 P230D-R231D	fwd:	CAGCCTCCCCAACCGCAGATGATCCTGGCCCATCTC
	rev:	GAGATGGGCCAGGATCATCTGCGGTTGGGGAGGCTG

Table 2-12 Sequencing primers

Name	**Sequence (5'-3')**
T7 fwd	TAATACGACTCACTATAGGG
T7 terminator	TATTGCTCAGCGGTGGCAGCAGC
pOPC rev	GCCCTCGAGACGCGT
pGEX5	CGTATTGAAGCTATCCCACAAATTGATAAG
GST rev	GAAGTCGAGTGGGTTGCACAAG
SP6	ATTTAGGTGACACTATA
pF5A fwd	GTGTCCACTCCCAGTTCA
pGBKT7 fwd	AAGACAGTTGACTGTATCGCCG
pGBKT7 rev	AAATCATAAGAAATTCGCCCGG
pGADT7 fwd	GATGAAGATACCCCACCAAACC
pGADT7 rev	TGGCCAAGATTGAAACTTAGAGG
pGADT7 fwd long	CGATGATGAAGATACCCCACCAAACC
pGADT7 rev long	AGAGGTTACATGGCCAAGATTGAAACTTAGAGG
CMV fwd	CAACGGGACTTTCCAAAATG
BGH reverse	TAGAAGGCACAGTCGAGG

3 Characterisation of the UL7-UL51 complex

3.1 Introduction

The aim of this study is to elucidate the molecular function of the UL7 and UL51 proteins during HSV-1 infection, which may also be applicable to their homologues from some or all other herpesviruses. As mentioned in the introduction, it was hypothesised that UL7 and UL51 could function as a complex during infection and that the complex may contribute to virus assembly and egress. This chapter describes attempts to characterise the UL7-UL51 interaction, the first section presents results from bioinformatic investigations performed on the UL7 and UL51 proteins and their homologues from viruses belonging to the other *Herpesviridae* subfamilies: VZV (α), HCMV (β), EBV(γ), KSHV (γ) and murid herpesvirus MHV (γ). The purpose of the bioinformatics was to gain a general understanding of the proteins and to identify conserved protein domains/regions that may aid the design of protein truncations for purification. The subsequent sections detail the efforts to purify recombinant UL7 and UL51 protein from *E.coli* for the generation of monoclonal antibodies, thereby enabling the study of the UL7 and UL51 proteins in the context of infection. Purified UL7 and UL51 protein samples (full-length and truncated) were also generated for use in pull-down experiments to investigate whether the UL7-UL51 interaction is direct and to map the UL7-binding region in UL51. At the same time, the proteins were purified with a view to using them for crystallisation experiments. While UL7 and UL51 from HSV-1 are the focus of this study, attempts were also made to purify their homologues from viruses belonging to other *Herpesviridae* subfamilies: HCMV, EBV, KSHV and MHV, to determine if the interaction is conserved between homologues and across the herpesvirus subfamilies. It was hoped that sufficient quantities of pure protein would be generated for crystallisation trials. Attempting to purify the homologues maximises the chance of obtaining sufficient quantities of soluble protein for X-ray crystallography.

3.2 Bioinformatic analysis of UL7 and UL51 proteins and their homologues

3.2.1 Sequence alignment

The primary sequences of the UL7 and UL51 proteins were compared with their human herpesvirus homologues: HSV-1, HSV-2, VZV, HCMV, EBV, KSHV, and homologues from murid herpesvirus MHV-68 (Table 3-1), to assess the extent of sequence conservation. Analysis of the sequence identity between UL7 proteins from HSV-1 and HSV-2 shows reasonable conservation at 79%, however, this drops to 29-32% when compared with the VZV homologue despite belonging to the same subfamily (Figure 3.1). There is low sequence identity between UL7 from HSV-1/2 and the beta and gamma herpesvirus homologues, at 16-19%. This pattern is replicated across the UL51

homologues, there is 76% sequence identity between the HSV-1 and HSV-2 proteins and 36% with VZV (Figure 3.2). Sequence identity between HSV-1 UL51 and the gamma herpesvirus homologues is 16-17%, while UL71 the HCMV homologue has only 12% sequence identity with the HSV-1 protein.

Table 3-1 Properties of the UL7 and UL51 proteins and their homologues
Table containing the length, predicted molecular mass and theoretical pI of UL7, UL51 and a selection of their homologues. GenBank accession numbers for the respective viral genomes are listed. *Herpesviridae* subfamily (α, β or γ) is shown in brackets.

Virus	Accession	Protein	No. aa's	Mass (kDa)	pI	Protein	No. aa's	Mass (kDa)	pI
HSV-1 (α)	JQ673480	UL7	296	33.0	7.01	UL51	244	25.5	5.87
HSV-2 (α)	NC_001798	UL7	296	33.0	8.29	UL51	244	25.7	5.88
VZV (α)	NC_001348	ORF53	331	37.4	8.36	ORF7	259	28.2	5.91
HCMV (β)	GU937742	UL103	249	28.6	6.26	UL71	361	29.9	4.99
EBV (γ)	V01555	BBRF2	278	31.2	8.82	BSRF1	218	23.8	4.67
KSHV (γ)	GQ994935	ORF42	278	31.2	6.7	ORF55	227	24.6	5.11
MHV (γ)	NC_001826	ORF42	253	28.6	7.66	ORF55	190	20.9	5.05

Figure 3.1 Amino acid sequence alignment of UL7 with homologues
Amino acid sequences of UL7 from HSV-1/2 and the homologues from VZV, HCMV, EBV, KSHV, and MHV were aligned using the M-Coffee server [289,290]. The images were generated in JalView [291]. Residues are coloured according to BLOSUM62 score: if a residue matches the consensus sequence at that position it is coloured dark blue, if it does not match the consensus residue but the two residues have a positive BLOSUM62 score it is coloured a lighter blue.

Figure 3.2 Amino acid sequence alignment of UL51 and homologues
Amino acid sequences of UL51 from HSV-1/2 and the homologues from VZV, HCMV, EBV, KSHV and MHV were aligned using the M-Coffee server [289,290]. The images were generated in JalView [291]. Residues are coloured according to BLOSUM62 score: if a residue matches the consensus sequence at that position it is coloured dark blue, if it does not match the consensus residue but the two residues have a positive BLOSUM62 score it is coloured a lighter blue. The boxed region of UL71 (aa. 34-55) contains a leucine zipper motif that is not conserved in the homologues. The boxed region of BSRF1, KSHV ORF55 and MHV ORF55 was matched to the small polypeptide Brk1/HSPC3000 by HHPred.

3.2.2 Secondary structure and disorder prediction

Protein secondary structure and disorder prediction were performed using NetSurfP and RONN [292,293]. NetSurfP predicts the relative surface accessibility of residues using artificial neural networks that have been trained on a set of experimentally solved protein structures. Each residue is assigned a value that estimates the probability of said residue being involved in the formation of a given secondary structure element. RONN (Regional Order Neural Network) predicts intrinsically disordered regions by aligning the query protein sequence with a series of sequences of known folding state i.e. ordered, disordered or both, the alignment score is then used to predict the probability that a given residue is in an ordered or disorder region of the protein. Figure 3.3 and Figure 3.4 show the

NetSurfP and RONN output for UL7, BBRF2, UL103, UL51, BSRF1 and UL71, appendix 2 (page 197) contains the output for the VZV, KSHV and MHV homologues. The UL7 proteins are predicted to be alpha-beta proteins with segregated alpha and beta regions, and to be largely folded. The UL51 proteins possess a conserved alpha-helical core domain (Pfam: herpes-U44 domain, residues 8-165 of UL51), which is flanked by poorly conserved, disordered regions at the N- and C-termini. HSV-1 UL51 is proline-rich, as are the homologues, with proline residues accounting for 10.2% of the protein (the median percentage of proline residues per human protein is 5.6% [294]). Proline is an anomalous amino acid with a restricted peptide bond that confers unique properties to protein structure and function [295,296]. Proline residues account for 24% of the amino acid residues in the UL51 C terminus (aa. 171-244), which explains why this region is predicted to be disordered, compared to the N-terminal region (aa. 1-170) where proline accounts for 4.7% of the residues (Figure 3.6). Disordered regions within proteins are often involved in protein-protein interactions and become structured upon binding with their partner [297,298]. Such conformational plasticity can offer advantages over folded domains by potentially enabling the protein to recognise many different partners in multiple cellular pathways [297]. A consecutive tri-proline sequence can fold into a right or left-handed polyproline helix (PP+N/G/A/Q/V/D/H/K can also form a left-handed helix), which will induce sharp turns in local geometry [294]. These motifs have be shown to be important in protein-protein interactions that mediate signal transduction, and all of the UL51 homologues, except ORF55 from MHV, contain the potential to form one or more polyproline helices in their C-terminal region. While these proteins could form polyproline helices, it is not clear whether they are conserved functional motifs. The disordered C terminus of HCMV UL71 (β) is substantially longer than the alpha and gamma homologues, and may represent a specific adaptation of this protein in the β-subfamily (Figure 3.2). A leucine zipper has been identified within residues 34-55 of UL71 (boxed in Figure 3.2), which has been linked with protein dimerisation, however, this motif is not conserved in the homologues [299].

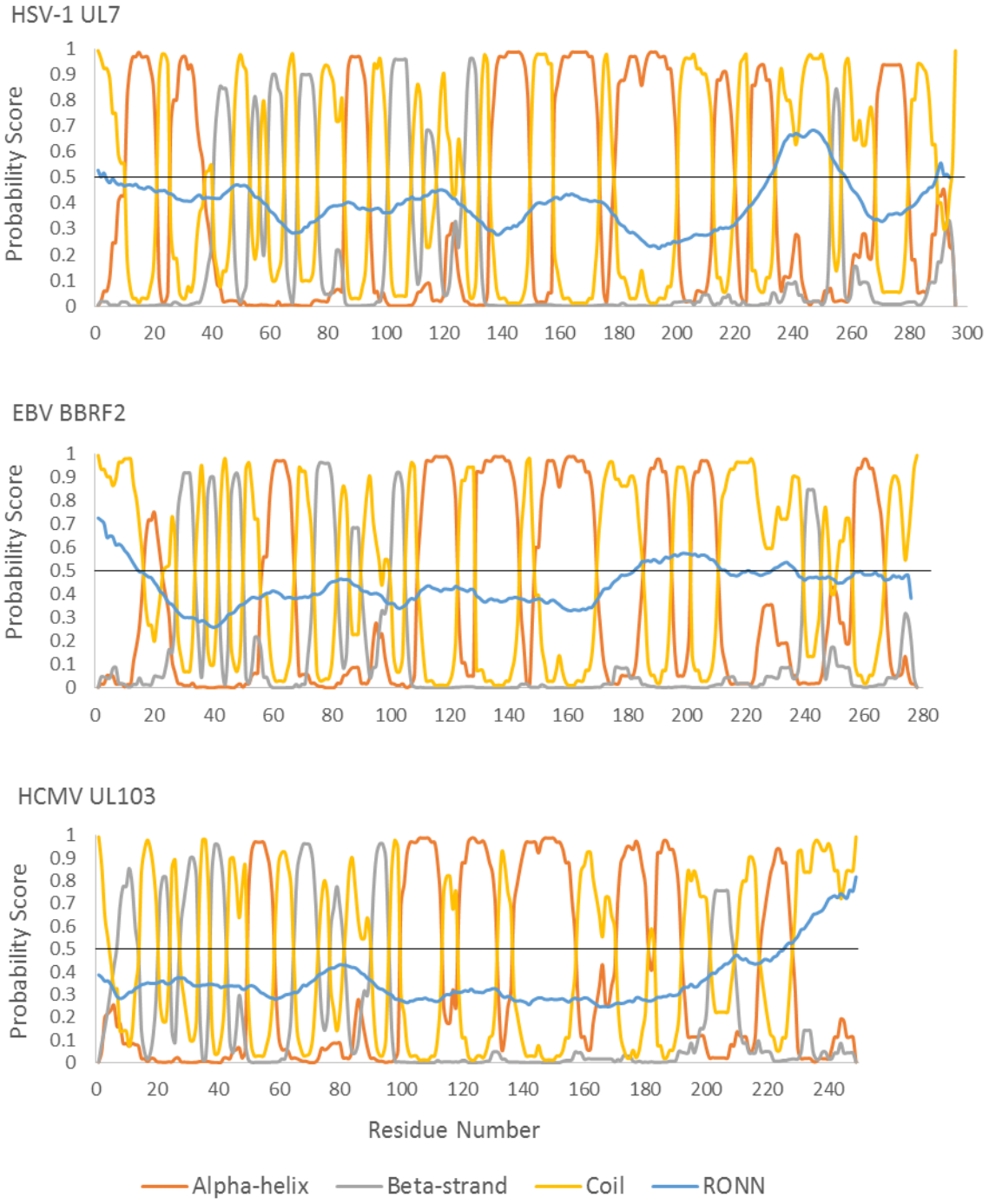

Figure 3.3 UL7 secondary structure and disorder prediction by NetSurfP and RONN
The predicted secondary structure and disorder profiles for UL7 (α), BBRF2 (γ) and UL103 (β) are shown. A RONN probability score (blue line) greater than 0.5 is classed as disordered. The proteins are predicted to have alpha-helix and beta-sheet secondary structure elements and are mostly folded based on the RONN disorder prediction profile. NetSurfP and RONN predictions for the homologues from VZV, MHV and KSHV, suggest that they too share similar secondary structure and disorder profiles, shown in Appendix 2, page 197.

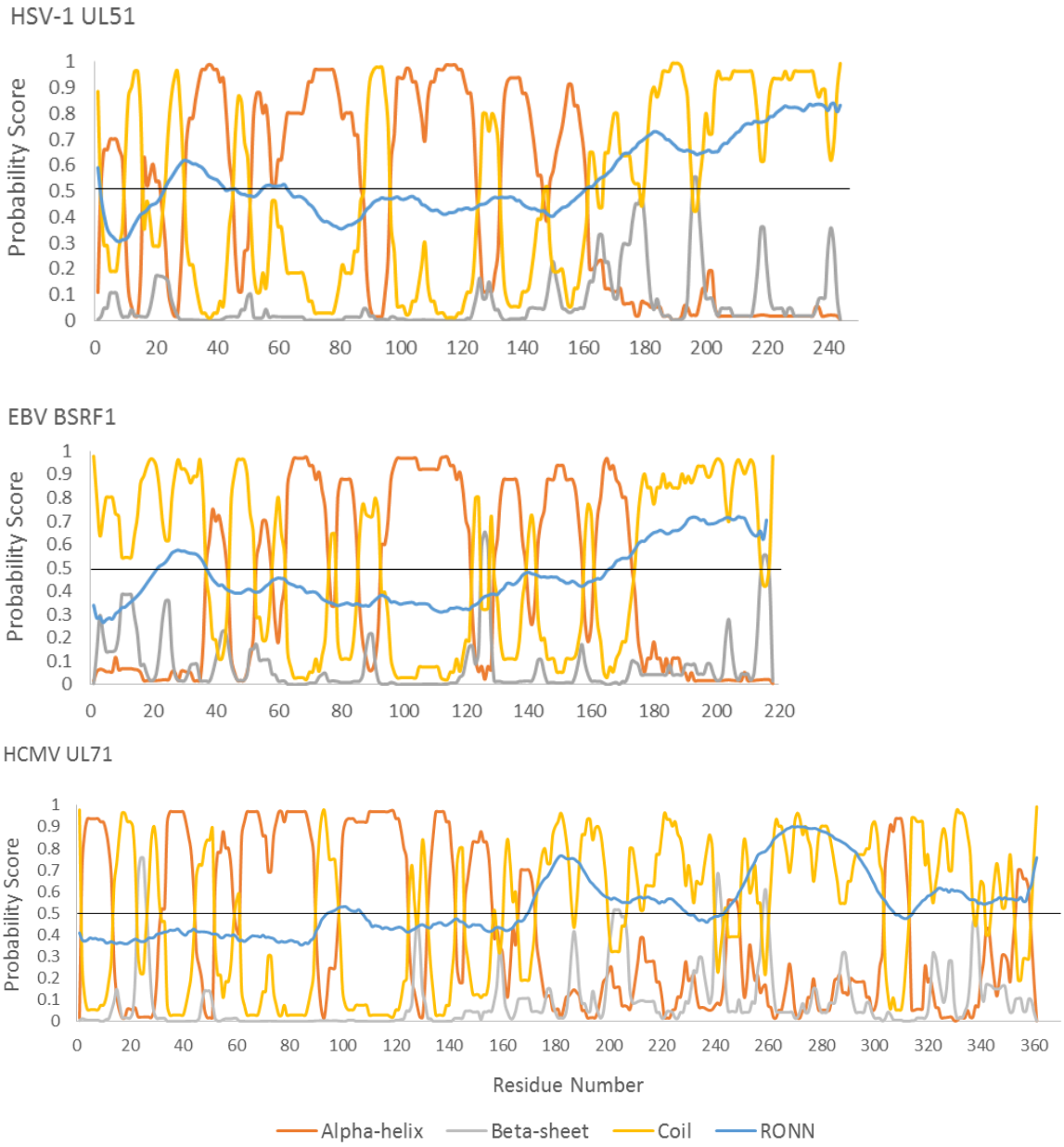

Figure 3.4 UL51 secondary structure and disorder prediction by NetSurfP and RONN
The predicted secondary structure and disorder profiles for UL51 (α), BSRF1 (γ) and UL71 (β) are shown. A RONN probability score (blue line) greater than 0.5 is classed as disordered. The UL51 N terminus is predicted to have alpha-helical secondary structure. A disordered region is predicted from residue 171 through to the C terminus. NetSurfP and RONN predictions for the homologues from VZV, MHV and KSHV, suggest that they too share similar secondary structure and disorder profiles, shown in Appendix 2, page 197.

3.2.3 Homology based structure prediction

Remote homology detection was performed for UL7, UL51 and their homologues using the HHPred server [300-302]. HHPred is a protein function and structure prediction server that generates a position-specific degree of conservation profile for a query protein based on multiple sequence alignment. HHPred then compares the query protein profile to a database of protein profiles in order to detect remotely related proteins. Database matches are scored based on the probability of a true relationship. The HHPred protein matches identified for UL7 had low sequence coverage (20-31 amino acids) and low probability scores (16-25%) so were not deemed reliable. The UL51 homologues from EBV, KSHV and MHV (BSRF1 aa. 78-109; KSHV ORF55 aa. 76-107; MHV ORF55 aa. 67-98) were matched with the small polypeptide Brk1/HSPC300 (PDB: 3PP5 and 3P8C) with a probability score of 46-52%, although the sequence coverage is low. Brk1 is a component of the Scar/WAVE complex and may serve as a precursor to the assembly of this complex. The Scar/WAVE complex bridges upstream signalling events with Arp2/3-complex-mediated actin nucleation and assembly in lamellipodia during cell migration. The matched region (boxed in Figure 3.2) is within the herpes-U44 domain so the fold may be conserved in the alpha herpesvirus homologues although the sequence is not.

3.2.4 Amphipathic helix prediction

Amphipathic helices have a hydrophobic face that enables them to associate with membranes, they can also act as a signal for palmitoylation [303,304]. It was hypothesised that the first helix predicted in the UL51 sequence might be amphipathic and would signal for palmitoylation of cysteine 9 (Figure 3.6). As shown in Figure 3.5, residues 1-20 of UL51 are predicted to form an amphipathic helix by the HeliQuest server.

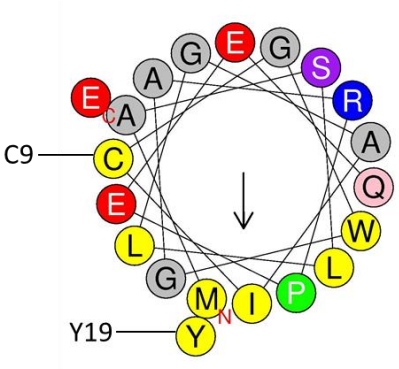

Figure 3.5 Amphipathic helix prediction for UL51 residues 1-20
UL51 residues 1-20 are predicted to form and amphipathic helix with a hydrophobic face encompassing residues: W11, L4, P15, I8, M1, G12, L5 and Y19. In this prediction, cysteine 9 is adjacent to a glutamic acid residue (E16) that in theory may impede membrane association, though there is evidence that one negatively charged residue in the hydrophobic face can be tolerated [303]. Prediction by HeliQuest server [305]. Residue colour coding: yellow, hydrophobic; purple, serine and threonine; blue, basic; red, acidic; pink, asparagine and glutamine; grey, alanine and glycine; green, proline; light blue, histidine. The arrow in the wheel is proportional to the hydrophobic moment.

3.2.5 Bioinformatics summary

Amino acid sequence alignment, protein secondary structure and disorder prediction was performed for UL7, UL51 and their homologues from a selection of alpha, beta and gamma herpesviruses. Despite the relatively poor sequence conservation between the subfamilies, secondary and domain structure is predicted to be conserved between the homologues. Currently, there is a lack of convincing structural homologues for UL7 and UL51, thus there is scope for structural characterisation to provide a useful insight into the nature of these proteins.

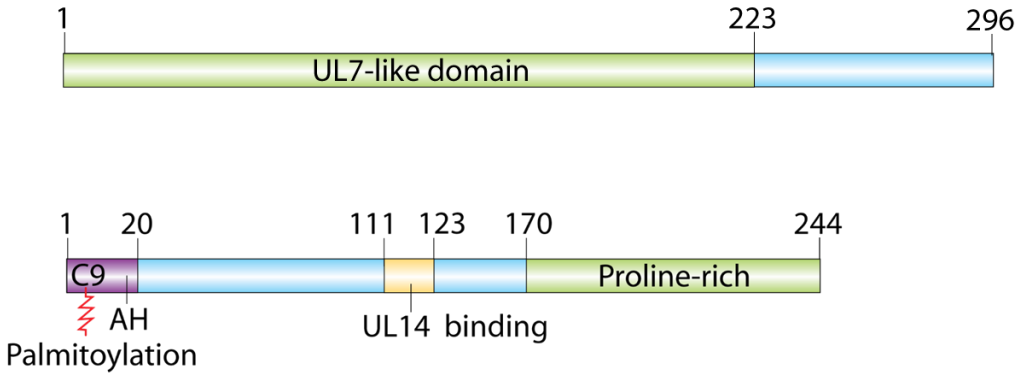

Figure 3.6 Schematic representation of UL7 and UL51 predicted domain architecture
Bioinformatic analysis of UL51 predicts the formation of an N-terminal amphipathic helix (AH, aa. 1-20), and that the C-terminal region (aa. 170-244) is disordered. UL51 is reported to be palmitoylated at cysteine 9 [278], and UL14 has been proposed to bind UL51 in the region spanning residues 111-123 [229]. Little is known about the domain architecture of UL7 but a UL7-like domain has been predicted bioinformatically.

3.3 Screening for optimal protein expression and purification conditions for UL7, UL51 and their homologues

3.3.1 Cloning and construct design

Attempts were made to express and purify HSV-1 UL7 and UL51 proteins from *E. coli* for the generation of monoclonal antibodies, for use in pull-down experiments and for protein crystallisation screens. Full-length UL7 and UL51 were cloned for expression with either an N-terminal or C-terminal His_6 tag. Additionally, shorter UL51 constructs, encompassing residues 1-170 and 29-170, were also cloned to exclude the predicted disordered region at the C terminus and the putative amphipathic helix at the N terminus. While intrinsically disordered regions may be valuable biologically, the low conformational stability can hamper crystallisation since proteins are less likely to self-organise into a highly-ordered crystal. In addition to the HSV-1 proteins, the homologues from HCMV, EBV, KSHV and MHV were also cloned as full-length proteins, as were comparable short construct for the UL51 homologues (Table 3-2). As mentioned in the introduction, HSV-1 strain KOS and strain 17 are frequently used to study gene function and pathogenesis. The genomes of the two strains differ by approximately 1024 SNPs and 272 insertion/deletions, however, the UL7 and UL51 amino acid sequences are identical in both strains.

Table 3-2 Full-length and truncated UL7 and UL51 proteins and their homologues
UL7, UL51 and their homologues were cloned into pOPTH and pOPTnH for expression with an N- or C-terminal His_6 tag, respectively. The molecular masses shown include the N-terminal (MAHHHHHH) and C-terminal (GSKHHHHHH) His_6 tag. The MHV and KSHV homologues are distinguished with either and M or K, respectively.

Virus	UL7 protein & homologues (kDa)	UL51 protein & homologues (kDa)	UL51 short construct aa. (kDa)
HSV-1 (α)	UL7 (34.1)	UL51 (26.5)	UL51 1-170 (19.1)
HCMV (β)	UL103 (29.7)	UL71 (41.0)	UL71 1-173 (20.6)
EBV (γ)	BBRF2 (32.3)	BSRF1 (24.9)	BSRF1 1-174 (20.4)
MHV (γ)	M_ORF42 (29.6)	M_ORF55 (21.9)	ORF55 1-163 (19.0)
KSHV (γ)	K_ORF42 (32.2)	K_ORF55 (25.6)	ORF55 1-170 (19.7)

3.3.2 High throughput expression and purification screen of UL7 and UL51 constructs from pOPTH and pOPTnH

In the first instance, a high throughput approach was taken to screen for optimal expression conditions by testing two *E. coli* strains: BL21 (DE3) pLysS and Rosetta™ (DE3) pLysS, and two induction temperatures: 22°C and 37°C. Soluble protein expression was ascertained by the presence of bands of the appropriate size in SDS-PAGE gels following a crude nickel affinity-purification step using magnetic Ni-NTA beads. Overall, for most proteins optimal purification was achieved following expression in BL21 (DE3) cells at 22°C. The results of the expression screen for UL51 and its homologues are shown in Figure 3.7A. Full-length and truncated UL51 was successfully purified, but only when the His_6 tag was at the N terminus. For simplicity the MHV and KSHV homologues are distinguished with either an M or K, respectively. The strongest expression is seen for M_ORF55, with either N- or C-terminal His_6 tags. Faint bands that may be BSRF1 are present, though these bands were stronger when expression was performed in Rosetta™ (DE3) pLysS cells at 37°C.

The result of the expression screen for UL7 and its homologues clearly shows successful purification of M_ORF42 with both N- and C-terminal His_6 tags (Figure 3.7B). Weak bands of appropriate size are also present for N-terminally tagged BBRF2 and K_ORF42, mass spectrometry confirmed the presence of BBRF2 but not K_ORF42. The UL7 proteins co-purify with a band at ≈65 kDa (boxed in Figure 3.7), which was identified by mass spectrometry to be chaperonin 60. Co-purification with a chaperone protein is an indication of misfolding, based on this finding, the expression was re-attempted using ArcticExpress™ (DE3) competent cells at 12°C. ArcticExpress™ cells are an *E. coli* strain that has been genetically engineered to encode cold-adapted chaperone proteins for optimal soluble protein expression at low temperature. Lowering the expression temperature slows the rate of protein synthesis, which may facilitate correct protein folding. Figure 3.7C shows bands of appropriate size for BBRF2, M_ORF42 and K_ORF42 following expression in ArcticExpress™ cells, but

UL7 is still not visible by SDS-PAGE. An immunoblot for His_6-tagged protein identified bands of appropriate size for BBRF2, M_ORF42, K_ORF42, and UL7. Protein expression appears to be higher when the His_6 tag is C-terminal for BBRF2, K_ORF42, M_ORF42 but N-terminal for UL7. Large-scale (4 L) expression of His_6-UL7 in ArcticExpress™ cells was attempted, followed by Ni-NTA affinity chromatography, but no UL7 protein was detected by SDS-PAGE, suggesting that the protein is unstable when expressed in *E. coli* cells.

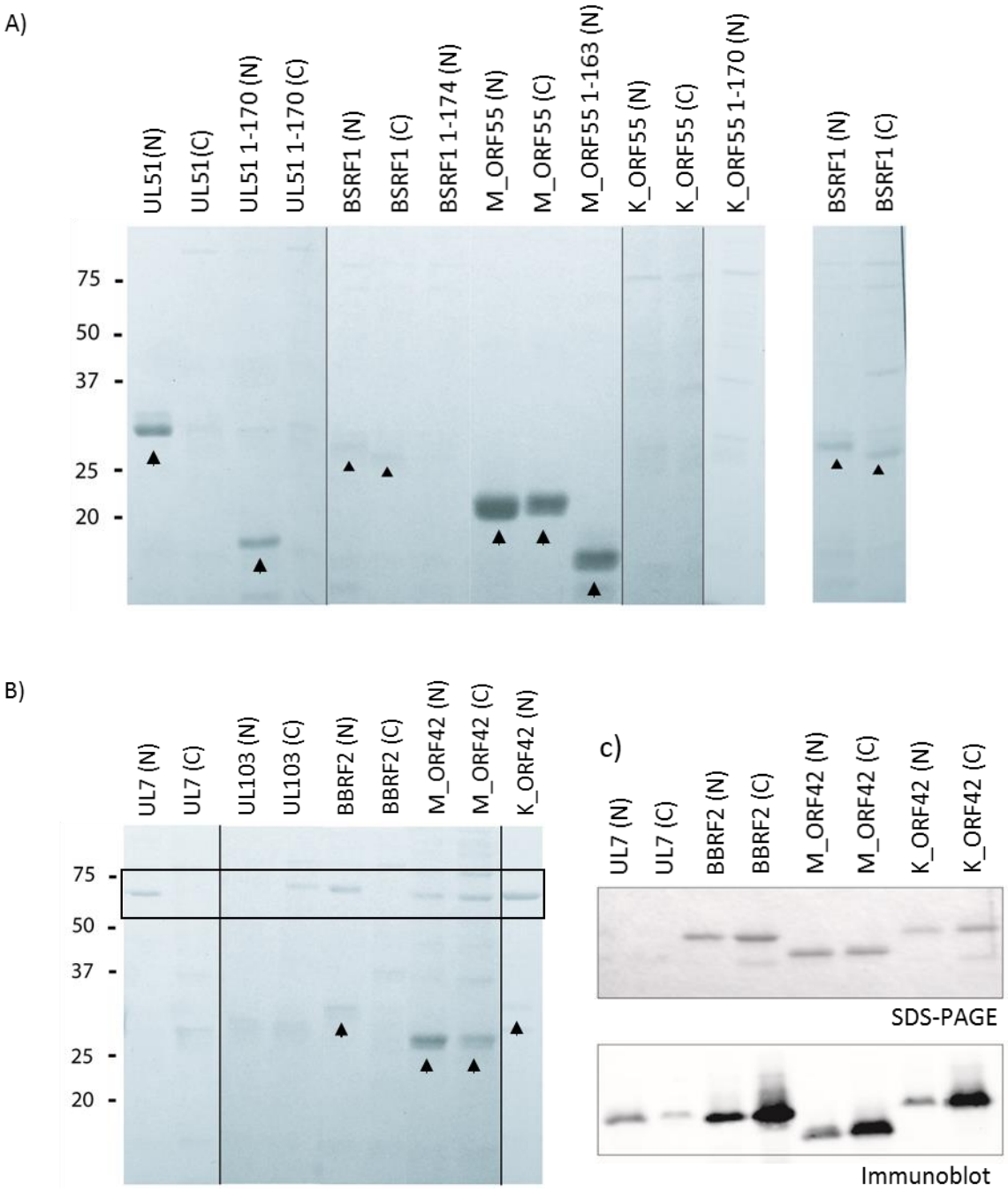

Figure 3.7 Small-scale test expression and purification of UL7, UL51 and homologues
UL7 and UL51 from HSV-1 and their homologues from HCMV, EBV, MHV and KSHV were cloned for expression with either an N- or C-terminal His_6 tag. Two *E. coli* strains: BL21 (DH3) pLysS and Rosetta™ (DH3) pLysS, and two expression temperatures: 22°C and 37°C were screened to identify optimal expression conditions. A small-scale affinity purification step was then performed using Ni-NTA beads to capture His_6-tagged protein, which was then eluted from the beads and analysed by SDS-PAGE. In general, optimal protein expression was achieved using BL21 (DE3) pLysS cells with an expression temperature of 22°C A) Results of the test purification for the UL51 constructs and UL51 homologues following expression in BL21 (DE3) pLysS cells at 22°C. The arrows indicate bands corresponding to the appropriate molecular mass for M_ORF55 (MHV) and UL51 with either an N- or C-terminal His_6 tag. The arrowheads highlight bands suspected to be BSRF1

(EBV), these bands were more intense in Rosetta™ (DE3) pLysS cell lysates. B) Results of the test purification for UL7 and the UL7 homologues following expression in BL21 (DE3) pLysS cells at 22°C. The arrows indicate bands corresponding to the appropriate molecular mass for M_ORF42 (MHV) and UL51 with either an N- or C-terminal His_6 tag. There are also weak bands at the appropriate molecular mass for BBRF2 (EBV) and K_ORF42 (KSHV). The boxed region highlights chaperonin 60 protein, as determined by mass spectrometry. C) His_6-tagged UL7 and the UL7 homologues were expressed in ArcticExpress™ cells at 12°C, followed by a small-scale affinity purification step. SDS-PAGE of the purified proteins shows that the expression of UL7 and the UL7 homologues was improved by switching to ArcticExpress™ cells and reducing the expression temperature to 12°C. Bands at the appropriate molecular mass for BBRF2, M_ORF42and K_ORF42 are clearly visible by SDS-PAGE. An immunoblot for the His_6 tag (α-His_5 antibody) detected bands of appropriate size for these proteins and shows limited expression of UL7.

3.3.3 Expression of UL7 from a codon-optimised synthetic gene

Heterologous gene expression in *E. coli* can be impaired by the presence of 'rare codons' within the transgene sequence, which can lead to inefficient and inaccurate translation as ribosomes stall. Low expression levels of transgenes and/or protein misfolding can sometimes be alleviated by using a gene sequence that has been optimised at the codon level for expression in the target organism. Codon-optimisation can also remove secondary structure elements encoded by the mRNA transcripts, and nucleotide bias, which may be beneficial given the high GC content of the HSV-1 genome. A synthetic gene for UL7 HSV-1 was purchased where the codon usage of the sequence had been optimised for expression in *E. coli*. The synthetic gene was cloned into pOPTH and pOPTnH for protein expression with either an N- or C-terminal His_6 tag, and pOPTG and pOPTnG for expression with either an N- or C-terminal GST tag, respectively. An expression screen, similar to that described in section 3.3.2, was performed to identify optimal expression conditions. Figure 3.8A shows expression of GST-tagged UL7, there are bands of appropriate size with Rosetta™ (DE3) pLysS and B834 cell strains but none for BL21 (DE3) pLysS. In Rosetta™ (DE3) pLysS and B834 cells N-terminally tagged UL7 is expressed at 22°C and 37°C, however, with the Rosetta™ cells there is a band at ≈65 kDa that co-purifies with GST-UL7 and is likely to be chaperonin 60. C-terminally tagged UL7 expressed in Rosetta™ (DE3) pLysS cells at 22°C and no chaperonin 60 band is present. Expression of His_6-tagged UL7 showed a slight improvement over expression from the wild-type gene, there are very faint bands of appropriate size for C-terminally tagged UL7 in conditions: Rosetta (DE3) pLysS and B834 cells at 22°C, and also N-terminally tagged UL7 in BL21 cells at 22°C, although this is accompanied with a strong band that is likely to be chaperonin 60.

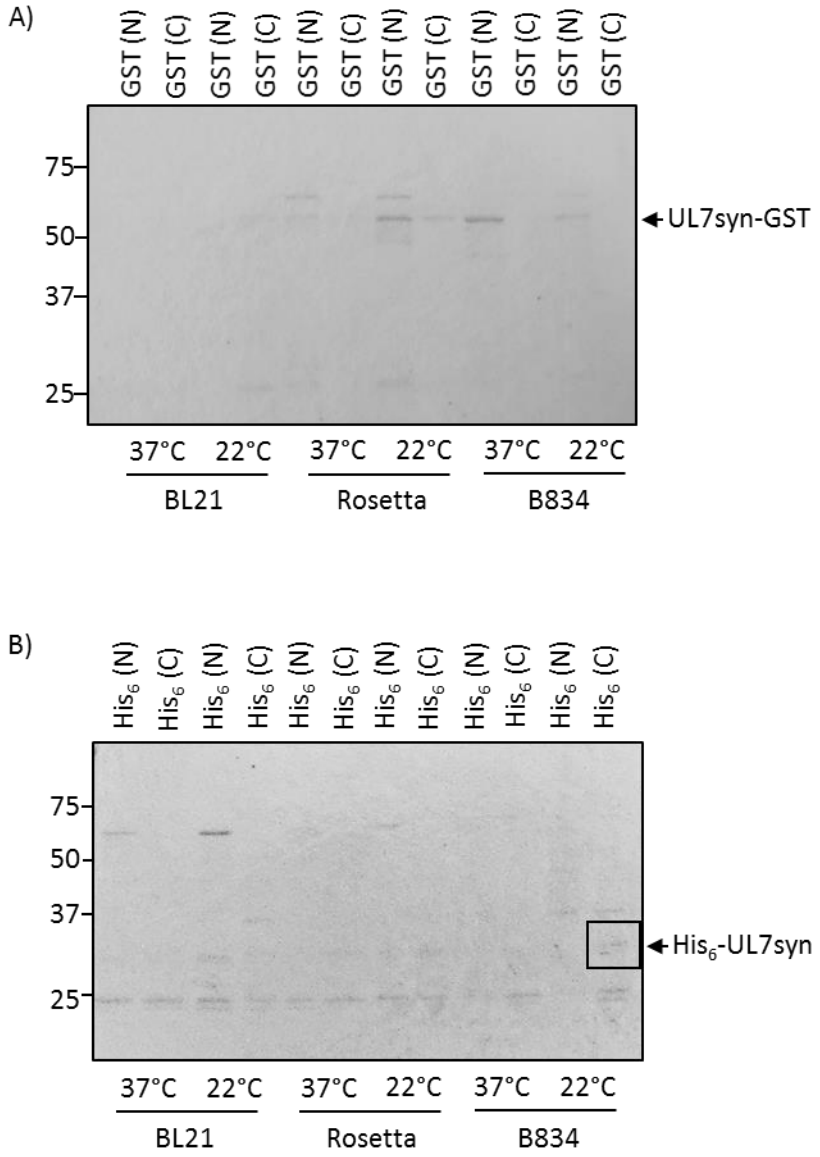

Figure 3.8 Small-scale test expression and purification of codon optimised UL7 with either a GST or His_6 tag

The UL7 gene was codon optimised for expression in *E. coli* and cloned for expression with either an N- or C-terminal GST or His_6 tag. Three *E. coli* strains: BL21 (DE3) pLysS, Rosetta™ (DE3) pLysS and B834 (DE3), and two expression temperatures: 22°C and 37°C were screened to identify optimal expression conditions. A small-scale affinity purification step was then performed using either GSH or Ni-NTA beads to capture GST and His_6-tagged protein, respectively. Purified protein was eluted from the beads and analysed by SDS-PAGE. A) Expression of either N- or C-terminally GST-tagged UL7 protein, the arrow indicates bands at the expected molecular mass for GST-UL7. B) Expression of either N- or C-terminally His_6-tagged UL7 protein. A faint band at the expected molecular mass for His_6-UL7 is highlighted by the box.

3.3.4 Summary of protein expression screening

In summary, with the exception of M_ORF42, the overall expression of the UL7 proteins at 22°C and 37°C was poor, but could be improved by lowering the induction temperature to 12°C and using ArcticExpress™ cells. Bands for BBRF2, M_ORF42 and K_ORF42 were clearly visible by SDS-PAGE when ArcticExpress™ cells were used, and an immunoblot detected limited expression of UL7. Use of a codon-optimised UL7 sequence enabled expression of UL7 to levels detectable in an SDS-PAGE gel, particularly when expressed with a GST tag. Full-length UL51 and M_ORF55 can be purified from BL21 (DE3) pLysS cells at 22°C, and also the truncated constructs of these proteins. Limited expression and purification of BSRF1 may have occurred and it may be worth repeating the expression using ArcticExpress™ cells. Proteins that expressed well in these initial screens: M_ORF42, M_ORF55, and UL51 were selected for large-scale expression and purification with His_6 tags. It was decided to express the UL7 protein from the codon optimised gene with a C-terminal GST tag in Rosetta™ (DE3) pLysS cells at 22°C overnight, and in B834 (DE3) cells with an N-terminal GST tag at 37°C for 4 h.

3.4 Large-scale expression and purification of UL7 and M_ORF42

3.4.1 Large-scale purification of ORF42 from MHV

M_ORF42 is the UL7 homologue from murid herpesvirus and, unlike UL7, it could be readily purified in the high throughput screen, making it an ideal candidate for large-scale expression. The aim was to produce His_6-tagged M_ORF42 for structural studies and GST-tagged M_ORF42 for pull-down experiments. BL21 (DE3) pLysS cells and an expression temperature of 22°C were selected for the expression of N-terminally tagged His_6-M_ORF42. Initially, a 2 L bacterial culture was grown and the protein was purified by affinity capture using Ni-NTA resin followed by size-exclusion chromatography (SEC). As shown in Figure 3.9A a reasonably pure sample His_6-M_ORF42 was obtained, though some lower molecular mass bands are present. These fractions were concentrated to 1.6 mg/ml at which point protein precipitation was evident. An overall yield of 2.0 mg/L of culture was achieved. Similarly, N-terminal GST-tagged M_ORF42 was purified from a 2 L culture of BL21 (DE3) pLysS cells grown at 22°C overnight, the SEC peak is quite broad and SDS-PAGE shows contamination of the later fractions with a band at 27 kDa that is likely to be GST (Figure 3.9B and C). The GST tag seemed to improved protein solubility, enabling the sample (fractions C7-C12) to be concentrated to 10.3 mg/ml with an overall yield of 2.5 mg/L of culture.

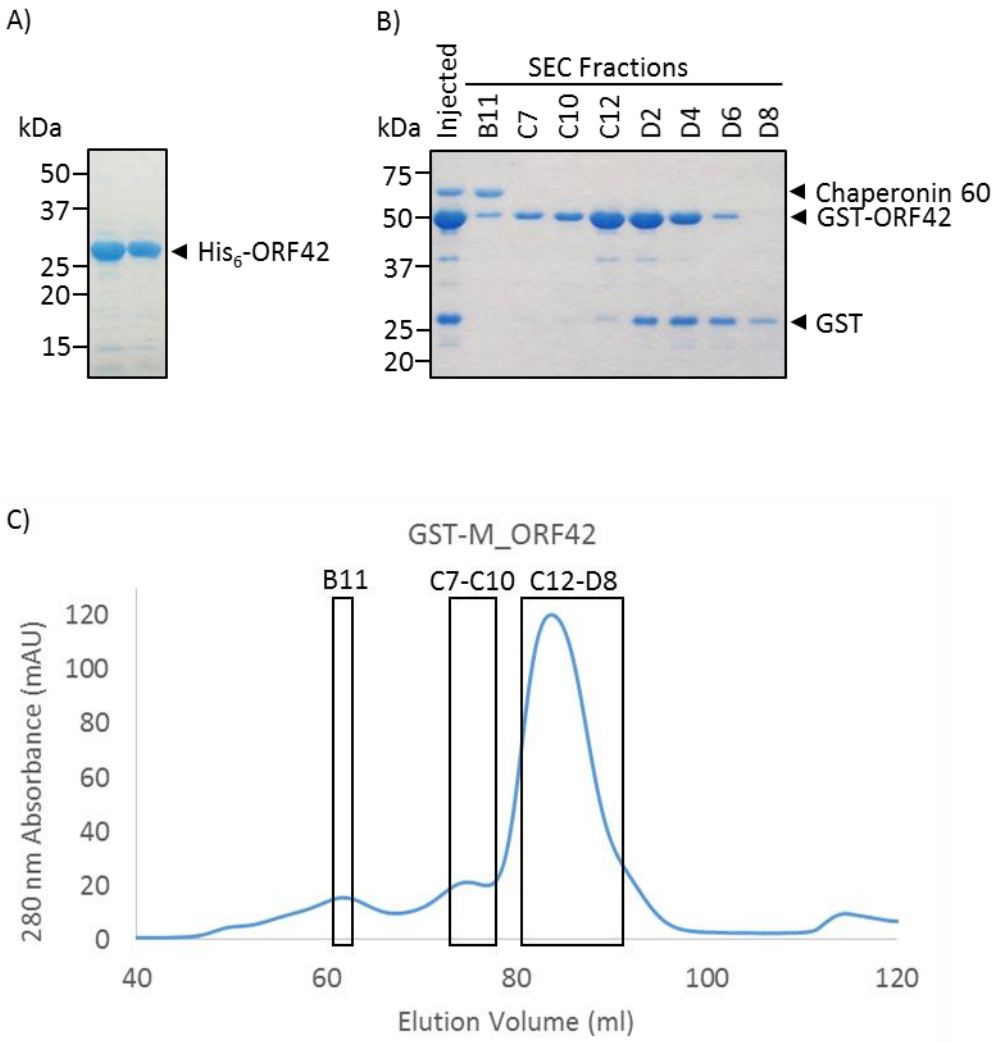

Figure 3.9 Purification of His_6-tagged and GST-tagged M_ORF42
M_ORF42 with either an N-terminal His_6 or GST tag was expressed in *BL21 (DE3) pLysS* (2 L bacterial culture) and purified using either Ni-NTA or GSH beads, respectively. The affinity purification step was followed by SEC. A) Purification of His_6-M_ORF42: SDS-PAGE of SEC fractions showing a band at the expected molecular mass for His_6-M_ORF42 (29.6 kDa). B) Purification of GST-M_ORF42: SDS-PAGE of the SEC fractions corresponding to the chromatogram in C. Bands are apparent at the expected molecular mass for GST-M_ORF42 (55.6 kDa). The band running at 27 kDa is likely to be GST alone. C) S200 16/600 SEC chromatogram for GST-M_ORF42.

3.4.2 Large-scale purification of UL7 from HSV-1

Expression of UL7 was achieved by switching to a synthetic gene that had been codon-optimised for expression in *E. coli*. As with M_ORF42, the aim was to produce GST-tagged UL7 for pull-down experiments and either untagged or His_6-tagged UL7 for monoclonal antibody generation and structural studies. Based on the outcome of the small-scale expression and purification screen (section 3.3.3), two expression conditions for GST-tagged UL7 protein were selected for expression in 2 L cultures: (i) N-terminally GST-tagged UL7 expressed in B834 (DE3) cells at 37°C for 4 h and, (ii) C-

terminally GST-tagged UL7 expressed in Rosetta™ (DE3) pLysS cells at 22°C overnight. The proteins were purified by GSH affinity capture followed by SEC. Expression in B834 (DE3) cells with an N-terminal GST tag produced a very small amount of UL7-GST protein, which co-purified with chaperonin 60. However, it was possible to produce a higher yield of C-terminal GST-tagged UL7 through expression in Rosetta™ cells at 22°C overnight that did not co-purify with chaperone protein. The SEC chromatogram shows two peaks (Figure 3.10A), the second of which contains UL7-GST (Figure 3.10B). The second peak fractions were pooled and concentrated to approximately 0.9 mg/ml without evidence of precipitation, giving an overall yield of 0.24 mg/L of culture.

The next aim was to produce UL7 for structural studies by expressing UL7 with a His_6 tag, or by expressing the GST-tagged construct and cleaving the tag from the recombinant protein to produce untagged UL7. The former was attempted through large-scale expression and purification of C-terminally His_6-tagged UL7 from B834 (DE3) cells at 22°C, however, this approach yielded very low levels of UL7 that co-purified with chaperone protein. Following on from the successful expression of C-terminally GST-tagged UL7 from Rosetta™ (DE3) pLysS cells at 22°C overnight, an 8 L preparation was attempted with the intention to cleave the GST tag. SEC was performed to remove glutathione from the protein sample after the GSH elution step, and SDS-PAGE of the SEC peak fractions confirmed the presence of UL7-GST. The fractions were pooled and incubated overnight with human rhinovirus 3C protease, however, the following day protein precipitation was visible in the tube. After centrifuging to remove the precipitated protein the sample was incubated with GSH beads to capture cleaved GST, any uncleaved UL7-GST and the GST-tagged protease. A small amount of cleaved UL7 was retrieved after SEC, however, the protein yield was low and the protein could not be concentrated beyond 0.35 mg/ml due to precipitation.

In conclusion, it was possible to express and purify sufficient quantities of GST-tagged UL7 protein suitable for pull-down experiments. The attempts to produce His_6-tagged or untagged UL7 failed in the first instance due to low expression levels and co-purification chaperone protein, and in the second due to precipitation of the untagged UL7 protein.

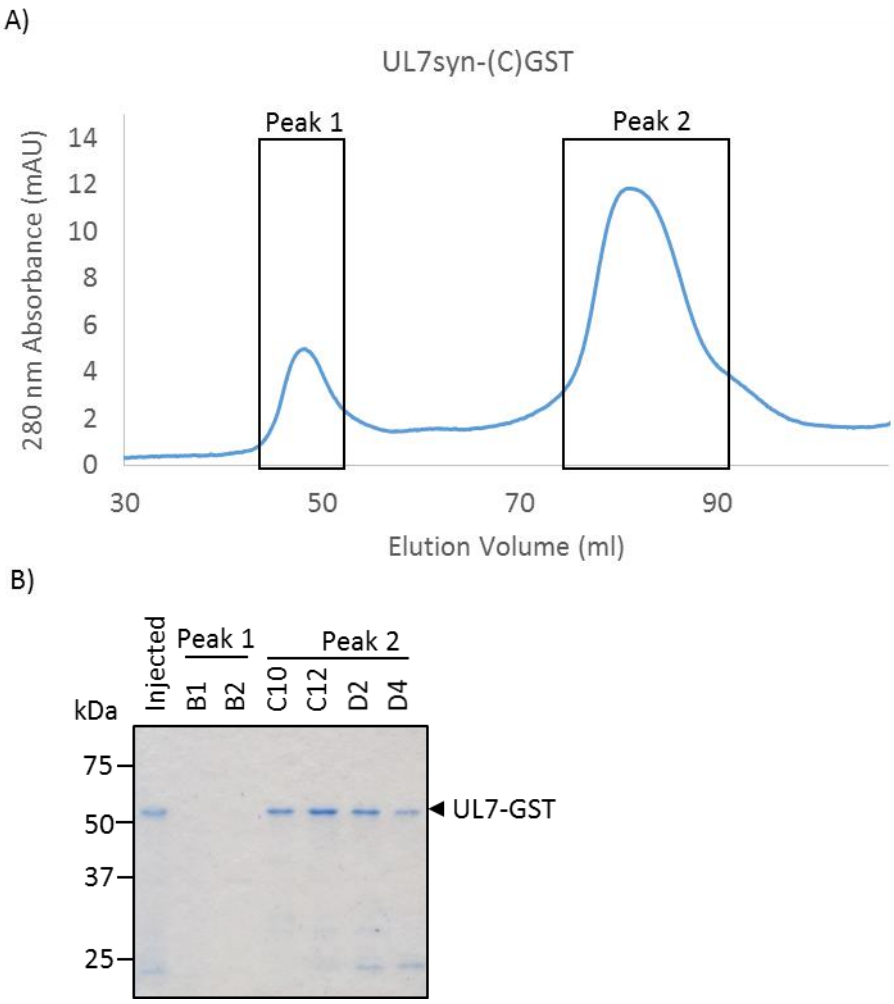

Figure 3.10 Large-scale purification of UL7-GST
GST-tagged (C-terminal) UL7 was expressed from a synthetic gene that had been optimised for expression in *E. coli*. The protein was expressed in Rosetta™ (DE3) pLysS cells at 22°C overnight (2 L bacterial culture), and purified by affinity capture using GSH beads followed by SEC. A) S200 16/600 SEC chromatogram for UL7-GST. B) SDS-PAGE of the SEC fractions for the UL7-GST purification showing bands at the expected molecular mass for UL7-GST (60.1 kDa).

3.5 Large-scale expression and purification of UL51 and M_ORF55

3.5.1 Purification of MHV His_6-ORF55 full-length and truncated constructs

M_ORF55 expressed well in the high throughput screen regardless of cell type and expression temperature, this remained the case when expressed in 2 L *E. coli* cultures. N-terminally His_6-tagged M_ORF55 was expressed in BL21 cells at 22°C overnight and purified by affinity chromatography followed by SEC. The SEC chromatogram for wild-type His_6-M_ORF55 shows a single asymmetric peak that is skewed to the right, SDS-PAGE analysis confirmed that this peak corresponded to M_ORF55 (Figure 3.11A and B). The asymmetry of the peak was attributed to the co-elution of higher molecular mass species, which run around 45 kDa, approximately twice the molecular mass of the monomer, and

at 80 kDa (Figure 3.11B). Purification of M_ORF55 1-163 produced a similar pattern in SDS-PAGE and SEC, with an additional band running at twice the molecular mass of the monomeric protein (Figure 3.11A and E). It was hypothesised that His_6-M_ORF55 may be forming dimers resistant to SDS, DTT and boiling, possibly through metal coordination since the concentrated full-length and 1-162 protein was visibly brown. As mentioned in the introduction, UL51 can be palmitoylated at a cysteine residue in position 9 (Cys9); M_ORF55 has two adjacent cysteine residues in positions 3 and 4 that were predicted to be homologous to cysteine 9 in UL51 and may undergo palmitoylation *in vivo*. Palmitoylated residues are surface-exposed, by extension it was predicted that Cys3 and Cys4 of M_ORF55 will be present on the protein surface. When expressed in *E. coli* these residues will not be palmitoylated, and therefore may be liable to form di-sulphide interactions. It was hypothesised that the higher molecular mass species that co-purify with monomeric M_ORF55 might be due to the formation of SDS/DTT resistant multimers that form via intermolecular di-sulphide bonds between labile cysteine residues. A high concentration of DTT would be expected to reduce the di-sulphide bonds and eradicate the oligomers. To test this hypothesis purified M_ORF55 FL was incubated with 50 mM DTT for 5 m on ice and injected onto an analytical S200 (10/300) column that was equilibrated in one of three test buffers:

1) 20 mM Tris pH 7.5, 200 mM NaCl, 10 mM DTT
2) 20 mM Tris pH 8.8, 350 mM NaCl, no DTT
3) 20 mM Tris pH 8.8, 350 mM NaCl, 10 mM DTT

The first buffer appeared to improve the sample by eliminating the ≈80 kDa band as shown by SDS-PAGE (Figure 3.11C). However, a band at ≈45 kDa was still present and the sample remained brown. Buffers 2 and 3 were intended to test whether charge-mediated self-association of purified M_ORF55 might be occurring, by switching to pH 8.8 (M_ORF55: pI 5.05) and increasing the salt concentration. However, despite these modifications to the buffer there was little change in the SEC trace and the higher molecular mass bands persisted.

To further investigate the possible role Cys3 and Cys4 of His_6-M_ORF55 may play in the formation of oligomers they were mutated to serine, an analogous amino acid that cannot form di-sulphide bonds, and the purification was repeated. The SEC trace of the mutant protein resembles that of the wild-type protein with a slight shift to a later elution volume (Figure 3.11A). The band at ≈45 kDa is present in the SDS-PAGE but appears weaker and the band at ≈80 kDa is absent (Figure 3.11D). There is a ladder of bands running below the His_6-M_ORF55 band that may be indicative of protein degradation, similar bands are also present in the gel for His_6-M_ORF55 1-163 (Figure 3.11E). Intriguingly, the mutated full-length and 1-163 protein samples were no longer brown in colour, one possible explanation for this observation could be the formation of iron-sulphur complexes between the surface cysteine residues of M_ORF55 and iron in the sample, resulting in the brown colouration. Iron-sulphur clusters readily occur when SNAP-25 is purified from *E. coli* cells and its cysteine residues

(Cys85, 88, 90 and 92) are lacking their palmitoyl modification [306]. The purified His_6-M_ORF55 C3S+C4S protein was soluble and could be concentrated to at least 15.1 mg/ml without signs of precipitation. Overall yields of 15.0 mg/Litre of culture of His_6-M_ORF55 C3S+C4S and 14.0 mg/Litre of culture of His_6-M_ORF55 C3S+C4S 1-163 could be achieved. Anion exchange was performed with the mutant protein in an attempt to separate the lower molecular mass bands, but was unable to remove these contaminants.

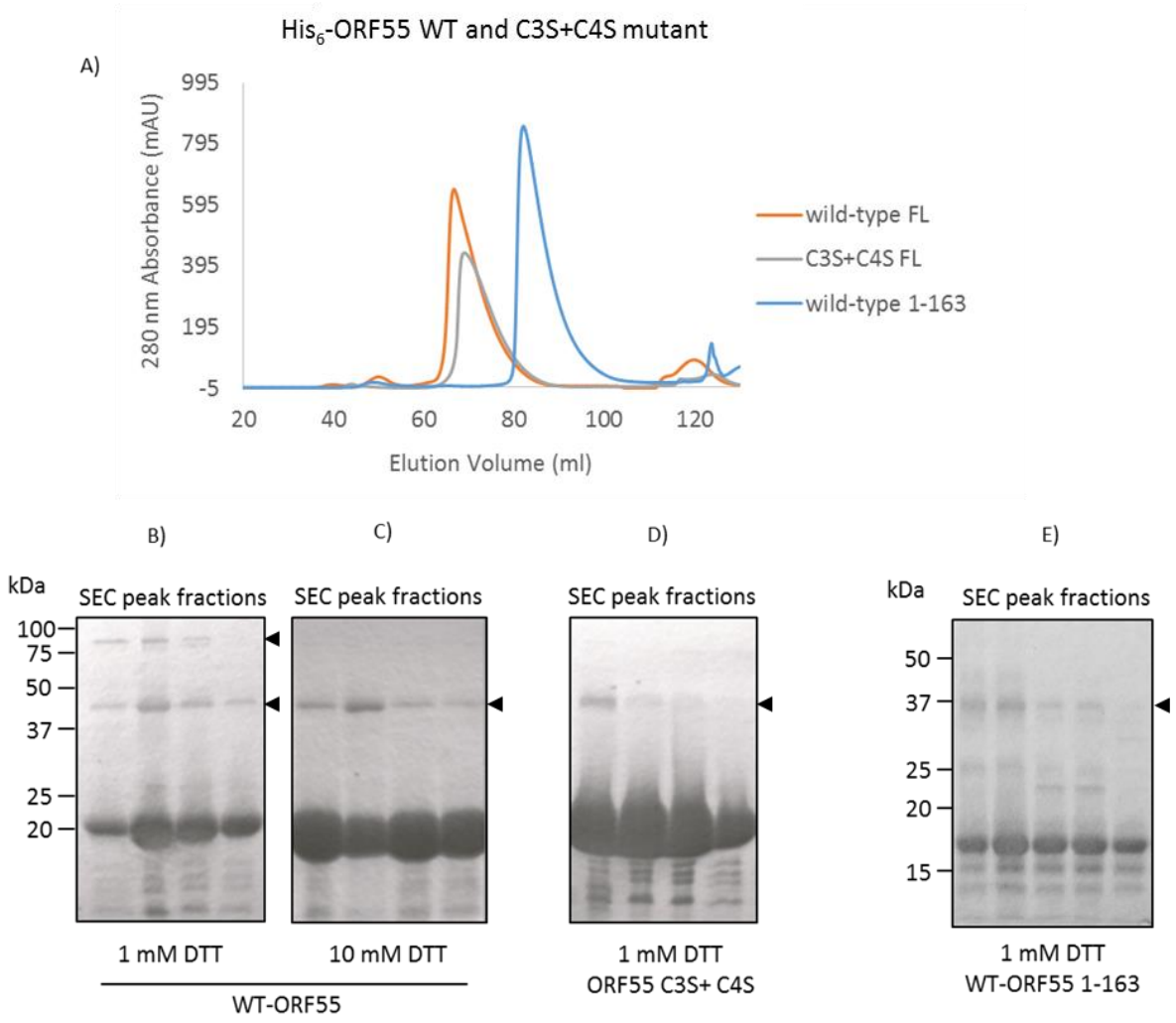

Figure 3.11 Purification of His_6-M_ORF55 wild-type and C3S+C4S mutant
N-terminally His_6-tagged M_ORF55 wild-type and the C3S+C4S mutant were expressed in BL21 (DE3) pLysS cells (2 L culture) at 22°C overnight and purified by affinity chromatography followed by SEC. A) S200 16/600 SEC chromatograms for full-length (FL) His_6-M_ORF55 wild-type (21.9 kDa), His_6-M_ORF55 C3S+C4S mutant (21.8 kDa) and His_6-M_ORF55 wild-type 1-163 (19.0 kDa). B) SDS-PAGE for His_6-M_ORF55 wild-type SEC peak fractions, showing a band at the expected molecular mass for His_6-M_ORF55 and two additional bands running at ≈45 kDa and ≈80 kDa. C) SDS-PAGE showing SEC fractions for the purification of His_6-M_ORF55 wild-type in the presence of 10 mM, the ≈80 kDa band is no longer present in the sample. D) SDS-PAGE of the His_6-M_ORF55 C3S+C4S mutant SEC fractions. Cys3 and Cys4 of M_ORF55 were mutated to serine to eliminate the potential for these residues to form di-sulphide bonds or chelate metal ions. The mutant protein was

purified with buffer containing 1 mM DTT. The mutant sample lacks the ≈80 kDa band and appears to have a lower amount of the ≈45 kDa species. E) SDS-PAGE of His_6-M_ORF55 wild-type 1-163 SEC fractions. Concentrated wild-type M_ORF55 full-length and 1-163 was visibly brown, while the mutant protein was colourless.

In an attempt to improve the sample by eliminating the suspected M_ORF55 degradation products, an additional His_6-M_ORF55 construct was designed encompassing residues 22-154. This construct excludes N-terminal residues that were predicted to exist in a coiled-coil conformation and also the cysteine residues in positions 3 and 4 (Appendix, page 197). The construct was expressed in BL21 (DE3) pLysS cells at 22°C overnight and purified by affinity chromatograph followed by SEC. The SEC peak resembles that of the full-length protein and SDS-PAGE shows the corresponding fractions to contain fewer degradation bands (Figure 3.12). The protein was soluble and could be concentrated to 10.2 mg/ml and a yield of 6.0 mg/L of culture could be achieved.

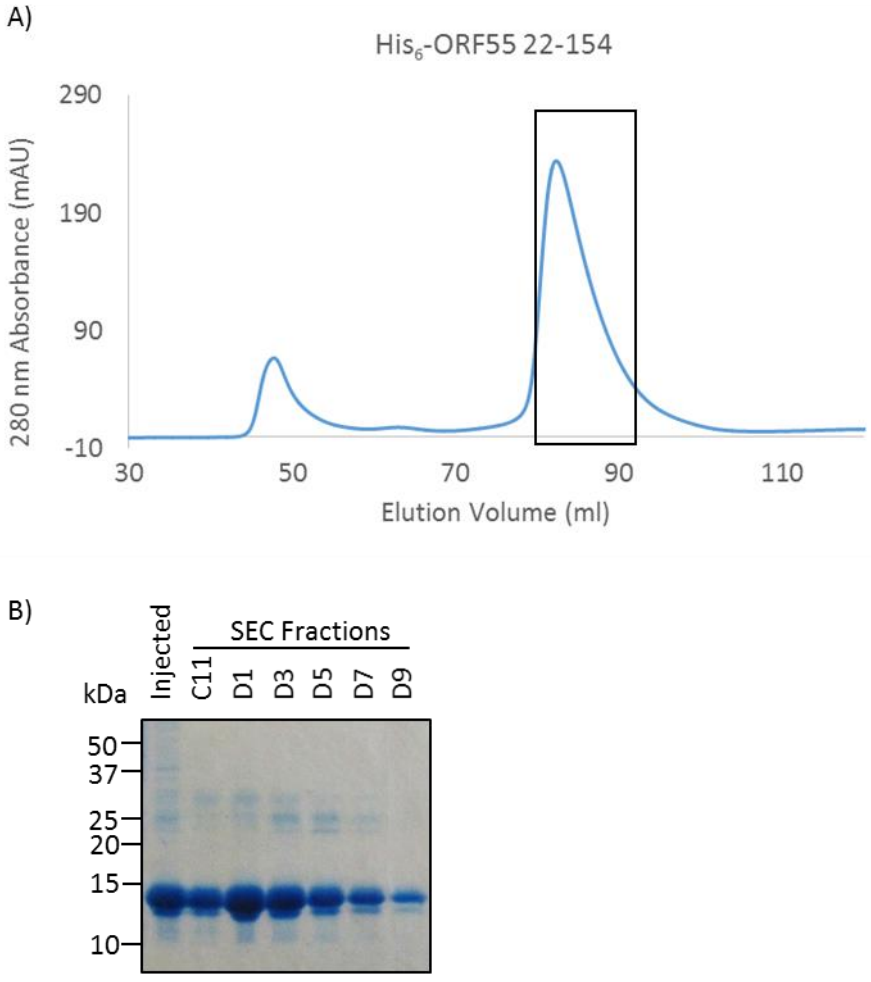

Figure 3.12 Purification of His_6-ORF55 22-154
N-terminally His_6-tagged M_ORF55 22-154 was expressed in BL21 (DE3) pLysS cells (2 L culture) at 22°C overnight and purified by affinity chromatography followed by SEC. A) S200 16/600 SEC chromatogram for His_6-M_ORF55 22-154 showing an asymmetric single peak.

B) SDS-PAGE gel of peak fractions showing a band that runs close to the predicted molecular mass of His_6-M_ORF55 22-154 (15.4 kDa).

3.6 Crystallisation screens for His_6-M_ORF55 constructs

Sparse-matrix crystallisation experiments were prepared for His_6-M_ORF55 C3S+C4S full-length (screens: CIMR1, 2, 3, 4, 5, 6, 7, 8, 9, 11, 12, 15; see Table 2-6, page 43) using a protein concentration of 15.1 mg/ml. Protein and reservoir drops were dispensed using an Innovadyne Screenmaker and plates were incubated at 20°C in a Formulatrix imaging robot. After 24 h, ≈25% of the drops were clear and the remainder contained either phase separation (≈25%) or granular (≈20%) and heavy (≈30%) precipitate. The drops were monitored during the following weeks and months, but after two years no crystalline material was apparent. Similarly, crystallisation experiments were prepared for His_6-M_ORF55 C3S+C4S 1-163 using protein at 11.3 mg/ml (screens: CIMR5, 6, 7, 11, 15; see Table 2-6) and 21.0 mg/ml (screens: CIMR 1-14 and 18; see Table 2-6). Drops prepared using protein at 21.0 mg/ml predominantly contained phase separation (≈45%) or heavy precipitation (≈30%), while drops prepared with 11.3 mg/ml protein were mostly clear. The drops were monitored over the following weeks and months, but after 2 years crystals were not forthcoming. Crystallisation screening with His6-ORF55 22-154 protein at 10.2 mg/ml and 4.3 mg/ml was also unsuccessful, the protein rapidly precipitated in all the conditions tested even at low concentration.

3.6.1 Purification of His_6-UL51 full-length and truncated constructs

Full-length UL51 and the 1-170 construct could be expressed and purified in the high throughput screen (Figure 3.7) but only when the affinity tag was positioned at the N terminus. Full-length His_6-UL51 was expressed in BL21 (DE3) pLysS cells at 22°C overnight and purified using affinity chromatography followed by SEC. The chromatogram shows a peak with an extended tail that is close to the void volume of the column (Figure 3.13A). SDS-PAGE shows a band at the appropriate size for His_6-UL51 in the main peak and in the tail region (Figure 3.13B). As with the purification of wild-type M_ORF55 there is also a band running at twice the predicted molecular mass of His_6-UL51, just above the 50 kDa marker. Anion exchange was attempted but failed to separate the higher band from His_6-UL51. The protein was concentrated to 4.5 mg/ml, an overall yield of 1.1 mg/L of culture was achieved.

Based on the reasons described in the previous section, a C9S mutation was introduced into the UL51 gene by QuickChange. The protein was expressed and purified by affinity chromatography and SEC as described above. As with the wild-type protein, the SEC chromatogram shows a peak with an extended tail and SDS-PAGE identified a band of appropriate size for UL51 in both the peak and the tail (Figure 3.13A). As shown in Figure 3.13C the suspected His_6-UL51 dimer band is substantially reduced with the C9S mutant compared to wild-type. Anion exchange was unsuccessful at removing the contaminating band that runs between the 15 and 20 kDa markers. The protein was soluble and

could be concentrated to 15.0 mg/ml with an overall yield of 2.8 mg/L of culture. For comparison, a sample of wild-type His_6-UL51 was incubated with either 50 mM β-mercaptoethanol or 50 mM DTT and analysed by SDS-PAGE alongside the C9S mutant. As shown in Figure 3.13D, treating the wild-type protein with reducing agent eradicates the higher molecular mass species from the sample such that it resembles the C9S mutant. Henceforth, all work on UL51 protein was conducted with the C9S mutant.

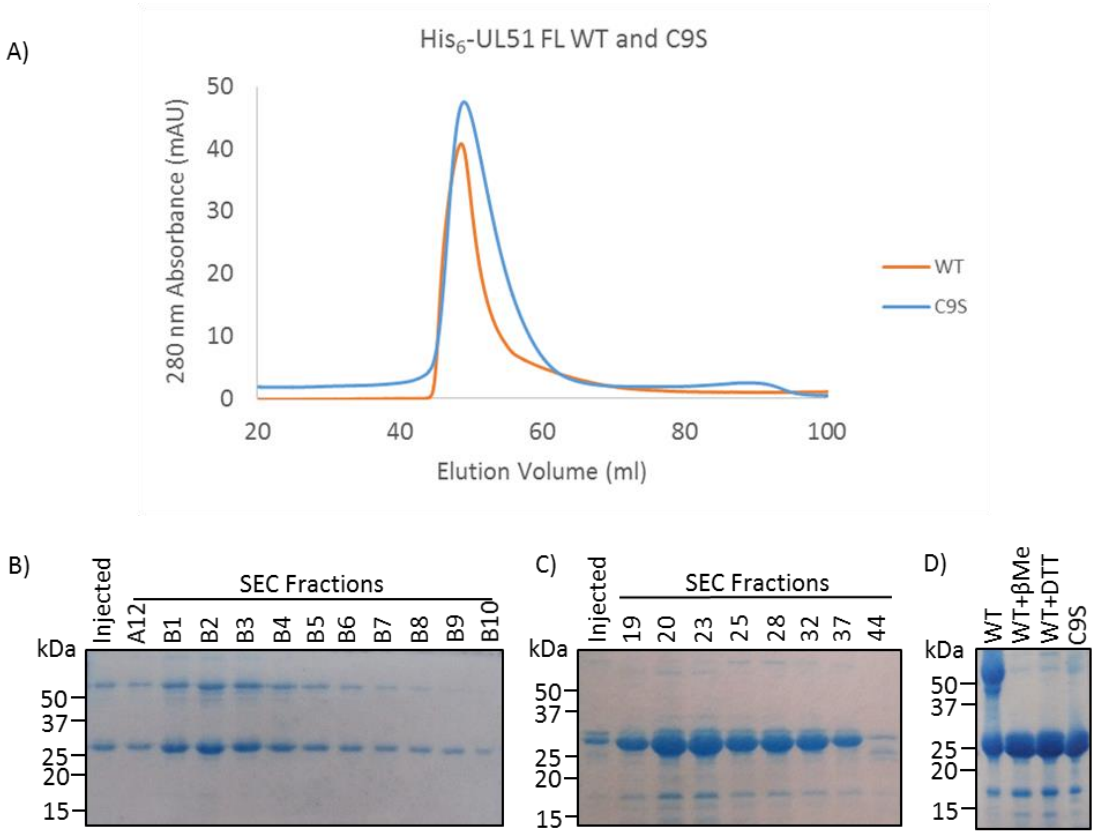

Figure 3.13 Purification of full-length His_6-UL51 wild-type and C9S mutant
N-terminally His_6-tagged UL51 wild-type and a C9S mutant were expressed in BL21 (DE3) pLysS cells (2 L culture) at 22°C overnight and purified by affinity chromatography followed by SEC. A) S75 16/600 SEC chromatogram for the full-length wild-type His_6-UL51 and the C9S mutant. B) Purification of wild-type His_6-UL51: SDS-PAGE of SEC fractions showing a band at the predicted molecular mass for His_6-UL51 (26.5 kDa) and a higher band running at the molecular mass expected for a His_6-UL51 dimer. C) Purification of His_6-UL51 C9S: SDS-PAGE of SEC fractions showing that the introduction of the C9S mutation eliminates the posited His_6-UL51 dimer band. D) Wild-type His_6-UL51 was treated with reducing agents, either DTT or β-mercaptoethanol, and analysed alongside the C9S mutant. Treating the wild-type sample with reducing agents eliminates the higher molecular mass band as does the C9S mutation.

In addition to the full-length His_6-UL51 protein a truncated construct was also purified, which encompasses residues 1-170 and thus excluding the C-terminal region that is predicted to be disordered. A C9S mutation was introduced into this construct and the protein was expressed in BL21

(DE3) pLysS cells at 22°C overnight. The SEC chromatogram (Figure 3.14) has two peaks and both contain a band of appropriate size for His_6-UL51 C9S 1-170. The first peak contains additional contaminant bands and is close to the void volume of the column, whereas the second peak fractions are cleaner. The shape of the second peak also resembles that of the full-length protein, there being an extended tail region. A SEC peak with a trailing tail can be indicative of conformational heterogeneity or interactions with the column matrix. Fractions corresponding to the second peak were pooled and concentrated to 3.5 mg/ml without signs of precipitation.

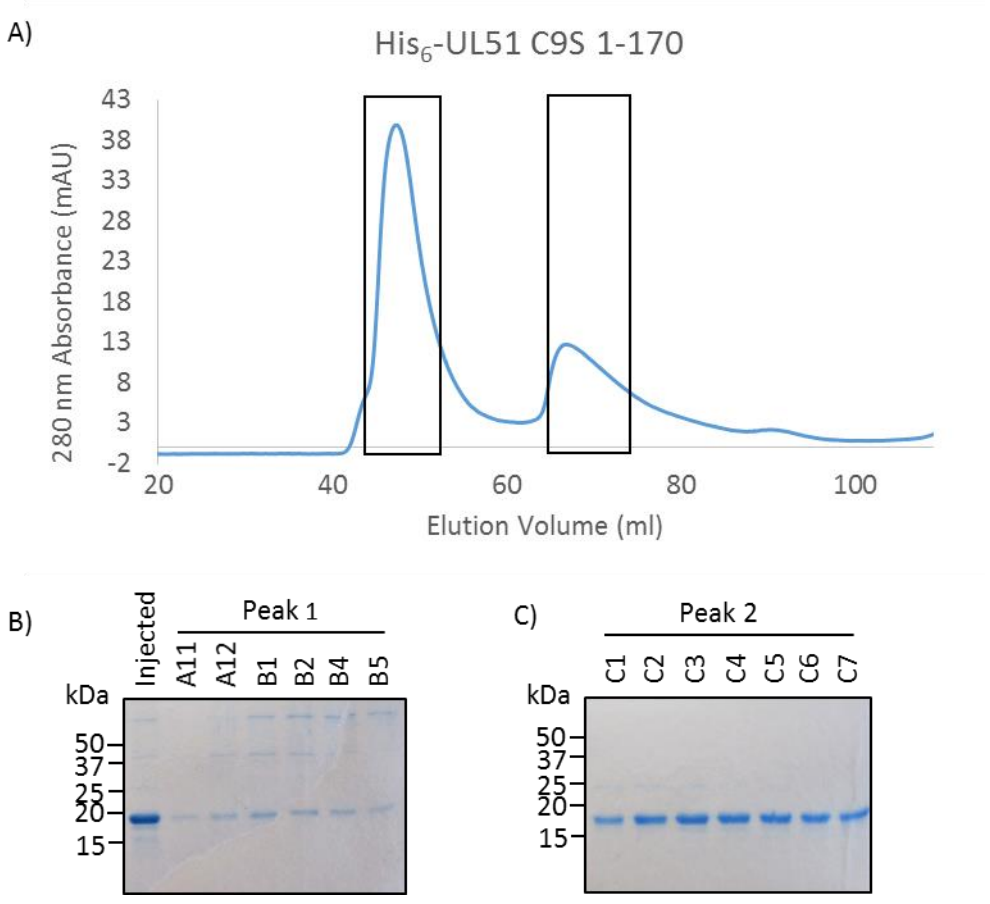

Figure 3.14 Purification of His_6-UL51 C9S 1-170
N-terminally His_6-tagged UL51 C9S 1-170 was expressed in BL21 (DE3) pLysS cells (2 L culture) at 22°C overnight and purified by affinity chromatography followed by SEC. A) S200 16/600 SEC chromatogram for His_6-UL51 C9S 1-170 showing two peaks. B) SDS-PAGE of the SEC fractions corresponding to peak 1, there is a band at the predicted molecular mass for His_6-UL51 (19.1 kDa) along with several higher molecular mass bands. This peak is close to the void volume of the column and is likely to contain aggregated protein. C) SDS-PAGE of SEC fractions corresponding to the second peak, there is a band at the expected size for His_6-UL51 and no other contaminating bands are visible.

3.6.2 Purification of UL51 29-170

An additional UL51 construct was designed encompassing residues 29-170, which excludes a predicted disordered region at the N terminus and matches the M_ORF55 22-154 construct. The

protein was expressed in BL21 (DE3) pLysS cells overnight at 22°C and purified as above, Figure 3.15 shows the SEC chromatogram and corresponding SDS-PAGE. As with previous attempts to purify UL51 constructs the elution peak is close to the void volume of the column and contains additional contaminating bands. The trailing tail of the peak contains bands that correspond to the UL51 29-170 protein (fractions B6-C3), and is an indication of conformational heterogeneity and/or interactions with the column matrix. SEC fractions A12-B3 were pooled and concentrated to 12.0 mg/ml for use in pull-down experiments.

In conclusion, full-length and truncated UL51 could be purified and sufficient amounts of protein were obtained for pull-down experiments and monoclonal antibody generation. However, the shape of the SEC peaks, particularly for the 29-170 construct, suggest that the proteins may not adopt a full-folded conformation, which can reduce the chance of protein crystallisation.

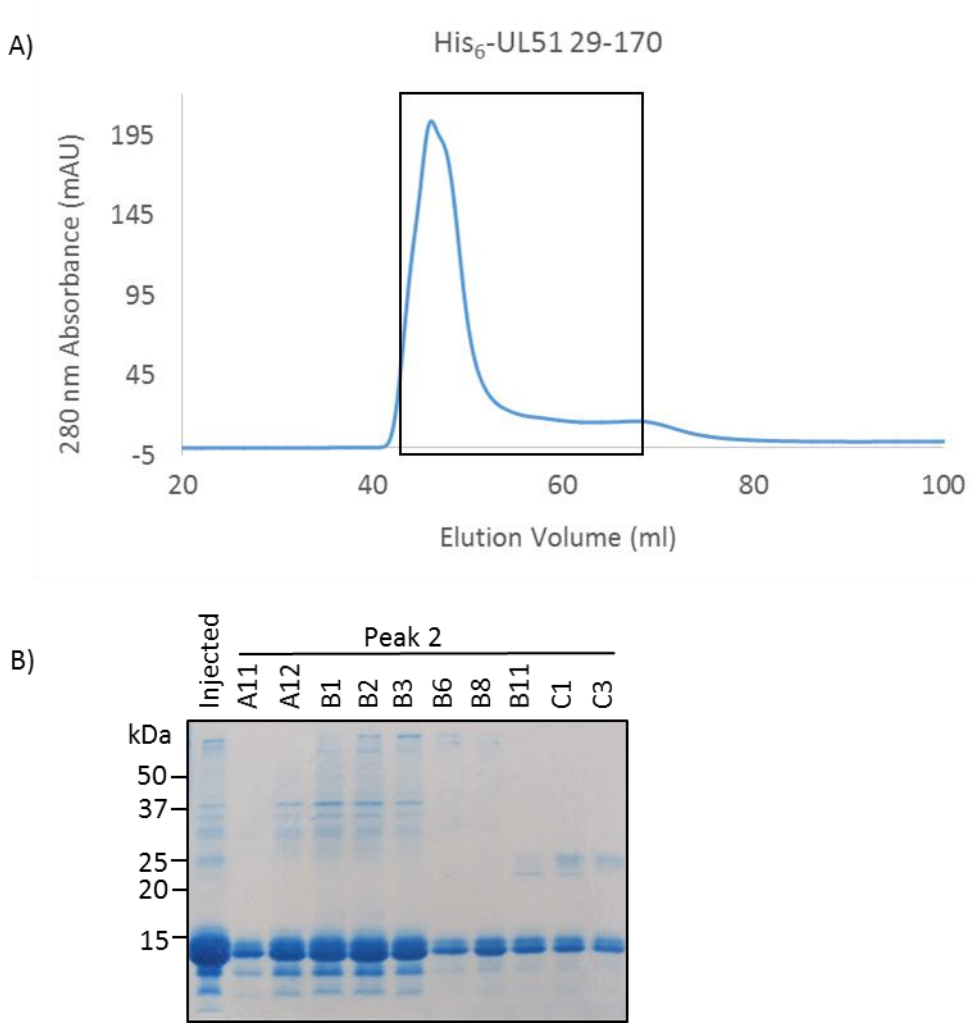

Figure 3.15 Purification of His_6-UL51 29-170
N-terminally His_6-tagged UL51 C9S 29-170 was expressed in BL21 (DE3) pLysS cells (2 L culture) at 22°C overnight and purified by affinity chromatography followed by SEC. A) S75 16/600 SEC chromatogram of His_6-UL51 29-170 showing an asymmetric peak with an extended tail. B) SDS-PAGE of SEC fractions, there is a band close to the expected molecular

mass of His_6-UL51 29-170 (16.1 kDa) that elutes across the SEC peak including the extended tail region. Such an elution profile is indicative of unfolded/misfolded protein.

3.7 Generation of monoclonal antibodies against UL7 and UL51

Purified full-length UL51 and UL7 were used to raise monoclonal antibodies, to enable the study of these proteins in the context of viral infection. Soluble wild-type, full-length His_6-UL51 protein was readily obtained from expression in BL21 cells and a small amount of soluble UL7 was obtained following expression in ArcticExpress™ cells, albeit contaminated with chaperonin 60. The chaperone contaminant was not considered a problem for this purpose because UL7 specific clones were to be selected during the hybridoma screening stage. The antibodies were generated in-house according to the following protocol: two BALBc mice were infected with 10^5 PFU of HSV-1 by ear scarification (performed by Dr Stacey Efstathiou), at two weeks post-infection the mice were immunised with purified UL7 or UL51 as an emulsion in Freund's adjuvant, using 50 µg per injection. After a further two weeks the mice were given a booster immunisation with purified UL7 or UL51 protein, and the spleens were harvested after three days. Hybridoma cell lines were produced by fusing homogenised spleen tissue with myeloma cells using polyethylene glycol, and were cultured in HAT (hypoxanthine-aminopterin-thymidine) medium by Susanna Colaco. Initial screening of the hybridoma supernatants was done by immunofluorescence (by Dr Colin Crump), identifying a single positive supernatant for detection of UL7 and many supernatants positive for UL51 detection, of which 24 were selected for validation by immunoblot, ELISA and immunoprecipitation. All 24 supernatants were suitable for detecting UL51 in cell lysates by immunoblot (four are shown in Figure 3.16A). ELISAs were performed with purified full-length and truncated (aa. 1-170) UL51 protein to distinguish between supernatants that recognise epitopes in the N- and C-terminal regions of UL51. Thirteen supernatants tested positive by ELISA: six recognised epitopes within the first 170 residues of UL51, the reminder were presumed to bind epitopes within the 171-244 region since they recognised full-length UL51 but not the N-terminal truncation. Four supernatants were tested for the ability to immunoprecipitate UL51: two of each recognising epitopes in the N- and C-terminal regions; of these one N-terminal binder and two C-terminal binders were able to immunoprecipitate GFP-UL51 from transfected HEK 293T cells (Figure 3.16B). Table 3-3 lists the hybridoma cell lines that were cloned out and cultured to larger volumes, supernatants were harvested and antibodies purified using a HiTrap Protein G HP column. Once purified, the antibodies were stored at 4°C in PBS supplemented with sodium azide. The 2A4 clone ceased to recognise UL51 after being cloned out and was not used for any experiments in this thesis.

Table 3-3 Mouse monoclonal αUL7 and αUL51 antibodies raised for this study
IP: Immunoprecipitation; WB: immunoblot.

Clone	Antigen	Binding region	Suitable for	Isotype
B1134	UL7	Unknown	IF, WB	IgG_{2B}
2C5	UL51	1-170	IF, ELISA, WB	Unknown
3D3	UL51	1-170	IF, ELISA, WB, IP	IgG_1
2A4	UL51	171-244	IF, ELISA, WB, IP	Unknown
2B3	UL51	171-244	IF, ELISA, WB, IP	IgG_1

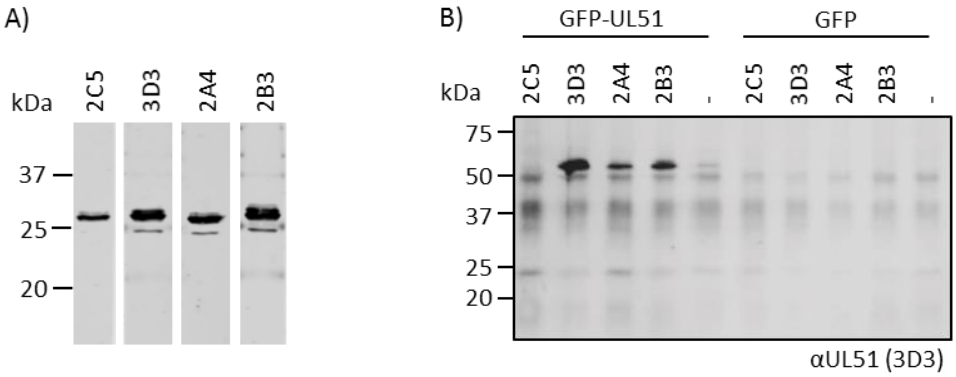

Figure 3.16 Validation of αUL51 antibodies for immunoblot and immunoprecipitation
A) Immunoblot of purified His_6-UL51 C9S full-length protein using four different UL51 antibody clones: 2C5, 3D3, 24A and 2B3. All four αUL51 clones detect the purified UL51 protein, of them 2C5 is the weakest and unlike the other three detects one not two bands. B) HEK 293T cells were transfected with GFP-UL51 or GFP only, the cells were lysed and incubated with the each of the UL51 antibodies. Protein A/G beads were used to capture the UL51 antibody and immunoprecipitate GFP-UL51. The αUL51 clones: 3D3, 2A4 and 2B3, but not 2C5, were able to immunoprecipitate GFP-UL51 and not GFP alone. Cell lysate was also incubated with Protein A/G beads in the absence of αUL51 antibody to control for non-specific binding to the beads, this sample lane is denoted by '-' in the image.

3.8 HSV-1 proteins UL7 and UL51 form a complex

3.8.1 Co-transfection of GFP-UL7 and untagged UL51

As mentioned in the introduction to this chapter, the HSV-1 UL7 and UL51 proteins are putative interaction partners based on Y2H screen data, and the comparable growth profiles of the single and double deletion viruses. To test this hypothesis a co-immunoprecipitation experiment was performed as follows: HEK 293T cells were co-transfected with GFP-UL7 and untagged UL51, after 24 h the cells were lysed and incubated with GFP-Trap™ beads for 1 h then washed and bound protein was eluted in SDS-PAGE loading buffer for analysis by immunoblot. This experiment appears to show an interaction between GFP-UL7 and full-length UL51, and a shorter UL51 construct encompassing

residues 1-207 (Figure 3.17). UL51 1-170 was not detected in the input lane in this or other transfection experiments, suggesting that the construct is not stable in cells. The UL51 full-length protein was always detected as two close bands when expressed in cells. The presence of multiple bands for UL51 was attributed to either phosphorylation or palmitoylation of the protein in cells. UL51 was not detected in lysates of cell that were co-transfected with GFP control plasmid as opposed to GFP-UL7, this was always the case when the experiment was repeated and indicates that UL51 protein may be unstable in cells when UL7 is absent. Therefore, it is not possible to rule out the possibility that UL51 could be binding GFP.

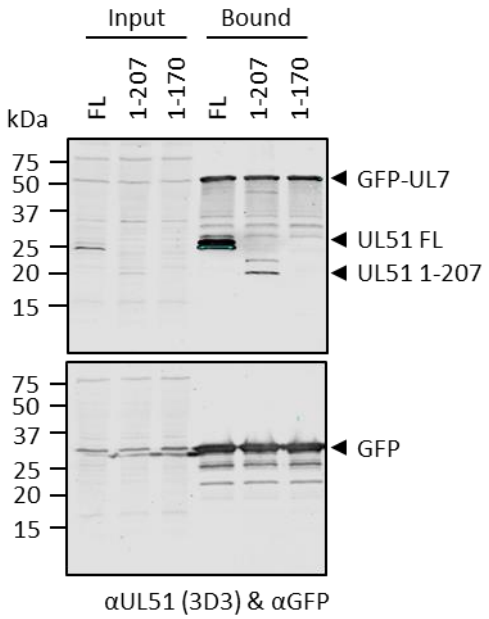

Figure 3.17 GFP-UL7 co-immunoprecipitates untagged UL51 from co-transfected cells
HEK 293T cells were co-transfected with EGFPC1-UL7 or EFGPC1 and pcDNA3-UL51 full-length, 1-207 or 1-170. GFP-UL7 was captured on GFP-Trap™ beads then washed. The bound sample was eluted in SDS-PAGE loading buffer. The samples were resolved by SDS-PAGE and visualised by western blot (αGFP and αUL51). The top image shows co-immunoprecipitation of GFP-UL7 with full-length UL51 and the UL51 1-207 truncation. UL51 1-170 was not visible in either the input or bound lanes. UL51 was not detected in lysates of cell that were co-transfected with EGFPC1 only as shown in the bottom blot, this was always the case when the experiment was repeated and suggests that UL51 may be unstable in cells when UL7 and/or other viral proteins are absent.

3.8.2 UL7-UL51 interaction is direct

Purified protein was used to ascertain whether the UL7-UL51 interaction is direct, and also to determine if the interaction is unique to HSV-1. To do this, an *in vitro* GST pull-down experiment was performed using purified HSV-1 proteins and the homologues from MHV. To perform the pull-down experiment a GST-tagged bait protein was immobilised on magnetic GSH beads, washed and then

incubated with prey protein. Ideally, the pull-down would be performed in both directions i.e. with GST-UL7 vs UL51 and GST-UL51 vs UL7, however, only the former was possible due to the inability to produce His_6-tagged or untagged UL7. The experiment was designed with GST-UL7 and GST-ORF42 bait proteins, which were then incubated with His_6-UL51 C9S and His_6-ORF55 C3S+C4S prey constructs as shown in Figure 3.18. Despite the concerns that the UL51 proteins may not be fully folded (based on SEC chromatograms), this experiment shows that there is a specific and direct interaction between UL7 and UL51, and also maps the binding region to within the U44-domain of UL51. The interaction is conserved between the MHV homologues, but not between the alpha and gamma herpesvirus proteins. Thus, the UL7-UL51 interaction is direct and conserved within at least one other herpesvirus.

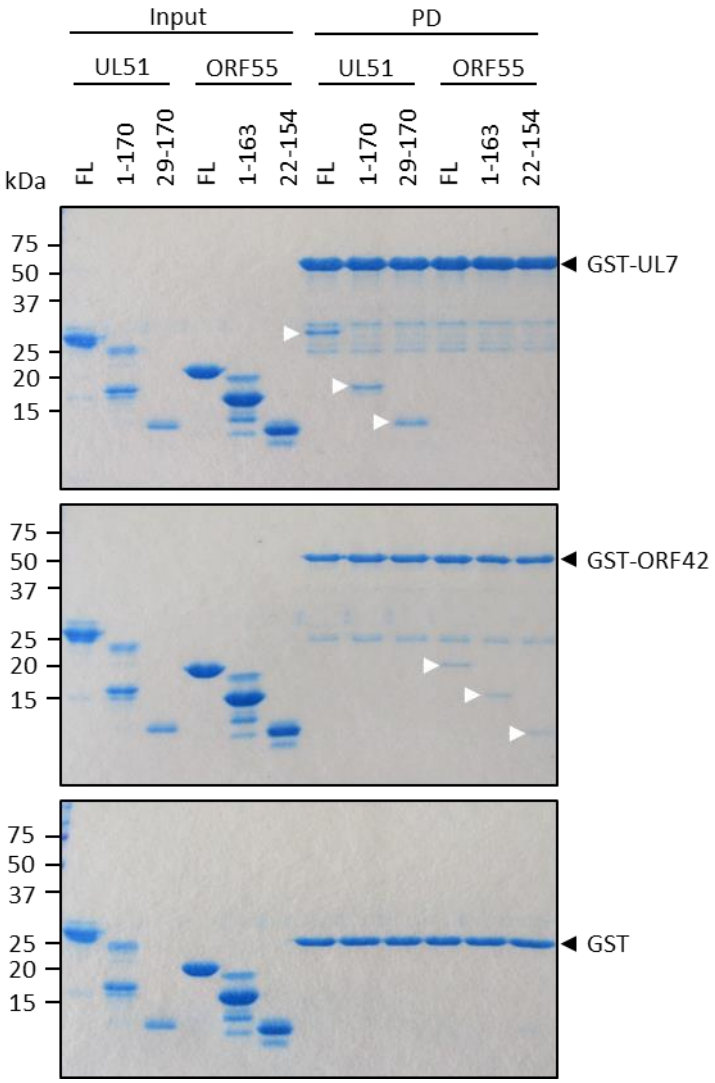

Figure 3.18 The UL7-UL51 interaction is direct and conserved
Purified GST-tagged UL7 and ORF42 were used as bait proteins to capture full-length and truncated His_6-UL51 C9S and His_6-M_ORF55 C3S+C4S prey proteins in GST pull-down experiments. All UL51 constructs are pulled-down by UL7, confirming that this is a direct interaction and mapping the binding region to within residues 29-170 of UL51. The M_ORF55 proteins are pulled-down by M_ORF42 demonstrating that the interaction is

conserved in at least one other herpesvirus, but not between the viruses since UL7 from HSV-1 is unable to pull-down M_ORF55 and *vice versa*.

3.8.3 The UL7-UL51 interaction occurs during infection

To determine whether the UL7-UL51 interaction occurs during infection, antibodies capable of specifically detecting the endogenous viral proteins were generated for immunoprecipitation and immunofluorescence experiments, as described in section 3.7. Immunoprecipitation of UL51 from infected cell lysates was performed using two antibodies: the 3D3 antibody that binds within residues 1-170 and the 2B3 antibody that recognises the 171-244 region of UL51. HaCaT cells were infected with wild-type HSV-1, ΔUL51 HSV-1 or mock infected, and harvested at 16 h.p.i.. The lysates were incubated with either the 3D3 or 2B3 antibody then captured on Protein A/G beads, the beads were washed then boiled in SDS-PAGE loading buffer. Panel A, of Figure 3.19 shows successful immunoprecipitation of UL51 with both antibodies, and co-immunoprecipitation of UL7 but only when the 2B3 antibody is used for UL51 capture. Since the 3D3 antibody binds to UL51 within the UL7 binding region, as determined by the *in vitro* pull-down experiment (section 3.8.2), it was concluded that the 3D3 antibody occludes the UL7 binding site. Interestingly, there is no detectable UL7 in the ΔUL51 cell lysate (Panel A, of Figure 3.19), it has also been observed that the ΔUL7 virus has lower levels of UL51 expression compared to wild-type HSV-1 [277]. These observations suggest that UL7 and UL51 are less stable when expressed alone, being perhaps more prone to misfolding or aggregation and subsequent degradation. It was not possible to perform this experiment in the opposite direction because the UL7 antibody does not efficiently capture UL7 in immunoprecipitation experiments, instead, HaCaT cells were infected with YFP-UL7 tagged HSV-1 virus, allowing YFP-UL7 to be captured on GFP-Trap^{TM} beads. Figure 3.19 panel C shows that YFP-UL7 is able to specifically immunoprecipitate UL51 from infected cells, thus the interaction can be detected in the reciprocal direction.

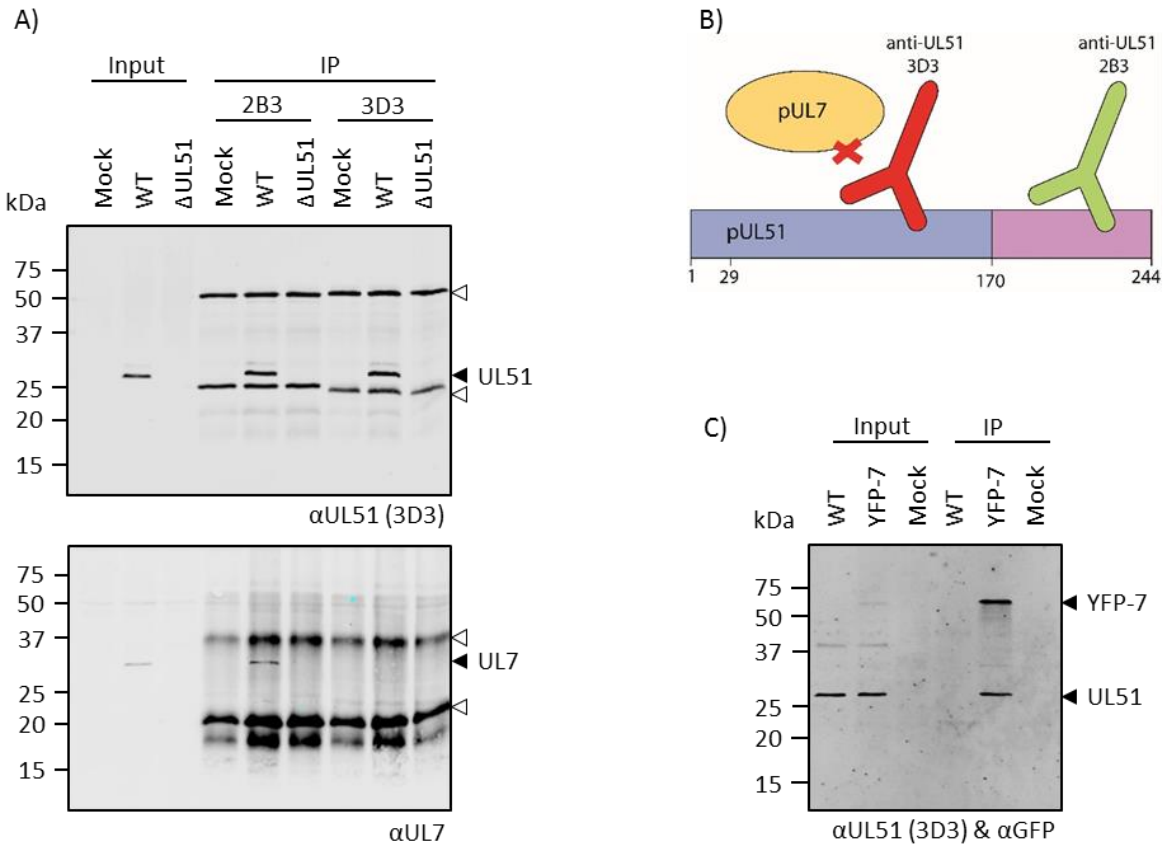

Figure 3.19 Immunoprecipitation of the UL7-UL51 complex from infected cells
HaCAT cells were infected with either wild-type (WT) HSV-1, a HSV-1 mutant lacking the UL51 gene (ΔUL51) or mock infected. Two αUL51 antibodies were used to immunoprecipitate UL51 from the infected cell lysates: 3D3 and 2B3. A) Western blot showing the immunoprecipitation of UL51 with both the 2B3 and 3D3 antibodies from WT HSV-1 infected cell lysates (top), and co-immunoprecipitation of UL7 with the 2B3 but not the 3D3 antibody (bottom). White arrowheads highlight the UL51 antibody heavy and light chains. B) The 3D3 antibody binds within the first 170 residues of UL51, which is within the UL7-binding region, thus the 3D3 antibody likely blocks the interaction between UL51 and UL7. C) GFP-Trap™ immunoprecipitation experiment from HaCaT cells infected with either WT or HSV-1 expressing YFP-tagged UL7 (YFP-7). A western blot was performed and the membrane was probed with αGFP and αUL51 (3D3). YFP-UL7 and UL51 are shown to co-immunoprecipitate.

3.9 Discussion

The aim at the start of this work was to express and purify samples UL7 and UL51 from *E. coli* in order to investigate the putative UL7-UL51 interaction, through the generation of monoclonal antibodies and their use in pull-down experiments. The aim was also to produce sufficient quantities of pure UL7, UL51 and their homologues for X-ray crystallography and biophysical studies. Large-scale expression was achieved for UL7, UL51 and the respective MHV homologues ORF42 and ORF55 with varying levels of success. The MHV proteins proved to be amenable to purification and gave high overall protein yields, however, the samples often contained degradation products that could not be

separated by anion exchange and failed to produce crystals. The proteins from HSV-1 were generally more difficult to work with, UL7 in particular, and produced much lower yields. Sufficient GST-tagged UL7 was produced for pull-down experiments, but it was not possible to produce the quantities of soluble protein required for structural studies. The UL51 constructs could be purified, though again, there was evidence of protein degradation occurring, which could not be separated, nor were any crystals forthcoming. While structural insights could not be achieved with these samples, they were used to demonstrate a direct interaction between UL7-UL51 and to show that this complex is also formed by the homologous proteins in MHV. The purified proteins were also used to generate monoclonal antibodies, which were successfully employed to provide evidence of the UL7-UL51 interaction in the context of HSV-1 infection.

Work done by Dr Anna Albecka provides further evidence for the UL7-UL51 interaction during infection. Dr Albecka performed immunofluorescence experiments on either transfected or HSV-1 infected cells. Her data show that UL7 and UL51 co-localise to focal adhesions in HSV-1 infected and co-transfected cells, but only when both proteins are present [277]. Expression levels of UL7 are diminished in the ΔUL51 virus and *vice versa*, suggesting that the stability and localisation of either UL7 or UL51 is dependent on the expression of the other. Cells infected with double-deletion HSV-1 (ΔUL7+ΔUL51) have less pronounced focal adhesions and detach from the tissue culture dish faster than wild-type infected cells. Therefore, the UL7-UL51 complex has been proposed to stabilise focal adhesions during infection [277]. A similar phenotype has been reported for cells infected with VZV deficient in the UL51 homologue ORF7 [307]. Focal adhesions are necessary for lamellipodium and filopodium extension and also for maintaining contacts to the extracellular matrix [308]. HSV-1-infected cells can form long filopodium-like projections that are thought to aid the transfer of virions to neighbouring cells [309]. By stabilising focal adhesions the UL7-UL51 complex could enhance cell-to-cell transmission, which may contribute to the small plaque phenotype reported for the mutant viruses [277].

During the course of this study, evidence of the UL7-UL51 interaction in infected cells was published by another group. Their data show co-localisation of UL7 and UL51 close to the nucleus and suggest that this is driven by palmitoylation-dependent membrane association of UL51 [139]. However, they did not report focal adhesion localisation, possibly due to the technical difficulty of visualising these structures in Vero cells, which they used in their study. The low stability of UL7 in cells in the absence of UL51 mirrors the behaviour of this protein when it is expressed and purified from *E. coli*. Based on this insight, it was decided that future attempts to purify the proteins for structural studies would focus on obtaining the UL7-UL51 complex rather than the individual proteins in isolation.

4 Expression, purification and crystallisation of the UL7-UL51 complex

4.1 Introduction

The experimental data presented in results chapter one shows that UL7 and UL51 from HSV-1 form a complex in infected cells and that the interaction is direct. While it was possible to purify enough protein for the *in vitro* pull-down experiments, sufficient quantities of high-purity untagged or His_6-tagged UL7 suitable for crystallisation experiments could not be obtained. Correct localisation of UL7 and UL51 during infection is dependent on the formation of the complex [277]. Furthermore, the expression levels of either protein in the absence of its partner is diminished during infection [277]. Thus, it was concluded at the end of results chapter one that any further attempts to purify UL7 and UL51 for structural studies would focus on obtaining the proteins as a complex rather than purifying them individually. This approach offers two advantages: Firstly, if the complex is the functional unit in the cell then its crystal structure could be more informative than the proteins on their own; Secondly, in many cases, proteins that form complexes in cells are poorly folded when expressed in a heterologous system without their cellular partner(s). The absence of a binding partner can result in the presence of solvent-exposed hydrophobic patches on the surface of the protein, which can lead to the formation of insoluble aggregates known as inclusion bodies. One indication of inclusion body formation is a thick, pale looking pellet after clearing the cell lysate by centrifugation, and this was often observed for the UL7 and UL51 proteins when expressed recombinantly in *E. coli*. It was hoped that protein expression and solubility would improve for both UL7 and UL51 when expressed as a complex. In addition to crystallisation experiments, there arose the opportunity to perform small angle X-ray scattering (SAXS). SAXS experiments generate low resolution structural data of a protein/complex in solution. The overall shape or 'envelope' of the protein molecule or complex can be determined by SAXS without requiring crystallisation. SAXS data for UL7-UL51 and ORF42-ORF55 would be useful to compare the overall shape of the complex.

This chapter details the efforts to co-express and co-purify UL7 and UL51 from *E. coli* cells to produce protein suitable for crystallisation and SAXS. In total, three different versions of the complex were expressed and purified each containing full-length UL7 and either UL51 C9S 1-170, UL51 29-170 or UL51 C9S 8-142. The rationale for producing each version of the complex, and how they were used, is outlined in the following sections.

4.2 Co-expression of UL7-GST and His_6-UL51 C9S 1-170 in *E. coli*

4.2.1 Construct design

Protein co-expression in *E. coli* can be achieved by transforming cells with two or more plasmids encoding the genes of interest or by expressing the genes from a single plasmid. Using the latter approach the genes may be under the control of a single promoter to produce one long polycistronic mRNA, or separate promoters, resulting in multiple mRNA transcripts. A polycistronic expression plasmid, pOPC, which expresses the proteins from single mRNA, was chosen for this study because it is compatible with the pOPT vector family [282]. This meant that the constructs already made for the work described in results chapter one could be sub-cloned, along with their affinity tags, directly into pOPC. UL51 was cloned into cassette 1 of pOPC, followed by GST-tagged UL7 in cassette 2. The interaction between UL7 and UL51 has been mapped to within the first 170 residues of UL51, and since the C-terminal residues 171-244 of UL51 are proline-rich and were predicted to be disordered by RONN, His_6-UL51 C9S 1-170 was used for co-expression as it was deemed most promising for structural studies.

4.2.2 Screening for optimal protein expression conditions

A small-scale protein co-expression and co-purification screen was performed by testing three *E. coli* strains: BL21 (DE3) pLysS, Rosetta™ (DE3) pLysS and B834 (DE3), and two expression temperatures: 22°C overnight and 37°C for 4 h. Protein purification was monitored by SDS-PAGE following a crude affinity-purification step using magnetic GSH beads. Expression of His_6-UL51 C9S 1-170 and UL7-GST was achieved in all three cells lines grown at 22°C after induction of protein expression, but not in cells grown at 37°C after induction (Figure 4.1).

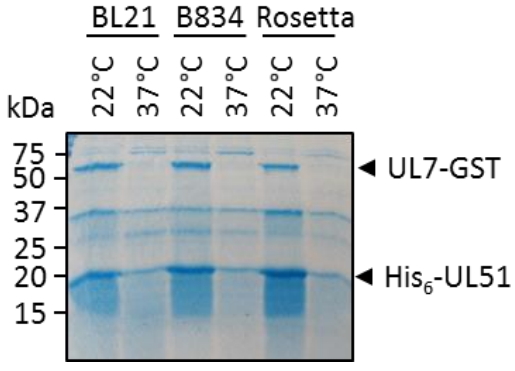

Figure 4.1 Small-scale test co-expression and co-purification of UL7-GST and His_6-UL51 C9S 1-170
N-terminally tagged His_6-UL51 C9S 1-170 and C-terminally GST-tagged UL7 were cloned into pOPC for co-expression in *E. coli* cells. Three *E. coli* strains: BL21 (DE3) pLysS, Rosetta™ (DE3) pLysS and B834 (DE3), and two expression temperatures: 22°C and 37°C were screened to identify optimal expression conditions. A small-scale affinity

purification step was then performed using GSH beads to capture GST-UL7 and associated His_6-UL51. Purified protein was eluted from the beads and analysed by SDS-PAGE. Bands at the expected molecular mass for GST-UL7 (60.1 kDa) and His_6-UL51 C9S 1-170 (19.1 kDa) are indicated by arrowheads.

4.2.3 Large-scale co-expression and purification of His_6-UL51 C9S 1-170 and UL7-GST

Large-scale co-expression of UL7-GST and His_6-UL51 C9S 1-170 was performed in BL21 (DE3) pLysS cells cultured overnight at 22°C. The aim was to co-purify UL7 and UL51 by capturing the complex on GSH beads. In brief, the cell lysate was incubated with GSH beads, these were then washed and any bound complex was eluted with glutathione - the success of this step depended on the complex remaining associated during the wash. Reduced glutathione was removed by SEC using resin equilibrated with glutathione-free buffer, and the recombinant protein was cleaved overnight to liberate the GST tag. The following day, the sample was incubated again with GSH resin to capture the free GST, any uncleaved UL7-GST and also the GST-tagged protease. The cleaved sample was further purified by SEC. For simplicity the purified UL7-UL51 complex will, henceforth, be referred to as FAB C9S 1-170 (for Focal Adhesion Binding complex containing untagged UL7 and His_6-UL51 C9S 1-170).

To determine the suitability of the purification protocol, the FAB complex was expressed and purified from a 2 L test culture. Figure 4.2 shows successful capture and co-elution of the GST-FAB C9S 1-170 complex from the GSH beads (A, 'eluate'), followed by efficient cleavage and removal of the GST tag (A, '+3C' and 'GSH FT2'). The sample injected for SEC contains UL7 and UL51 as the major species (Figure 4.2C, 'Injected') but some smaller bands are also evident. The SEC chromatogram shows a single peak with a slight trailing tail on the right (Figure 4.2B), SDS-PAGE of the peak fractions confirms the presence of cleaved UL7 and His_6-UL51 C9S 1-170. The complex was predicted to form in a 1:1 ratio based on coomassie-stained SDS-PAGE bands. An extinction co-efficient for the complex was estimated as the theoretical extinction co-efficient of the combined polypeptide sequences of the two proteins, assuming a 1:1 ratio, as calculated using the ProtParam server [310]. This was used to calculate protein concentration from 280 nm absorbance values. The test purification yielded approximately 0.5 mg/L of culture, the complex was purified repeatedly using this protocol and with practice a routine yield of ≈1.0 mg/L of culture could be achieved. Compared to the proteins on their own, the complex was much more soluble and could be concentrated to at least 14.3 mg/ml with little precipitation. There are some additional bands that run below the UL51 protein in the SDS-PAGE gel (Figure 4.2C), which were predicted to be UL51 degradation products because a similar pattern is observed when His_6-UL51 C9S 1-170 is purified alone, furthermore, these bands could be detected by an αUL51 (3D3) antibody (Figure 4.2D).

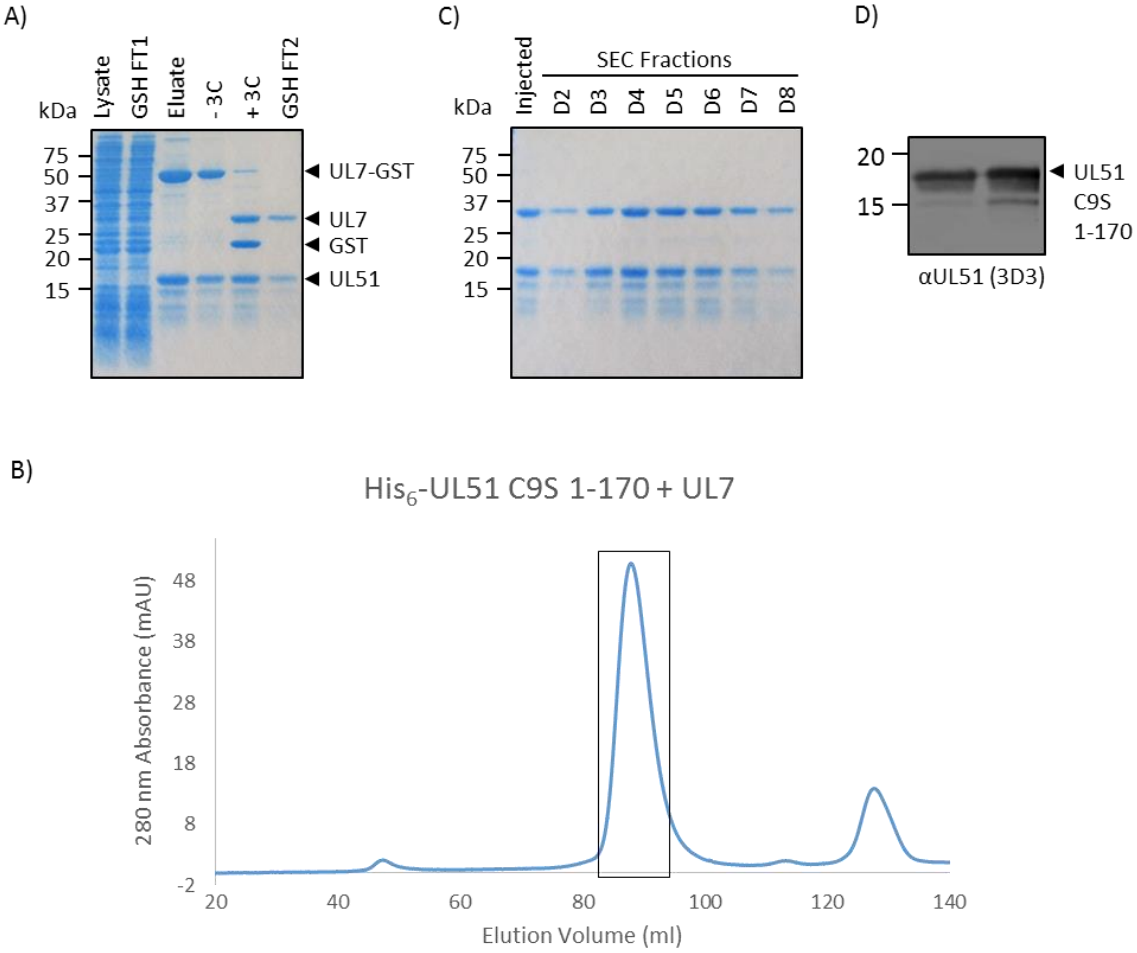

Figure 4.2 Purification of UL7 and His_6-UL51 C9S 1-170 (FAB C9S 1-170)
N-terminally His_6-tagged UL51 C9S 1-170 and C-terminally GST-tagged UL7 were co-expressed in BL21 (DE3) pLysS cells (2 L culture) at 22°C overnight. UL7-UL51 complex (GST-FAB C9S 1-170) was purified by GSH affinity chromatography, followed by the removal of the GST tag and SEC. A) GSH affinity purification of the GST-FAB C9S 1-170: bands at the expected molecular mass for UL7-GST and His_6-UL51 C9S 1-170 are present in the sample eluted from the GSH beads. The sample was incubated with PreScission 3C protease to remove the GST tag, before (-3C) and after (+3C) protease treatment lanes show successful cleavage of the GST tag from UL7. GSH beads were used to capture the free GST, the GST-tagged protease and any uncleaved GST-UL7. The Flow-through (GSH FT2) contains bands for cleaved UL7 (33.2 kDa) and His_6-UL51 C9S 1-170 (19.1 kDa). B) The GSH FT2 sample was further purified by SEC chromatography using an S200 16/600column. C) SDS-PAGE of the peak fractions showing co-elution of UL7 and His_6-UL51 C9S 1-170 from SEC, indicating that the complex remains intact. D) Immunoblot of purified complex for UL51 using the αUL51 (3D3) antibody, showing a UL51 degradation band.

4.3 Crystallisation of FAB C9S 1-170

4.3.1 Nanolitre-scale sparse-matrix screening for FAB C9S 1-170

Initial screening of crystallisation conditions for the FAB C9S 1-170 complex was performed using commercially available sparse-matrix screens and different protein concentrations. An Innovadyne Screenmaker robot was used to dispense reservoir and protein drops (200 nl : 200 nl) into 96-well MRC sitting drop plates, pre-filled with 96 different precipitant conditions. Plates were stored and imaged at 20°C by a Formulatrix imaging robot. A list of the commercial sparse-matrix screens that were available is presented in Table 2-6, page 43.

Crystallographic experiments were attempted using a number of different crystallisation screens and FAB C9S 1-170 complex at: 7.6 mg/ml, 10.1 mg/ml, 12.3 mg/ml and 14.3 mg/ml. Several conditions from these initial screens produced either interesting phase separation, granular precipitation, spherulites or very small crystalline particles (Table 4-1). The most promising conditions were from screen CIMR7, wells: C7, D7 and E5, which produced many, very fine needles at a protein concentration of 10.1 mg/ml. The needles took between 11 and 22 days to grow and were hardly visible in the images taken by the Formulatrix robot. Drops containing protein at 7.6 mg/ml remained mostly clear for several days before some light precipitation occurred. After 11-22 days fine needles, this time resembling pincushions, grew in well F7 of the CIMR5 screen at 7.6 mg/ml. In an attempt to increase the size of the crystals, crystallisation experiments were attempted using the same commercial screens with FAB C9S 1-170 protein at 14.3 mg/ml. Of the drops prepared at this concentration, 65% contained either spherulites or promising granular precipitate that appeared within 12 h, but none contained crystalline material - such observations are indicative of rapid nucleation occurring when using the proteins at high concentration (14.3 mg/ml). In an attempt to slow the rate of nucleation, follow-up experiments were performed using protein at a concentration of 12.3 mg/ml, and a selection of screens were incubated at 4°C. At this concentration the spherulites no longer appeared, nor did any crystalline material. Reducing the incubation temperature to 4°C did not result in any crystal growth. Thus, the fine needles and pincushions that grew at 10.1 mg/ml and 7.6 mg/ml respectively could not be improved upon nor were they reproducible in the same conditions at any other protein concentration.

Table 4-1 FAB C9S 1-170 crystallisation hits from sparse-matrix screens

Well	Condition	Concentration	Image
CIMR5 F7	0.1 M di-sodium succinate, 12% PEG 3,350	7.6 mg/ml	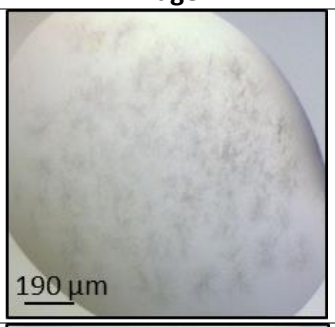
CIMR7 C7	0.2 M NaCl, 0.1 M HEPES pH 7.0, 20% PEG 6,000	10.1 mg/ml	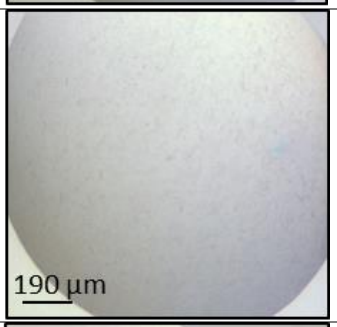
CIMR7 D7	0.2 M NaCl, 0.1 M Tris pH 8.0, 20% PEG 6,000	10.1 mg/ml	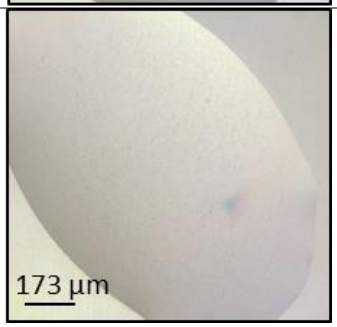
CIMR7 E5	0.2 M sodium nitrate, 20% PEG 6,000	10.1 mg/ml	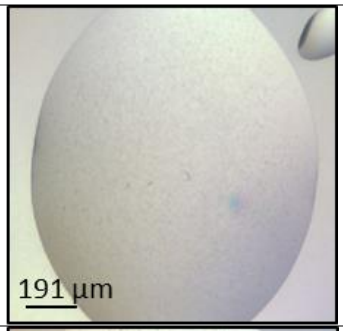
CIMR7 C7	0.2 M NaCl, 0.1 M HEPES pH 7.0, 20% PEG 6,000	14.3 mg/ml	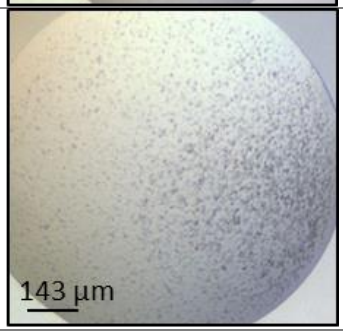

Well	Condition	Concentration	Image
CIMR5 E6	0.2 M sodium malonate pH 6.0, 20% PEG 3,350	14.3 mg/ml	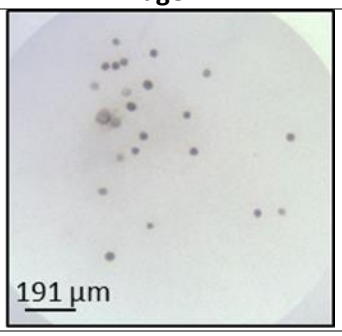

4.3.2 4-row optimisation screens for FAB C9S 1-170

Preliminary crystallisation conditions, which yielded fine needles, were identified by the sparse-matrix screens as outlined in section 4.3.1. Needles are one dimensional crystals that provide a promising starting point for further optimisation. 4-row optimisation experiments were performed for the conditions where needles grew: CIMR7, wells C7, D7, E5 and CIMR5 well F7, such experiments screen around the condition by adjusting the precipitant concentration and the protein-to-reservoir drop ratio, thus altering the equilibration kinetics. For CIMR7 conditions the FAB C9S 1-170 protein was used at 9.6 mg/ml, and at 7.6 mg/ml for the CIMR5 screen. A dilution series starting at 100% precipitant solution and being diluted in 5% steps to 45% with Milli-Q^{TM} water was prepared across the four rows of a 96-well plate. Four drop ratios were tested, one for each row: 100 nl protein (P): 100 nl reservoir (R), 200P:100R, 100P:200R, 200P:200R. The precipitant solutions were made by combining and diluting pre-made stocks from Molecular Dimensions salt and buffer kits. The drops were dispensed using an Innovadyne Screenmaker and the plates were stored and imaged in a Formulatrix imaging robot. Unfortunately, the crystals could not be reproduced in any of the conditions tested, instead the protein rapidly precipitated in all conditions. To rule out possible variations in buffer composition, the experiment was repeated using the complete ready-made commercial buffers for conditions: CIMR7, well C7 and CIMR5, well F7, but again the protein rapidly precipitated in all drops. Temperature was ruled out as a variable by equilibrating the optimisation screen at the same temperature as the original screen before dispensing the drops. And the order in which the drops were dispensed was switched i.e. dispensing the protein drop into the reservoir drop when preparing the experiment and *vice versa,* but did not prevent the protein from rapidly precipitating.

4.3.3 48-well grid screening for FAB C9S 1-170

Grid-screening was also employed to optimise the crystallisation conditions. Grid-screens systematically sample two variables from the original crystallisation condition e.g. pH and precipitant concentration. Three conditions from the preliminary sparse-matrix screens were selected for grid screening: CIMR7, wells C7 and D7 (at 9.6 mg/ml) and also CIMR5, well F7 (at 7.6 mg/ml). These were

dispensed by hand in 48-well sitting drop plates (1 µl protein : 1 µl reservoir). Figure 4.3 shows the screen designed for CIMR7 C7 - salt and buffer concentration remain constant while buffer pH and PEG 6,000 concentration vary. Similarly, salt and buffer concentration were held constant for CIMR7 D7 while pH and PEG 6000 were varied as follows: pH 7.8, 8.0, 8.2, 8.4 versus PEG 6,000 at 16%, 18%, 20%, 22%, 24%, 26%. For CIMR5 F7 the grid-screen was designed as follows: di-sodium succinate at 0.08 M, 0.09 M, 0.1 M, and 0.12 M versus PEG 3,500 at 8%, 10%, 12%, 15%, 16%, and 18%. As was observed with the 4-row optimisation screens, the FAB C9S 1-170 protein precipitated almost immediately in all drops, including in the original conditions from the sparse-matrix screens.

		PEG 6,000 (%)					
		16	18	20	22	24	26
pH	6.8						
	7.0			x			
	7.2						
	7.4						

Figure 4.3 Grid screen designed to sample around the CIMR7 C7 condition
Sparse-matrix screening for crystallisation conditions was performed with the FAB C9S 1-170 protein sample. The following condition yielded crystals: 0.1 M HEPES pH 7.0, 0.2 M NaCl, 20% PEG 6,000. Grid screening was performed around this condition in an attempt to optimise the crystals. The grid-screen was performed in 46-well plates, the concentration of PEG 6,000 and the pH of the HEPES buffer whilst salt and buffer concentration was maintained.

4.3.4 Limited proteolysis of FAB C9S 1-170

Limited proteolysis of the FAB C9S 1-170 complex was attempted, this approach uses a low concentration of a non-specific protease to excise regions of the protein that exhibit enhanced flexibility i.e. unfolded regions and flexible loops, whilst maintaining the core protein fold intact [311]. The technique is typically used to probe for protein conformational changes and to identify protein domains that can fold autonomously. Limited proteolysis can increase the chance of crystallisation by generating conformationally-stable protein domains/folds. The FAB C9S 1-170 complex was pre-incubated with subtilisin in a 1:5000 molar ratio before use in crystallisation experiments. In this instance, subtilisin treatment had little effect on the UL7 and UL51 proteins based on a side-by-side comparison of treated and untreated samples by SDS-PAGE (Figure 4.4), nor did subtilisin treatment yield crystals in the sparse-matrix screens tested (CIMR5, 7, 11 and 15) using FAB C9S 1-170 at 10.1 mg/ml or 12.3 mg/ml.

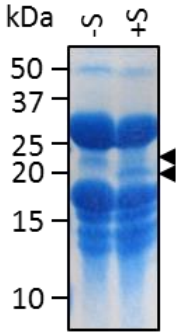

Figure 4.4 Subtilisin treatment of FAB C9S 1-170
The FAB C9S 1-170 complex was incubated with subtilisin in a 1:5000 molar ratio. SDS-PAGE shows the sample before (-S) and after (+S) treatment. The samples are almost identical except for the presence of the bands indicated by the arrowheads. This may represent a protein band shift as a result of subtilisin treatment, alternatively the band in the +S lane could be subtilisin itself (predicted molecular mass ≈26 kDa).

4.3.5 Large-scale expression and purification of untagged FAB C9S 1-170

After extensive sparse-matrix screening with FAB C9S 1-170, which only yielded fine needles, and the failed attempts to optimise these needles, it was decided to re-examine the UL51 construct used in the protein sample. Differences of a few residues at the N or C terminus can have dramatic effects on protein solubility and protein crystallisation. Also, purification tags can impinge on protein folding, so for this reason it was decided to remove the His_6 tag from UL51 since it is not required for the purification. QuickChange was used to delete the His_6 tag from the co-expression construct, and the complex was expressed and purified as described in section 4.2.3. This construct had a lower yield, ≈0.5 mg/L of culture compared to the ≈1.0 mg/L of culture that could be achieved with the His_6-tagged FAB C9S 1-170 construct. Figure 4.5A shows that the SEC peak fractions contain fewer degradation bands compared to the tagged FAB C9S 1-170 sample (Figure 4.2), this might be due to removal of the His_6 tag or a result of switching from a S200 16/600 to a higher resolution S200 10/300 column. There is however a notable band at ≈13 kDa that was present in all purification attempts of this construct and was suspected to be a UL51 degradation product. The sample was soluble and could be concentrated to at least 9.9 mg/ml; the latter fractions show co-elution of GST with the complex and for this reason they were excluded.

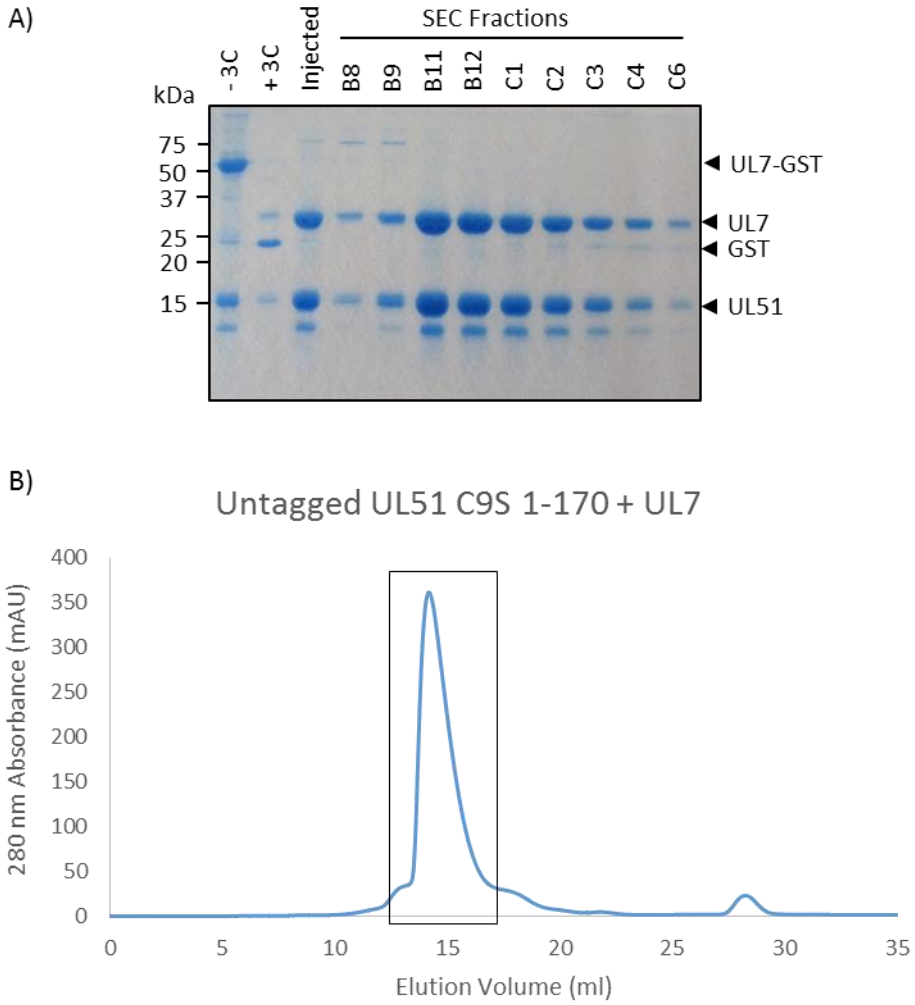

Figure 4.5 Purification of UL7 and untagged UL51 C9S 1-170 (untagged FAB C9S 1-170) Untagged UL51 C9S 1-170 and C-terminally GST-tagged UL7 were co-expressed in BL21 (DE3) pLysS cells at 22°C overnight. UL7-UL51 complex (untagged FAB C9S 1-170) was purified by GSH affinity chromatography, followed by the removal of the GST tag and SEC. A) SDS-PAGE of fractions after GSH affinity purification of the complex and cleavage of the GST tag from UL7 by 3C PreScission Protease. Samples taken before (-3C) and after (+3C) overnight incubation with human rhinovirus 3C protease are shown. The injected sample shows successful capture of the cleaved GST, uncleaved UL7-GST and the GST-tagged protease. The SEC fractions contain bands at the expected molecular mass for untagged UL7 (33.2 kDa) and untagged UL51 C9S 1-170 (18.1 kDa), showing that both proteins co-elute from SEC, indicating that the complex is intact. B) S200 10/300 SEC chromatogram corresponding to the fractions shown in panel A.

4.3.6 Crystallisation screens for untagged FAB C9S 1-170

Sparse-matrix crystallisation screening experiments for untagged FAB C9S 1-170 were performed using protein at 9.2 mg/ml (screens: CIMR5 and 13) or 9.9 mg/ml (CIMR4, 7, 8, 11 and 15). After 8 months there was no crystalline material in any of the drops, nor was it possible to reproduce the crystals that grew with His_6-tagged FAB C9S 1-170 in CIMR7. Of the 672 conditions, 31% drops remained clear, 48% contained light precipitation and 21% contained heavy precipitation.

4.3.7 Reductive methylation of untagged FAB C9S 1-170

Reductive methylation is a standard crystallisation “rescue” strategy, aimed at improving the crystallisation properties of a protein by reducing the conformational entropy of intrinsically flexible surface lysine residues [312]. A way to achieve this is through lysine methylation, thereby, switching the lysine side chain functional group from a primary to a tertiary amine to promote intermolecular interactions over solvent interactions. Reductive methylation was attempted for untagged FAB C9S 1-170: UL51 C9S 1-170 contains three lysine residues and UL7 contains five. Tris buffer is unsuitable for reductive methylation because it contains primary amines that are capable of reacting with the methylation reagents (dimethylamine borane complex and formaldehyde). Therefore, it was necessary to purify the untagged FAB C9S 1-170 in an amine-free buffer, and HEPES was chosen. The initial purification stages progressed well. However, following the overnight cleavage of the GST tag from UL7, flakes of precipitation were visible in the protein sample. The sample was incubated again with GSH resin to capture the free GST, any uncleaved UL7-GST and also the GST-tagged protease, then was further purified by SEC. SDS-PAGE of the SEC peak fractions only show a band of the appropriate size for UL51 and no band for cleaved UL7 (Figure 4.6). It was concluded that HEPES buffer resulted in UL7 protein precipitation, either by directly destabilising the UL7 protein and causing it to precipitate or by disrupting the UL7-UL51 interaction. Reductive methylation remains to be attempted, a buffer besides Tris or HEPES, needs to be identified that can maintain the complex in solution e.g. phosphate buffer.

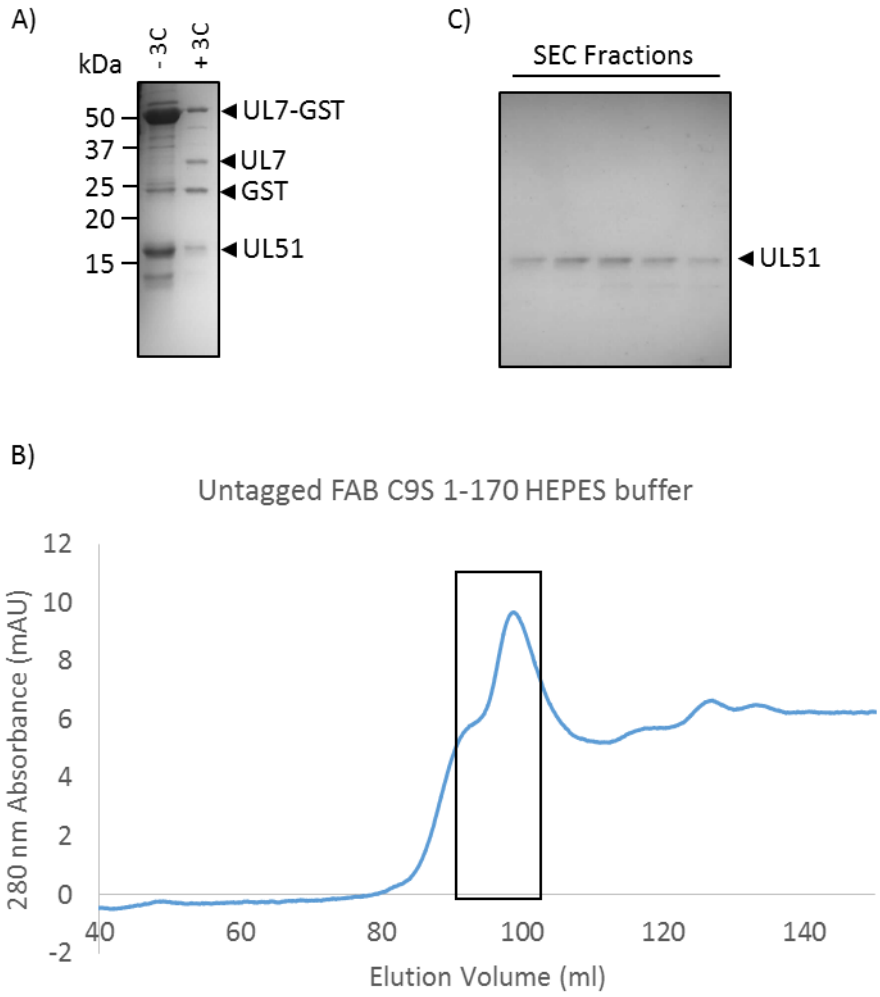

Figure 4.6 Purification of untagged FAB C9S 1-170 in HEPES buffer
Untagged UL51 C9S 1-170 and C-terminally GST-tagged UL7 were co-expressed in BL21 (DE3) pLysS cells at 22°C overnight. UL7-UL51 complex (untagged FAB C9S 1-170) was purified by GSH affinity chromatography, followed by the removal of the GST tag and SEC. The protein was purified in HEPES buffers, as opposed to Tris, so that reductive methylation could be performed. A) SDS-PAGE of the complex before (-3C) and after (+3C) overnight incubation with human rhinovirus 3C protease, showing cleavage of the GST tag from UL7. B) S200 16/600 SEC chromatogram after free GST, uncleaved UL7 and the GST-tagged protease was removed by GSH affinity purification. C) SDS-PAGE of the SEC peak fractions showing only His_6-UL51 C9S 1-170 and no cleaved UL7.

4.3.8 Summary of crystallisation attempts with tagged and untagged FAB C9S 1-170

Extensive sparse-matrix screening, condition optimisation (i.e. 4-row optimisation and grid-screening) and several rescue strategies (i.e. limited proteolysis, affinity tag removal, and reductive methylation) were utilised whilst trying to crystallise FAB C9S 1-170. The most promising outcomes were fine needles, pincushions, granular precipitate and spherulites. It is not known whether the needles and pincushions were protein or salt since they were too small to harvest for diffraction

experiments, and unfortunately it was not possible to improve on the needles nor reproduce them in the optimisation screens or in sparse-matrix screens at different concentrations. There are many variables that could explain the inability to replicate the original needles in the 4-row optimisation and grid screens: i) batch variation in FAB C9S 1-170 protein; ii) fresh protein versus protein that had been thawed after plunge freezing in liquid nitrogen; iii) slight difference in the protein concentration used; iv) order in which the drops were dispensed i.e. protein then reservoir and *vice versa;* v) temperature and, vi) the origin of the reagents. It was possible to rule out temperature, drop order, reagents and fresh vs plunge frozen protein as the possible cause, but not batch variation. Doubt was also cast on the reliability of the Innovadyne Screenmaker, which was found at a later date to be dispensing inaccurate volumes of liquid. Upon discovering this defect the dispensing robot was replaced.

4.4 Large-scale co-expression of UL7-GST and His_6-UL51 29-170

Following on from the unsuccessful attempts to reproducibly crystallise the tagged and untagged FAB C9S 1-170, it was decided to look again at the UL51 construct used to generate the complex. In order to improve the heterogeneity of the sample, and thus the chances of crystallisation, a new pOPC plasmid was cloned for the expression of His_6-UL51 29-170 and UL7-GST. The 29-170 UL51 construct was shown to interact with UL7 in results chapter one, and so it was expected to co-purify with UL7-GST. Protein expression and purification proceeded as described in section 4.2.3. Figure 4.7 shows the purification of a 4 L pellet, the SEC chromatogram is a single asymmetric peak with a tail on the right-hand side, SDS-PAGE of the peak fractions shows bands at the expected molecular mass for UL7 and His_6-UL51 29-170. There is still a contaminating protein band running at ≈13 kDa. An extinction co-efficient for the complex was estimated as the theoretical extinction co-efficient of the combined polypeptide sequences of the two proteins, assuming a 1:1 ratio, as calculated using the ProtParam server [310], and this was used to calculate protein concentration. A yield of ≈1.4 mg/L of culture was achieved and the protein could be concentrated to at least 9.5 mg/ml, but considerable protein precipitation was observed during concentration, more so than with the FAB C9S 1-170 constructs.

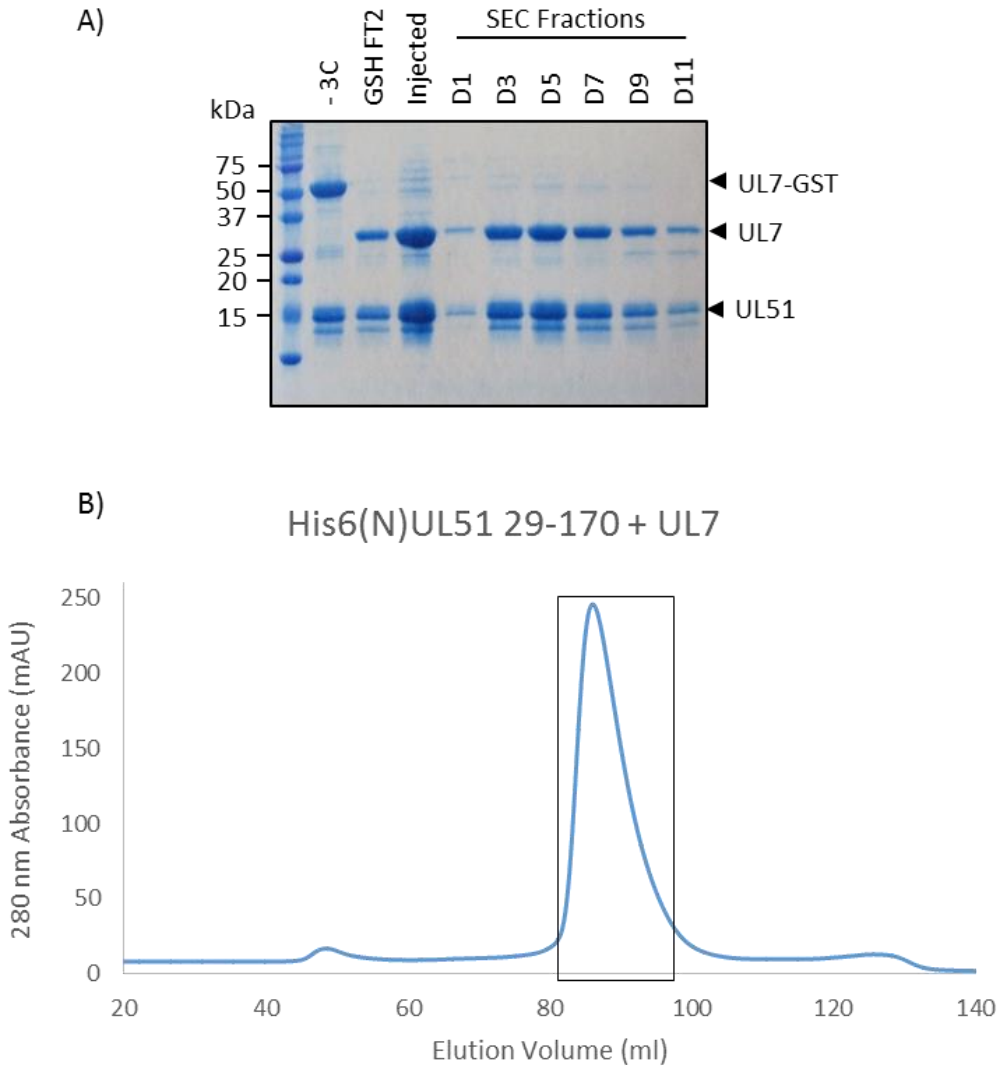

Figure 4.7 Purification of UL7 and His_6-UL51 29-170 (FAB 29-170)
N-terminally His_6-tagged UL51 29-170 and C-terminally GST-tagged UL7 were co-expressed in BL21 (DE3) pLysS cells at 22°C overnight. FAB 29-170 was purified by GSH affinity chromatography, followed by the removal of the GST tag and SEC. A) SDS-PAGE after GSH affinity purification of the complex and cleavage of the GST tag from UL7 by human rhinovirus 3C protease. GSH FT2 is the flow-through after capture of the cleaved GST, uncleaved UL7-GST and the GST-tagged protease. Bands at the predicted molecular mass for cleaved UL7 (33.2 kDa) and His_6-UL51 29-170 (16.1 kDa) are present in the sample injected for SEC and SEC peak fractions. B) S200 16/600 SEC chromatogram corresponding to the fractions presented in panel A.

4.4.1 Nanolitre-scale sparse-matrix crystallisation screening for FAB 29-170

Crystallisation experiments were performed using FAB 29-170 at 9.5 mg/ml and the following sparse-matrix screens: CIMR1, 2, 3, 4, 5, 6, 7, 8, 9, 11 and 12 (Table 2-6, page 43). After 24 h, granular and heavy precipitation was observed in ≈70% of the conditions and no crystalline material appeared during the following weeks. Given these observations and the reduced solubility of the FAB 29-170 protein during the purification, no further attempts to crystallise this complex were made.

4.5 Characterising the oligomeric state of the untagged FAB C9S 1-170 and FAB 29-170 complexes

SEC-MALS (multi-angle light scattering) experiments were performed to probe the oligomeric state of the UL7-UL51 complex and to determine the actual extinction coefficient for accurate concentration calculation. SEC-MALS combines high resolution SEC with MALS and differential refractive index measurements to determine the molecular mass of a protein or complex, independent of hydrodynamic radius. The intensity of scattered light and protein concentration is accurately measured and used to calculate the molar mass. Once known, the overall value of the molar mass can be used to deduce the stoichiometry of the complex based on the predicted masses for each protein component. SEC-MALS can provide an insight into the behaviour of proteins in solution, which is crucial to the success of SAXS experiments.

Samples of untagged FAB C9S 1-170 and FAB 29-170 were subjected to SEC-MALS at a range of concentrations. The predicted masses for complexes of different stoichiometry are shown in Table 4-2. Figure 4.8 shows the SEC-MALS traces along with the calculated molecular mass for each sample. As with the SEC chromatograms the peaks corresponding to the complex in the SEC-MALS traces are skewed to the left. Two key observations can be made from these data: Firstly, the calculated masses suggest a UL7:UL51 ratio of between 1:1 and 1:2; Secondly, there is a concentration dependent shift in molar mass for each complex. While these findings mean that it is not possible to draw a conclusion on the precise stoichiometry of the complex they do provide some insight into the behaviour of the complex in solution, since they are consistent with self-association and the formation of higher order oligomers. Importantly, these samples are thought to contain a UL51 degradation product (band at ≈13 kDa in Figure 4.5 and Figure 4.7) that co-purifies with UL7, therefore it is possible that heterogeneous complexes could exist within each sample, which contain either the complete and/or degraded UL51 species – alternatively, if the UL51 degradation products results from a cut loop it may still form part of the core UL51 fold in solution, only becoming apparent as a separate species during SDS-PAGE. Interestingly, it was noted from the 254 nm SEC-MALS trace that there was additional unexpected absorbance around the complex peak that is suggestive of nucleic acid contamination (Figure 4.10, bottom left panel). The 260/280 absorbance ratio for this complex was 1.12, which is also indicative of nucleic acid contamination. Co-purification of nucleic acid with the sample could explain the inconsistent molecular mass calculated by SEC-MALS, and also contribute to the self-association behaviour. A monodisperse sample is required for SAXS, so in light of the observations above these samples were deemed unsuitable for SAXS and are sub-optimal for crystallisation trials. To improve the quality of the protein sample three approaches were taken to tackle the issues mentioned above: i) to search for buffer components that might stabilise the formation of a monodisperse complex; ii) to adapt the purification protocol to remove the suspected nucleic acid contamination and finally, iii) to eliminate the presumed UL51 degradation band by expressing a further truncated form of UL51.

Table 4-2 Possible stoichiometry of the UL7-UL51 complex and predicted molecular mass
Monomeric molecular mass predictions were calculated from the primary sequence using ProtParam [310]: UL7 after GST tag removal is 33.2 kDa, untagged UL51 C9S 1-170 is 18.2 kDa and His_6-UL51 29-170 is 16.1 kDa.

Complex	Ratio	UL51 1-170 (kDa)	UL51 29-170 (kDa)
UL7:UL51	1:1	51.3	49.3
UL7:UL51	1:2	69.4	65.4
UL7:UL51	2:1	84.6	82.6

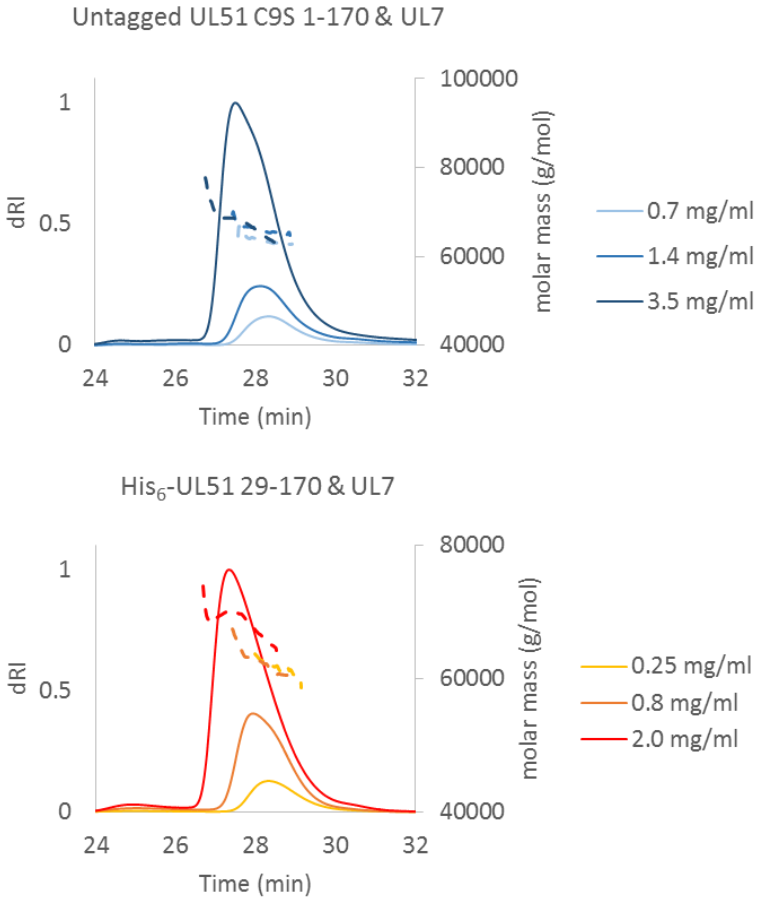

Average molecular mass calculated by SEC-MALS:

Untagged FAB C9S 1-170	
Conc^n (mg/ml)	Mass (kDa)
0.7	63.6
1.4	66.1
3.5	67.2

Average molecular mass calculated by SEC-MALS:

FAB 29-170	
Conc^n (mg/ml)	Mass (kDa)
0.25	63.0
0.8	62.5
2.0	68.6

Figure 4.8 SEC-MALS data for untagged FAB C9S 1-170 and His_6-FAB 29-170
Purified FAB samples were analysed by SEC-MALS at a range of concentrations. The concentrations of the injected complex are listed. The curves show relative differential refractive index for each experiment and the calculated molecular mass for each peak. The values for the average molecular masses calculated for each experiment are presented in the tables, although it is noted that the masses change substantially across the elution peaks.

4.6 Differential scanning fluorimetry with untagged FAB C9S 1-170

In light of the findings from SEC-MALS, differential scanning fluorimetry (DSF) was performed to identify buffer additives (e.g. salts, detergents, ligands, co-factors etc.) that might stabilise the untagged FAB C9S 1-170 complex. This assay uses a thermal shift to monitor the stability of a protein(s) in the presence of different buffer components. Protein unfolding, due to incremental increases in temperature, results in exposed hydrophobic patches that would otherwise be protected within the protein fold. Unfolding is measured by an increase in fluorescence from Protein Thermal Shift™ dye (ThermoFisher Scientific), which fluoresces upon binding to hydrophobic patches of the protein, any unbound dye is quenched by water. There is additional complexity in interpreting DSF data for a complex since multiple melting events can occur: i) disassembly of the complex and ii) unfolding of one or both of the proteins. Protein aggregation can also complicate the interpretation of DSF data. The RUBIC additive screen was used to test 95 possible additives [313]; the protein buffer was 20 mM Tris pH 8.0, 200 mM NaCl, 1 mM DTT. By plotting the fluorescence data as a function of temperature it is possible to determine the melting temperature (T_m) of the protein/complex in the presence of each additive. A selection of curves are shown in Figure 4.9 for additives that resulted in a higher T_m compared to the ultrapure water control. Ideally, the melting curve would be sigmoidal and the inflection point would give the T_m. However, for a protein complex the shape of the curve will be influenced by the multiple melting events possible (particularly where aggregation occurs) as was the case for this sample as seen in Figure 4.9. Given the uncharacteristic sigmoidal shape of most of the curves produced, the calculated T_m values alone cannot be relied upon, and must be considered along with the shape of the curve itself. 5% and 20% glycerol did result in an increased T_m and the curves for these are fairly sigmoidal. The increase in T_m is slightly greater with 20% versus 5% glycerol, suggesting that there is a concentration-dependent stabilising effect. It was decided to include 5% glycerol in the gel filtration buffer of future purification attempts.

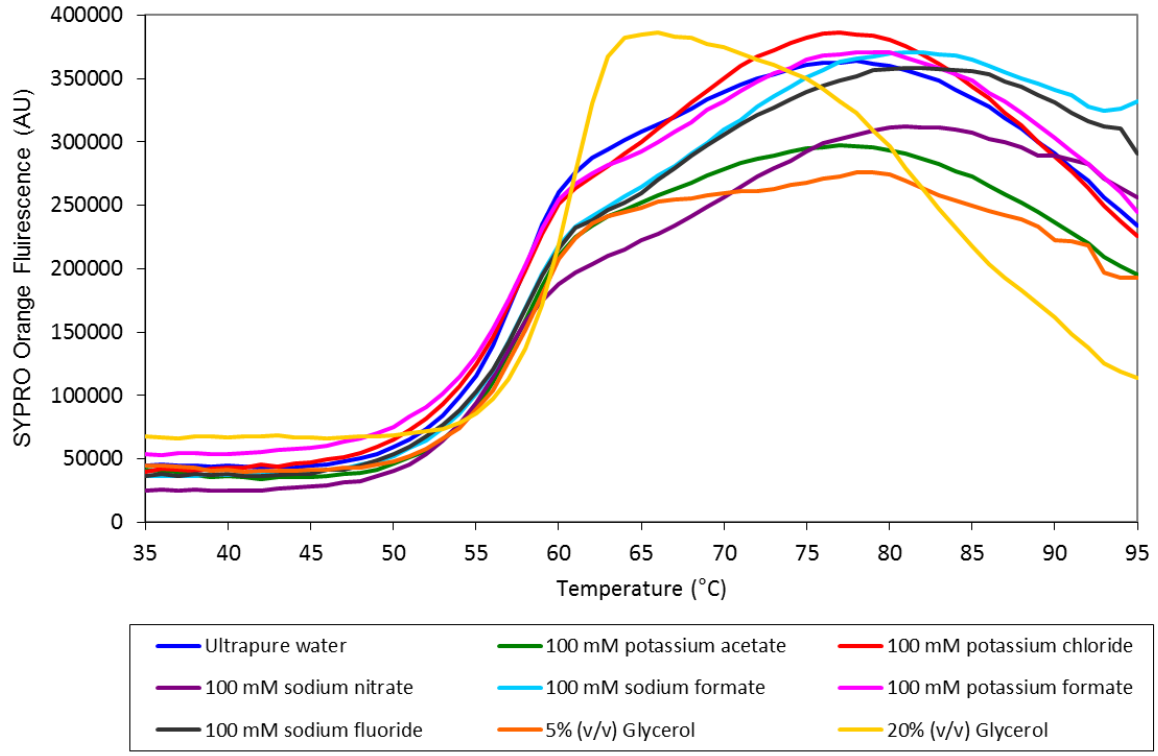

Figure 4.9 Differential scanning fluorimetry curves for untagged FAB C9S 1-170
A selection of DSF curves for purified untagged FAB C9S 1-170 in the presence of different additives. The melting temperature (T_m) for each condition were calculated using the Boltzmann equation in GraphPad Prism, the data were then plotted in Excel. The curves shown are for additives that increased the T_m compared to ultrapure water alone, there were also additives that reduced the T_m compared to ultrapure water.

4.7 Removal of nucleic acid contamination

The SEC-MALS traces for untagged FAB C9S 1-170 and FAB 29-170 show unexpected absorbance at 254 nm (Figure 4.10), which is characteristic of the presence of nucleic acid. A new purification protocol was designed, taking a three pronged approach towards the removal of nucleic acid contamination: i) switching from Tris to phosphate buffer during the affinity purification steps, which can displace bound nucleic acids by mimicking the phosphate backbone; ii) treating the sample with benzonase, which degrades DNA and RNA, followed by iii) a high salt wash to dissociated any bound nucleic acid fragments by disrupting ionic interactions. An outline of the protocol is shown section 2.2.6.2 (page 37). Untagged FAB C9S 1-170 was purified according to the new protocol using phosphate buffers up to the gel filtration stage, at which point the buffer was switched to Tris, due to concerns of phosphate crystal formation in the crystallisation screens. SEC-MALS was performed on the purified protein and, as shown in Figure 4.10, the modified protocol removed the additional peaks in the chromatogram measured at 254 nm, compared to the standard protocol. Furthermore, the 260/280 ratio was more consistent with the expected value for pure protein (≈0.5), supporting the view that the new protocol is able to remove the nucleic acid contamination.

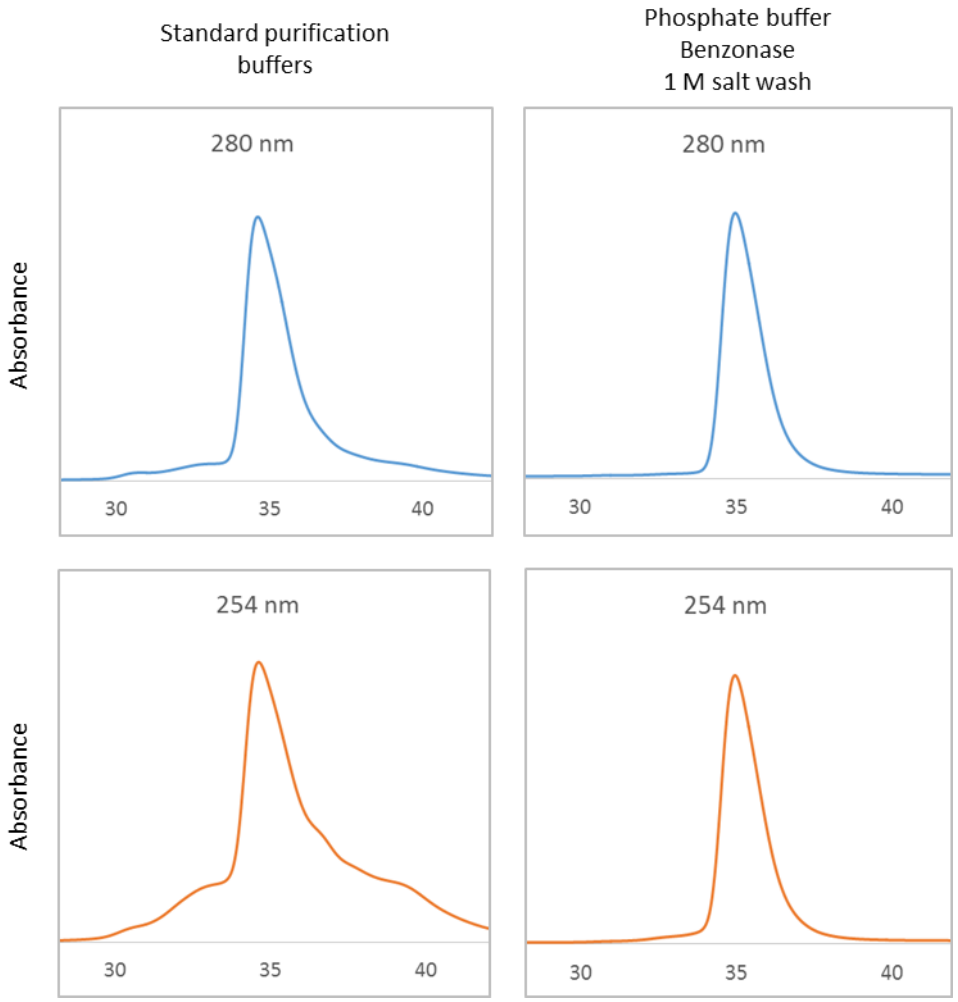

Figure 4.10 Comparison of the 254 nM absorbance for untagged FAB C9S 1-170
S200 10/300 chromatograms for untagged FAB C9S 1-170 at 280 nm and 254 nm after purification with either the standard Tris purification protocol or the new phosphate/benzonase purification protocol geared towards the removal of nucleic acid contamination. The 254 nm trace for the protein sample purified using the phosphate/benzonase protocol shows a sharper peak, suggesting that the nucleic acid contamination has been removed.

4.7.1 Nanolitre-scale sparse-matrix crystallisation screening for FAB 1-170 C9S after purification with the new protocol

Crystallisation experiments were performed using FAB 1-170 C9S purified using the protocol designed to remove nucleic acid contamination. The protein was used at 9.9 mg/ml and the following sparse-matrix screens were prepared: CIMR 4, 5, 7, 8, 11 and 15 (Table 2-6, page 43). After 5 days, granular and heavy precipitation was observed in ≈40% of the conditions, the remainder contained either light precipitation or were clear. The plates were checked regularly up to 5 months and finally after 1 year but no crystalline material was observed.

4.8 Large-scale purification of untagged FAB C9S 8-142

Since FAB C9S 1-170 and FAB 29-170 proved refractory to crystallisation, attempts were made to improve the FAB sample by removing UL51 heterogeneity. A ≈13 kDa protein consistently co-purified with the FAB complex (Figure 4.5 and Figure 4.7). The band was extracted from an SDS-PAGE gel and submitted for mass spectrometry. As suspected, the band was confirmed to be a UL51 degradation product and mapped to residues 8-142. The pOPC co-expression plasmid was modified by QuickChange to express untagged UL51 C9S 8-142 and UL7-GST.

Untagged FAB 8-142 was expressed in BL21 (DE3) pLysS cells at 22°C overnight and purified according to the new protocol outlined in section 4.7, including 5% glycerol in the gel filtration buffer. As shown in Figure 4.11 the complex remains intact during the washes and SEC, the SEC peak is also more symmetrical than previously achieved with the complex. SDS-PAGE of the SEC peak fractions shows that the sample is more homogenous than the purification attempts for FAB C9S 1-170 and FAB 29-170. Interestingly, purified untagged FAB C9S 8-142 exhibited peculiar behaviour when concentrated to ≈6.0 mg/ml or higher. At this point, the spectrophotometer was unable to give an absorbance measurement. However, if the sample was diluted to below ≈6.0 mg/ml the absorbance could be measured using the spectrophotometer. This behaviour was consistent with all batches of untagged FAB C9S 8-142. Protein aggregation at higher concentrations might explain this observation since it could result in excessive scattering of light as it passes thought the sample, which might prevent the instrument making a measurement. The concentration of samples above ≈6.0 mg/ml was determined by Bradford assay.

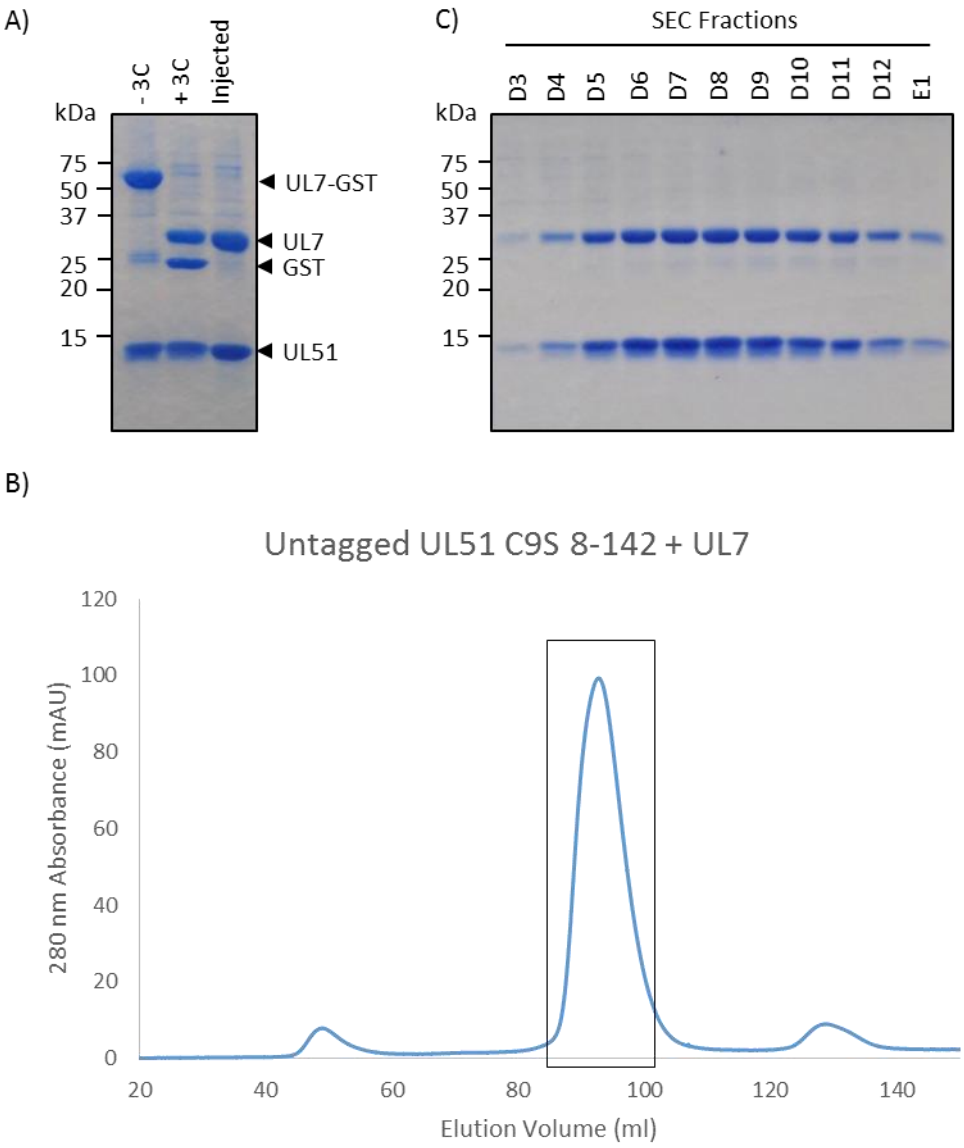

Figure 4.11 Purification of UL7-GST and Untagged UL51 C9S 8-142 (FAB C9S 8-142)
Untagged UL51 C9S 8-142 29-170 and C-terminally GST-tagged UL7 were co-expressed in BL21 (DE3) pLysS cells at 22°C overnight. FAB C9S 8-142 was purified by GSH affinity chromatography, followed by the removal of the GST tag and SEC. A) SDS-PAGE after GSH affinity purification of the complex and cleavage of the GST tag from UL7 by human rhinovirus 3C protease. The sample before (-3C) and after (+3C) incubation with human rhinovirus 3C protease is shown. The sample injected for SEC contains bands at the appropriate size for cleaved UL7 (33.2 kDa) and untagged UL51 C9S 8-142 (14.7 kDa). B) S200 16/600 SEC chromatogram for FAB C9S 8-142 after removal of the GST tag. C) SDS-PAGE of the SEC peak fractions showing that the FAB C9S 8-142 complex remains intact during SEC.

4.9 Characterising the oligomeric state of the untagged FAB C9S 8-142

Given the improved quality of the FAB sample SEC-MALS was repeated with the untagged FAB C9S 8-142 sample. 5% glycerol was present in the gel filtration and SEC-MALS buffer. The predicted molecular mass for a complex with a UL7:UL51 ratio of 1:1 is 47.9 kDa, and 1:2 is 62.6 kDa. The trace at 254 nm shows that the suspected nucleic acid contamination is not present (Figure 4.12B). However, despite the obvious improvement in sample quality, as is evident from the increased symmetry of the peak, there continues to be a concentration dependent shift in molecular mass measured by SEC-MALS, suggesting that self-association is still occurring. Unfortunately, this meant that the sample was not suitable for SAXS experiments.

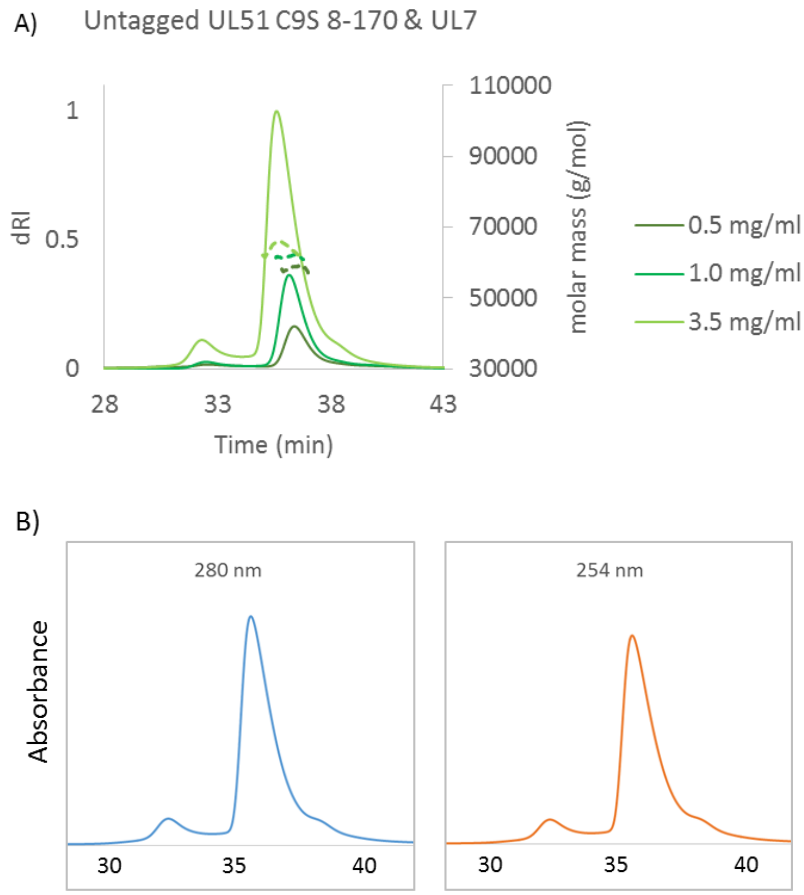

Average molecular mass calculated by SEC-MALS:

Untagged FAB C9S 8-142	
Conc^{n} (mg/ml)	Mass (kDa)
0.5	58.4
1.0	61.6
3.5	64.6

Figure 4.12 SEC-MALS trace for untagged FAB C9S 8-142
SEC-MALS was performed with untagged FAB C9S 8-142 that had been purified using a protocol designed to eliminate nucleic acid contamination. The buffer also contained 5% glycerol in an attempt to stabilise the complex and reduce self-association. A) SEC-MALS peaks for FAB C9S 8-142 at three injected concentrations and calculated molecular masses B) 254 and 280 nm traces of the SEC-MALS peak at 3.5 mg/ml.

4.10 Crystallisation trials of untagged FAB 8-142

4.10.1 Nanolitre scale sparse-matrix screening for untagged FAB C9S 8-142

Sparse-matrix crystallisation experiments were attempted using FAB C9S 8-142 protein at 10.0 mg/ml based on previous experience with the FAB C9S 1-170 protein. Protein concentration was determined by Bradford assay since the 280 nm absorbance for this complex could not be measured at concentrations greater than ≈6.0 mg/ml. Two screens (CIMR5 and 7) were attempted initially to assess the suitability of this protein concentration, all the drops in both plates contained heavy precipitation within 24 h. Based on this feedback the protein concentration was reduced to 5.9 mg/ml, as determined by absorbance at 280 nm and confirmed by Bradford assay, for further sparse-matrix screening (CIMR3, 5, 7, 8, 11, 12 and 15, page 43). Precipitation was present in the majority of drops after 24 h, ranging from light to heavy. After two days, one condition, well G4 of screen CIMR11, yielded crystalline material (Figure 4.13). Similar crystals also appeared after two days in screen CIMR13 well H8 with a protein concentration of 4.2 mg/ml (Figure 4.13). Crystals from each of these conditions were harvested for X-ray diffraction and cryo-protected in reservoir solution plus 5% glycerol. The crystals were flexible thin plates and adhered to the crystallisation stage making them difficult to harvest. None diffracted, although this is most likely due to damage occurring to the fragile crystals during mounting into loops for the diffraction experiment.

4.10.2 4-column optimisation for untagged FAB C9S 8-170

The small thin plates that grew in the sparse-matrix screens were difficult to harvest and did not produce any X-ray diffraction. 4-column optimisation screens were performed for conditions CIMR11 G4 and CIMR13 H8, with untagged FAB C9S 8-142 protein at 5.9 mg/ml and at 4.2 mg/ml respectively, the aim being to grow larger, diffracting crystals that would also be easier to mount. Stock precipitant solutions were made by combining and diluting pre-made stocks from Molecular Dimensions salt and buffer kits; the design of the screen is outlined in Figure 4.13B. The conditions were, screen CIMR11 well G4: 0.1 M carboxylic acids, 0.1 M Morpheus buffer system 1 (MES and Imidazole) pH 6.5, 50% precipitant mix 4; and screen CIMR13 well H8: 0.1 M sodium cacodylate pH 6.0, 0.05 M calcium acetate, 25% MPD. Drops were dispensed using a TTP Labtech Mosquito robot (1P:1P means 100 nl protein:100 nl reservoir). Unlike the previous attempts to reproduce FAB C9S 1-170 crystals from sparse-matrix screens, the untagged FAB C9S 8-142 crystal were reproducible, from both conditions. However, there was no improvement i.e. increase in size or change in crystal morphology (Figure 4.13).

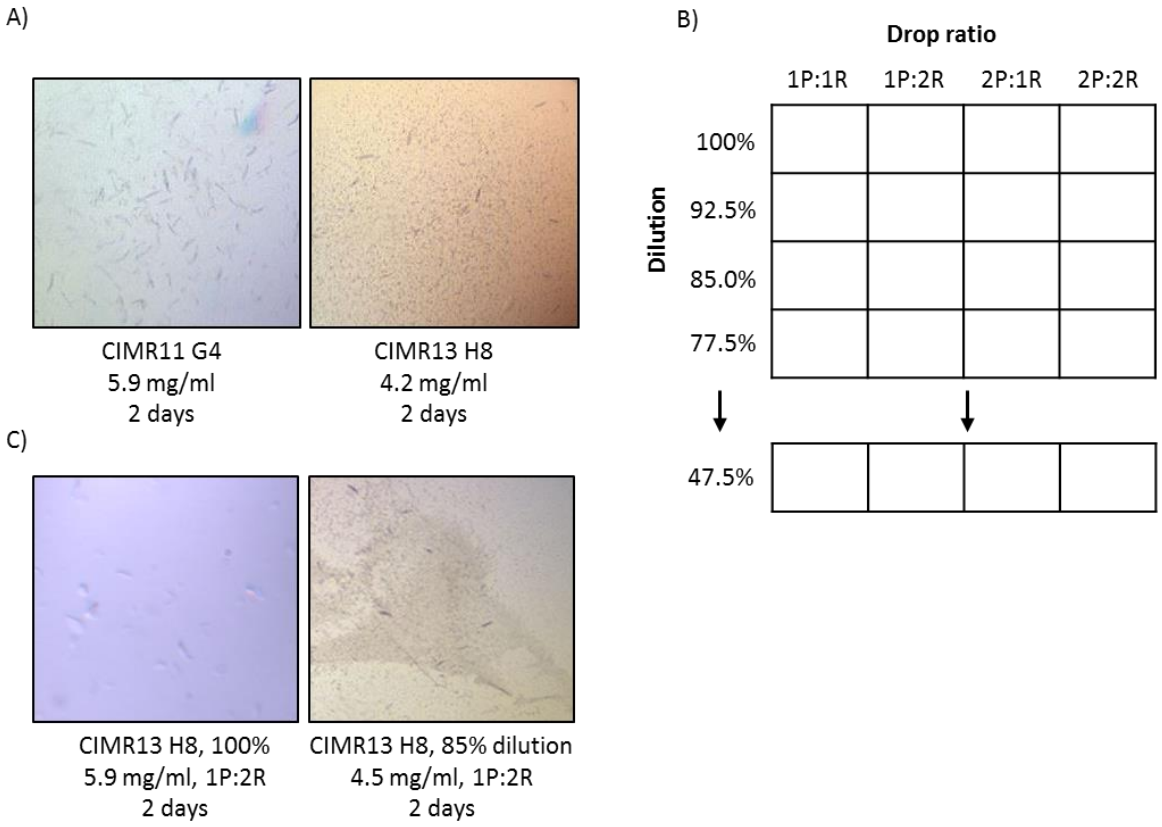

Figure 4.13 Sparse-matrix screening and 4-column optimisation of FAB C9S 8-142
Sparse-matrix screening for crystallisation conditions was performed with the FAB C9S 8-142 protein sample. A) Small crystals grew in two conditions from the sparse-matrix screens: CIMR11 G4 and CIMR13 H8. B) In an attempt to increase the size of these crystals, a four-column optimisation screen was designed to sample incremental changes in the crystallisation conditions. The concentration of reservoir solution (dilution) and drop ratio (1P:1P means 100 nl protein:100 nl reservoir) were varied as shown. C) Crystals from both conditions were reproduced in the 4-column optimisation screen, but there was no increase in crystal size.

4.10.3 Additive Screen for untagged FAB C9S 8-170 around CIMR13 H8

Additive screening is a quick optimisation approach for small but reproducible crystals. The technique utilises small molecules to enhance crystallisation by either stabilising the protein or complex, or to promote the formation of crystal contacts. An additive screen (Jena Bioscience) was performed for untagged FAB C9S 8-170 (4.5 mg/ml) around the CIMR 13 H8 condition. Small needles grew in many wells, which were similar in appearance to those that grew in the sparse-matrix and 4-column optimisation screens. More promisingly, the additive potassium cyanate resulted in some small crystals, shown in Table 4-3, which were unlike the crystal seen previously for this protein. Interestingly, after five days the crystals deteriorated and took on an appearance closer to phase separation. Three other additives: ethanolamine, 1,8-diaminooctane and 1,6-diaminooctane produced

similar phase separation but crystals were never observed, it is possible that crystals may have formed with these additives then deteriorated more rapidly than with potassium cyanate.

A further optimisation screen was performed in 48-well sitting drop tray using CIMR 13 H8 (85%) reservoir condition and potassium cyanide additive whilst varying the drop ratio and volume, also two protein concentrations were tested: 4.5 mg/ml and 6.0 mg/ml. The drops were scaled up to microliter volumes, which can sometimes yield larger crystals. The crystals were reproducible in all conditions, larger and fewer crystals were obtained at the higher concentration. Micro-seeding was attempted with seed stocks prepared from crushed crystals and used to streak seed pre-equilibrated drops set-up with 70% reservoir condition and potassium cyanate additive. The seed stock was also used to seed drops that contained the other three additives mentioned above. Crystals grew along the streak for the conditions with potassium cyanide but there was no increase in crystal size. No crystals grew with the other additives. Crystals from a selection of drops were harvested and cryo-protected in 5% glycerol. Unfortunately, the new crystals were confirmed to be salt by X-ray diffraction at the Diamond Light Source.

Table 4-3 Additive Screen for FAB C9S 8-142

Condition	Additive	Image
CIMR13 H8 (85%)	Potassium cyanate	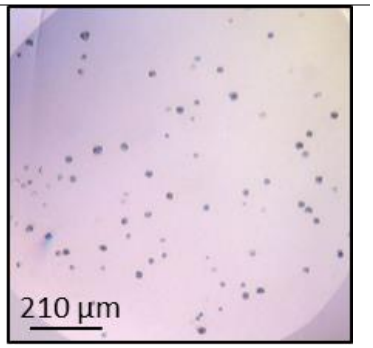 After 24 h 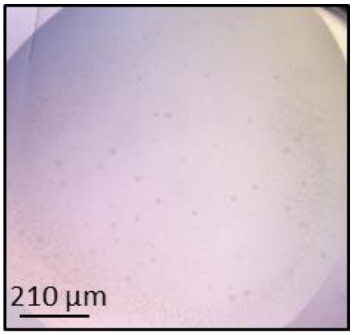 After 5 days
CIMR13 H8 (85%)	Ethanolamine	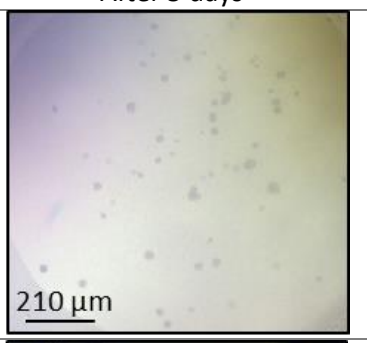
CIMR13 H8 (85%)	1,8-Diaminooctane	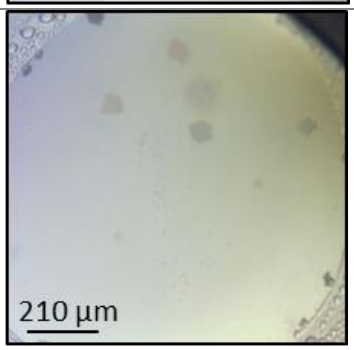

Condition	Additive	Image
CIMR13 H8 (85%)	1,6-Diaminooctane	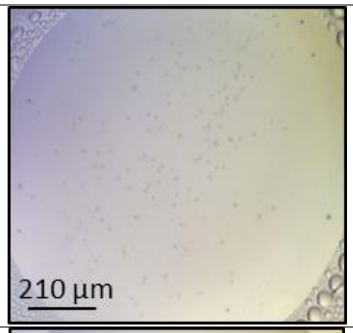
CIMR13 H3 (85%)	Potassium sulphate	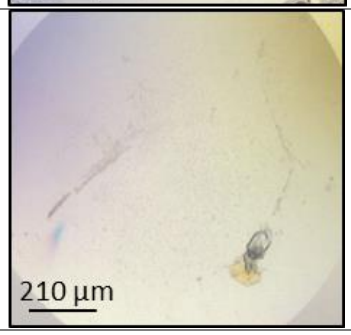

4.11 Expression and Purification of ORF42-ORF55 C3S+C4S 1-162 complex

The UL7-UL51 interaction is conserved between the homologues from murid herpesvirus (MHV), ORF42 and ORF55, respectively. In results chapter one the MHV homologues were shown to be more amenable to large-scale bacterial expression, when expressed alone, than UL7 and UL51. Attempts were made to crystallise the ORF42-ORF55 complex with the view that any structural insight gleaned could be extrapolated to the homologous UL7-UL51 interaction. Purified ORF42 and ORF55 C3S+C4S 1-163 were diluted and combined in a 1:1 ratio. Unexpectedly, there was extensive precipitation in the tube upon combining the proteins, despite their having been soluble beforehand and in the same buffer. This observation suggested that upon formation of the ORF42-ORF55 complex the protein(s) were no longer soluble. To address this issue co-expression and purification of ORF42-GST and His_6-ORF55 C3S+C4S 1-163 from *E. coli* was attempted, with the view that the proteins will undergo co-folding in cells to form a stable complex that will be selected for during the purification process, this complex was named GAB C3S+C4S 1-163.

Based on the assumption that the GAB C3S+C4S 1-163 might bind nucleic acid, as was the case for the FAB complexes, the purification protocol (described in section 4.7) that minimised nucleic acid contamination was used. Initially a 4 L pellet was purified, the lysate was incubated with GSH beads and at this point it was noted that the lysate appeared opaque and the unbound lysate fraction was very slow to run through the column – two observations that are indicative of precipitated protein in the lysate. SEC was performed to remove glutathione and the protein sample was incubated overnight with human rhinovirus 3C protease. GSH beads were used to capture any uncleaved ORF42, free GST tag and the GST-tagged protease followed by SEC. The SEC chromatogram in Figure 4.14 (blue) shows

two peaks, the first corresponds to a small amount of GAB C3S+C4S 1-163 complex and the second peak is ORF42 alone (Figure 4.14C). ORF55 C3S+C4S 1-163 protein is present in the lysate fraction as shown in Figure 4.14B, however, the majority does not purified with GST-ORF42 beyond this step suggesting that the protein had precipitated during the lysis in the phosphate buffer. The purification was repeated, from a 6 L pellet, this time using Tris buffers throughout, whilst also performing the treatment with benzonase and the high salt wash. The lysate was again opaque and a large pellet was observed after centrifuging the eluted and concentrated protein. The second chromatogram in Figure 4.14 (orange) again shows two peaks, this time the first peak is higher and corresponds to the complex while the second peak is ORF42 alone. An extinction co-efficient for the complex was estimated as the theoretical extinction co-efficient of the combined polypeptide sequences of the two proteins, assuming a 1:1 ratio, as calculated using the ProtParam server [310]. This was used to calculate the protein concentration from 280 nm absorbance values as measured by spectrophotometer. The first peak fractions were pooled and concentrated to 5.8 mg/ml without signs of precipitation, a yield of 0.58 mg purified complex was achieved from 6 L of *E. coli* culture. Unfortunately, the 260/280 ratio for the purified complex was 1.14, which is suggestive of nucleic acid contamination and, therefore, the sample is not suitable for SAXS experiments and is sub-optimal for crystallisation.

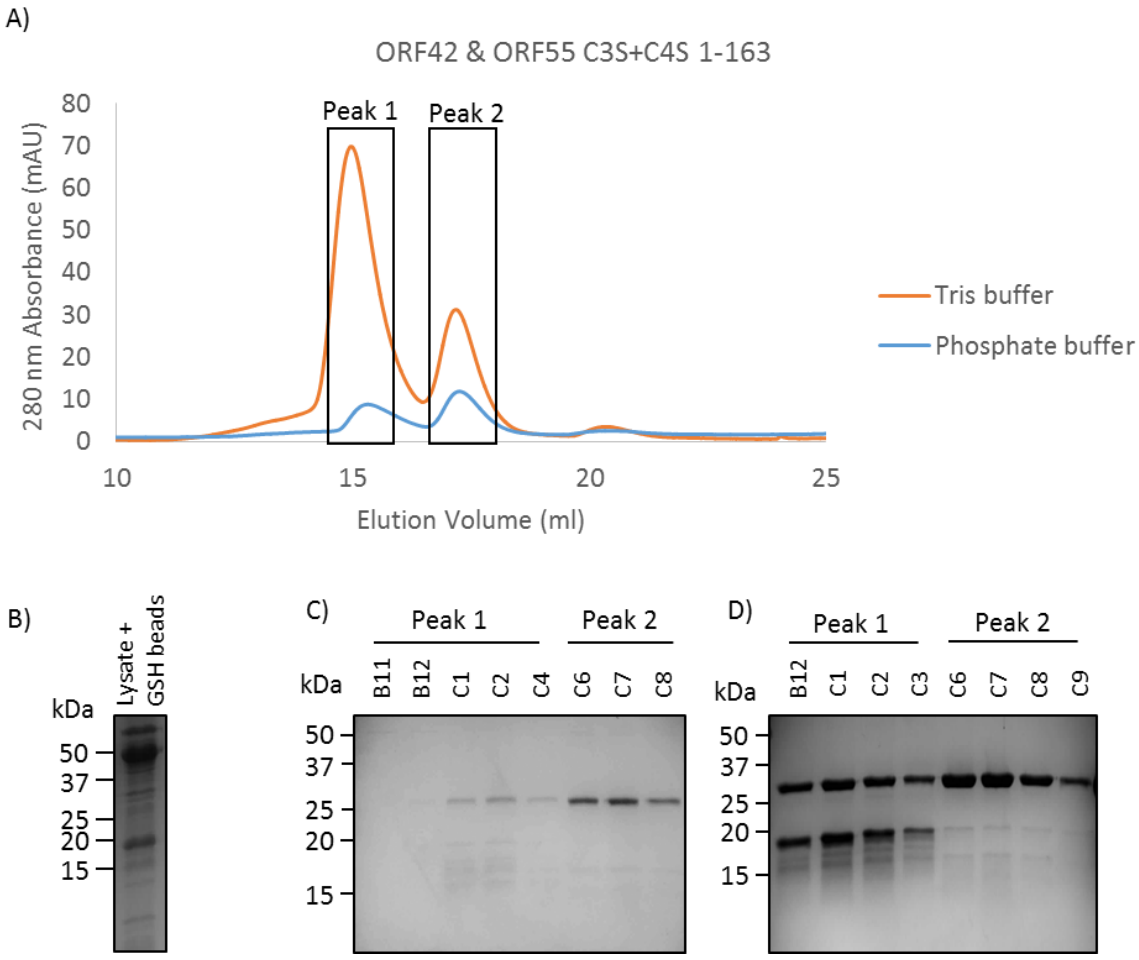

Figure 4.14 Purification of ORF45 and His_6-ORF55 C3S+C4S 1-163 (GAB C3S+C4S 1-163)
N-terminally His_6-tagged ORF55 C3S+C4S 1-163 and C-terminally GST-tagged ORF42 were co-expressed in BL21 (DE3) pLysS cells at 22°C overnight. GAB C3S+C4S 1-163 was purified by GSH affinity chromatography, followed by the removal of the GST tag and SEC. A) S200 10/300 SEC chromatograms for purification attempts with either Tris or phosphate based buffers. B) SDS-PAGE of the cell lysate after centrifugation, taken after GSH beads were added. Bands at the expected molecular mass for ORF42-GST (54.9 kDa) and His_6-ORF55 C3S C4S 1-163 (19 kDa) are present. C) SDS-PAGE of SEC peak fractions following purification in phosphate buffers. There is a band at the expected molecular mass for untagged ORF42 (28.9 kDa) but not His_6-ORF55 C3S C4S 1-163. D) SDS-PAGE of SEC peak fractions following purification in Tris buffers. Bands at the predicted molecular mass for untagged ORF42 and His_6-ORF55 C3S C4S 1-163 are present in SEC fractions corresponding to peak 1.

4.12 Discussion

This chapter describes the attempts to co-express and purify the UL7-UL51 complex for crystallisation and small-angle X-ray scattering experiments. Co-expression of UL7 and UL51 greatly improved protein solubility and yield, which is in line with the observation that expression levels of either protein in the absence of its partner is diminished during infection of human cells. Extensive sparse-matrix screening for crystallisation conditions was conducted with the FAB 1-170 complex, and did yield some small crystals, though unfortunately these were irreproducible. Nucleic acid contamination and the presence of UL51 degradation products in the sample increases the scope for batch variation, which could explain the inability to reproduce the crystals. These problems were overcome by modifying the purification protocol and by re-cloning UL51 to express a shorter, more stable, construct. The outcome was a more symmetrical SEC peak and a higher-purity sample as assessed by SDS-PAGE. Sparse-matrix screening with FAB C9S 8-142 yielded small crystals that are reproducible, and the next step is to determine whether they are protein or salt. *In situ* diffraction might be a way to address this questions since the crystals are small and difficult to harvest. Additive screening did not improve the crystals from CIMR13 H8, and this approach has yet to be attempted for the CIMR11 G4 condition. Other options available for optimising the crystals are grid-screening and micro-seeding. Reductive methylation of the complex is also a viable option, since the complex is stable in phosphate buffer, and surface entropy reduction by mutagenesis of selected residues predicted to be on the surface of the protein could also be attempted.

There was the option to perform small-angle X-ray scattering with the UL7-UL51 complex. However, it was not possible to produce a monodisperse sample, which is crucial to the success of this technique. The behaviour of the sample in SEC-MALS experiments was characteristic of self-association, and the addition of glycerol to the buffer was unable to combat this. In hindsight it might be worth investigating other additives from the DSF screen, such as those that lowered the T_m value compared to water; it might be that these additives increased fluorescence at lower temperatures by limiting self-association i.e. the fluorescence was a result of the fluorescent dye binding to exposed hydrophobic patches on the surface rather than dissociated of the complex unit or protein unfolding. However, self-association behaviour might be expected given the very nature of these proteins, as tegument proteins their typical environment as part of the virus is within the protein-dense tegument layer. Tegument proteins form an extensive network of interactions and during the course of this study an interaction between UL51 and UL14 was reported [229], there is also some evidence to suggest that UL51 might also bind gE [168,229]. The absence of UL14 and gE in the purified UL7-UL51 sample could result in exposed hydrophobic patches on the surface of the complex leading to a propensity for self-association. Co-expression of UL7-UL51 and UL14 might be a productive avenue for producing a crystal containing the UL7-UL51 complex.

5 Yeast two-hybrid screening for UL7 and UL51 interaction partners

5.1 Introduction

Results chapters one and two described attempts to generate structural information for the HSV-1 UL7-UL51 complex by X-ray crystallography and small-angle X-ray scattering. Protein structure determination can provide an insight into protein function through inference i.e. if protein folds and features of known function are identified in the crystal structure. Biochemical approaches are also available for the determination of protein function. One such approach is to identify protein interaction partners through library screening, which can elucidate the metabolic processes or cellular pathway(s) within which a given protein functions. In this study, Y2H screening was employed to identify host-cell interaction partners for the proteins UL7 and UL51. Given the hypothesis that UL7 and UL51 are involved in virus assembly and egress, it was anticipated that they would interact with proteins that mediate intracellular vesicular transport. Similarly, focal adhesion proteins would also be likely candidates, given that the UL7-UL51 complex is known to co-localise with these structures. This chapter presents the results of a Y2H screen and attempts to validate the interactions between viral protein and the host-cell proteins identified as putative interaction partners.

5.2 Yeast two-hybrid screen

5.2.1 Autoactivation test

Y2H screening was performed using the Clonetech Mate & Plate^{TM} Library Screen system. To perform a Y2H screen, yeast expressing the protein of interest (bait) fused with a Gal4-myc DNA-binding domain are mated with yeast expressing a library of protein fragments (prey), in this case human proteins, fused to a Gal4-myc DNA activation domain. If an interaction occurs between the protein of interest and a library fragment, the complementary Gal4-DNA binding and Gal4-DNA activation domains combine to stimulate the transcription of reporter genes, resulting in colony growth. Matchmaker^{TM} Gold yeast were transformed with bait constructs expressing UL7 and UL51 fused to a Gal4-myc-DNA-binding domain. Expression of the UL7 and UL51 fusion proteins in the yeast cells was confirmed by immunoblotting yeast cell extract with αMyc antibody (Figure 5.1B). Before proceeding with the Y2H library screen, the bait proteins were tested for autoactivation, which occurs when the bait fusion protein is able to stimulate reporter gene transcription in the absence of a Gal4-DNA activation domain. In this test, autoactivation is indicated by the growth of blue colonies due to the cleavage of the colorimetric substrate X-α-gal by the yeast galactosidase enzyme that is under the control of the Gal4 promoter. As shown in Figure 5.1A, the UL7 bait protein alone was able to activate reporter gene expression, while UL51 was not. Thus, the UL7 construct is unsuitable for library

screening and the Y2H screen was performed for UL51 interaction partners only. The Y2H screen was performed before co-dependence of UL7 and UL51 for folding was known, hence the proteins were screened individually.

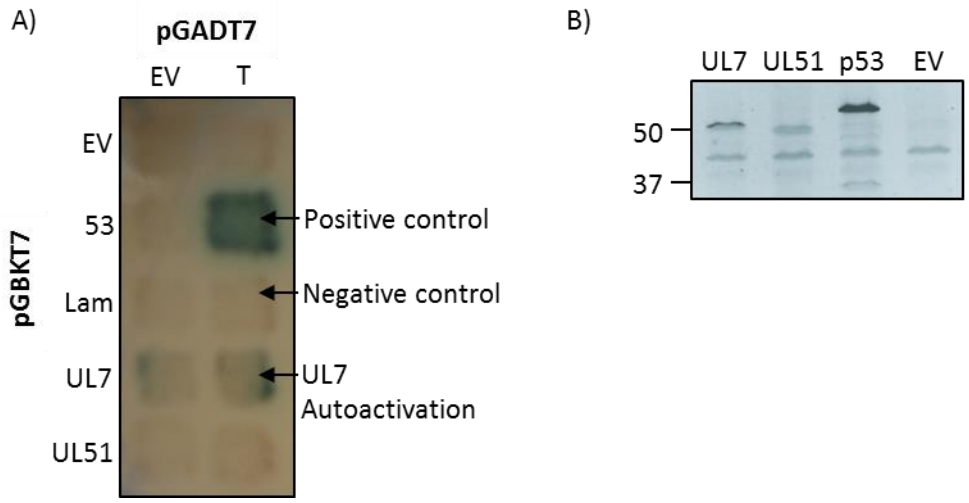

Figure 5.1 Autoactivation test for UL7 and UL51 fusion proteins in yeast
Y2H bait constructs were generated by cloning UL7 and UL51 into pGBKT7 for expression as fusion products with a Gal4-DNA binding domain. These constructs were tested for autoactivation, which occurs when occurs when the bait fusion protein is able to stimulate reporter gene transcription in the absence of a Gal4-DNA activation domain, resulting in the growth of blue colonies. A) Matchmaker™ Gold yeast cells were transformed with either empty pGADT7 vector (EV) or SV40 T-antigen conjugated to a Gal4-activation domain (T). Y187 yeast were transformed with either UL7, UL51, human p53 or human laminin (Lam) conjugated to a Gal4-DNA binding domain (pGBKT7), or empty pGBKT7 vector (EV) as a negative control. The yeast strains were mated in the combinations shown and plated on nutrient selection (lacking adenine, His, Trp, Leu) agar plates, supplemented with X-α-Gal and Aureobasidin A. The positive control interaction between p53 fused to Gal4-DNA binding domain and the SV40 T-antigen fused to Gal4-activation domain results in the growth of blue colonies as expected. Similarly, the negative control interaction: Lam with T-antigen, does not result in colony growth as expected. UL51 fused to a Gal4-DNA binding domain does not result in the growth of blue colonies suggesting that does not autoactivate and is thus suitable for Y2H screening. However, UL7 fused to a Gal4-DNA binding domain does result in the growth of blue colonies, which is a clear indication of autoactivation rendering this construct unsuitable for Y2H screening. B) The bait constructs contain a myc epitope between the Gal4-DNA binding domain and the protein of interest e.g. UL51. Thus the expression of the fusion proteins can be detected by immunoblotting for the myc epitope. The yeast cells, transformed with the bait constructs, were lysed and analysed by immunoblot using αmyc antibody. Bands for Gal4-myc-UL7 (53.9 kDa) and Gal4-myc-UL51 (45.8 kDa) were detected.

5.2.2 Yeast two-hybrid screen with UL51 bait protein against human library

Yeast expressing the UL51 bait protein were mated with yeast expressing a library of human prey protein fragments fused to a Gal4-activation domain. Mated yeast were plated onto quadruple-drop-out (QDO) nutrient selection (lacking adenine, His, Trp, Leu) agar plates. If UL51 interacts with a

library fragment, the complementary Gal4-DNA binding and Gal4-DNA activation domains combine to stimulate transcription of the reporter genes, the yeast cells in which this occurs are then able to produce the nutrients lacking in the QDO plates, resulting in growth and the appearance of yeast colonies. Mating efficiency was calculated to be 30% (> 2.5% mating efficiency is considered successful), meaning approximately 5.6 million clones were screened (screening of > 1 million clones is generally sufficient to sample the library). From the initial QDO plates, 108 colonies were picked and streaked onto QDO agar supplemented with X-α-Gal and Aureobasidin A. Positive clones on the QDO/X/A plates appear blue, and 90 blue colonies were picked from these plates and re-streaked on fresh QDO/X/A plates. All 90 of the re-streaked colonies grew and were blue. Colony PCR was performed on 90 colonies, of these 59 were successfully amplified and sent for sequencing. In total, 22 unique protein hits were identified by the screen and the sequences were confirmed to be in-frame and to correspond with coding regions of the gene, these are shown in Table 5-1. Several hits were selected for further investigation, based on their links with vesicular transport and/or the frequency of unique clones i.e. different overlapping fragments of the same protein (Table 5-2).

Table 5-1 Sequenced hits from the yeast two-hybrid screen are putative UL51 interaction partners

Hits identified by BLASTp	No. Unique Clones
CPAP (Centrosome Protein J, CENPJ)	**3**
Nipsnap homolog 3A (*C. elegans*) (NIPSNAP3A aka. NIPSNAP4)	**2**
Peroxiredoxin 3 (PRDX3)	**2**
Homo sapiens annexin A7 (ANXA7)	**1**
Stathmin-2 (STMN2), transcript variant 1, mRNA	**1**
TOX high mobility group box family member 4 (TOX4)	1
Prostaglandin E receptor 3 (subtype EP3) (PTGER3)	1
BRWD3 bromodomain and WD repeat domain containing 3	1
Homo sapiens adenosine deaminase domain containing 1 (testis-specific) (ADAD1)	1
Splicing factor 3b, subunit 1 (SF3B1)	1
Ankyrin repeat and sterile alpha motif domain containing 1B (ANKS1B)	1
Leucine aminopeptidase 3 (LAP3)	1
Proline-rich coiled-coil 1 (PRRC1)	1
Zinc finger and BTB domain containing 20 (ZBTB20)	1
Origin recognition complex, subunit 4 (ORC4)	1
Tectonic family member 3 (TCTN3)	1
Protoporphyrinogen oxidase (PPOX)	1
3-hydroxy-3-methylglutaryl-CoA synthase 2 (mitochondrial) (HMGCS2)	1
COP9 signalosome subunit 5 (COPS5)	1
Ubiquitin specific peptidase 7 (USP7)	1
Sulfide:quinone oxidoreductase, mitochondrial [SQOR]	1
Homo sapiens LanC lantibiotic synthetase component C-like 1 (bacterial) (LANCL1)	1

Table 5-2 Yeast two-hybrid hits selected for validation

Y2H Hit	Length aa.	Molecular mass (kDa)	Pathway
CPAP	1338	153.0	Centriole elongation and replication; Microtubule nucleation and polymerisation; Cilium assembly.
NIPSNAP4	247	28.5	Putative role in vesicular transport.
PRDX3	256	26.7	Cell redox homeostasis; Cellular response to oxidative stress.
ANXA7	488	52.7	Autophagy; Membrane fusion; Regulation of cell shape.
STMN2	179	20.8	Regulation of microtubule (de-) polymerisation; Regulation of neuron projection development; Cellular response to nerve growth factor.

5.2.3 Overview of the yeast two-hybrid screen hits selected for validation

Out of the 22 putative UL51 binding partners identified in the Y2H screen, 5 were selected for further investigation: CPAP, NIPSNAP4, PRDX3, ANXA7 and STMN2 (Table 5-2). NIPSNAP4 is a ubiquitously expressed protein with a putative role in vesicular transport; it has been shown to associate with intracellular vesicles and partly localise in detergent insoluble 'lipid rafts' in membranes [314,315]. The *Salmonella* virulence factor SpiC targets NIPSNAP4, and in doing so is thought to prevent phagosome-lysosome fusion [316]. NIPSNAP4 was deemed a hit worthy of further investigation in light of the hypothesis that UL51 has a role in virus assembly and egress, and because it was identified as two unique overlapping clones i.e. two different but overlapping regions of the gene. Similarly, ANXA7, a calcium-dependent phospholipid binding protein, is predicted to promote membrane fusion and play a role during exocytosis [317-319]. The N terminus of Annexin A7 is highly hydrophobic and predicted to be membrane associated [318,320]. Additionally, Annexin A1, A2 and A5 were detected in extracellular HSV-1 virions, with A2 being the most abundant [58].

CPAP was selected for further investigation because it was detected as three unique overlapping clones. CPAP is a centriolar scaffold protein involved in microtubule assembly and elongation at the MTOC, the principal microtubule nucleating centre in cells [321,322]. The microtubule network is utilised for the transport of virus particles during entry and egress, [22,60,82,83,183,323] and HSV-1 tegument proteins UL36 and UL37 have been shown to recruit microtubule motor proteins *in vitro* [59]. Many viruses, including HSV-1 [324,325], vaccinia virus [326,327], adenovirus [328], rotavirus [329,330] and African swine fever virus [331] have been shown to reorganise the microtubule network and/or affect the centrosome during infection. In HSV-1-infected cells the microtubule cytoskeleton is remodelled, with microtubule depolymerisation occurring at the plasma membrane and new microtubule bundles forming close to the nucleus [324].

The reorganisation of the microtubules in HSV-1-infected cells is also associated with fragmentation and dispersal of the Golgi apparatus [332]. Staining for gamma tubulin, an MTOC marker, and CPAP binding protein, suggests that the MTOC is absent in HSV-1 but not PrV-infected cells at 6 h.p.i. [333]. Without the MTOC serving as principal organising centre in HSV-1-infected cells, microtubules nucleate at dispersed locations throughout the cytoplasm [333]. Interestingly, CPAP depletion by siRNA was shown to impair HSV-1 replication (personal communication Dr Colin Crump [334]). While the role of the microtubule network in virus transport has been intensively studied, the precise role of the centrosome has not been fully explored. A second protein identified in the Y2H screen, stathmin-2 (STMN2), also has a role in microtubule dynamics by regulating the cytoplasmic pool of tubulin available for microtubule growth. To do this, STMN2 sequesters αβ-tubulin dimers to prevent their incorporation into microtubules [335,336]. When phosphorylated, STMN2 releases tubulin for microtubule assembly [335,336]. STMN2 can also act directly on microtubule ends to promote disassembly [337]. In HSV-1-infected cells, STMN1 levels were shown to be upregulated at early stages, i.e. before 6 h.p.i [338].

PXRD3 is the final putative UL51 binding protein identified in the Y2H screen that was selected for validation. PXDR3 was included despite having no obvious link with vesicular trafficking and egress, but because two unique clones were detected in the screen. It is an abundant antioxidant protein and has been detected in mature HSV-1 virions by mass spectrometry [58].

5.2.4 Yeast two-hybrid hits were cloned for expression using the wheat germ cell-free expression system

Selected protein hits from the Y2H screen were cloned for expression using the wheat germ cell-free expression system (Promega). The aim was to perform a GST pull-down experiment using GST-tagged UL51 bait protein and wheat germ expressed prey proteins. The prey constructs were designed based on the gene fragments detected in the Y2H screen and also secondary structure predictions. Full-length NIPSNAP4, PXRD3 and STMN2 were sequenced from the yeast clones, and so the complete gene was cloned into pF3A vector for expression with an N-terminal myc-tag. The two NIPSNAP4 clones differ slightly in sequence, one aligns perfectly with the NM_015469.1 sequence while the second contains the substitutions: I15V and V231A. The NIPSNAP4 sequence corresponding to NM_015469.1 was amplified from a HeLa cDNA library and cloned into pF3A, the gene contains the mutation R100Q, which is a known natural variant. Fragments of the CPAP (aa. 950-1230; 991-1253; 990-1253) and ANXA7 (aa. 308-488) genes were sequenced from the yeast clones. Secondary structure and domain predictions, along with crystal structures where available, were used to aid construct design. A CPAP construct encompassing residues 988-1338 was designed, which maps to a C-terminal domain termed the G-box [339,340]. ANXA7 constructs encompassing residues 189-488 and 266-488 were designed (Figure 5.2). ANXA7 contains four C-terminal annexin repeats spanning residues 189-

485, which fold into a globular domain. The fragment detected in the screen spans part of the 2nd annexin repeat and both the 3rd and 4th repeats. The ANXA7 189-488 construct includes all four annexin repeats, while the 266-488 construct includes the 2nd, 3rd and 4th annexin repeats.

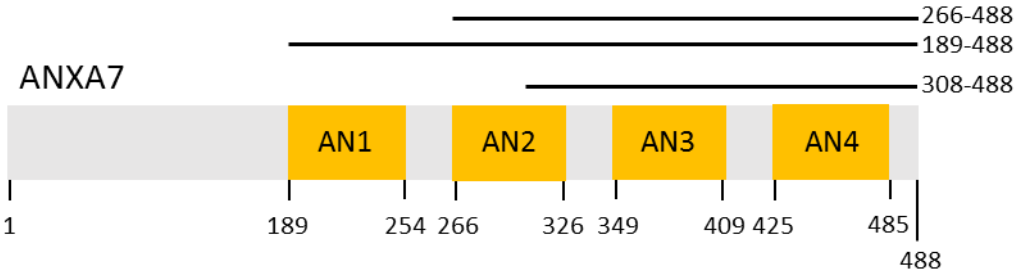

Figure 5.2 Annexin A7 construct map
Annexin A7 contains 4 C-terminal annexin repeats (AN1-4) that span residues 189-485. The construct identified in the Y2H screen encompasses part of AN2 and all of AN3 and AN4. Two constructs were design for expression using the wheat germ system: 189-488 that spans AN1-AN4 and 266-488 that spans AN2-AN4.

5.2.5 Validation of Y2H hits with GST-UL51 bait protein and wheat germ expressed prey

Full-length GST-UL51 was expressed and purified from *E. coli* by affinity chromatography followed by SEC (Figure 5.3). The protein was concentrated to 2.0 mg/ml without signs of precipitation, and a total yield of 0.25 mg/L of culture was achieved. The putative UL51 binding partners identified in the Y2H screen were expressed using the wheat germ cell-free expression system and then incubated with GST-UL51 bait protein in a pull-down experiment. Figure 5.4 shows the successful expression of all constructs except ANXA7$^{189-488}$. In repeat experiments, ANXA7$^{189-488}$ expression was never detected, and expression of ANXA7$^{266-488}$ was often absent, suggesting that ANXA7 truncations may not be stable. Of the constructs that did express, myc-CPAP$^{988-1338}$ was specifically and consistently pulled-down by GST-UL51. Since ANXA7 and STMN2 are calcium binding proteins, the experiment was repeated in the presence of supplemental $CaCl_2$ (2.5 mM). Despite the addition of calcium, expression levels of ANXA7 and STMN2 and their ability to bind UL51 were unaltered.

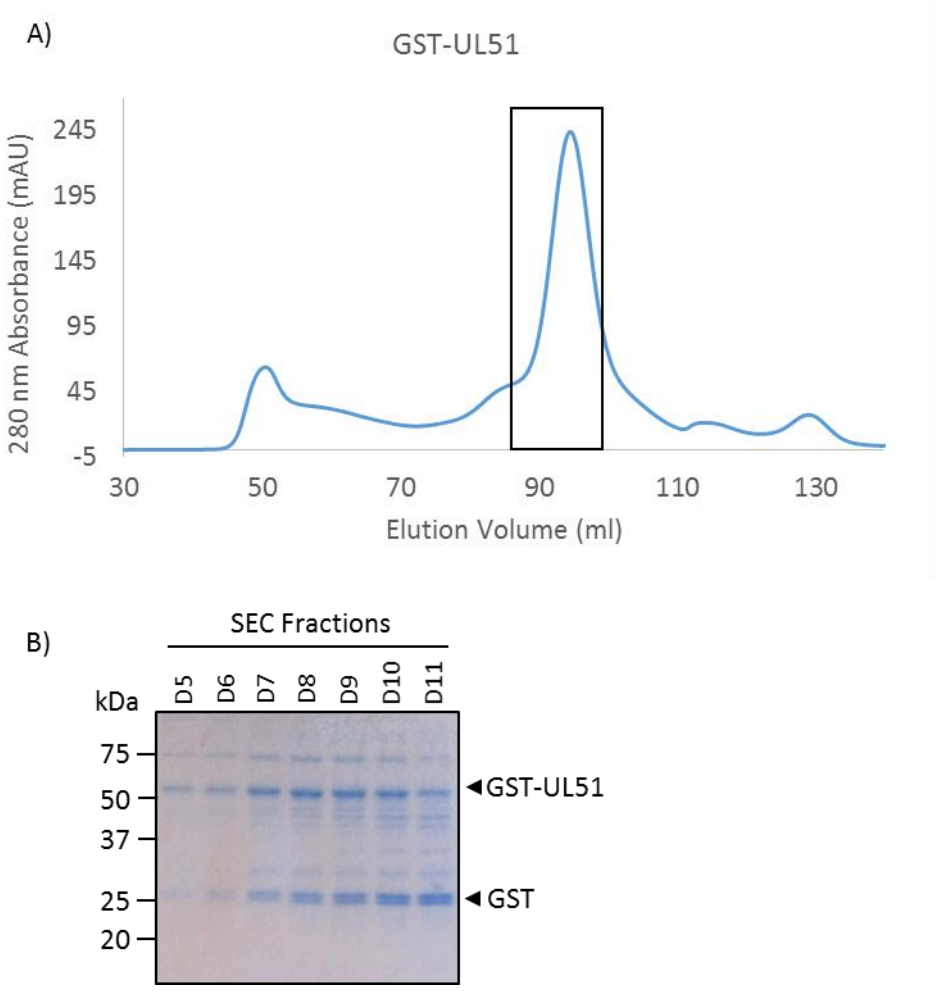

Figure 5.3 Purification of GST-UL51 full-length
N-terminally GST-tagged UL51 wild-type was expressed in BL21 (DE3) pLysS cells at 22°C overnight (2 L bacterial culture). The protein was purified by GSH affinity chromatography followed by SEC. A) SEC S200 16/600 chromatogram for GST-UL51 full-length. B) SDS-PAGE of SEC peak fractions showing a band corresponding to the predicted molecular mass of GST-UL51 (52.6 kDa) and a lower band that is likely to be free GST (26 kDa).

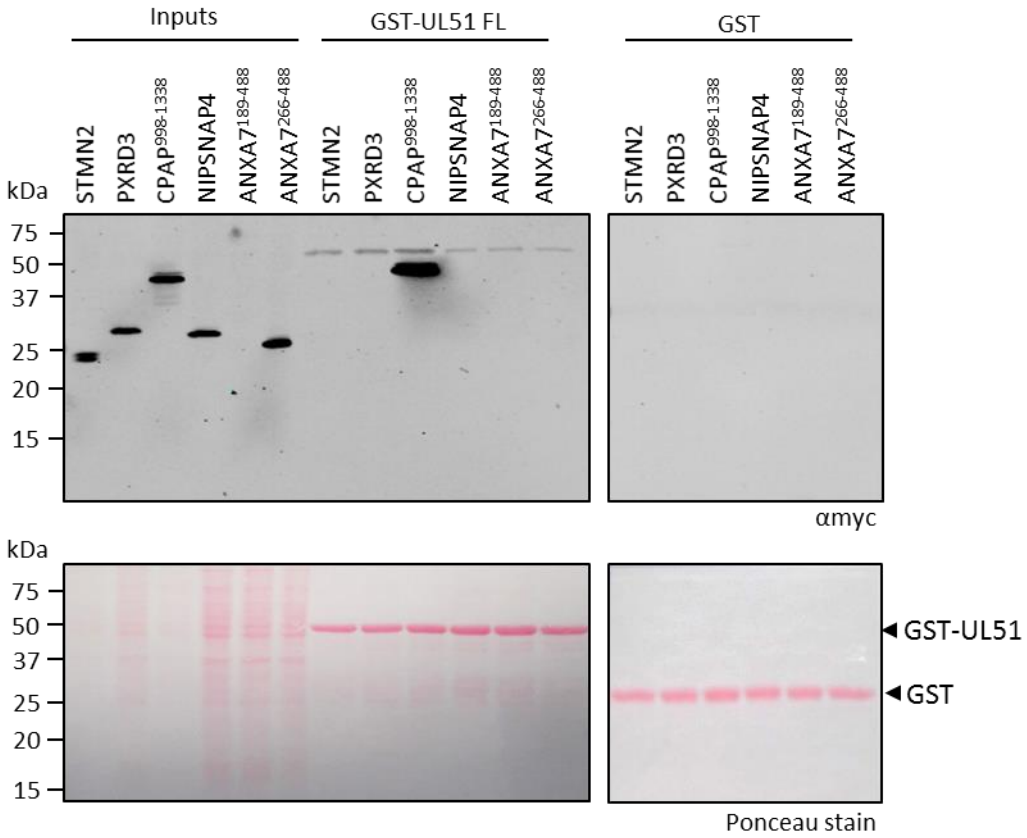

Figure 5.4 Validation of yeast two-hybrid hits by GST-UL51 pull-down
Putative UL51 binding partners identified during the Y2H screen were expressed with N-terminal myc epitope tags in a wheat germ cell-free expression reaction. All constructs except ANXA7$^{189-488}$ expressed well. GST-UL51 and GST bait proteins were immobilised on magnetic GSH beads and incubated with myc-tagged prey proteins. The presence of bait protein in the samples was confirmed by ponceau staining the membrane before probing with αmyc antibody. A strong band for CPAP in the pull-down sample indicates that this protein fragment interacts with GST-UL51, there is no corresponding band in the GST-control condition indicating that the interaction is specific. The predicted molecular masses for these constructs are: myc-STMN2 (23.3 kDa); myc-PXRD3 (29.2 kDa); myc-CPAP$^{988-1338}$ (43.0 kDa); myc-NIPSNAP4 (31.0 kDa); myc-ANXA7$^{189-488}$ (35.3 kDa); myc-ANXA7$^{266-488}$ (28.2 kDa).

5.3 UL51 interacts with human CPAP via the G-box domain

5.3.1 UL51 interacts with CPAP G-box domain in co-transfected cells

The pull-down experiment described in section 5.2.5 demonstrates an interaction between UL51 purified from *E. coli* and a CPAP fragment expressed in wheat germ cell extract. To create an environment closer to that of an infected cell, myc-CPAP$^{988-1338}$ was co-transfected into HEK 293T cells with GFP-UL51 alone, GFP-UL51 in the presence of untagged UL7, and also of GFP-7 with untagged UL51. GFP-Trap™ beads were used to capture the GFP-tagged protein, the beads were washed, and bound protein eluted into SDS-PAGE loading buffer. Figure 5.5 (bottom panel) shows that myc-CPAP$^{988-1338}$ co-immunoprecipitated with GFP-UL51 alone and in the presence of untagged UL7 (IP samples 1 &

2), and the amount of CPAP captured may be enhanced when UL7 is also present (IP sample 2). Similarly, GFP-UL7 can immunoprecipitate CPAP$^{988-1338}$ when untagged UL51 is also present (IP sample 4). CPAP is not immunoprecipitated by the GFP negative control (IP sample 3). This experiment shows that the interaction between UL51 and CPAP$^{988-1338}$ is not disrupted by the UL51-UL7 interaction, rather that interaction between the UL7-UL51 complex and CPAP may be stronger than UL51 alone, perhaps due to enhanced stability of UL51 due to UL51-UL7 co-folding. Furthermore, the interaction is not inhibited by the presence of other mammalian proteins, though it is important to be aware that the bait and prey proteins are overexpressed in this experiment.

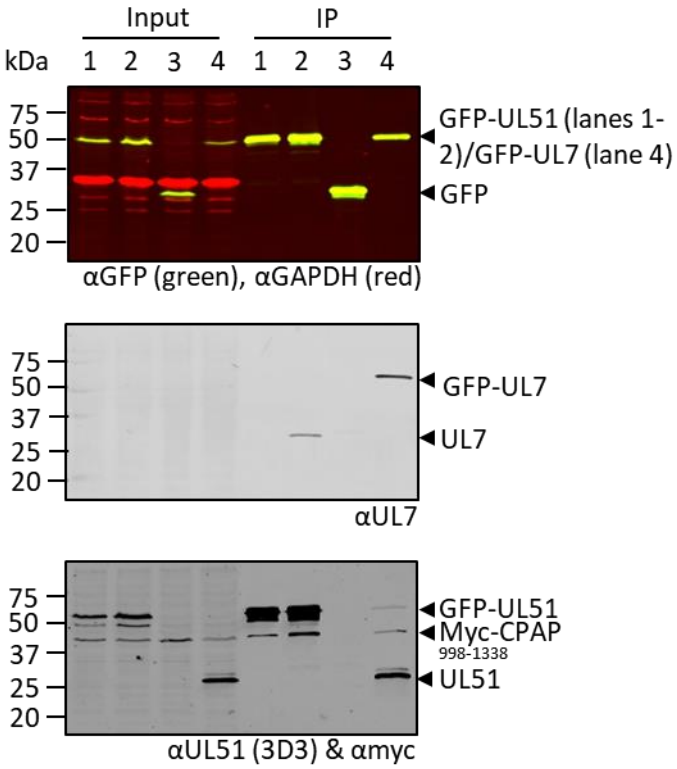

Figure 5.5 GFP-UL51 immunoprecipitation of myc-CPAP$^{988-1338}$ from co-transfected cells
HEK 293T cells were co-transfected in the following combinations: (1) GFP-UL51 + myc-CPAP$^{998-1338}$; (2) GFP-UL51 + UL7 + myc-CPAP$^{998-1338}$; (3) GFP + myc-CPAP$^{998-1338}$; (4) GFP-UL7 + UL51 + myc-CPAP$^{998-1338}$. The cells were lysed after 48 h and incubated with GFP-Trap^{TM} beads. Myc-CPAP$^{998-1338}$ is present wherever UL51 is immunoprecipitated from the lysates, either GFP-tagged or untagged. Predicted molecular masses are: GFP-UL51 (52.5 kDa); GFP-UL7 (60 kDa); myc-CPAP$^{988-1338}$ (43.0 kDa); untagged UL51 (25.5); untagged UL7 (33 kDa); GAPDH (37 kDa).

5.3.2 GST-CPAP is able to pull-out UL51 and UL7 from infected cell lysates

To determine if CPAP is able to interact with UL51 in the context of infection, a pull-down experiment was performed from infected cell lysates using purified GST-CPAP$^{1153-1338}$ bait protein. GST-CPAP$^{1153-1338}$ was expressed in *E. coli* cells and purified by affinity chromatography followed by SEC

(Figure 5.6). HaCaT cells were infected with wild-type HSV-1 or ΔUL51 HSV-1 virus and harvested at 16 h.p.i.. The CPAP bait protein was immobilised on GSH resin and incubated with the cell lysates, the beads were washed, and bound protein was eluted with glutathione. Figure 5.7 shows successful pull-down of UL51 and UL7 from wild-type HSV-1 infected HaCaT cell lysates with the GST-CPAP$^{1153-1338}$ bait protein and not with the GST control.

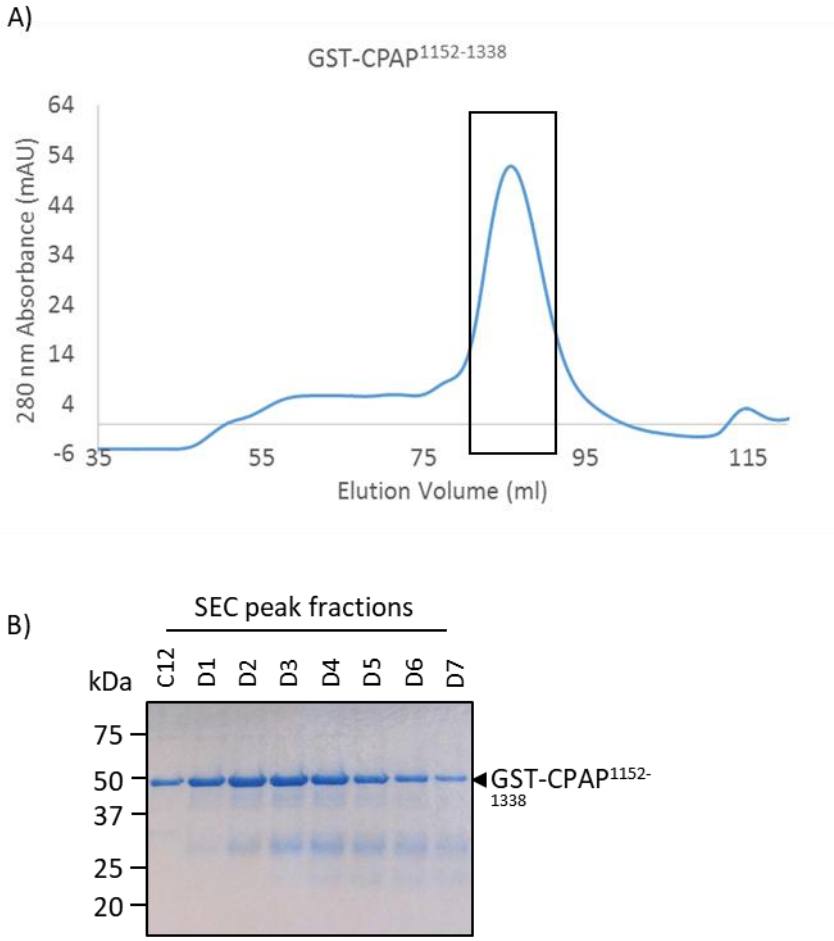

Figure 5.6 Purification of GST-CPAP$^{1153-1338}$
N-terminally GST-tagged CPAP 1151-1338 was expressed in BL21 (DE3) pLysS cells at 22°C overnight (2 L bacterial culture). The protein was purified by GSH affinity chromatography followed by SEC. A) S200 16/600 SEC chromatogram for GST-CPAP$^{1151-1338}$. B) SDS-PAGE of SEC peak fractions showing a band corresponding to the predicted molecular mass of GST-CPAP$^{1153-1338}$ (48.6 kDa).

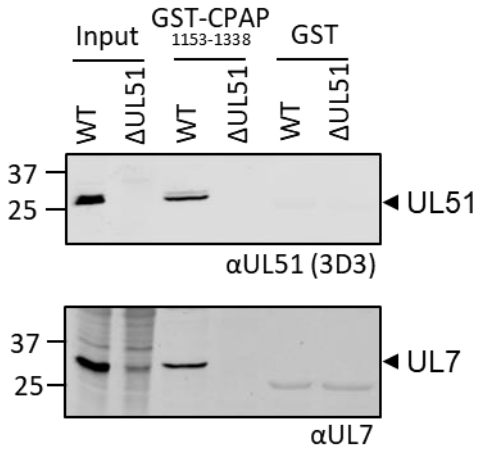

Figure 5.7 GST-CPAP$^{1153-1338}$ interacts with the UL7-UL51 complex from infected HaCaT cell lysates.
HaCaT cells were infected with wild-type (WT) HSV-1 or ΔUL51 HSV-1 at MOI 5.0. After 16 h the cells were harvested and cell lysates were incubated with human GST-CPAP$^{1152-1338}$ or GST only immobilised on GSH beads. The beads were washed and bound protein was eluted with reduced glutathione. The samples were analysed by immunoblot for the presence of UL7 and UL51. UL51 and UL7 are pulled-down by the CPAP fragment from lysate of cells infected with WT HSV-1. In the absence of UL51 (ΔUL51 virus), UL7 is not pulled-down by CPAP, confirming that the interaction is mediated by UL51.

5.3.3 Attempt to immunoprecipitate endogenous CPAP from transfected cells

To determine if UL51 can immunoprecipitate endogenous CPAP, HEK 293T cells were co-transfected with GFP-UL51 and untagged UL7. GFP-Trap™ beads were used to capture GFP-tagged protein and an αCPAP antibody was used to probe for endogenous CPAP. As shown in Figure 5.8 (top panel), GFP-UL51 and the GFP negative control were successfully captured by the beads. The predicted molecular mass of endogenous CPAP is 153 kDa, although it has been reported to run above the 170 kDa marker in SDS-PAGE [341]. The αCPAP antibody recognises many bands around the 150 kDa marker (Input lanes, bottom panel of Figure 5.8) and it is not clear if any or all of these bands correspond to endogenous CPAP. Assuming CPAP is detected by the antibody, there is no evidence of a specific interaction between UL51 and endogenous CPAP in the pull-down samples (Figure 5.8, IP lanes in the bottom panel). A band at ≈50 kDa (black arrowhead) is present in the GFP-UL51 pull-down lane and not the GFP negative control lane, which is likely to be cross-reactivity of the αCPAP antibody with GFP-UL51 (52.5 kDa). The experiment was repeated multiple times using both HEK 293T and HeLa M cells, and there was never any convincing evidence that GFP-UL51 could immunoprecipitate endogenous CPAP.

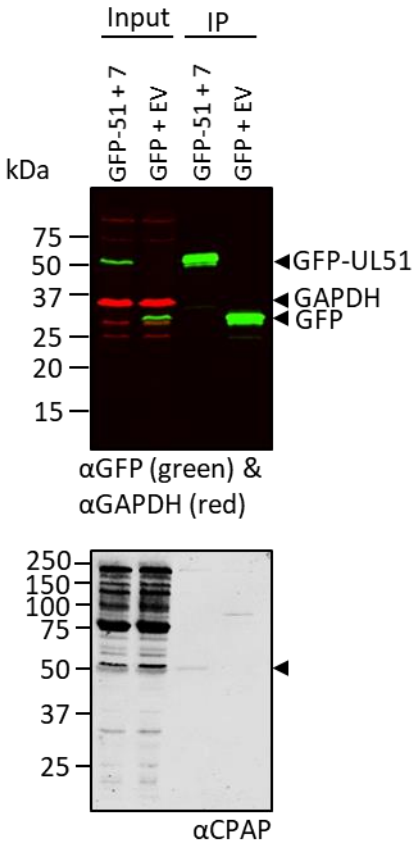

Figure 5.8 Attempt to co-immunoprecipitate endogenous CPAP with GFP-UL51
HEK 293T cells were co-transfected with GFP-UL51 and untagged UL7, or GFP and empty vector (EV). GFP-tagged protein was captured using GFP-Trap™ beads and eluted into SDS-PAGE loading buffer. The samples were analysed by immunoblot, the top blot shows successful capture of GFP-UL51 and GFP by the GFP-Trap™ beads (IP). However, the bottom blot shows that there is no evidence of CPAP co-immunoprecipitation (predicted molecular mass 150 kDa) with GFP-UL51. A band at ≈50 kDa (black arrowhead) is present in the GFP-UL51 pull-down lane and not the GFP negative control lane, which is likely to be cross-reactivity of the αCPAP antibody with GFP-UL51 (52.5 kDa).

5.3.4 Attempt to Immunoprecipitate endogenous CPAP from synchronised cells

CPAP expression levels are known to fluctuate with the cell cycle: levels gradually increase from early S-phase until mitosis, and then decrease significantly after mitosis as cells enter early G1-phase [341]. Expression levels of endogenous CPAP are likely to be low given that CPAP is a centriolar scaffold protein and each cell possess only two centrioles unless undergoing cell division. Therefore, the ability to immunoprecipitate endogenous CPAP may be enhanced if the experiment is performed when CPAP levels are maximal, i.e. during G2/M-phase. To achieve this, Hela M cells were transfected with UL51 then treated with nocodazole to stimulate G2/M phase cell-cycle arrest. The first question was whether nocodazole treatment increases CPAP levels. Figure 5.9A, compares CPAP levels in transfected and un-transfected (UN) cells, as well nocodazole treated (sync) and untreated (async) cells. There are two prominent bands in these samples, the band indicated by the black arrow is

enriched in transfected and nocodazole treated cells, and the band indicated by the black arrowhead is only present in cells that have not been treated with nocodazole. Neither of these bands correspond to the predicted molecular mass of CPAP (153 kDa), however, CPAP has been reported to present at 170 kDa in SDS-PAGE, which approximately corresponds to the band indicated with the black arrow [341]. A co-immunoprecipitation experiment was performed using the αCPAP antibody and lysate from Hela M cells transfected with UL51, with and without nocodazole treatment. The aim was to immunoprecipitate CPAP directly from the lysate in an attempt to maximise the amount of CPAP in the pull-down sample, then to probe for UL51. Cells were transfected with full-length UL51 and UL51 1-170 in an attempt to map the CPAP binding region in UL51. As shown in Figure 5.9B (bottom immunoblots), full-length UL51 but not UL51 1-170 was detected in the input lanes, this is consistent with other experiments where UL51 1-170 was not detected in cell lysates. In Figure 5.9B (top immunoblots), the band suspected to be full-length CPAP (black arrow) is present in the pull-down lanes, but UL51 is not detected in these samples.

While there is clear evidence for an interaction between co-transfected UL51 and $CPAP^{998-1338}$, or UL51 and wheat germ expressed $CPAP^{998-1338}$, there is not yet evidence for an interaction between UL51 and full-length CPAP. However, this does not rule out the possibility of a UL51-CPAP interaction in cells. For instance, if CPAP is immunoprecipitated from these cells then it is possible that the αCPAP antibody occludes the UL51 binding site, which would explain why UL51 is not co-immunoprecipitated. Or perhaps other viral proteins are required to disrupt the centrosome/centriole structure before UL51 can access CPAP.

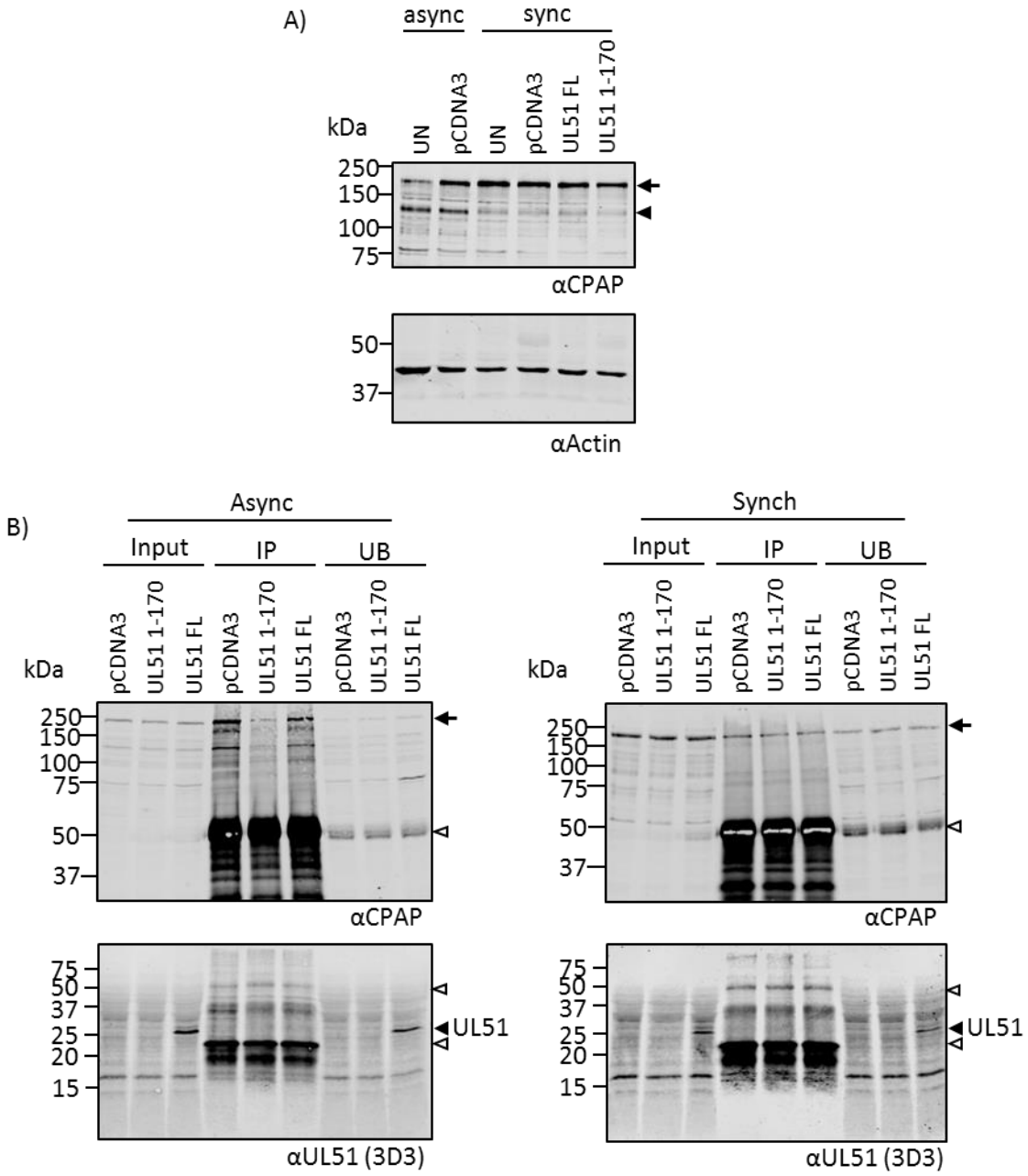

Figure 5.9 Immunoprecipitation of endogenous CPAP from synchronised cells
A) A test to determine the impact of transfection and nocodazole treatment on CPAP expression levels. HeLa M cells were either un-transfected (UN), or transfected with empty vector (pcDNA3) or UL51, and treated with nocodazole (synch), or left untreated (asynch). The band indicated by the black arrow is enriched in cells following transfection and nocodazole treatment, and is suspected to be full-length CPAP. B) Immunoprecipitation experiment from UL51-transfected HeLa M cells, with (synch) or without (asynch) nocodazole treatment. Expression of UL51 FL is indicated by the black arrowhead, antibody heavy and light chains are highlighted by the white arrowheads. The band suspected to be full-length endogenous CPAP is indicated by the black arrow.

5.3.5 Attempt to immunoprecipitate endogenous CPAP from infected cells

Though it was not possible to immunoprecipitate endogenous CPAP from cells transfected with UL51, attempts were made to co-immunoprecipitate UL51 and endogenous CPAP from infected cells. Both available αUL51 antibodies were tested: 3D3 and 2B3, the former recognises an epitope within residues 1-170 of UL51 and the latter an epitope within residues 171-244. UL7 co-immunoprecipitates with UL51 when the 2B3 antibody is used but not with the 3D3 antibody. HaCaT cells were infected with either wild-type HSV-1, ΔUL51 HSV-1 or mock infected. The experiment was performed multiple times with cells being harvested at either 7 or 16 h.p.i.. After harvesting the cells were lysed and the lysates were incubated with either the 3D3 or 2B3 antibody. Figure 5.10 shows immunoprecipitation of UL51 with both antibodies (bottom immunoblots) from lysates harvested at 7 h.p.i.. Probing for endogenous CPAP (top immunoblots) produces a similar banding pattern in the input lanes as previously seen with the αCPAP antibody (Figure 5.8). The αCPAP antibody detects a band at ≈100 kDa in infected but not mock infected cell lysates. This band was later identified using an αICP0 antibody, HSV-1 ICP0 is 110 kDa and so it is likely that the αCPAP antibody cross-reacts with ICP0. Despite successful immunoprecipitation of UL51, there is no evidence of CPAP co-immunoprecipitation in the IP samples. Similar results were observed for UL51-immunoprecipitation experiments performed from lysates harvested at 16 h.p.i (not shown).

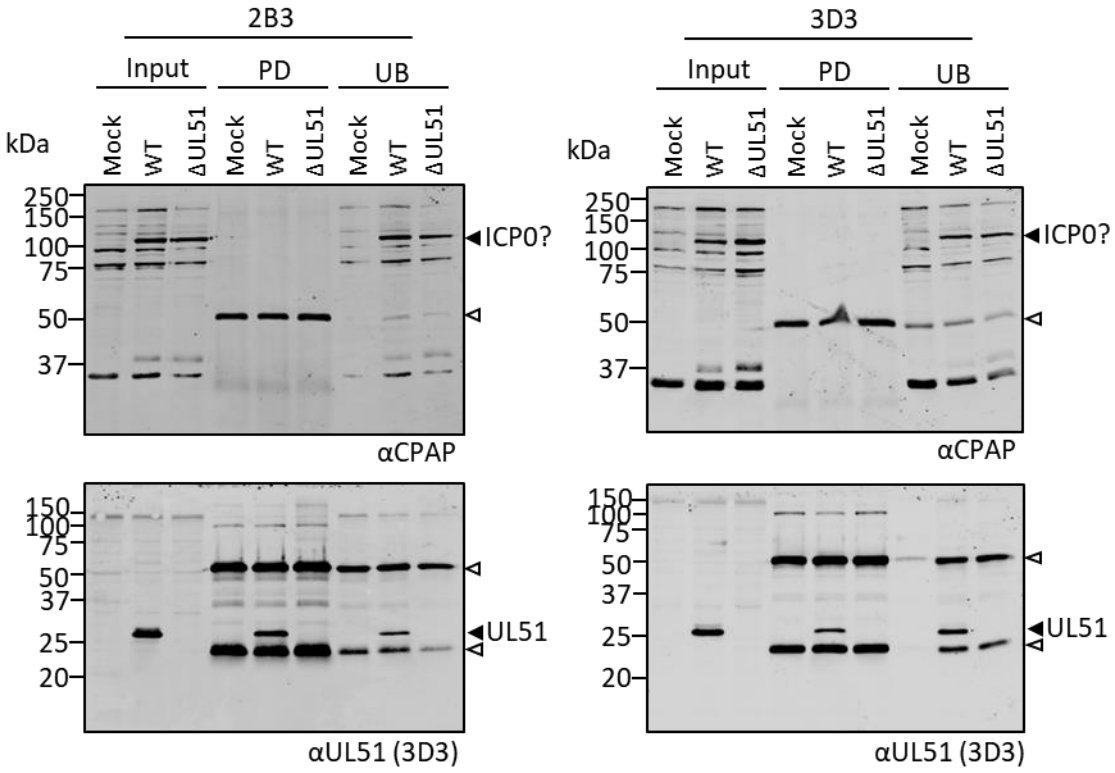

Figure 5.10 Attempt to co-immunoprecipitate UL51 and CPAP from infected cells
HaCaT cells were infected with either wild-type HSV-1 (WT), ΔUL51 HSV-1 or mock-infected (MOI 5.0). Cells were harvested at 7 h.p.i. and cell lysates were incubated with either 3D3 or 2B3 antibody to immunoprecipitate UL51 (and UL7 when the 2B3 antibody was used). UL51 was successfully immunoprecipitated (IP lanes, bottom blots) from WT infected cells, though some UL51 is also present in the unbound fraction (UB). However, there is no evidence of CPAP co-immunoprecipitation (predicted molecular mass 150 kDa) in the top blots. The white arrowheads indicate the UL51 antibody heavy and light chains. The CPAP antibody is thought to cross-react with HSV-1 protein ICP0.

5.3.6 Summary

The previous sections present the following evidence in favour of an interaction between the HSV-1 protein UL51 and a C-terminal fragment of the cellular protein CPAP: 1) In a pull-down experiment purified GST-UL51 bait protein was able to capture a CPAP fragment expressed in wheat germ cell extract; 2) CPAP was immunoprecipitated from cells that were co-transfected with a CPAP fragment and GFP-UL51(or GFP-UL7 with untagged UL51); 3) Purified GST-CPAP$^{1152\text{-}1338}$ was able to capture the UL7-UL51 complex from infected cell lysates. However, attempts to immunoprecipitate the endogenous CPAP protein were deemed unsuccessful, partly due to the ambiguity in interpreting the bands detected by the αCPAP antibody. Assuming the antibody was able to correctly detect endogenous CPAP then UL51 (+UL7) was unable to immunoprecipitate the endogenous CPAP protein in these experiments. The inability to co-immunoprecipitate proteins does not necessarily mean that they do not interact in cells. Complexes formed through weak and transient interactions are likely to be difficult to co-immunoprecipitate. Immunoprecipitation experiments have many caveats that can

prevent protein co-immunoprecipitation, e.g. the lysis and wash buffers may destabilise the interaction, the antibody or affinity tags used could interfere with complex formation, or a protein partner(s) may precipitate during the incubation and centrifugation steps (a problem particularly associated with filamentous cytoskeletal proteins). With this mind, further characterisation of the UL51-CPAP interaction using biochemical techniques was considered worthwhile despite the inability to co-immunoprecipitate endogenous CPAP with UL51.

5.4 UL51 binds human CPAP in a manner similar to STIL

5.4.1 The CPAP-STIL interaction

Centrioles are evolutionally conserved barrel-shaped organelles with characteristic 9-fold radial symmetry [342,343] (Figure 5.11B). Two centrioles and pericentriolar material (PCM) form the centrosome, which is the primary MTOC in eukaryotic cells [344]. Centrosome duplication precedes mitosis and enables mitotic spindle formation. Upon cell division, each daughter cell receives a single centrosome [342]. Most centrioles consist of a core centriole structure that is surrounded by nine sets of microtubule triplets (Figure 5.11B) [343]. Extensive genetic studies, mostly in *Drosophila melanogaster*, have identified the main protein components required for centriole assembly, extension and duplication. The centriole core is composed of a small number of conserved structural proteins: CPAP/SAS-4, PLK4/SAK, SAS-6, STIL/Ana2, CEP152/Asl and CEP135 [342,345].

Human centriolar protein CPAP (SAS-4 in worms and flies) is a large (153 kDa) multi-domain protein (Figure 5.11A) that acts as a scaffold for centriole assembly and as a regulator of centriole elongation together with CEP120, CEP135 and SPICE1 [341,346-348]. The elongation rate of centriolar microtubules is significantly slower than that of cytoplasmic microtubules [349-351]. The restricted growth of centriolar microtubules has recently been attributed to CPAP, which purportedly acts as a plus-end microtubule 'cap' to dampen elongation [339,352]. CPAP also contains a MT destabilising motif (PN2-3 with 112 amino acids) that is able to depolymerise taxol-stabilised MTs in a manner similar to that of another known MT destabilising protein, stathmin [353]. CPAP regulation is finely tuned, and exogenous overexpression of CPAP results in abnormally long centrioles [341,354-356].

The CPAP protein comprises a tubulin-binding domain (PN2-3), a microtubule-binding domain (MBD), a coiled-coil dimerisation domain, and a C-terminal G-box (TCP10) domain (Figure 5.11A). As mentioned previously, the CPAP fragment identified in the Y2H screen spans the human G-box domain. Crystal structures of the zebra fish (*Danio rerio*) and *Drosophila melanogaster* G-box domains reveal a unique conformation, comprising a single solvent-exposed β-sheet containing 17-20 antiparallel consecutive β-strands [286,357] (Figure 5.11B). In solution, purified *D. rerio* CPAP G-box domain self-associates in a head-to-tail manner to form a continuous sheet resembling amyloid fibrils [357]. The G-box domain mediates the interaction between CPAP and another core centriole protein, STIL

[286,340,348,358]. STIL, in concert with PLK4 and SAS-6, has been shown to influence centriole number; overexpression of STIL triggers centriole duplication [359-361]. Furthermore, depletion of either STIL, PLK4 or SAS-6 blocks centriole duplication [359,361].

Co-crystallisation of the G-box domain of *D. rerio* CPAP$^{937-1124}$ (DrCPAP) in complex with a peptide of *D. rerio* STIL$^{408-428}$ (DrSTIL) shows the STIL peptide binding in a polyproline helical conformation via a proline-rich motif (PDB: 4BXR and 4LZF) [286,340]. Similarly, the *D. melanogaster* G-box domain was also shown to bind a *D. melanogaster* STIL peptide in an analogous manner [340]. Based on these studies, a proline-rich CPAP-binding motif in STIL was defined with the consensus sequence: PRxxPxP. Interestingly, the proline-rich C-terminal region of UL51 contains two partial PRxxPxP sequences, highlighted in Figure 5.11C. In the DrCPAP-DrSTIL structure, STIL residues P417, P421 and P423 pack against aromatic residues F978, Y994 and F1015 of CPAP (PDB: 4BXR). Residue R418 of STIL makes a cation-π interaction with the phenyl ring of Y998, and is involved in a water-mediated H-bonding network with CPAP residues H1003 and T1005 [340]. Finally, side-chain interactions occur between the STIL peptide and CPAP residues Y994, Q1019, E1021 [286,340]. Human and *D. rerio* CPAP share 64.5% sequence identity and all CPAP residues involved in the interaction with STIL are conserved between DrCPAP and Human CPAP (HsCPAP). DrCPAP and HsCPAP contain additional aromatic residues further towards the C terminus of the beta-sheet that are arranged in a similar conformation to those interacting with the STIL peptide. Interestingly, the DrSTIL peptide contains conserved proline residues (P435 and P438) that are predicted to be positioned such that they could interact with these additional aromatic residues in an analogous manner [340]. The two partial PRxxPxP sequences in the C terminus of UL51 span residues 221-227 and 230-236, and are highlighted in Figure 5.11C. In each of the putative UL51 CPAP-binging motifs, equivalent UL51 residues are present for three out of four of the STIL residues involved in the DrCPAP-DrSTIL interaction (e.g. P417, R418, P421 and P423) (Figure 5.11C). The first putative motif in UL51 (aa. 221-227) lacks a proline residue equivalent to P421 in DrSTIL, possessing an alanine instead. Alanine will not replicate the stacking interaction formed between DrSTIL-P421 and DrCPAP-Y998, but is also unlikely to disrupt the interaction since it is a small non-polar residue. Another discrepancy between the UL51 sequence and DrSTIL is the threonine in position 224 of UL51, which is a serine residue in DrSTIL. However, given that both serine and threonine are similar in size and are both non-polar, this difference is unlikely to disrupt the interaction. The second putative motif in UL51 (aa. 230-236) lacks a proline residue equivalent to P423 in DrSTIL, possessing an arginine instead. Arginine chemistry differs considerably to that of proline and it is likely that this substitution will influence the interaction. UL51 also has a proline residue at position 239 that is equivalent to P435 of DrSTIL.

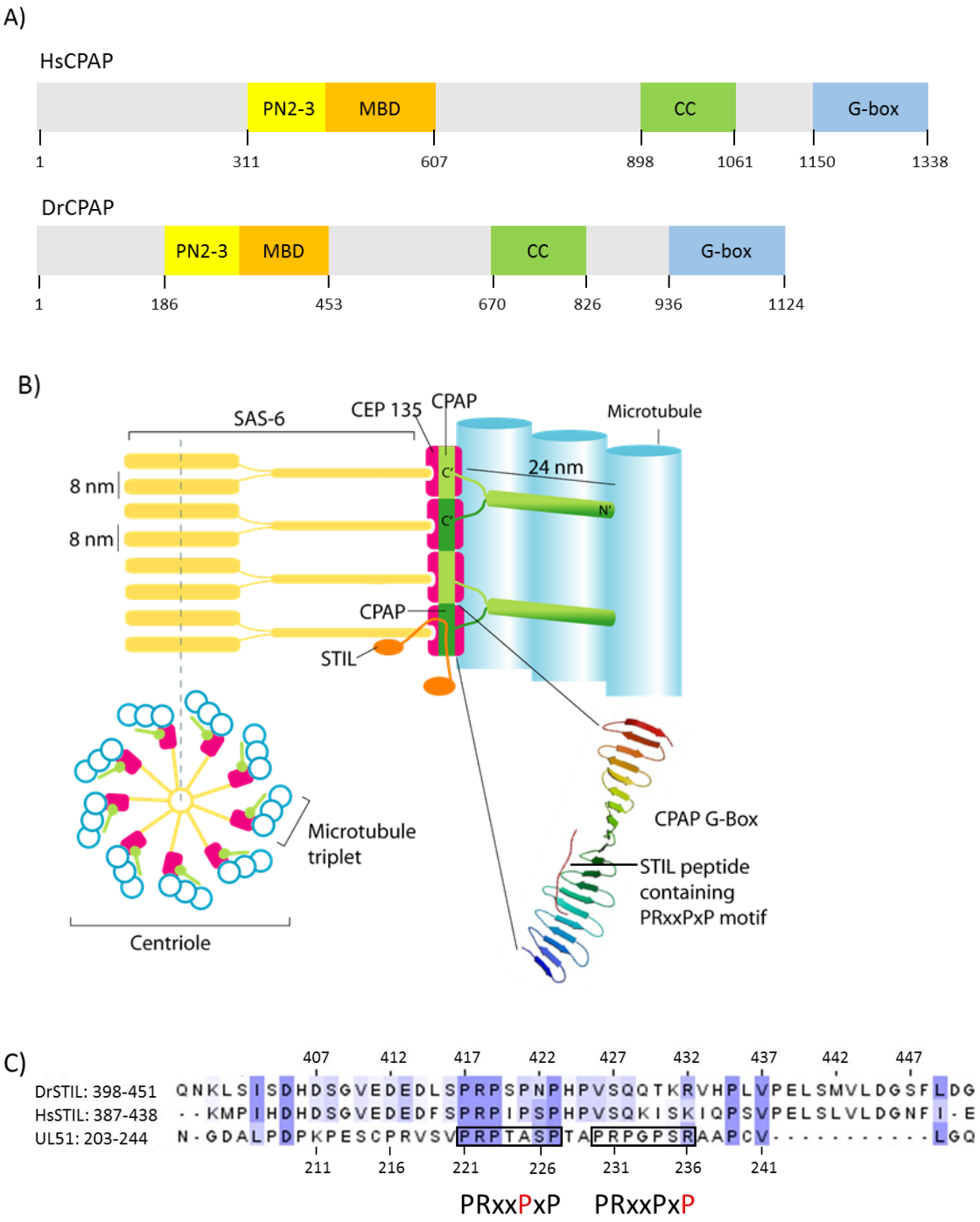

Figure 5.11 Mapping the interaction between DrCPAP and DrSTIL

A) Domain architecture of human (Hs) and *D. rerio* (Dr) CPAP, highlighting the tubulin-binding domain (PN2-3), microtubule-binding domain (MBD), a coiled-coil dimerisation domain (CC), and C-terminal G-box/TCP10 domain. B) Schematic representation of centriole assembly showing microtubule triplets arranged in 9-fold radial symmetry around the centriole core. The crystal structure shown is of the DrCPAP G-box domain in complex with DrSTIL peptide (PDB: 4BXR, [340]). C) Multiple sequence alignment of STIL fragments from *D. rerio* (aa. 398-451) and human (aa. 387-488) with UL51 (aa. 203-244). The PRxxPxP CPAP-binding consensus sequences spans DrSTIL residues 417-423 (top residue numbering). UL51 contains two partial consensus sequences, which are boxed in the figure. The bottom residue numbering corresponds to UL51.

5.4.2 UL51 binds HsCPAP in a manner similar to STIL

As described in the previous section, UL51 contains proline-rich sequences that resemble the CPAP-binding motif in STIL. It was hypothesised that these sequences might mediate the UL51-CPAP interaction. To test this, full-length and C-terminal UL51 truncations were cloned for expression in the wheat germ cell-free expression system. GST-HsCPAP$^{1153\text{-}1338}$ was purified and used as bait protein in a pull-down experiment with full-length and truncated UL51 (Figure 5.6). As shown in Figure 5.12A, the UL51 truncations that lack the putative CPAP binding motifs are not pulled-down by GST-CPAP$^{1153\text{-}1338}$. Furthermore, binding of the UL51 1-227 species, which contains only one of the putative motifs, appears to be weaker compared to constructs containing both motifs (Figure 5.12A).

To further investigate the role of these putative motifs in CPAP binding, a series of UL51 point mutations were designed that were intended to disrupt the interaction. Two mutated, full-length UL51 constructs were generated: UL51 P221D+R222D and UL51 A225E+P226D. The P221D+R222D mutations were intended to eradicate the potential for analogous stacking interactions to form between the UL51 proline residues and CPAP residues F978 and Y994. The A245E+P227D mutations were primarily designed to disrupt a hydrophobic pocket in CPAP, by substituting alanine in position 225 with glutamic acid, which is charged and bulky compared to alanine. The pull-down experiment was repeated using GST- HsCPAP$^{1153\text{-}1338}$ bait and the UL51 mutants as prey. Figure 5.13 demonstrates that the P221D+R222D mutations were sufficient to disrupt the CPAP-UL51 interaction, while A225E+P227D were not. Also, a C-terminal fragment of UL51 encompassing residues 171-244 was sufficient to bind CPAP (Figure 5.13). These data show the UL51-HsCPAP interaction to be mediated by a motif in UL51 that is analogous to the CPAP-binding motif in STIL. Furthermore, two UL51 point mutations have been identified that abolish the UL51-HsCPAP$^{1153\text{-}1338}$ interaction.

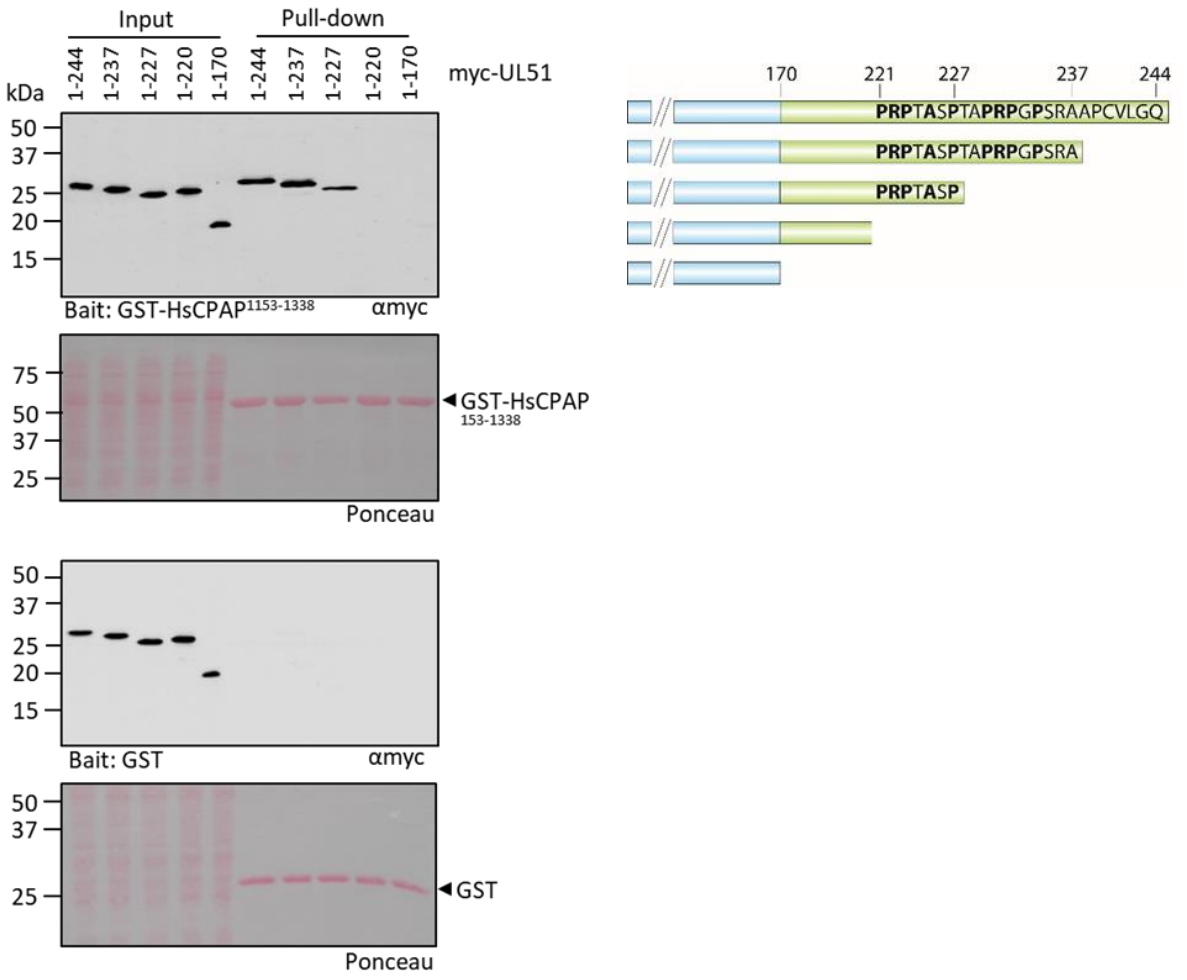

Figure 5.12 Mapping the UL51 CPAP-binding site
A pull-down experiment was performed using purified GST-HsCPAP$^{1153-1338}$ bait protein and myc-tagged UL51 truncations that were expressed in the wheat germ cell-free expression system. The immunoblot shows myc-tagged UL51 truncation constructs that bound GST-HsCPAP$^{1153-1338}$, with a schematic of the UL51 truncations shown on the right.

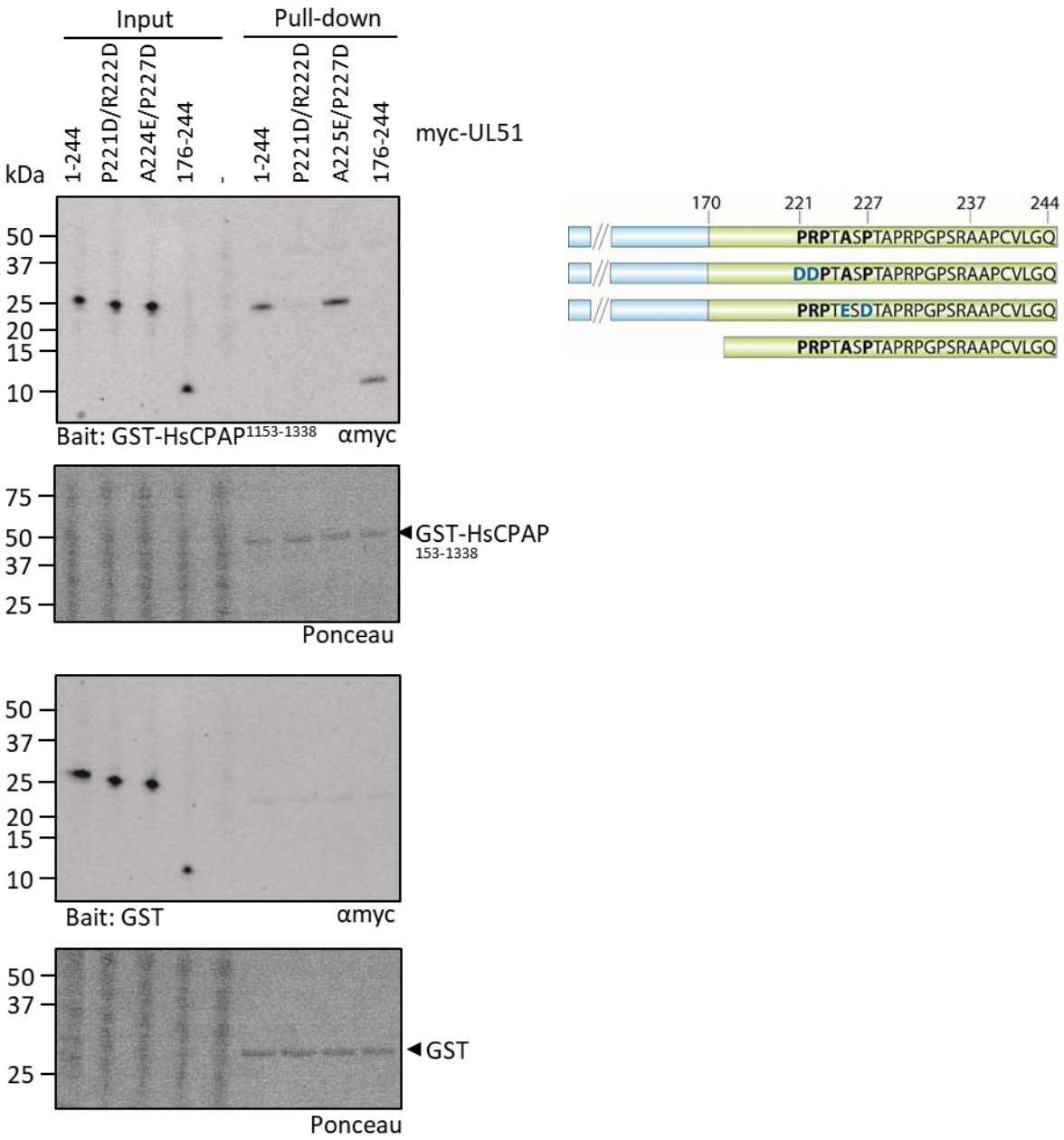

Figure 5.13 Mapping UL51 residues involved in the interaction with CPAP
A pull-down experiment was performed using purified GST-HsCPAP$^{1153-1338}$ bait protein and myc-tagged UL51 mutants expressed in the wheat germ cell-free expression system. The UL51$^{P221D+R222D}$ mutant no longer binds CPAP.

5.4.3 Crystallisation of UL51 peptide with DrCPAP fragment

In the previous section, UL51 was shown to bind CPAP in a manner similar to STIL. With knowledge of the UL51 binding site, it was possible to try and replicate the DrCPAP-DrSTIL crystal structure with a UL51 peptide in place of STIL (Published DrCPAP-DrSTIL structures: 4LD3, DrCPAP$^{943-1121}$-DrSTIL$^{398-450}$; 4LZF, DrCPAP$^{943-1121}$-DrSTIL$^{414-428}$; 4BXR, DrCPAP$^{943-1121}$-DrSTIL$^{408-428}$). Two synthetic UL51 peptides were ordered for co-crystallisation experiments with the CPAP G-box domain: UL51 217-229 (RVSV**PRPTASP**TA) that is equivalent to a DrSTIL$^{413-425}$ peptide, and UL51 217-237

(RVSV**PRPTASP**TA**PRP**G**P**SRA), which is equivalent to a DrSTIL$^{413-433}$ peptide. The pull-down experiments presented in section 5.4.2 were performed with purified human GST-tagged CPAP G-box. However, attempts to purify sufficient quantities of human CPAP$^{1153-1338}$ for crystallisation experiments were unsuccessful; expression levels were low and protein precipitation was evident upon concentrating the sample beyond ≈2.0 mg/ml (Figure 5.14B). A decision was made to express and purify the published *Danio rerio* CPAP$^{943-1121}$ construct from a plasmid kindly provided by Dr Vakonakis [286]. The DrCPAP$^{943-1121}$ G-box was expressed in BL21 (DE3) pLysS cells and purified in accordance with the published protocol [286]. Switching CPAP species greatly improved expression levels, and the protein could be purified and concentrated to at least 7.0 mg/ml without precipitation (Figure 5.14). A pull-down experiment was performed to confirm that the DrCPAP G-box domain is able to interact with UL51. As shown in Figure 5.15, both *D. rerio* and Human CPAP G-box domains are able to interact with GST-UL7+UL51 C9S full-length. DrCPAP does not interact with GST-UL7+UL51 C9S 1-170, as predicted. Unexpectedly, there is a small amount of HsCPAP present in the pull-down lane with the UL51 C9S 1-170 bait, suggesting that there may be an additional CPAP-binding site in UL51 not yet characterised, or that due to the low solubility of purified HsCPAP$^{1153-1338}$ some protein may have precipitated onto the GSH beads.

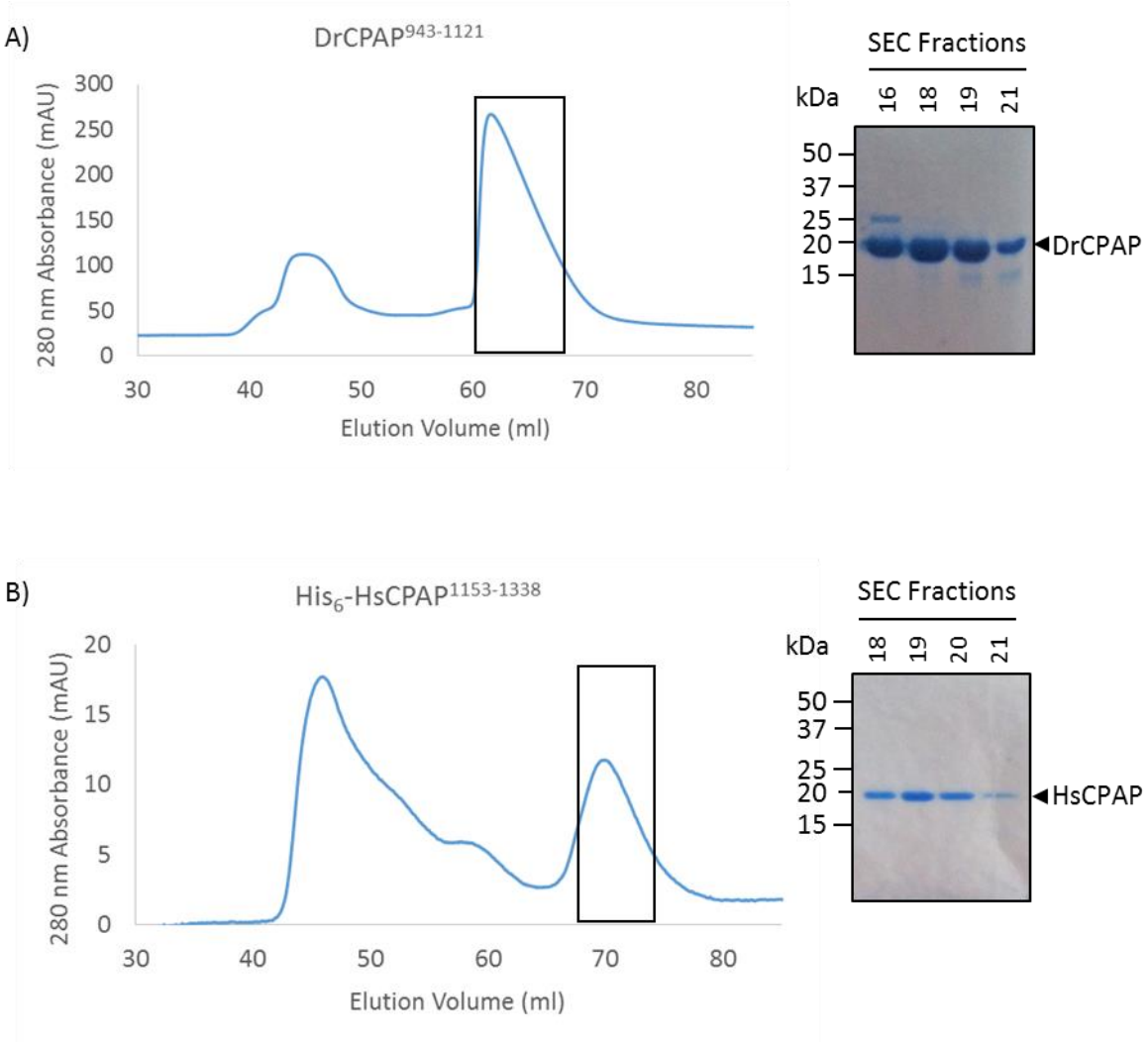

Figure 5.14 Purification of DrCPAP$^{943-1121}$ and HsCPAP$^{1153-1338}$
N-terminally GST-tagged DrCPAP$^{943-1121}$ and N-terminally His$_6$-tagged HsCPAP$^{1153-1338}$ were expressed in BL21 (DE3) pLysS cells at 22°C overnight. The proteins were purified using an appropriate affinity chromatography step followed by SEC. The GST tag was cleaved from DrCPAP$^{943-1121}$ by incubating the sample with 3C PreScission protease before SEC was performed. A) SEC S75 16/600 chromatogram for DrCPAP$^{943-1121}$ and SDS-PAGE of SEC peak fractions showing a band corresponding to the predicted molecular mass of DrCPAP$^{943-1121}$ (20.7 kDa). B) SEC S75 16/600 chromatogram for His$_6$-HsCPAP$^{1153-1338}$ and SDS-PAGE of SEC peak fractions showing a band corresponding to the predicted molecular mass of HsCPAP$^{1153-1338}$ (21.9 kDa).

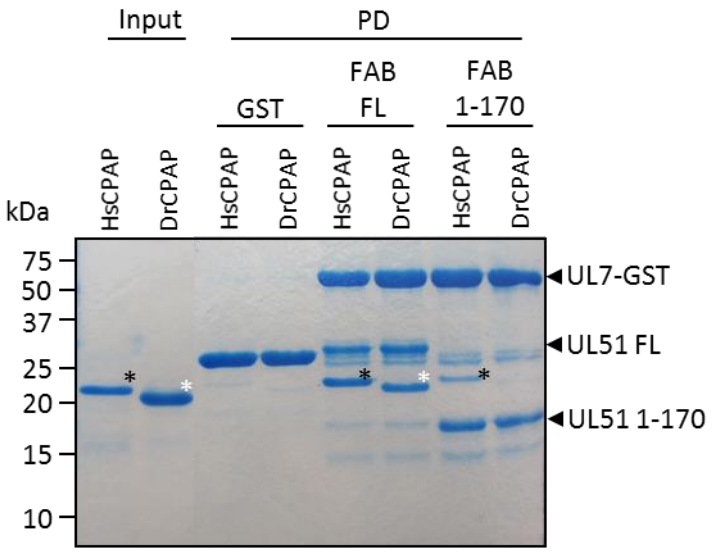

Figure 5.15 Purified HsCPAP and DrCPAP G-box domains interact with FAB C9S FL
A pull-down experiment was performed to determine if DrCPAP$^{943-1121}$ (white star) and HsCPAP$^{1153-1338}$ (black star) could interact with GST-UL7+UL51 C9S full-length bait (FAB FL). GST-UL7+UL51 C9S 1-170 (FAB 1-170) was included as a negative control since UL51 1-170 lacks the CPAP-binding motif. SDS-PAGE analysis shows that FAB FL is able to interact with both HsCPAP and DrCPAP. Unexpectedly, FAB 1-170 was able to interact with HsCPAP despite lacking the CPAP-binding motif.

Co-crystallisation experiments were prepared with DrCPAP$^{943-1121}$ and either one of the UL51 peptides. DrCPAP$^{943-1121}$ protein and UL51 peptide were combined in a ≈1:3 molar ratio (peptide in excess), which equated to DrCPAP$^{943-1121}$ protein at 7.0 mg/ml (341 µM) combined with 1 mM of UL51 peptide. The DrCPAP-UL51 peptide samples were incubated on ice for 10 m. Initially, two 96-well nanolitre sparse-matrix screens were prepared: Morpheus® HT and the PEG/Ion screen. These screens were selected because they contain conditions similar to those that produced DrCPAP-DrSTIL crystals used for structure solution. Crystallisation reservoir and protein drops were dispensed in a 1:1 (200 nl : 200 nl) ratio, and the plates were stored at 20°C. After less-than 24 h, ≈65% of the Morpheus® HT conditions containing the CPAP-UL51$^{217-237}$ sample had many large crystals (Table 5-3). This protein sample also produced crystals in the PEG/Ion screen, where ≈30% of the conditions contained crystalline material. Similarly, crystals were present in drops prepared with the CPAP-UL51$^{217-229}$ sample in both the Morpheus® HT and PEG/Ion screens. However, fewer conditions produced crystals for the CPAP-UL51$^{217-229}$ sample compared to CPAP-UL51$^{217-237}$, the crystals took longer (1-3 days) to grow and were round in appearance (Table 5-3).

Table 5-3 Images of DrCPAP$^{943-1221}$ co-crystallised with either UL51$^{217-229}$ or UL51$^{217-237}$

Well	Condition	Peptide	Image
PEG/Ion 44	0.2 M Ammonium phosphate dibasic 20% w/v polyethylene glycol 3,350	UL51$^{217-237}$	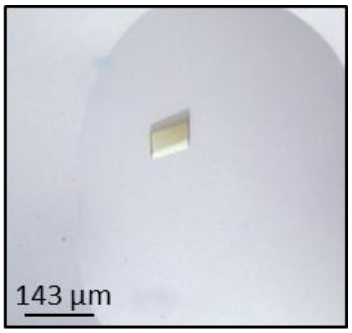
Morpheus® E3	0.12 M ethylene glycol 0.1 M Buffer System 1 pH 6.5 50% v/v Precipitant Mix 3	UL51$^{217-237}$	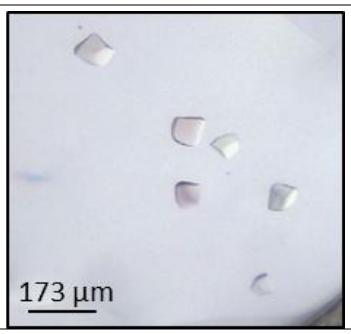
Morpheus® E9	0.12 M ethylene glycol 0.1 M Buffer System 3 pH 8.5 50% v/v Precipitant Mix 1	UL51$^{217-237}$	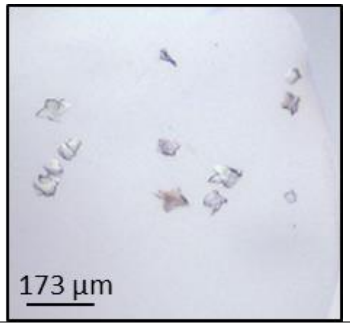
Morpheus® H2	0.1 M amino acids 0.1 M Buffer System 1 pH 6.5 50% v/v Precipitant Mix 2	UL51$^{217-237}$	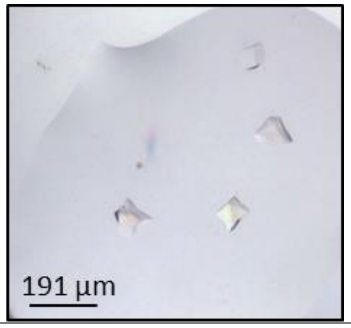
Morpheus® F5	0.12 M monosaccharides 0.1 M Buffer System 2 pH 7.5 50% v/v Precipitant Mix 1	UL51$^{217-229}$	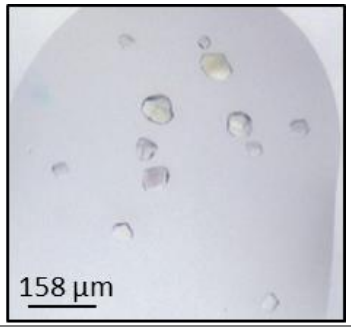

Well	Condition	Peptide	Image
PEG/Ion2 15	4% v/v Tacsimate™ pH 7.0 12% w/v polyethylene glycol 3,350	UL51$^{217-229}$	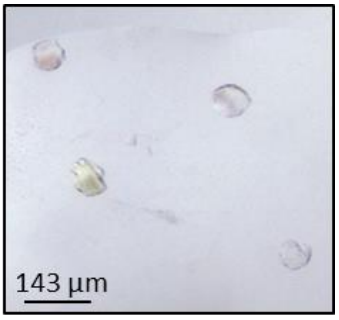

5.4.4 X-ray diffraction experiments for DrCPAP-UL51 crystals

A selection of crystals prepared using the UL51$^{217-229}$ and UL51$^{217-237}$ peptides were harvested for X-ray diffraction experiments. Several crystals from different crystallisation conditions were mounted and cryoprotected in mother liquor supplemented with 25% glycerol, before plunge cryo-cooling in liquid nitrogen. X-ray diffraction data were collected using the synchrotron facilities at the Diamond Light Source in Oxford and xia2 was used for data processing. Data collection statistics for three of these crystals are shown in Table 5-4. The DrCPAP G-box domain was solved by molecular replacement using DrCPAP (PDB: 4LD1, [286]) as a starting model with the solvent molecules removed. The crystals tested produced datasets with resolution ranging from 1.57-2.43 Å, but none contained electron density consistent with the presence of a bound UL51 peptide. Representative electron density maps for two datasets, of crystals from the PEG/Ion screen condition 44 (blue) and Morpheus® HT screen well H2 (magenta) are shown in Figure 5.16. Due to the absence of UL51 peptide in the structure no further refinement was performed.

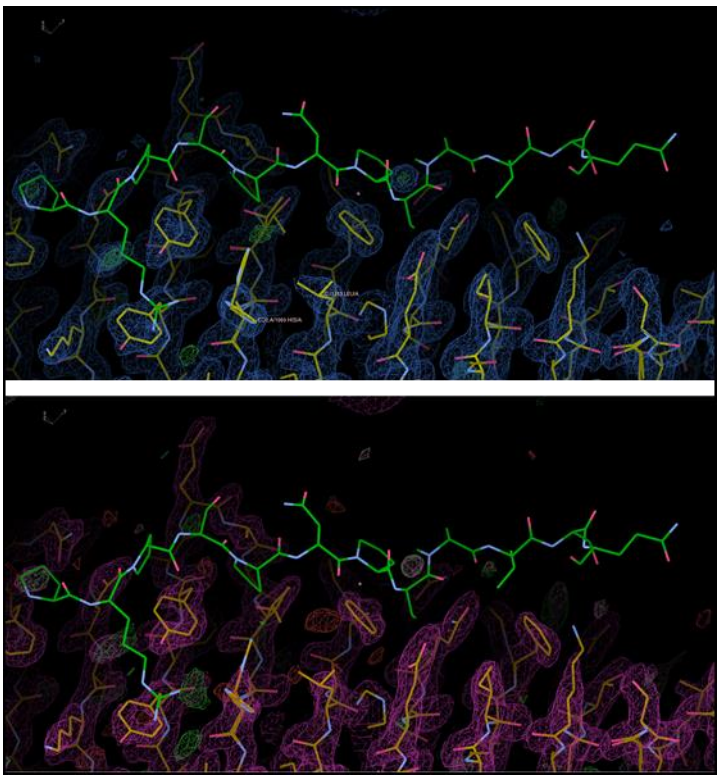

Figure 5.16 Electron density maps for the DrCPAP- UL51$^{217-237}$ peptide 'co-crystals'
Crystals from two conditions: PEG/Ion screen condition 44 (blue map) and Morpheus® HT screen well H2 (magenta map), diffracted to 1.57 Å and 1.59 Å, respectively. Molecular replacement was performed using the DrCPAP$^{943-1121}$ (PDB: 4LD1, [286]) structure as a starting model with solvent molecules removed. STIL$^{414-428}$ peptide was superimposed on the DrCPAP model from the crystal structure PDB: 4LZF [286] to illustrate where peptide binding would be expected. There is no electron density consistent with the presence of bound UL51 peptide. Images were generated in Coot [362].

Table 5-4 X-ray diffraction data collection statistics
X-ray diffraction data statistics for co-crystallisation experiments with DrCPAP$^{943-1121}$ and UL51$^{217-229}$ or UL51$^{217-237}$ peptide

Statistics	**PEG/Ion 44**	**Morpheus H2**	**PEG/Ion2 15**
UL51 peptide	217-237	217-237	217-229
Space group	$P2_1$	$P2_1$	$P2_1$
Cell dimensions:			
a, b, c (Å)	41.6, 49.9, 59.7	41.6, 49.4, 60.0	41.6, 50.0, 59.7
α, β, γ (°)	90.0, 107.9, 90.0	90.0, 107.6, 90.0	90.0, 107.9, 90.0
Resolution (Å)	1.57	1.59	1.78
Rmerge (I)	0.832	0.990	1.041
<I\σI>	1.5	1.2	1.0
CC half	0.901	0.748	0.492
Completeness (%)	98.2	98.1	80.7
Multiplicity	6.0	4.6	3.6

5.4.5 Fluorescence anisotropy with DrCPAP fragment

The interaction between the DrCPAP$^{937-1124}$ G-box domain and DrSTIL$^{404-448}$ peptide (equivalent to UL51$^{208-244+}$) had a K_d value ≈2 µM, as determined by isothermal titration calorimetry [340]. The HsCPAP G-box domain and HsSTIL$^{385-433}$ peptide (equivalent to UL51$^{202-244+}$) were shown to interact with a K_d of 0.55 µM in fluorescence polarisation experiments [286]. To determine the K_d of the DrCPAP$^{943-1121}$ G-box interaction with UL51, a fluorescent UL51$^{217-237}$ peptide was synthesised for fluorescence polarisation experiments. The UL51 peptide has an N-terminal FITC fluorophore linked via an aminohexanoyl group (NH_2-CH_2-CH_2-CH_2-CH_2-CH_2-COOH). Fluorescence polarisation experiments measure the affinity of an interaction between an unlabelled protein and a fluorescently labelled peptide by measuring changes in fluorescence anisotropy across a series of protein concentrations. The fluorescent peptide is excited with plane-polarised light, if the peptide is unbound it tumbles/rotates freely in solution and, as a result, depolarised light is emitted. However, if the peptide is bound by a large molecule, e.g. a protein, then the effective molecular volume of the peptide is increased and it tumbles/rotates more slowly in solution. As a result, the light emitted by the bound peptide is in the same or a similar plane as the plane-polarised excitation light. Thus, in this experiment, unbound peptide emits de-polarised light, while the bound peptide emits highly polarised light. Fluorescence emission is measured in parallel and perpendicular planes to the plane of the excitation light, and anisotropy is given as the weighted average of the two values. The degree of binding is found by measuring the change in anisotropy of partially-bound, free, and fully-bound peptide by protein titration.

In this instance, the fluorescent UL51$^{217-237}$ peptide concentration remained constant at 10 nM and this was titrated against a 2-fold serial dilution of DrCPAP$^{943-1121}$ prepared with a maximum concentration of 0.5 mM. GST protein was used as a negative control and was prepared in the same way. Fluorescence polarisation was measured and anisotropy calculated using a SpectraMax i3 microplate reader and accompanying software. The change in fluorescence anisotropy was plotted against DrCPAP$^{943-1121}$ concentration to produce the binding curve shown in Figure 5.17. The binding curve shows evidence of UL51 peptide binging to DrCPAP$^{943-1121}$, but despite using a relatively high protein concentration the curve does not plateau, and saturation of binding is not achieved. An approximate K_d value of 160 µM was determined using this data, though in reality it is likely to be higher because the interaction does not reach saturation. Such a high K_d value is indicative of weak, possibly non-specific, binding. Furthermore, there may evidence of non-specific binding between GST and the UL51 peptide. However, increased viscosity of the solution at high protein concentration would also restrict peptide rotation and result in linearly increasing anisotropy, which may be occurring with the GST sample. Therefore, this UL51 peptide binds DrCPAP$^{943-1121}$ with low affinity and is possibly non-specific, which could explain the failure to co-crystallise.

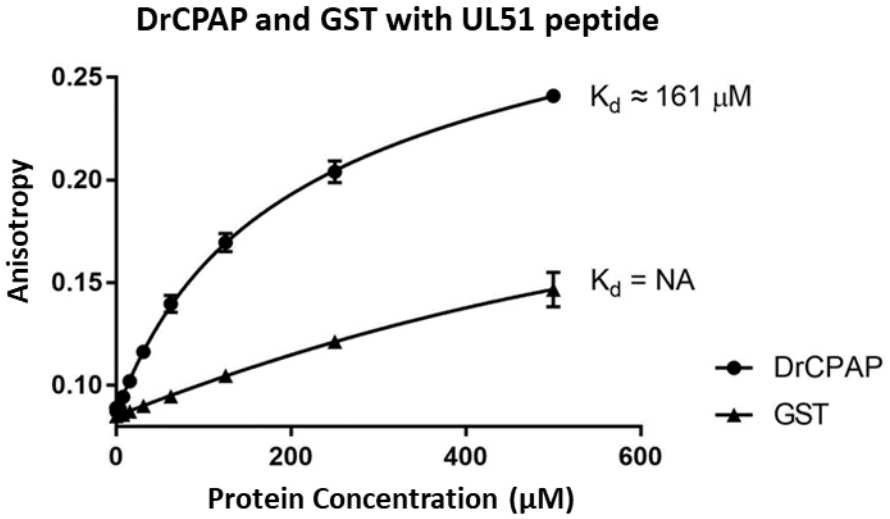

Figure 5.17 Binding curve for DrCPAP with FITC-Ahx-UL51$^{217-237}$ peptide
Fluoresce anisotropy was measured to determine the binding affinity of a fluorescent UL51$^{217-237}$ peptide and DrCPAP$^{943-1121}$ protein. DrCPAP protein was titrated against a constant concentration (10 nM) of fluorescent UL51$^{217-237}$ peptide. The experiment was repeated with GST as a negative control. A SpectraMax i3 plate reader was used to measure fluorescence, and anisotropy was calculated by the accompanying software. The titration was performed in triplicate and the data were plotted in GraphPad Prism 6.0. An approximate K_d value for UL51-DrCPAP binding was determined by fitting the data with a hyperbola (single-site binding) in GraphPad prism.

5.4.6 SEC-MALS of UL7-UL51 complex with and without DrCPAP$^{943-1121}$

Despite evidence of an interaction between full-length UL51 protein and DrCPAP$^{943-1121}$, as demonstrated by the pull-down experiment in section 5.4.3, it was not possible to conclusively demonstrate the interaction using the UL51 peptides in either co-crystallisation experiments or fluorescence anisotropy. Low affinity UL51 peptide binding, as determined by fluoresce polarisation experiments, could explain the failure to co-crystallise the UL51 peptide in complex with DrCPAP$^{943-1121}$. The unexpectedly low affinity of UL51 peptide binding might be due to incorrect folding of the peptide in the absence of the whole protein, though this region is predicted to be largely unfolded. Alternatively, the lack of an additional, unknown binding site in the full-length UL51 protein, might also explain the low affinity. To address these questions, SEC-MALS was performed with purified UL7-UL51 complex (untagged UL7 + His_6-tagged UL51 C9S full-length, aka. FAB FL) and DrCPAP$^{943-1121}$. As shown in Figure 5.18, DrCPAP$^{943-1121}$ and the UL7-UL51 complex do not co-elute during SEC. These data confirm the fluorescence polarisation experimental data, by showing that the interaction between UL51 and DrCPAP$^{943-1121}$ is low affinity and too weak for the proteins to co-elute during SEC.

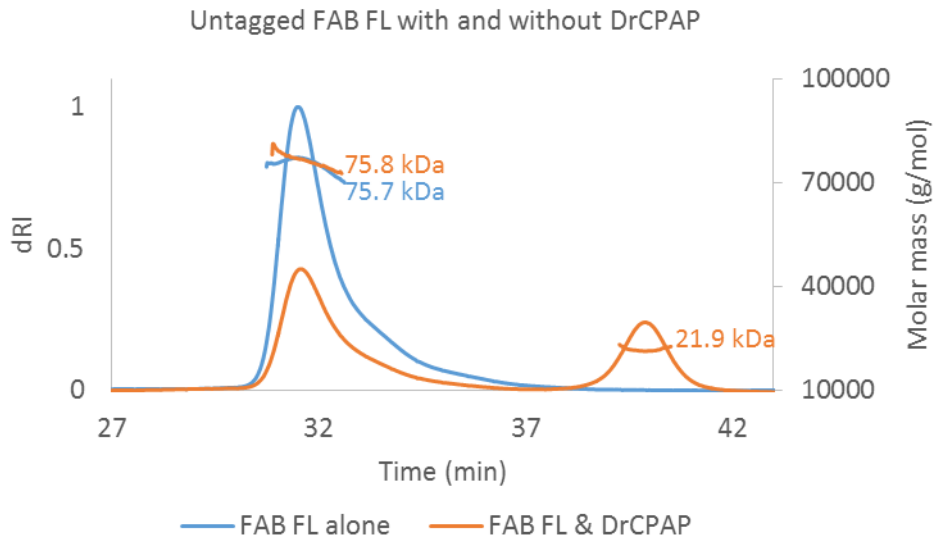

Figure 5.18 SEC-MALS data for the UL7-UL51 FL complex and DrCPAP$^{943\text{-}1121}$
Purified UL7-UL51 (untagged UL7 + His$_6$-UL51 C9S full-length, aka FAB FL) complex alone (blue) and after incubation with DrCPAP$^{943\text{-}1121}$ (orange) was analysed by SEC-MALS. The curves show relative differential refractive index for each experiment and the calculated molar mass for each peak. The UL7-UL51 complex and DrCPAP$^{943\text{-}1121}$ do not co-elute during SEC. Values for the average molecular masses calculated for each experiment are shown next to the peaks. The predicted molecular mass of DrCPAP$^{943\text{-}1121}$ is 20.7 kDa (including N-terminal 'GPLGS' residues remaining after cleaving the GST tag from the fragment).

5.4.7 HSV-1 UL51 P221D+P222D mutant virus phenotype

It was not possible to confidently determine if UL51 is able to interact with endogenous CPAP in co-immunoprecipitation experiments from infected cells (section 5.3.5), partly due to the ambiguity inherent in the detection of endogenous CPAP using the available αCPAP antibody. Since the αCPAP antibody is likely to cross-react with the HSV-1 protein ICP0, it was not possible to look for co-localisation of UL51 and CPAP infected cells by fluorescent microscopy. As such, it was unknown whether the UL51-CPAP interaction demonstrated in pull-down experiments was genuine and biologically relevant in the context of HSV-1 infection, particularly given that DrCPAP$^{943\text{-}1121}$ failed to co-elute with the UL7-UL51 complex during SEC-MALS. To tackle this question, a HSV-1 mutant was constructed carrying P221D+R222D point mutations in UL51 (virus made by Viv Connor). These mutations were sufficient to abolish the UL51-CPAP interaction in pull-down experiments (section 5.4.2). If the mutant virus produced a phenotype in infected cells that differed from the wild-type virus, then this could be an indication that the UL51-CPAP interaction is genuine and biologically relevant. To this end, a single-step growth curve was performed by infecting HaCaT cells with wild-type HSV-1, ΔUL51 HSV-1 or HSV-1 UL51$^{P221D+R222D}$ at MOI 5.0, and harvesting at 2, 4, 6, 8, 12 and 24 h.p.i.. Harvested cells were titrated by plaque assay using Vero cells to determine the whole-cell virus titre at each time-point. The single-step growth curves, shown in Figure 5.19, are as expected for the wild-type and

ΔUL51 HSV-1 viruses, with the ΔUL51 virus resulting in a ≈10-fold lower titre. Crucially, there is no difference between the single-step growth curves of wild-type HSV-1 and the UL51 $^{P221+R222D}$ mutant HSV-1. Assuming the UL51 interaction was completely abolished by the point mutations, then it is possible to conclude that blocking the UL51-CPAP interaction has no impact on viral replication in cell culture. Alternatively, the UL51-CPAP interaction detected *in vitro* may be an artefact and not occur during HSV-1 infection.

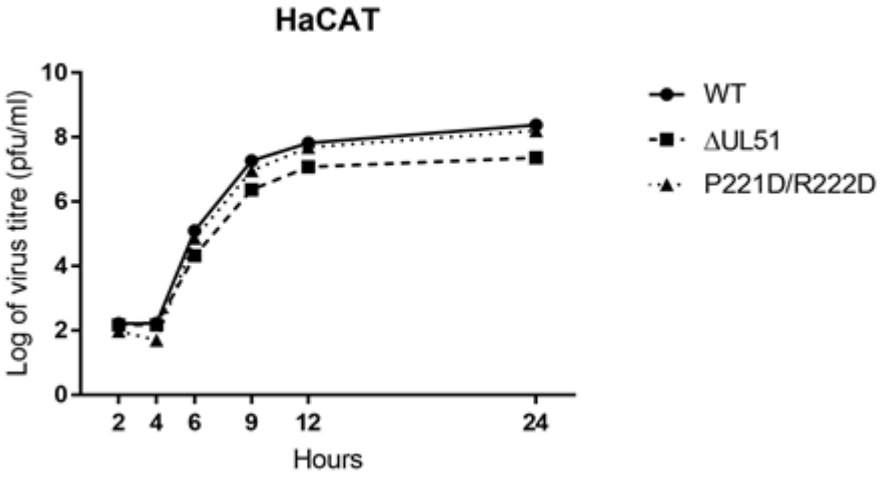

Figure 5.19 Single-step growth curves for wild-type, UL51 deletion and mutant HSV-1
HaCaT cells were infected with wild-type (WT), UL51 deletion (ΔUL51) and UL51 mutant (P221D/R222D) HSV-1 at MOI 5.0. Samples were harvested at the indicated times and viral titres were determined by plaque assay using Vero cells. Data are presented as the mean of duplicates of one experiment. Error bars for the standard error of the mean were calculated but they are shorter than the symbols so were not plotted by GraphPad Prism 6.0.

5.4.8 Discussion

The work presented in this chapter details the efforts to identify host-cell interaction partners for UL51 by performing a Y2H screen. This approach was not suitable for UL7 due to autoactivation of the UL7-pGBKT7 construct. In total, 21 human proteins were identified as putative UL51 binding partners, five of which were selected for further validation. Host-cell proteins with links to vesicular trafficking and exocytosis were prioritised. The initial attempt to confirm the interactions was to perform a pull-down experiment using GST-UL51 bait protein with the Y2H protein hits, expressed using a wheat germ cell-free system, as prey. This experiment was able to validate an interaction between UL51 and the G-box domain of centriole protein CPAP. Neither full-length NIPSNAP4, STMN2, PXRD3 nor the ANXA7 fragments were able to interact with GST-UL51 in this experiment. It is possible that the interactions detected in the Y2H screen were indirect, i.e. mediated by a yeast protein, which might explain the inability to recapitulate the interactions in the pull-down experiment with GST-UL51

or that the interactions require post-translational modification(s) that are not provided by the wheat germ expression system. It was also possible to co-immunoprecipitate myc-tagged CPAP G-box domain from cells co-transfected with GFP-UL51 and untagged UL7 (and *vice versa*). The same was attempted with myc-tagged NIPSNAP4, PXRD3 and the ANXA7 fragments, but these proteins failed to express in the HEK 293T cells despite multiple attempts. Therefore, the possibility that NIPSNAP4, PXRD3, ANXA7 and STMN2 interact with UL51 in a cellular context cannot be discounted. Purified GST-CPAP G-box domain was able to capture UL7 and UL51 from lysate of cells infected with wild-type HSV-1, but could not capture UL7 in the absence of UL51. Thus far, all experiments had been performed using only the CPAP G-box domain, and it was not known if UL7-UL51 could interact with full-length endogenous CPAP. Unfortunately, the available αCPAP antibody detects multiple bands in cell lysates and it is not clear which if any of these bands are endogenous CPAP. However, the antibody was able to specifically detect wheat germ expressed myc-CPAP$^{998\text{-}1338}$ in an immunoblot (Figure 5.20). Assuming CPAP is recognised by the antibody, there was no evidence of an interaction between GFP-UL51-UL7 and endogenous full-length CPAP, nor was it possible to co-immunoprecipitates endogenous CPAP with UL51 from infected HaCaT cells using either the 2B3 or 3D3 αUL51 antibody (Figure 5.8, Figure 5.9 and Figure 5.10).

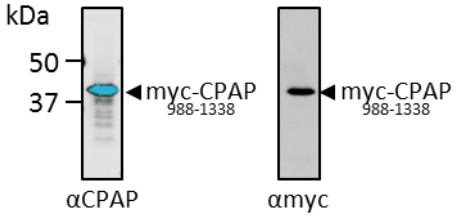

Figure 5.20 Testing the αCPAP antibody
Myc-HsCPAP$^{988\text{-}1338}$ was expressed using the wheat germ cell-free expression system and resolved by SDS-PAGE. Immunoblots were performed using αCPAP and αmyc antibodies. Both antibodies recognises myc-CPAP$^{998\text{-}1338}$ Additional lower molecular mass bands are also detected by the αCPAP but not the αmyc, these could be CPAP degradation product or other proteins present in the wheat germ cell extract.

Centriole duplication depends upon an interaction between CPAP and centriolar protein, STIL [340,358,361]. Genetic mutations linked to autosomal recessive primary microcephaly (MCPH) in humans all occur in proteins that localise to centrioles and/or centrosomes/spindle poles. One such mutation in the CPAP G-box domain (human E1235V, equivalent residue in *D. rerio* is E1021) is present at the CPAP-STIL interface, and has been shown to reduce the binding affinity of the CPAP-STIL interaction [340]. A proline-rich consensus sequence (PRxxPxP) in STIL mediates the interaction with CPAP, and it was noted that the proline-rich C terminus of UL51 contains two regions that resemble the CPAP-binding motif in STIL. A series of C-terminal truncations in UL51 were designed to test the

hypothesis that the interaction between CPAP and UL51 may be analogous to that between CPAP and STIL. Truncation mapping identified a motif in UL51 that mediates the interaction with CPAP, and two point-mutations (P221D+P222D) in this motif abolished the interaction, supporting the hypothesis that UL51 binds CPAP in a manner analogous to STIL. Despite convincing evidence of an interaction between UL51 and the CPAP G-box domain, evidence that the UL51 could interact with full-length CPAP was lacking. Assuming UL51 could interact with endogenous CPAP, it was not known whether the interaction would have any relevance in the context of viral infection. To address this, a virus incorporating the UL51 point mutations (P221D+P222D) was generated and analysed compared to wild-type HSV-1 by single-step-growth curve. No difference was evident between the UL51 mutant virus and wild-type HSV-1 based on their single-step growth curves, suggesting that abolition of a potential UL51-CPAP interaction does not impact viral replication in cell culture.

Attempts were made to characterise the UL51-CPAP interaction using biophysical techniques. It was possible to crystallise DrCPAP in complex with UL51 peptide, crystals prepared with $UL51^{217-229}$ (equivalent to $DrSTIL^{413-425}$) or $UL51^{217-237}$ (equivalent to $DrSTIL^{413-433}$) peptide were tested for X-ray diffraction but none showed any evidence of UL51 peptide binding in their electron density maps.

Fluorescence polarisation (FP) experiments measured low affinity binding between $DrCPAP^{943-1121}$ and the $UL51^{217-237}$ peptide, which could explain their failure to co-crystallise. Unfortunately, it was not possible to make FP measurements using human CPAP G-box domain due to the low solubility of the purified domain. In hindsight, a longer UL51 peptide might have been more suitable for the FP experiments; while the published crystal structures contain STIL peptides of only 12 or 20 residues the ITC and FP published experiments use much longer (44-48 residue) STIL peptides [286,340]. Thus, the CPAP-binding motif in STIL may determine the specificity, but regions flanking the motif may be required to contribute to the binding affinity. However, full-length UL51 was present in the UL7-UL51 complex that did not co-elute with $DrCPAP^{943-1121}$ during SEC-MALS, suggesting that the regions flanking the CPAP-binding motif in UL51 do not provide a sufficient boost to the binding affinity. Furthermore, the $UL51^{217-237}$ peptide may have also bound the GST negative control in the FP experiments, which is indicative of a non-specific interaction.

While Y2H screening is a convenient and sensitive technique for identifying protein-protein interactions, it is known to yield high rates of false positives and false negatives. The evidence presented in this chapter that favours a specific CPAP-UL51 interaction is currently outweighed by the evidence suggesting that the interaction is weak and unlikely to be relevant for HSV-1 infection.

6 Screening for UL7 and UL51 interaction partners using quantitative proteomics

6.1 Introduction

In addition to Y2H screening, a SILAC-based (stable isotope labelling by amino acids in cell culture) quantitative proteomics approach was employed to identify host-cell interaction partners for UL7 and UL51 proteins. This technique utilises isotope-labelled amino acids and mass spectrometry to compare the relative abundance of proteins in test and control samples, which in combination with immunoprecipitation, enables the identification of novel protein-protein interactions. Unlike Y2H screening, SILAC experiments are performed using labelled mammalian cells, which facilitates post-translational modifications and correct cellular localisation of bait and prey proteins, and can lead to the identification of whole protein complexes. These advantages can lead to fewer false positive identifications in SILAC-immunoprecipitation experiments compared to Y2H screening.

6.2 SILAC experiments

6.2.1 SILAC experimental design

SILAC experiments were designed to identify enriched host-cell proteins in immunoprecipitation (IP) experiments using UL7 and UL51 as bait proteins. The cell lines used (HEK 293T or HaCaT) were passaged at least five times in DMEM media containing stable isotope-labelled arginine and lysine. Three cell populations were generated: 'Light' containing unlabelled amino acids, 'Medium' containing arginine R6 ($^{13}C_6$) and deuterated lysine K4 (D_4), and 'Heavy' containing arginine R10 ($^{13}C_6$, $^{15}N_4$) and lysine K8 ($^{13}C_6$, $^{15}N_2$). Figure 6.1 provides a schematic overview of the SILAC experimental design. Three SILAC screens were performed during the course of this study:

1) Immunoprecipitation of GFP-tagged UL7 and UL51, or GFP alone from transfected cells
2) Immunoprecipitation of UL51 from infected cells using the αUL51 (2B3) antibody at 16 h.p.i.
3) Immunoprecipitation of UL51 from infected cells using the αUL51 (2B3) antibody at 7 h.p.i.

The following sections outline the specific experimental details, data analysis, results for each SILAC screen and the attempts to validate the putative interactions ("hits") identified in the screens.

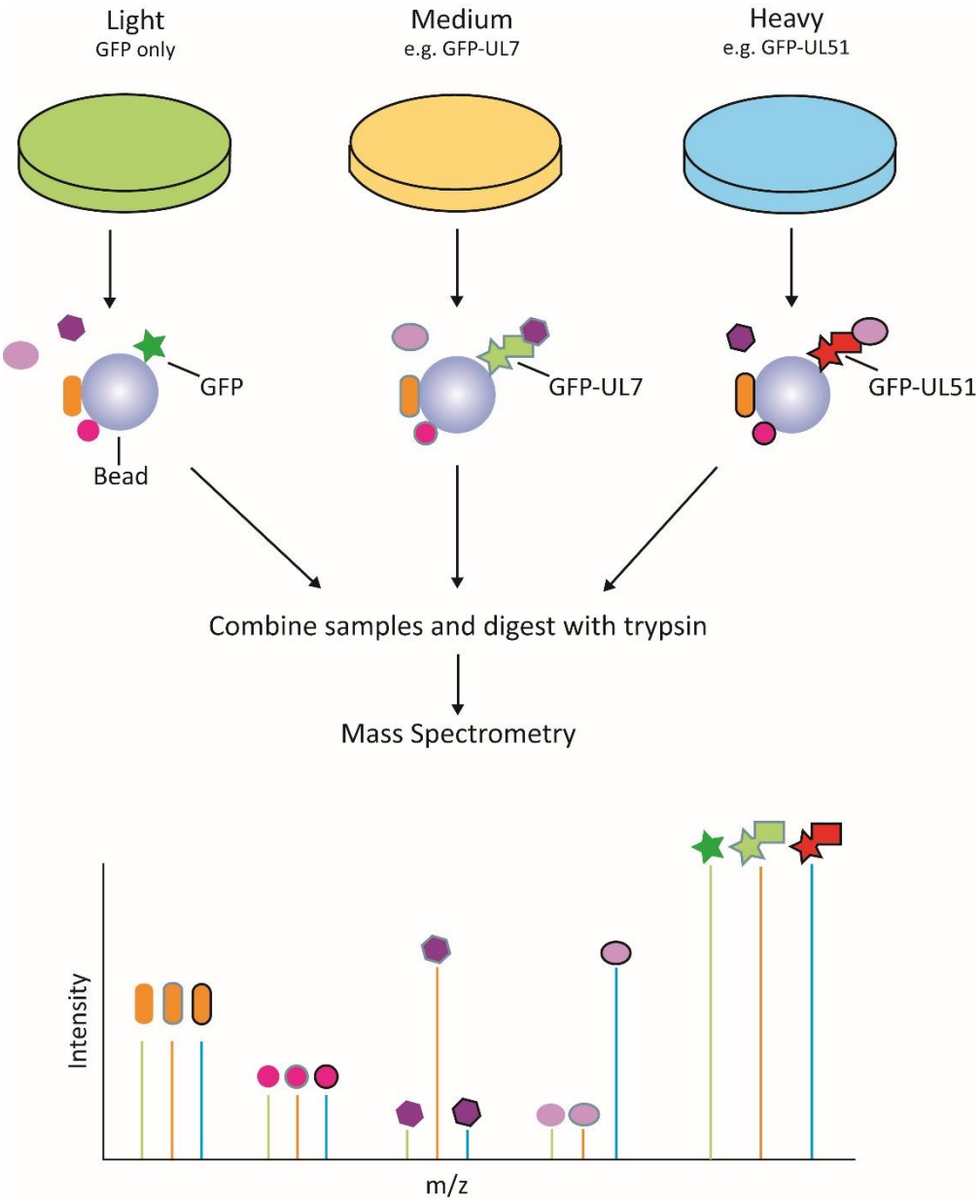

Figure 6.1 Schematic of the SILAC experimental design
Three different SILAC cell populations were cultivated: 'Light' containing unlabelled amino acids, 'Medium' containing arginine R6 ($^{13}C_6$) and deuterated lysine K4 (D_4), and 'Heavy' containing arginine R10 ($^{13}C_6$, $^{15}N_4$) and lysine K8 ($^{13}C_6$, $^{15}N_2$). In this example, the light-cell population was transfected with GFP only, the medium population with GFP-UL7 and the heavy with GFP-UL51. The bait proteins are expressed for 24-48 h then the cells are harvested and lysed. Normalised cell lysates are incubated with GFP-Trap™ beads to capture the bait protein. Some cellular proteins bind the beads non-specifically, for example, the orange and magenta shapes. The relative abundance of peptides from proteins that bind non-specifically should be consistent across all three IP samples, as shown in the mass spectrum. GFP, GFP-UL7 and GFP-UL51 bind the beads and are detected as peaks in the mass spectrum. The proteins shown in dark and light purple are specifically immunoprecipitated by GFP-UL7 and GFP-UL51, respectively. They appear enriched in the mass spectrum, for example, the dark purple hexagon is enriched in the medium sample compared to the light and heavy sample, thus this would be identified as a putative UL7 binding partner. Similarly, the light purple oval is enriched in the heavy sample indicating that this peptide is a putative UL51 binding partner.

6.2.2 SILAC screen 1: Immunoprecipitation of GFP-tagged UL7 and UL51 or GFP control

6.2.2.1 Specific experimental design

HEK 293T cells were cultured in isotope-labelled media for a minimum of five passages before use in immunoprecipitation experiments. The SILAC screen was performed in triplicate, and cells were transfected with either GFP, GFP-UL7 or GFP-UL51 as outlined in Table 6-1. The labelling for experiment 3 was switched to control for any differences in protein expression that may be introduced by isotope labelling. After 26 h the cells were harvested, lysed in mild buffer and kept on ice to help maintain protein-protein interactions. The cell lysates were normalised based on protein concentrations determined by BCA assay, this is to ensure that equal amounts of protein were incubated with the beads during the immunoprecipitation step. GFP-Trap™ beads were used to capture GFP and the GFP-tagged bait proteins, the beads were washed and bound protein was eluted in SDS-PAGE loading buffer. The presence of bait protein in the IP (bound) samples was determined by immunoblot as shown in Figure 6.2, this blot also shows there to be roughly equal amounts of bait protein in each sample. The absence of GAPDH in the IP samples indicates that the washes were sufficient for the removal of most unbound cellular proteins. SDS-PAGE analysis of the IP samples may have indicated the success of the immunoprecipitation experiment at enriching prey proteins in addition to the GFP-tagged bait proteins, though this was not performed at the time. The nine immunoprecipitation experiments were performed separately, then equal volumes of IP sample were combined into three experiment samples for analysis by mass spectrometry, according to Table 6-1. Samples from different labelled cell populations can be combined and analysed together, this is possible because labelled peptides will be identified as belonging to either light, medium or heavy samples due to the mass differences produced by labelling, for example, a peptide from the medium population and containing a single arginine will be 6 kDa heavier than the same peptide from the light population. The experiment samples were sent to The University of Bristol Proteomics Facility, where they were fully trypsinised following SDS-PAGE, before being analysed by liquid chromatography-mass spectrometry (LC-MS/MS). Since trypsin cleaves at the carboxyl group of arginine and lysine, most of the peptides generated from the medium and heavy cell populations will be labelled.

Table 6-1 Experimental design for SILAC screen 1
The SILAC screen was performed in triplicate (Experiment 1-3), with each experiment containing immunoprecipitation samples from unlabelled GFP control and labelled GFP-UL7 and GFP-UL51 bait. The labelling of the third experiment is switched to control for any differences that may be introduced as a result of isotope labelling.

Experiment (biological repeat)	Light (Lys0-Arg0)	Medium (Lys4-Arg6)	Heavy (Lys8-Arg10)
1	GFP	GFP-7	GFP-51
2	GFP	GFP-7	GFP-51
3	GFP	GFP-51	GFP-7

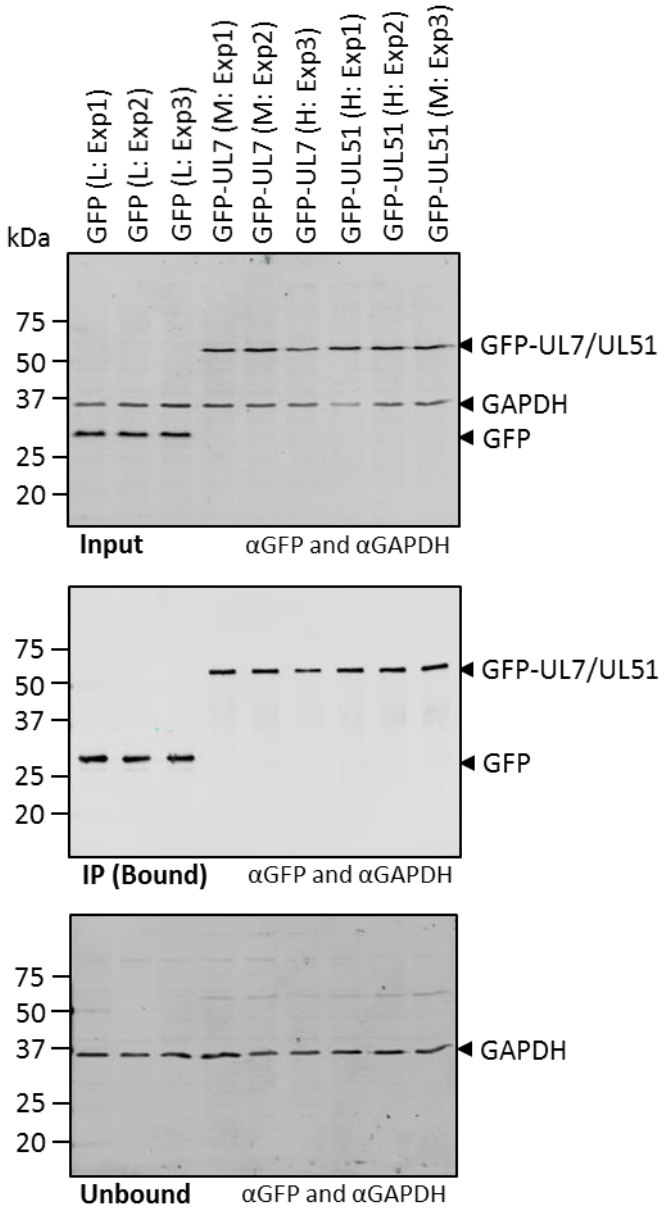

Figure 6.2 Immunoblot of SILAC screen 1 immunoprecipitation samples
HEK 293T cells were cultured in labelled media designated: L (light), M (medium) and H (heavy) in the image. The cells were transfected with either GFP-UL7, GFP-UL51 or GFP only, then lysed after 24 h. GFP-tagged protein was captured using GFP-Trap™ beads and eluted into SDS-PAGE loading buffer, the samples were then analysed by immunoblot. The middle blot shows successful capture of GFP (27 kDa), GFP-UL7 (60.0 kDa) and GFP-UL51 (52.5 kDa) by the GFP-Trap™ beads (IP). The lack of GAPDH in the IP samples is an indication that the washes were successful. The IP samples were sent for analysis by mass spectrometry.

6.2.2.2 Results for SILAC screen 1

Due to the high sensitivity achieved with mass spectrometry, the majority (>90%) of peptides detected in a SILAC-immunoprecipitation experiment will be contaminants and must be distinguished from genuine hits during the data analysis stage. The relative abundance of each protein is determined by calculating the ratio of peak intensities between the samples in a particular experiment (i.e. GFP-UL7/GFP or GFP-UL51/GFP) [363]. A protein is excluded from the analysis if it was identified by only one unique peptide. Once calculated the ratios are $\log_2$-transformed and plotted in GraphPad Prism as a frequency distribution, the data are then fitted with a Gaussian curve to generate the mean and standard deviation [363]. In theory, proteins that bind non-specifically will be equally enriched in both the control sample (i.e. GFP) and the sample containing the protein of interest (e.g. GFP-UL7), and therefore should cluster with a $\log_2$ SILAC ratio of zero. High-confidence interaction partners ("hits") will have significantly higher 'protein of interest/control' (e.g. GFP-UL7/GFP) ratios compared to background and their $\log_2$ SILAC ratio will be positive, while proteins enriched in the control sample will have a negative $\log_2$ SILAC ratio. High-confidence hits are filtered by setting a threshold value equal to the mean plus 1.96 times the standard deviation ($\mu + 1.96\sigma$), leading to a false discovery rate of 2.5% [363]. Figure 6.3 shows histograms for the logarithmised SILAC ratios for all three biological repeats, they follow a normal distribution centred on zero as would be expected for an ideal experiment. The cut-off threshold values for significance were calculated and are shown in Table 6-2.

Table 6-2 Threshold values calculated for the SILAC 1 data
Threshold was calculated as the mean plus 1.96 times the standard deviation ($\mu + 1.96\sigma$), which gives a false discovery rate of 2.5%.

	GFP-UL7/GFP	GFP-UL51/GFP	GFP-UL7/GFP-UL51	GFP-UL51/GFP-UL7
Experiment 1	0.9535	1.7047	0.6532	1.2782
Experiment 2	0.9982	0.2452	1.2394	0.4347
Experiment 3	0.9703	1.0272	1.0045	1.0676

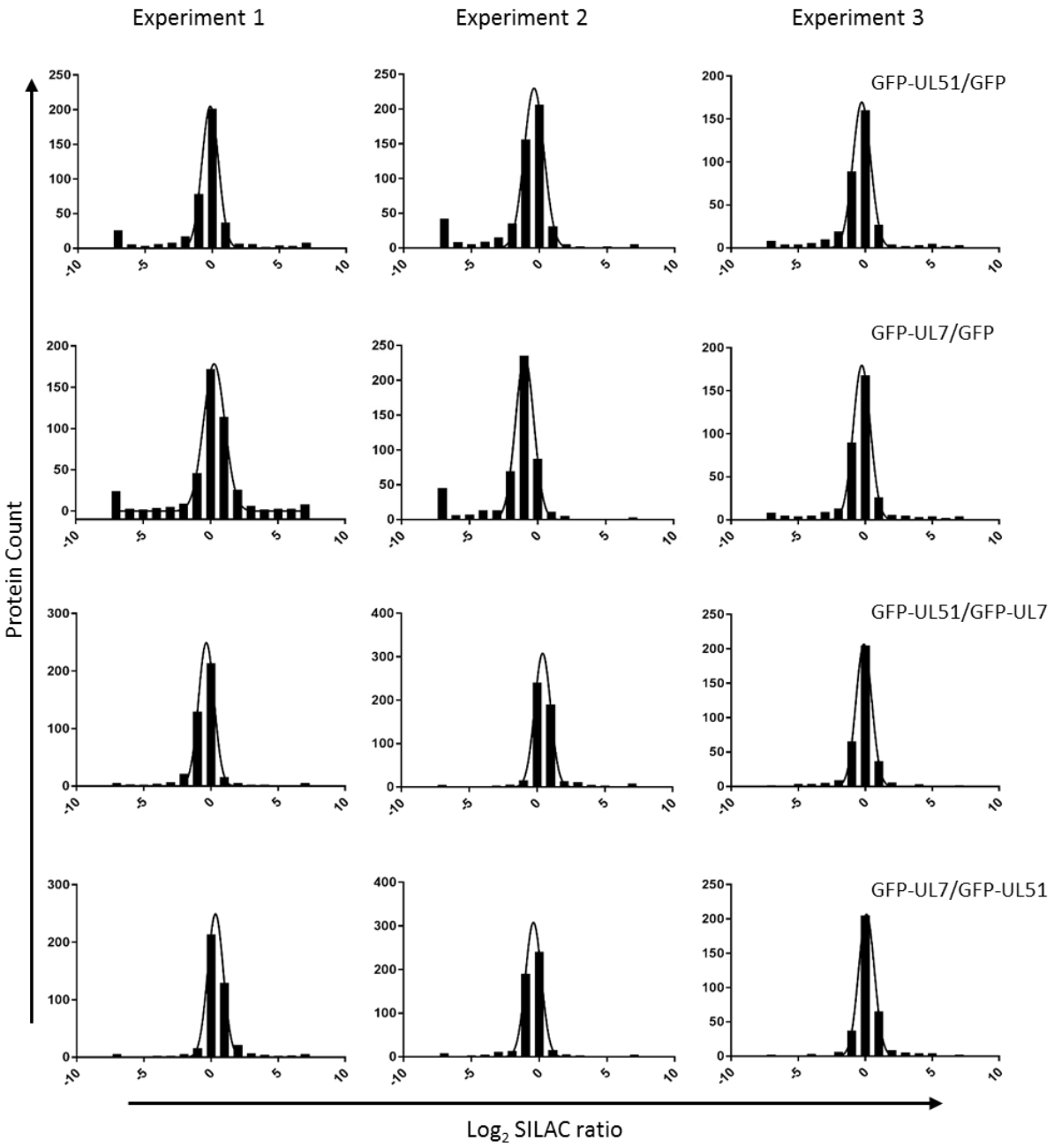

Figure 6.3 Frequency histograms of Log_2 SILAC ratios for the three biological repeats
Frequency histograms of the logarithmised SILAC ratio distributions for all three biological repeats for SILAC screen 1. The data for most samples are well centred on zero, suggesting that the sample loading was equivalent between experiments.

A total of 1172 proteins were identified in the IP samples by mass spectrometry, of these 139 (GFP-UL7) and 145 (GFP-UL51) were quantified for the three biological repeats. High-confidence hits are those that were significantly enriched in GFP-UL7 or GFP-UL51 samples compared to GFP, and are presented in Table 6-3. Strikingly, the majority of the hits are known heat shock or chaperone proteins, which suggests the GFP-UL7 and GFP-UL51 bait proteins may not be correctly folded. In hindsight, these findings are consistent with those presented in results chapters one and two, where the UL7 and UL51 proteins were found to be much less stable when expressed and purified individually compared

to the UL7-UL51 complex. In particular, the UL7 protein was shown to co-purify with the *E. coli* chaperone protein chaperonin 60 when expressed without UL51, this was not known at the time of the SILAC experiment. Furthermore, the GFP tag was positioned at the N-terminus of the bait proteins, which could have the potential to disrupt the normal localisation of the proteins, and UL51 in particular by blocking membrane association via palmitoylation at cysteine 9, however, this was not realised at the time. Subsequently, it was decided that the SILAC experiment should be repeated with the aim to immunoprecipitate the UL7-UL51 complex, since the proteins are more likely to be correctly folded when part of the complex. It was also thought that performing the immunoprecipitation from lysates of infected cells might increase the chances of identifying genuine UL7/UL51 interaction partners. These consideration were factored into the experimental design for SILAC screens 2 and 3.

Table 6-3 Putative binding partners for GFP-UL7 and GFP-UL51

Data from the SILAC-immunoprecipitation experiments (SILAC screen 1) were analysed to identify putative binding partners for GFP-tagged UL7 and UL51 bait proteins. The table presents proteins that were identified in two or more experiments with sample/mock Log_2 ratios greater than the threshold value (μ + 1.96σ, where the μ = mean and σ = standard deviation, shown in Table 6-2). Italicised proteins were identified for both GFP-UL7 and GFP-UL51.

Log_2 SILAC ratio GFP-UL7/GFP (number of peptides identified)			**Name/Description**
Exp1	**Exp2**	**Exp3**	
1.8 (2)	4.5 (2)	2.8 (3)	RUVBL1, RuvB-Like 1 (chaperone-like)
N/A	2.3 (10)	2.9 (8)	RUVBL2, RuvB-Like 2 (chaperone-like)
3.8 (4)	N/A	3.7 (7)	CCT2, T-complex protein 1 subunit beta (chaperone)
1.8 (2)	*1.3 (3)*	*N/A*	*FLJ76863, Highly similar to stress-induced phosphoprotein*
2.6 (7)	*2.5 (10)*	*N/A*	*HSPA6, Highly similar to heat shock 70 kDa protein 6*
N/A	*1.4 (2)*	*2.8 (2)*	*DNAJA2, DnaJ homologue subfamily A member 2*

Log_2 SILAC ratio GFP-UL51/GFP (peptide no)			**Name/Description**
Exp1	**Exp2**	**Exp3**	
1.6 (3)	0.9 (2)	1.1 (3)	UBC, Polyubiquitin-C
3.1 (9)	2.1 (9)	1.7 (7)	FLJ93166, highly similar to heat shock 70 kDa protein 6
3.3 (21)	2.5 (22)	2.2 (13)	HSPA8, Heat shock 70 kDa protein 1A/1B
2.8 (16)	2.0 (20)	N/A	HSPA8, Heat shock cognate 71 kDa protein
2.4 (2)	1.1 (3)	N/A	*FLJ76863, Highly similar to stress-induced phosphoprotein*
N/A	0.9 (2)	1.2 (2)	*DNAJA2, DnaJ homologue subfamily A member 2*

6.2.3 SILAC screen 2: Immunoprecipitation of UL51 from infected cells using the αUL51 2B3 antibody at 16 h.p.i.

6.2.3.1 Specific experimental design

Infection experiments were performed using HaCaT cells that had been passaged in isotope-labelled media a minimum of five times. The cells were infected with either wild-type HSV-1, ΔUL51 HSV-1 or were mock infected as outlined in Table 6-4. At 16 h.p.i. the cells were harvested and lysed on ice; the lysates were then normalised based on protein concentration measurements determined by BCA assay. Normalised cell lysates were incubated with αUL51 (2B3) antibody for 1 h, protein A/G beads were added and the sample was incubated for an additional hour. The beads were washed and bound protein was eluted into SDS-PAGE loading buffer. An immunoblot confirms the presence of UL51 in the IP samples (Figure 6.4). The nine immunoprecipitation experiments were performed separately, then equal volumes of IP sample were combined into three experiment samples for analysis by mass spectrometry, according to Table 6-4. The experiment samples were sent to The University of Bristol Proteomics Facility, where they were fully trypsinised following SDS-PAGE before being analysed by LC-MS/MS mass spectrometry.

Table 6-4 Experimental design for SILAC screen 2
The SILAC screen was performed in triplicate (Experiment 1-3), with each experiment containing immunoprecipitation samples from unlabelled mock-infected cells and labelled cells infected with either wild-type (WT) or ΔUL51 HSV-1. The labelling of the third experiment is switched to control for any differences that may be introduced as a result of isotope-labelling.

Experiment (biological repeat)	Light (Lys0-Arg0)	Medium (Lys4-Arg6)	Heavy (Lys8-Arg10)
1	Mock	ΔUL51	WT
2	Mock	ΔUL51	WT
3	Mock	WT	ΔUL51

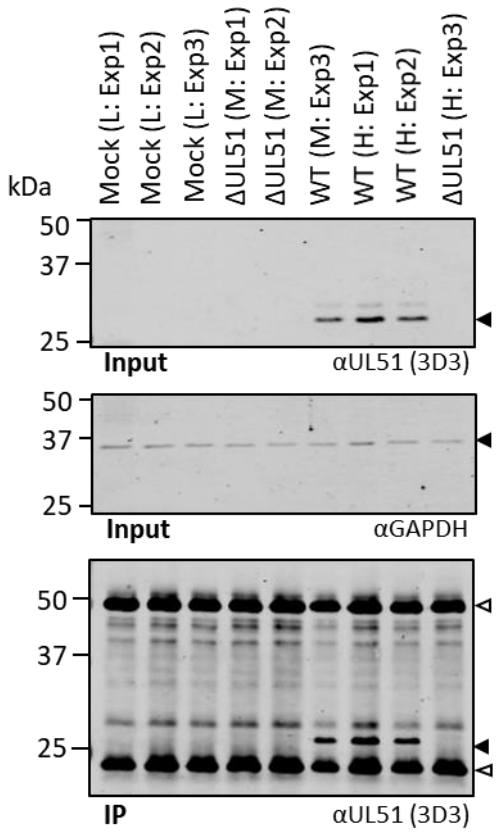

Figure 6.4 Immunoblot of SILAC screen 2 immunoprecipitation samples
HaCAT cells were cultured in labelled media designated: L (light), M (medium) and H (heavy) in the image. Cells were infected with wild-type (WT) HSV-1, ΔUL51 HSV-1 or mock-infected. After 16 h the cells were harvested and cell lysates were incubated with αUL51 (2B3) antibody for 1 h, protein A/G beads were added and the samples were incubated for an additional hour. The beads were washed and bound protein was eluted in SDS-PAGE loading buffer. The samples were analysed by SDS-PAGE followed by immunoblot for UL51. UL51 was successfully immunoprecipitated (IP) from the WT HSV-1 infected cells (bottom immunoblot).

6.2.3.2 Results for SILAC screen 2

SILAC data were analysed as described in section 6.2.2.2 and reference [363]. Figure 6.5 shows histograms for the logarithmised SILAC ratios for all three biological repeats, most of which follow a normal distribution centred on zero as would be expected for an ideal experiment. The histograms for Experiment 2 Δ51/Mock and Experiment 3 WT/Mock are not centred on zero, instead they are shifted to the left suggesting a high abundance of contaminants in these samples. The cut-off threshold values for significance were calculated and are shown in Table 6-5.

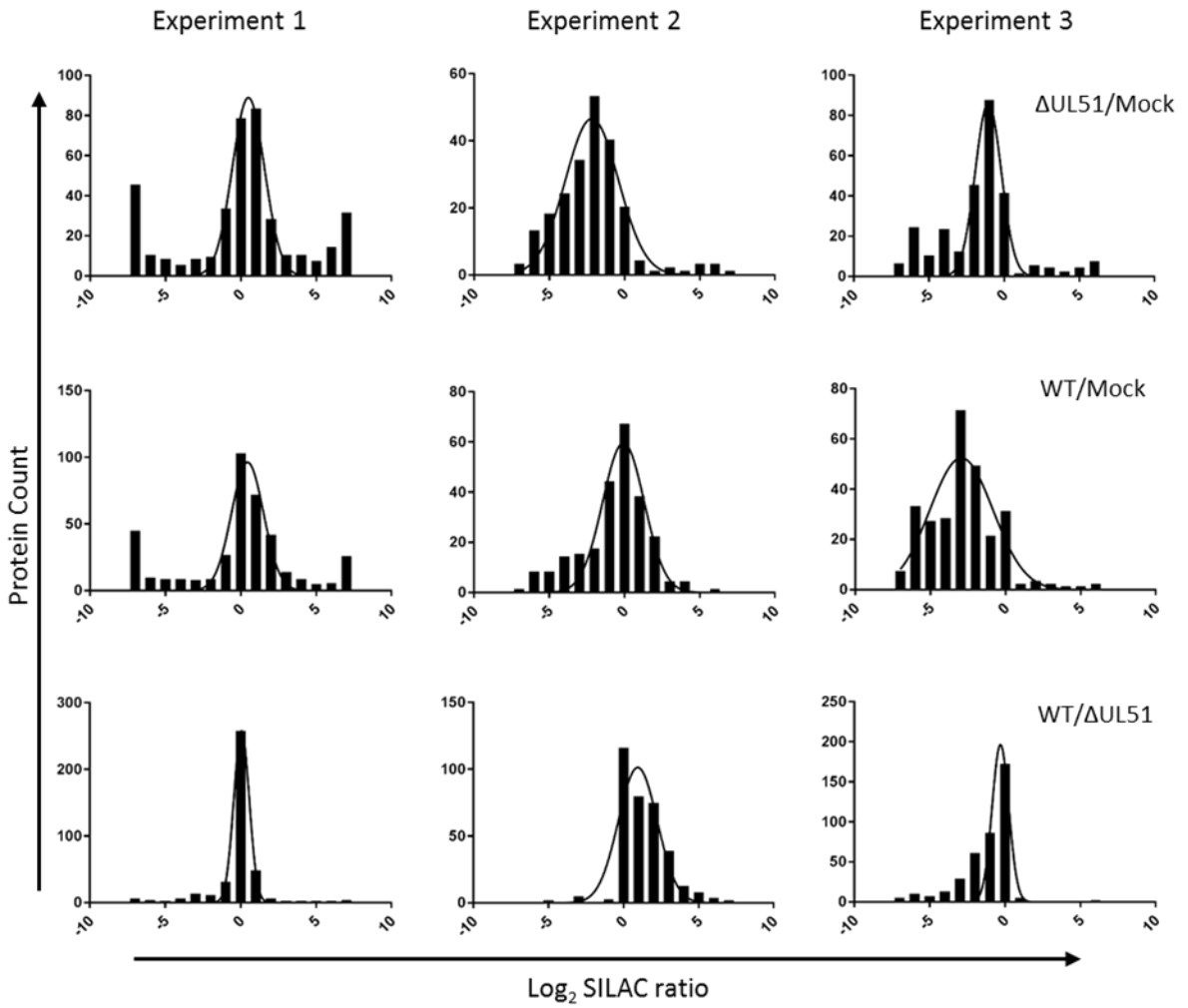

Figure 6.5 SILAC screen 2 frequency histograms of Log_2 SILAC ratios
Frequency histograms of the logarithmised SILAC ratio distributions for all three biological repeats for SILAC screen 2. The data for most samples are well centred on zero, suggesting that the sample loading was equivalent between experiments.

Table 6-5 Threshold values calculated for the SILAC screen 2 data
Threshold was calculated as the mean plus 1.96 times the standard deviation (μ + 1.96σ)

	ΔUL51/Mock	WT/Mock	WT/ΔUL51
Experiment 1	2.5199	2.3960	0.4437
Experiment 2	1.1722	2.6026	3.4421
Experiment 3	0.5863	1.2147	0.2411

Proteins with WT/Mock and WT/ΔUL51 SILAC ratios greater that the cut-off threshold were classed as high-confidence hits and are listed in Table 6-6. Notably, the heat shock and chaperone protein hits detected in SILAC screen 1 were not identified in this screen, suggesting that UL51(-UL7) were folded in the IP. Several HSV-1 proteins are among the hits, three of which have functional roles involving nucleic acids (UL12, UL29 and UL40) and two other that have previously been reported to interact with UL51 (UL14 and glycoprotein gE (US8)) [168,229,277]. Glycoprotein gE forms a heterodimeric complex with gI (US7), which was also identified as a high-confidence hit. The gI-gE

complex acts as an Fc receptor that binds human immunoglobulin G [169,170]. This complex also recognises rabbit IgG antibodies but should not recognise the mouse-derived IgG_1 αUL51 antibody used for the IP. Interestingly, gE is known to interact with cellular proteins NIPSNAP 1 and NIPSNAP 2 (personal communication from Firoz Ahmed, awaiting publication), which were also identified hits in this screen. The possible scenarios that could lead to the identification of NIPSNAP 1 and 2 as significant hits in this experiment are: i) UL51 directly interacts with NIPSNAP 1/2, ii) UL51 interacts with NIPSNAP 1/2 via gE(-gI), or iii) the αUL51 antibody can directly co-immunoprecipitate gE-gI with NIPSNAP 1/2. To test these hypotheses the immunoprecipitation experiment was repeated and an immunoblot was performed to analyse the samples for the presence of UL51, NIPSNAP 1/2, and gE. Figure 6.6A (page 167) shows successful immunoprecipitation of UL51 from wild-type infected cell lysates (top immunoblot). Endogenous NIPSNAP 1 and 2 share a similar molecular mass to the IgG light chain making them difficult to distinguish in the immunoblots. However, it is possible to see two faint bands (highlighted with stars) at the appropriate molecular mass for NIPSNAP 1/2. These bands are present in the wild-type and ΔUL51 HSV-1 infected IP samples but not mock infected. Glycoprotein gE is also present in both IP samples where NIPSNAP 1/2 bands were detected, even in the absence of UL51 (Figure 6.6B). Thus, it was concluded that the αUL51 (2B3) antibody is also able to immunoprecipitate gE and that this likely explains the presence of NIPSNAP 1/2 in the IP samples.

Host-cell proteins, RuvB-Like 1 (a.k.a. pontin) and RuvB-like 2 (a.k.a. reptin) were identified as high-confidence hits in this SILAC screen. They were also identified in the first SILAC screen but only with the GFP-UL7 bait protein and not with GFP-UL51 (Table 6-3). While the αUL51 (2B3) antibody has previously been shown to co-immunoprecipitate the UL7-UL51 complex, UL7 protein was only detected in one biological repeat (Exp 3). In practice, if a peptide is not detected by mass spectrometry this does not necessarily mean it was not present in the sample. Mass spectrometers can fail to detect peptides originating from different sample proteins that differ significantly in abundance if they arrive at the detector simultaneously, i.e. a significantly more abundant peptide can mask the detection of a less abundant peptide if they arrive at the detector at the same time. This may explain why UL7 was not detected in two of the three biological repeats. Thus, it was not entirely clear whether RuvB-Like1 and RuvB-like 2 are interacting with either or both UL7 and UL51, or possibly with another protein present in the sample as was the case for NIPSNAP 1 and 2. However, RuvB-Like1 and RuvB-like 2 were hits deemed worthy of further investigation and the validation attempts are presented in the next section.

Table 6-6 High-confidence hits from SILAC screen 2

Data from the SILAC-immunoprecipitation experiments were analysed to identify putative binding partners for UL51(-UL7). The table presents proteins that were identified in two or more experiments with WT/mock and WT/ΔUL51 Log_2 ratios greater than the threshold value ($\mu + 1.96\sigma$, where the μ = mean and σ = standard deviation).* Protein only quantified on one biological repeat.

Log_2 SILAC ratio WT/mock (number of peptides identified)			**Log_2 SILAC ratio WT/ΔUL51 (number of peptides identified)**			**Name/Description**
Exp1	**Exp2**	**Exp3**	**Exp1**	**Exp2**	**Exp3**	
		Cellular proteins				
2.4 (2)	3.8 (2)	N/A	0.6 (2)	4.2 (2)	N/A	Proteasome subunit alpha type
4.4 (5)	3.4 (4)	4.6 (4)	3.2 (5)	5.5 (4)	5.5 (4)	RUVBL1, RuvB-like 1 (a.k.a. pontin)
N/A	4.1 (7)	6.3 (7)	N/A	5.0 (7)	6.6 (7)	RUVBL2, RuvB-like 2 (a.k.a. reptin)
6.4 (4)	N/A	4.0 (3)	5.2 (4)	N/A	3.1 (3)	FLJ58042, highly similar to Protein NIPSNAP 1
5.8 (4)	N/A	4.0 (3)	5.7 (4)	N/A	3.2 (3)	GBAS, Protein NIPSNAP homolog 2
		HSV-1 proteins				
5.4 (6)	6.6 (5)	6.6 (2)	N/A	5.2 (5)	3.9 (2)	UL12, DNA exonuclease

Log_2 SILAC ratio WT/mock (number of peptides identified)			**Log_2 SILAC ratio WT/ΔUL51 (number of peptides identified)**			**Name/Description**
Exp1	**Exp2**	**Exp3**	**Exp1**	**Exp2**	**Exp3**	
		HSV-1 proteins				
N/A	6.6 (2)	6.6 (2)	N/A	3.6 (2)	6.6 (2)	UL29, Single-stranded DNA binding protein
6.6 (4)	6.6 (3)	6.6 (2)	0.5 (4)	N/A	3.8 (2)	UL40, Ribonuclease reductase
6.6 (3)	6.6 (2)	6.6 (3)	0.5 (3)	N/A	1.2 (3)	UL34, Capsid exit from nucleus
N/A	4.2 (4)	6.6 (5)	N/A	6.6 (4)	6.6 (5)	UL14, Tegument protein that is reported to bind UL51
6.6 (3)	6.6 (3)	6.6 (3)	0.6 (3)	N/A	1.3 (3)	US7, Glycoprotein I: Virus spread, forms a complex with gE
6.6 (12)	6.6 (11)	6.6 (13)	0.7 (12)	N/A	1.2 (13)	US8, Glycoprotein E: Fc receptor, forms a complex with gI
N/A	N/A	5.5 (3)	N/A	N/A	6.6 (3)	*UL7, Tegument protein that forms a complex with UL51

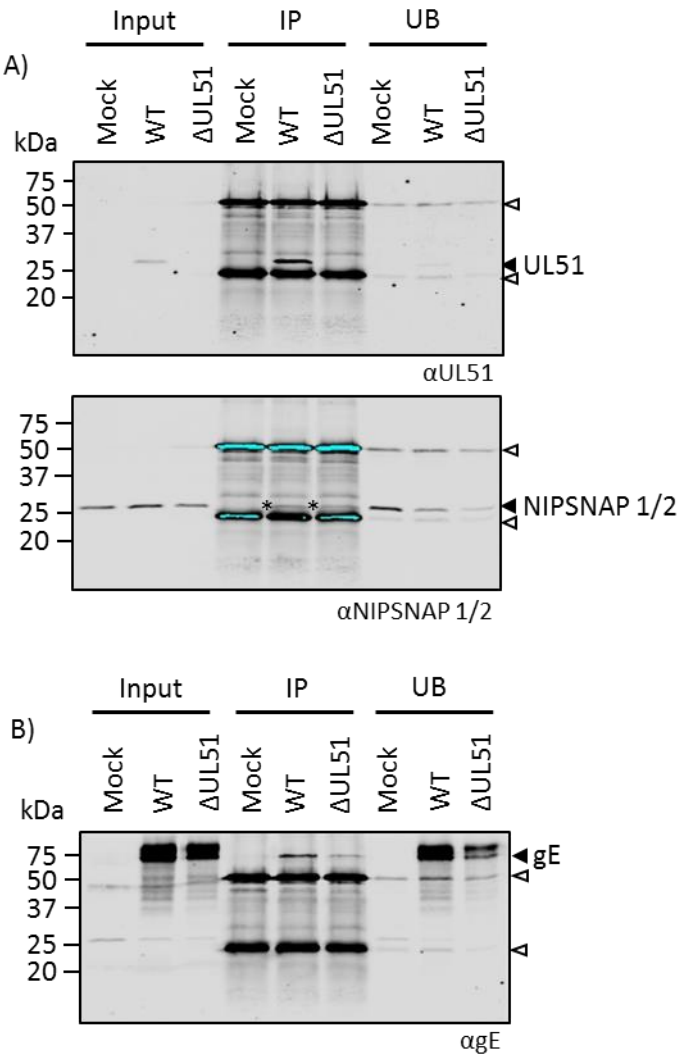

Figure 6.6 Co-immunoprecipitation of UL51 and NIPSNAP1/2 from infected cells
A) HaCaT cells were infected with wild-type (WT) HSV-1, ΔUL51 HSV-1 or mock-infected. After 16 h the cells were harvested and cell lysates were incubated with αUL51 (2B3) antibody for 1 h, protein A/G beads were added and the samples were incubated for an additional hour. The beads were washed and bound protein was eluted in SDS-PAGE loading buffer. The samples were analysed by SDS-PAGE followed by immunoblot for UL51 and endogenous NIPSNAP1 and 2. UL51 is immunoprecipitated (IP) from the WT HSV-1 infected cells (top immunoblot). Two co-immunoprecipitated bands are detected by the NIPSNAP1/2 antibody (middle immunoblot, starred bands) in IP samples from WT and ΔUL51 HSV-1 infected cells. B) The same IP samples were probed with αgE antibody, this immunoblot shows that gE is present in the IP samples from WT and ΔUL51 HSV-1-infected cells. NIPSNAP 1/2 are known to interact with gE (personal communication from Firoz Ahmed).

6.3 Validation of RuvB-like 1 and RuvB-like 2 (a.k.a. pontin and reptin)

Acknowledgement: The experiments presented in this section were performed by Alice Fletcher-Etherington as part of her undergraduate Part-II project under the supervision of Danielle Owen.

Pontin and reptin are highly conserved, essential AAA+ proteins (ATPases associated with diverse cellular activities) that share homology with the bacterial RuvB helicase [364-366]. Like RuvB, pontin and reptin exhibit DNA helicase activity [367-370] and also have roles in chromatin remodelling [371-373], transcriptional regulation [372,374], and DNA damage repair [365]. Pontin and reptin interact to form a dodecameric complex comprising two heterohexameric rings with alternating pontin and reptin monomers [367]. In the absence of reptin, pontin alone can assemble into a hexameric ring and *vice versa* [370,375]. Given their DNA-related functions, pontin and reptin exhibit nuclear localisation but are also present in the cytoplasm where they are involved in the formation of perinuclear aggresomes [376,377]. Aggresomes are 1-3 µl spherical inclusions that develop when abnormally high levels of misfolded or partially folded proteins are generated, such as during cellular stress [377-381]. Misfolded proteins that may be toxic to the cell, are stored at aggresomes before subsequent refolding or degradation through the ubiquitin-proteasome system and/or autophagy [381]. Aggresomes form close to the MTOC and a pool of cytoplasmic chaperones and proteasomes [382-387]. Mitochondria are also recruited to aggresomes, possibly to supply the ATP required by chaperone proteins and the proteasome [378,382]. In connection with aggresomes, pontin and reptin are proposed to possess a chaperone-like activity and interact directly with misfolded proteins to promote disaggregation [377]. Unfolded protein stimulates pontin-reptin ATPase activity and siRNAs against pontin or reptin suppress aggresome formation [377]. Other AAA+ proteins, such as Hsp104 and ClpB, are known to serve as molecular chaperones and often function in concert with Hsp70 and Hsp40 to promote disaggregation [388-390]. Pontin and reptin are also posited to possess a chaperone-like activity that enables them to assist in the assembly of large cellular complexes, such as RNA polymerase II and small nucleolar (sno) RNPs [391,392].

It is possible that pontin and reptin were detected as putative UL7/UL51 interaction partners through their generic ability to recognise misfolded proteins, particularly in the first SILAC screen since the GFP-UL7 bait was likely to be misfolded in the absence of UL51. Alternatively, the interaction may be mediated though non-specific interactions with nucleic acids since the UL7-UL51 complex purified from *E. coli* was shown to co-purify with nucleic acids. It was necessary to keep these possibilities in mind when designing experiments to validate the interaction between UL7/UL51 and pontin and reptin.

6.3.1 Attempt to co-immunoprecipitate endogenous pontin and reptin

Endogenous pontin and reptin protein bands overlap with the αUL51 (2B3) antibody heavy chain in SDS-PAGE. Thus, it was not possible to validate the putative interaction between UL51(-UL7) and pontin and reptin by repeating the SILAC-immunoprecipitation from infected cells and immunoblotting with αpontin and αreptin antibodies. Instead, an immunoprecipitation experiment was designed to determine if endogenous pontin and reptin could bind UL51 and/or UL7 in transfected cells in the absence of other viral proteins. HEK 293T cells were transfected with GFP-UL7, GFP-UL51 or co-transfected with GFP-UL7 and untagged UL51. GFP-tagged UL56 was included as a bait protein in this experiment to control for the possibility of pontin and reptin recognising misfolded protein, HSV-1 UL56 (aa. 1-207) protein is known to be misfolded based on circular dichroism experiments (personal communication from Julia Muenzner). GFP-Trap™ beads were used to capture GFP and GFP-tagged bait proteins, the beads were washed and bound protein was eluted in SDS-PAGE loading buffer. Phosphate buffers were used for all immunoprecipitation steps in an attempt to eliminate the potential for nucleic acid-mediated interactions. The samples were also treated with benzonase to degrade excess nucleic acids. Figure 6.7 shows successful capture of the bait proteins (bottom immunoblot). Pontin was detected in the lysates but there was no evidence of pontin co-immunoprecipitation with any of the bait proteins. Reptin was detected in all immunoprecipitation samples including the sample from un-transfected cells, which is suggestive of a non-specific interaction with the GFP-Trap™ beads. Unfortunately, no untagged UL51 was detected in the co-transfected cell lysates, so it is not possible to conclude whether or not the UL7-UL51 complex is able to immunoprecipitate pontin and reptin.

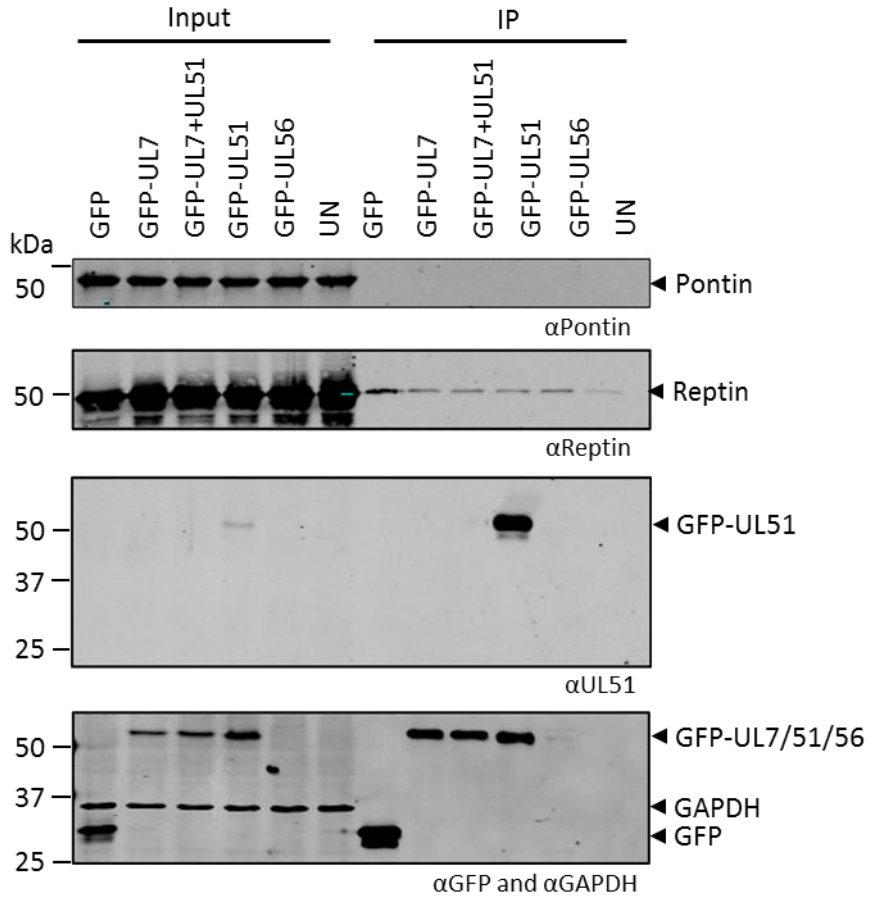

Figure 6.7 Attempt to co-immunoprecipitate pontin and reptin with GFP-UL7/UL51
HEK 293T cells were transfected with GFP-UL7, GFP-UL51, GFP-UL56 (aa. 1-207), co-transfected with GFP-UL7 and untagged UL51, or un-transfected (UN). GFP-UL56 was included as a control bait protein. GFP-Trap™ beads were used to capture the bait proteins, the beads were washed and bound protein (IP) was eluted in SDS-PAGE. The samples were analysed by immunoblot using αGFP, αUL51 (3D3), αGAPDH, αpontin and αreptin antibodies. No pontin was detected in the IP samples, and reptin was present in all lanes suggesting that it binds non-specifically to the GFP-Trap™ beads. *This experiment was performed by undergraduate student Alice Fletcher-Etherington under the supervision of Danielle Owen.*

6.3.2 Pontin and reptin interact with purified UL7-UL51 complex

Purified GST-tagged UL7-UL51 complex (UL7-GST+His_6-UL51 C9S FL, a.k.a. FAB FL) was used as bait in a pull-down experiment with myc-tagged pontin and reptin that was expressed using the wheat germ cell-free expression system. GST-UL56 (aa. 1-207) and VPS18 were included as bait and prey negative control proteins. As mentioned in section 6.3.1, GFP-UL56 (aa. 1-207) is known to be misfolded and was included as a control to test the ability of pontin and reptin to bind misfolded protein. Phosphate buffers and benzonase treatment of the UL7-UL51 complex was utilised in an attempt to eliminate the potential for nucleic acid-mediated interactions. As shown in Figure 6.8, the UL7-UL51 bait was able to pull-down pontin and reptin when they were expressed in the same wheat germ reaction but not when they were expressed separately (top immunoblot), demonstrating that

the formation of the pontin-reptin complex is required for UL7-UL51 binding. VPS18 was not pulled-down with the UL7-UL51 complex, nor were pontin and reptin pulled-down by GST alone (bottom immunoblot). However, pontin and reptin were pulled-down by GST-UL56 to the same extent as with the UL7-UL51 complex. It is likely that the pontin-reptin complex is acting as a molecular chaperone in recognising the unfolded N terminus of UL56 and, by extension, may be interacting with UL7-UL51 in the same way. It is possible to envisage hydrophobic patches on the surface of the UL7-UL51 complex that, in the context of infection, would be bound by cellular or viral proteins (e.g. UL14). Such patches would be exposed in the purified complex and may be prone to recognition by cellular chaperones. Furthermore, the SEC-MALS data presented in results chapter two demonstrated a tendency for UL7-UL51 to self-associate, which might well resemble protein aggregates to the pontin-reptin complex. If the phosphate buffers and benzonase treatment did not ensure the complete removal of nucleic acids then the interaction between pontin-reptin and UL7-UL51 may also be mediated by nucleic acid.

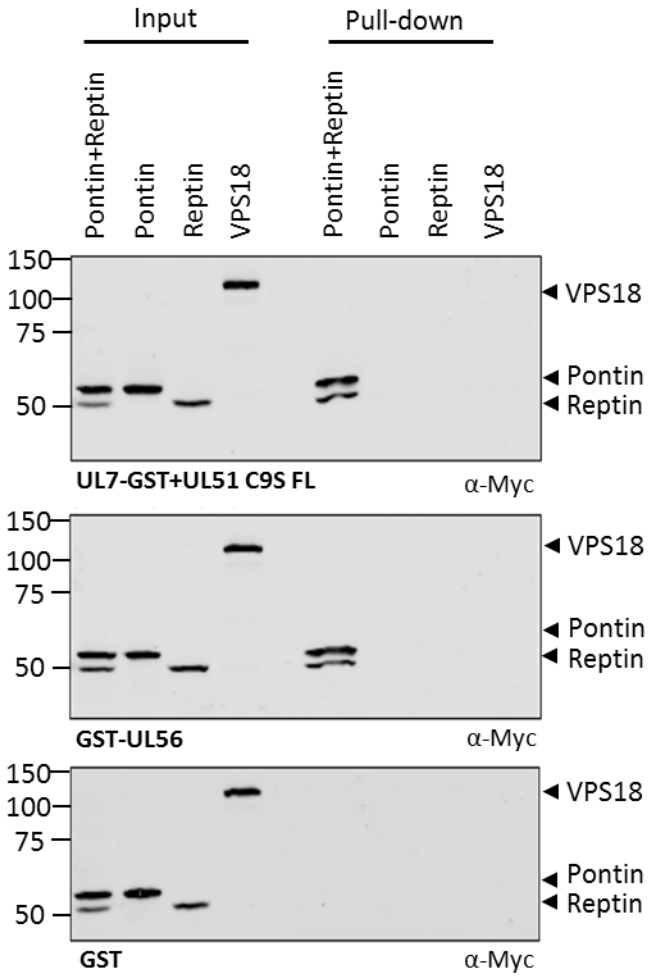

Figure 6.8 purified UL7-UL51 complex interacts with the pontin-reptin complex
Purified GST-tagged UL7-UL51 complex (UL7-GST+His_6-UL51 C9S FL, a.k.a. FAB) was used as bait in a pull-down experiment with wheat germ expressed myc-tagged pontin and reptin. Purified GST-UL56 and wheat germ expressed VPS18 were included as bait and prey negative controls, respectively. The pull-down samples were analysed by immunoblotting for αmyc. When expressed in the same wheat germ reaction, pontin and reptin form a complex that interacts with UL7-UL51. The pontin-reptin complex also interacts with GST-UL56. Only the pontin-reptin complex is able to interact with UL7-UL51 and UL56, and not the proteins on their own. *This experiment was performed by undergraduate student Alice Fletcher-Etherington under the supervision of Danielle Owen.*

6.3.3 Intracellular localisation of pontin and reptin in infected cells

The previous experiment established that the pontin-reptin and UL7-UL51 complexes do interact. However, it is not clear whether the pontin-reptin complex acts as a molecular chaperone in this interaction, or whether the interaction was mediated by nucleic acids. As mentioned in section 6.3, both pontin and reptin are implicated in aggresome formation. Upon infection, cytoplasmic DNA viruses such as poxviruses, African swine fever virus and herpesviruses induce the formation of virus assembly compartments/factories (VACs), which have be noted to resemble aggresomes [393-396]. Like aggresomes, VACs localise close to the MTOC, require an intact microtubule network for assembly,

recruit mitochondria and cellular chaperones, and cause a rearrangement of intermediate filaments [393,394]. It is possible that viruses may usurp aggresomal pathways to concentrate viral and host-cell proteins, mitochondria and membranes in order to enhance viral replication efficiency [396]. Theoretically, confinement to aggresome-like structures may make the virus more susceptible to autophagy: to counter this HSV-1 has developed mechanism to inhibit autophagosome recruitment through the action of ICP34.5, which targets autophagy protein beclin-1 [395,397]. Alternatively, the formation of aggresome-like structures during viral infection could be an innate cellular survival response to cope with high levels of 'foreign' viral proteins.

It was hypothesised that pontin-reptin may facilitate virus assembly by acting as molecular chaperones at VACs. Evidence of pontin-reptin co-localisation with UL7/UL51 at virus-induce assembly compartments would support this. To assess this, fluorescence microscopy was performed: HFF-Tert cells were mounted on glass coverslips and infected with HSV-1 expressing UL7-mCherry and UL51-EYFP, or mock infected. At 15 h.p.i. the cells were fixed and probed with antibodies that recognise pontin or reptin. As expected, the UL7-UL51 complex localises to focal adhesions (yellow arrowheads) and close to the nucleus (magenta arrowheads, Figure 6.9). Pontin expression and localisation was unaltered in HSV-1-infected cells compared to mock-infected cells (Figure 6.9), pontin localises at nuclear foci (white arrowheads) that have been identified as nuclear fibrilar centres [376]. However, there is no evidence of pontin co-localisation with UL7/UL51 close to the nucleus or at focal adhesions. The inset image (Figure 6.9) appears to show co-localisation of UL7 with pontin at nuclear fibrilar centres. However, this is likely the result of bleed-though since the Alexa Flour 663 and mCherry have overlapping excitation spectra, and the images of mock-infected cells show fluorescence in the red channel in the absence of UL7. Unfortunately, the signal for reptin antibody was too poor to determine reptin localisation. These results do not support the hypothesis that pontin-reptin facilitate virus assembly by acting as molecular chaperones at VACs.

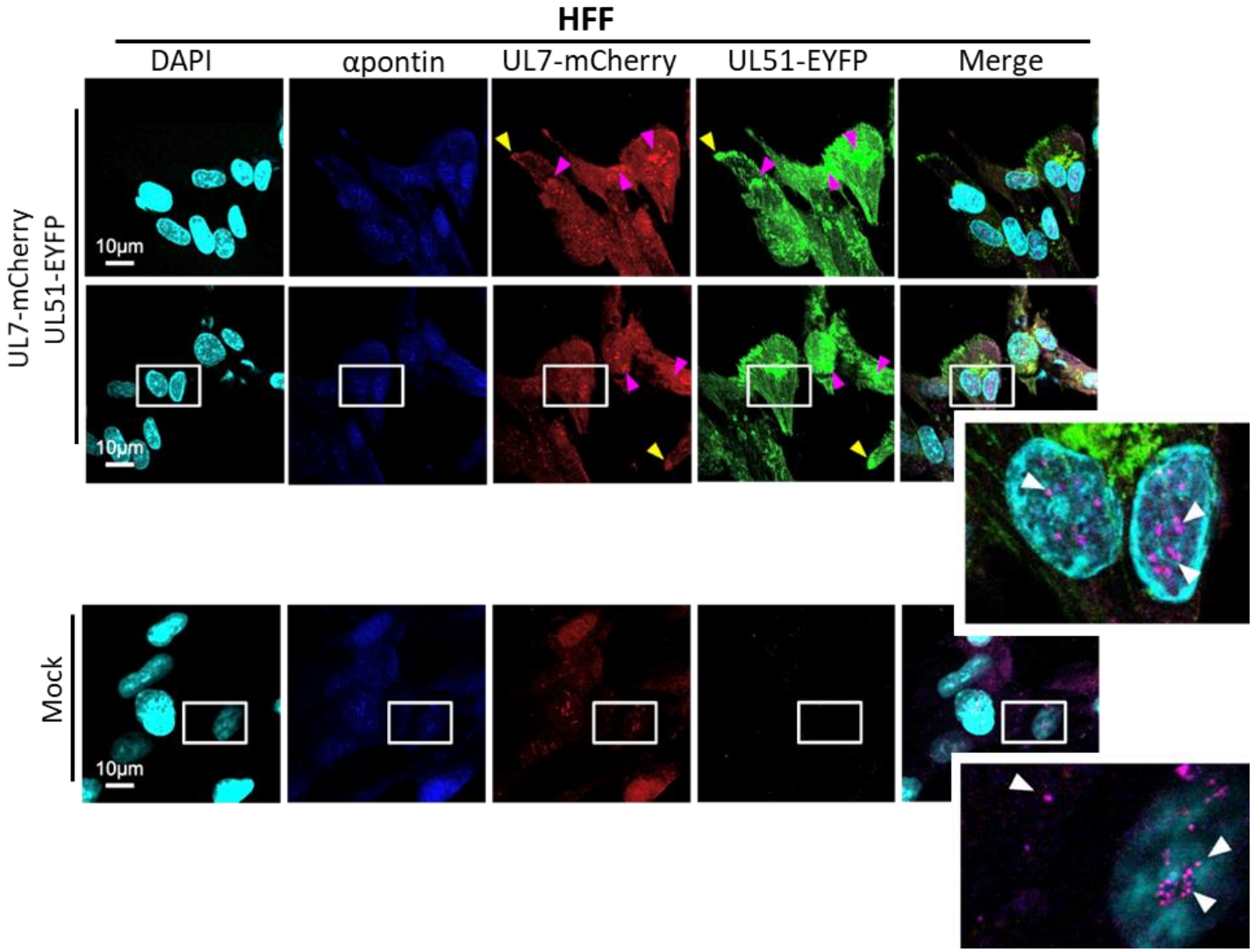

Figure 6.9 localisation of UL7, UL51 and pontin in infected cells

HFF cells were infected with HSV-1 expressing C-terminally tagged UL7-mCherry and UL51-EYFP, or mock infected. At 15 h.p.i. the cells were fixed, permeabilised and probed using mouse αpontin antibody and αmouse Alexa Flour 633. *Adapted from a figure made by Alice Fletcher-Etherington.*

6.3.4 SILAC data analysis with MaxQuant and Perseus

At a later date, a new integrated method for analysing SILAC data became available in the lab that utilises MaxQuant software for peak detection, peptide scoring, protein identification and quantification, followed by the use of Perseus software for interpretation and statistical analysis. MaxQuant uses correlation analysis and graph theory to carry out three-dimensional peak and isotope pattern detection in m/z, elution time and signal intensity space [398]. The software corrects for linear and non-linear offsets by integrating multiple mass measurements, to achieve greater mass accuracy [398,399]. As such, this software has become the gold-standard for analysing SILAC datasets. In light of this, the SILAC screen 2 data were re-analysed using the new method, with the view that previously missed hits may be identified. The raw mass spectrometry data were processed using MaxQuant and searched against the Uniprot Human database (UP000005640, dated 9th March, 2017) and a custom file containing the HSV-1 KOS strain (JQ673480.1) protein sequences. The MaxQuant analysis was imported into Perseus for further processing using the normalised SILAC ratios generated by MaxQuant. The dataset was the same as that used in section 6.2.3.2 and the experimental design is outlined in Table 6-4. Following the reanalysis, a total of 141 unique proteins were quantified across the replicate experiments. Close to 43% (60 proteins) were identified in all three biological repeats, and 84 (59.6%) were present in at least two biological repeats (Figure 6.10A). The distribution histograms of $\log_2$ SILAC ratios fit a Gaussian distribution centred on zero as would be expected for an ideal experiment (Figure 6.10B). Proteins were only considered if they were detected in at least two biological repeats. To identify significantly enriched proteins, a two-sided one-sample t-test against a $\log_2$ ratio of 0 (no change in abundance) was performed with a threshold p-value of 0.05. Proteins with a greater than 2-fold increase in abundance ($\log_2$ fold-change = 1) in the WT/mock and WT/ΔUL51 data were considered to be putative UL51 interaction partners, and these are shown in the volcano plots presented in Figure 6.11A and B. Pontin (RUVBL1) and reptin (RUVBL2) were enriched in both the WT/mock and WT/ΔUL51 data and not in the ΔUL51 /mock, NIPSNAP 1 and 2 were not found to be enriched based on this analysis. Glutathione-S-transferase (GSTP1) was enriched in the WT/mock data and not WT/ΔUL51, but it was also enriched in the detected in the ΔUL51/mock sample and is therefore likely to be non-specific. Re-analysis of the data using MaxQuant and Perseus confirmed the result of the original analysis, and was successful in identifying NIPSNAP1 and 2 as non-specific. However, no new putative UL51(-UL7) interaction partners were identified.

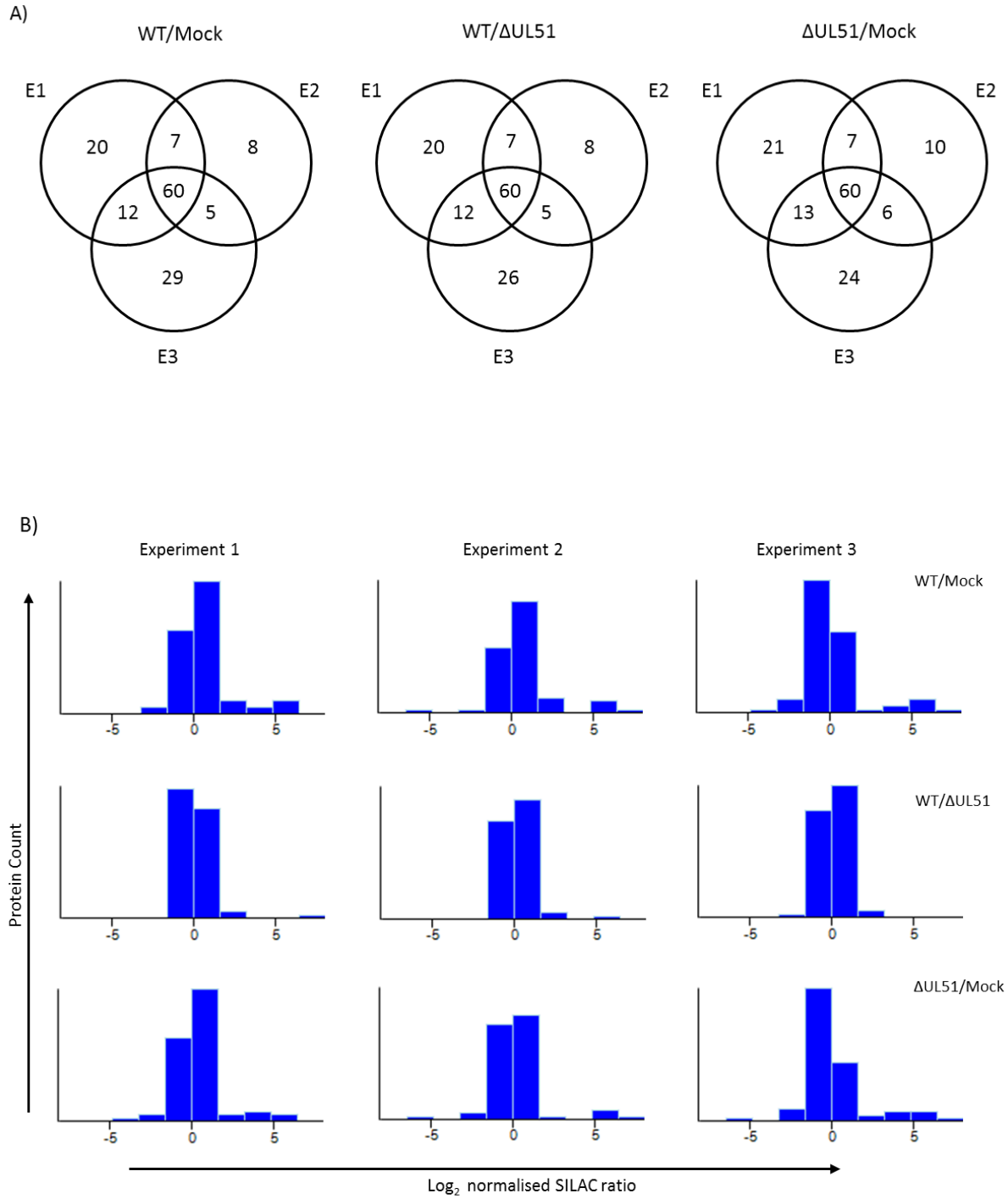

Figure 6.10 Re-analysis of the SILAC screen 2 data after quantification using MaxQuant
A) Venn diagrams showing the number of quantified proteins across the three biological repeats (E1, E2 and E3) for the WT HSV-1 samples over mock or ΔUL51 HSV-1 and ΔUL51 HSV-1 over mock. B) Log_2 normalised SILAC ratio distributions for all three biological repeats. This is a reanalysis of the raw data previously analysed in section 6.2.3.2.

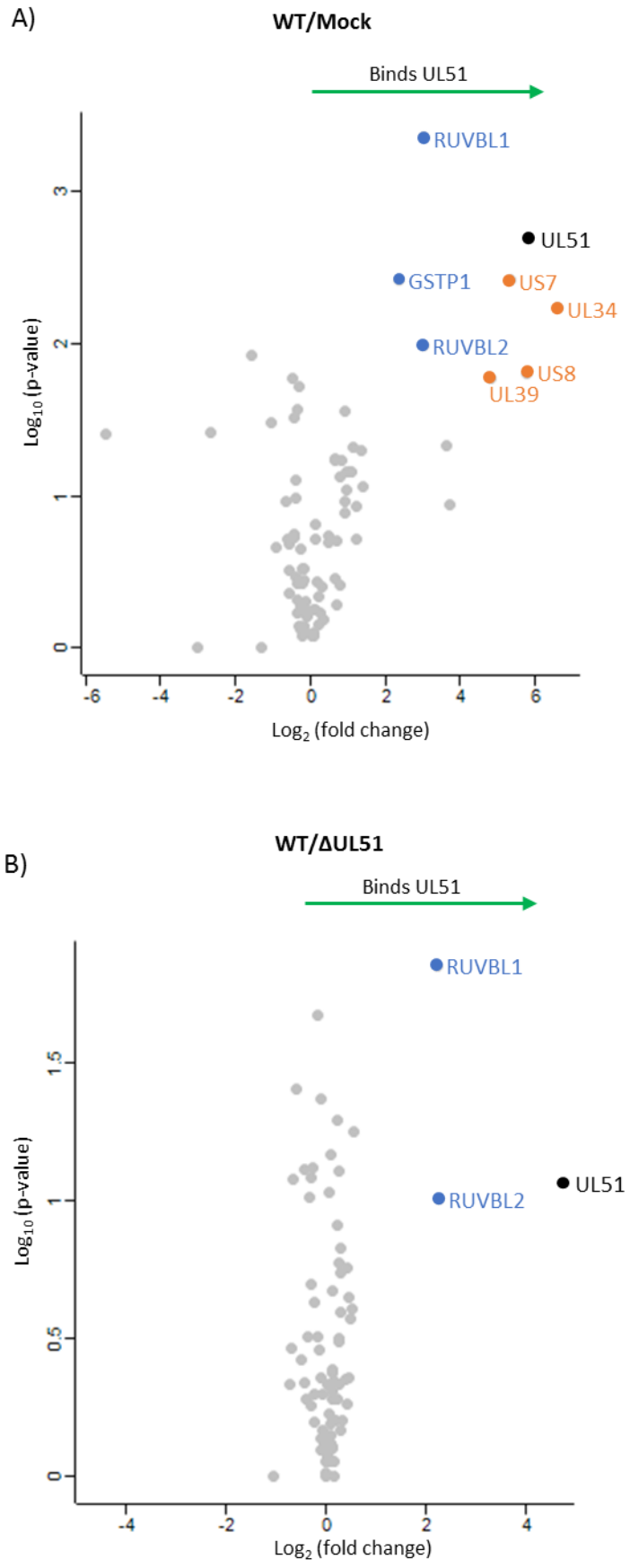
A)
WT/Mock
Binds UL51
RUVBL1
UL51
GSTP1
US7
UL34
RUVBL2
US8
UL39
Log10 (p-value)
Log2 (fold change)
B)
WT/ΔUL51
Binds UL51
RUVBL1
UL51
RUVBL2
Log10 (p-value)
Log2 (fold change)

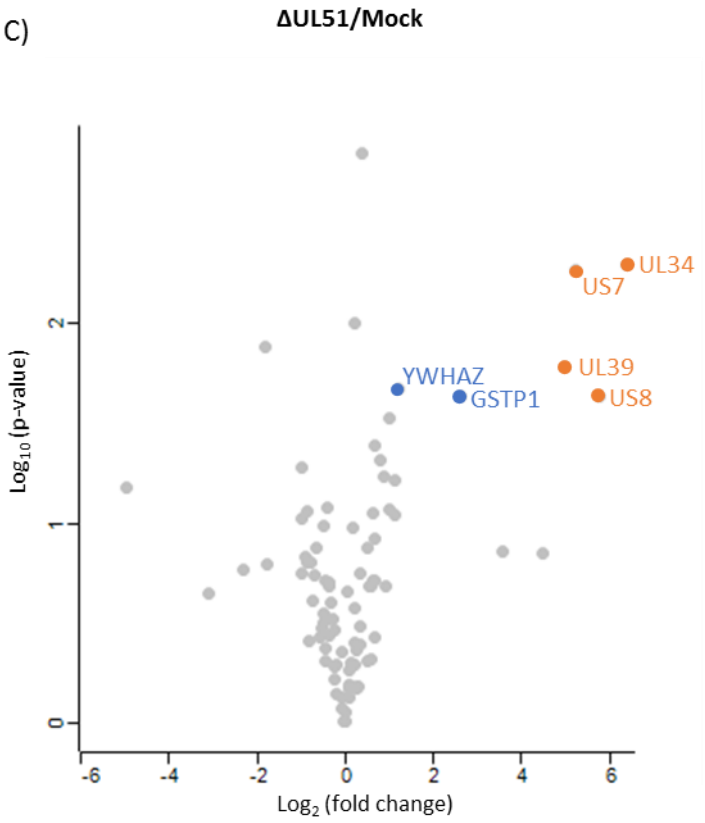

Figure 6.11 Potential UL51 interaction partners following re-analysis of the SILAC screen 2 data using MaxQuant
A and B) Volcano plots showing the $\log_2$ fold-change for WT HSV-1 samples over mock or ΔUL51 HSV-1. C) Volcano plot showing ΔUL51 HSV-1 sample over mock. Proteins with a fold-change > 2 and a $p < 0.05$ were deemed hits and are highlighted blue (cellular proteins) or orange (HSV-1 proteins). RUVBL1 and RUVBL2 are the gene names for pontin and reptin, respectively.

6.4 SILAC Screen 3: Immunoprecipitation of UL51 from infected cells using the α-UL51 2B3 antibody at 7 h.p.i.

6.4.1.1 Specific experimental design

The previous SILAC-immunoprecipitation experiment was performed at 16 h.p.i., and while this guarantees that there will be a high amount of UL51 (-UL7) in the cell, it is a relatively late stage of infection. It is conceivable that by 16 h.p.i. high levels of UL7 and UL51 (and possibly other viral proteins) could form clusters in the cytoplasm that may resemble protein aggregates, which could explain the detection of pontin and reptin in SILAC screen 2. Alternatively, as demonstrated in results chapters one and two, UL7 and UL51 may be unstable when not part of the UL7-UL51 complex, high levels of these proteins in the cell late during infection could result in the presence of un-complexed UL7 and UL51 that could be recognised as misfolded by the pontin-reptin complex. Given that the cellular environment will alter during the course of HSV-1 infection, and that UL7/UL51 may have different functional roles at different stages of

infection, it seemed reasonable to repeat the SILAC-immunoprecipitation experiment at an earlier stage of infection. The SILAC experiment was repeated as described in section 6.2.3.1, this time harvesting the cells at 7 h.p.i. instead of 16 h.p.i. An immunoblot confirmed the presence of a limited amount of UL51 in the IP samples for experiment 1 (WT, heavy) and experiment 3 (WT, medium) but not experiment 2 (WT, heavy) (Figure 6.12). A different batch of purified αUL51 (2B3) antibody was used for this immunoprecipitation experiment, which may explain the reduced efficiency of the UL51 capture compared to the previous SILAC-immunoprecipitation (shown in Figure 6.4). Ideally, the immunoprecipitation experiment would have been repeated in an attempt to increase the amount of UL51 captured prior to performing mass spectrometry, but this was not possible for due to time limitations. The samples were combined into the experiment samples shown in Table 6-4 and were sent to The University of Bristol Proteomics Facility, where they were fully trypsinised following SDS-PAGE before being analysed by LC-MS/MS mass spectrometry.

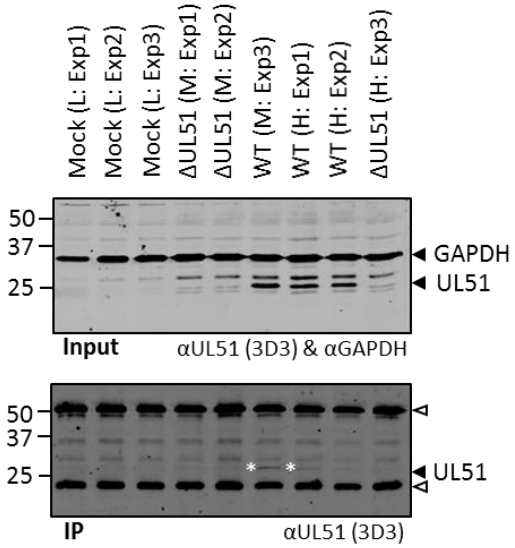

Figure 6.12 Immunoblot of SILAC screen 3 samples
HaCAT cells were cultured in labelled media designated: L (light), M (medium) and H (heavy) in the image. Cells were infected with wild-type (WT) HSV-1, ΔUL51 HSV-1 or mock-infected. After 7 h the cells were harvested and cell lysates were incubated with αUL51 (2B3) antibody for 1 h, protein A/G beads were added and the samples were incubated for an additional hour. The beads were washed and bound protein was eluted in SDS-PAGE loading buffer. The input (cell lysate) and immunoprecipitated (IP) samples were analysed by SDS-PAGE followed by immunoblot. A small amount of UL51 was immunoprecipitated from the wild-type (WT) HSV-1 infected cell lysates in Exp1 (heavy) and Exp3 (medium) but not Exp2 (heavy) (white stars, bottom immunoblot). UL51 antibody heavy and light chains are highlighted with white arrowheads.

6.4.1.2 Results for SILAC screen 3

The SILAC data were analysed as described in section 6.3.4 using MaxQuant and Perseus, excluding the data for experiment 2 since the immunoprecipitation of UL51 from WT lysates for experiment 2 was not successful. Any effect of isotope labelling is still controlled for because the WT infected cells used for experiments 1 and 3 were heavy and medium labelled, respectively. Following the data analysis, a total of 74 unique proteins were quantified across the replicate experiments. Close to 68% (50 proteins) were identified in both biological repeats (Figure 6.13A). The distribution histograms of log_2 SILAC ratios fit a Gaussian distribution centred on zero as would be expected for an ideal experiment (Figure 6.13B). To identify significantly enriched proteins, a two-sided one-sample t-test against a log_2 ratio of 0 (no change in abundance) was performed with a threshold p-value of 0.05. Proteins with a greater than 2-fold increase in abundance (log_2 fold-change = 1) in the WT/mock and WT/ΔUL51 samples were considered to be putative UL51 interaction partners. The volcano plots presented in Figure 6.14B show UL51 enrichment based on WT/mock and WT/ΔUL51 ratios, again UL7 was not detected in the SILAC data. Despite UL51 enrichment, no high-confidence protein hits were identified based on both the WT/mock and WT/ΔUL51 ratios. Notably, pontin and reptin were not enriched in this screen further suggesting that the interaction with UL51(-UL7) previously identified (section 6.2.3.2) might be non-specific. Tubulin alpha (TUBA1) and tubulin beta (TUBB1) were shown to be enriched based on the WT/Mock ratios, but not WT/ΔUL51 ratios, as was Myosin-9 (MYH9) and pyruvate kinase KPM. While an interaction between UL51(-UL7) and tubulin is possible, both tubulin alpha and beta score highly when screened against a common contaminant repository (CRAPome server [400]) for affinity-purification mass spectrometry data, being respectively identified as contaminants in 389 and 382 out of 411 experiments deposited on the sever. Similarly, PKM and Myosin-9 were respectively identified in 249 and 203 out of 411 experiments in the same contaminant repository, and so are likely to be non-specific. Thus, this SILAC screen did not identify any high-confidence putative interaction partners for UL51(-UL7) despite UL51 bring enriched.

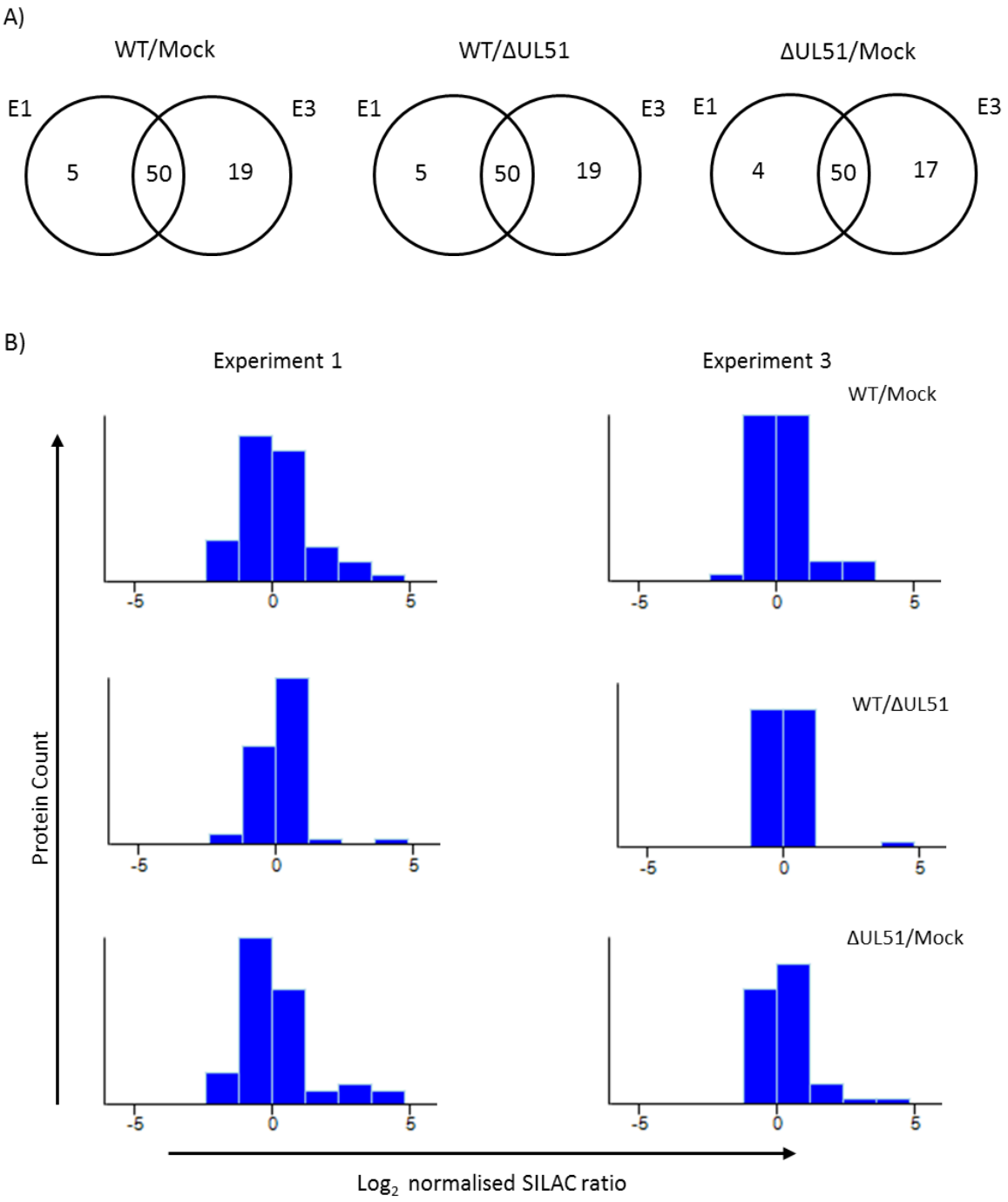

Figure 6.13 SILAC ratio distributions and quantification statistics for screen 3
A) Venn diagrams showing the number of quantified proteins across the two biological repeats (E1 and E3) for the WT HSV-1 samples over mock or ΔUL51 HSV-1 and ΔUL51 HSV-1 over mock. B) Log_2 normalised SILAC ratio distributions for all three biological repeats.

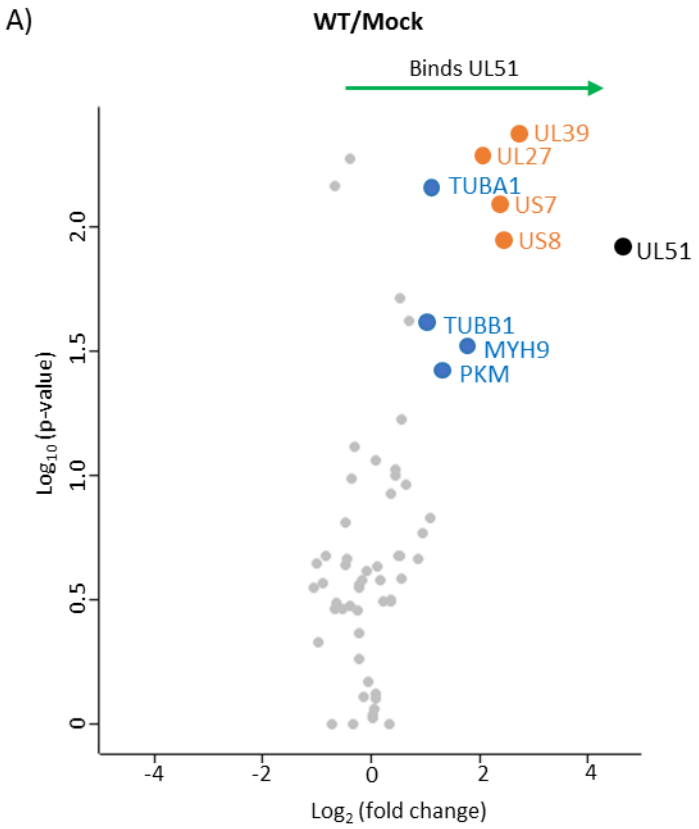
A)
WT/Mock
Binds UL51
UL39
UL27
TUBA1
US7
US8
UL51
TUBB1
MYH9
PKM
Log10 (p-value)
Log2 (fold change)
0
0.5
1.0
1.5
2.0
-4
-2
0
2
4

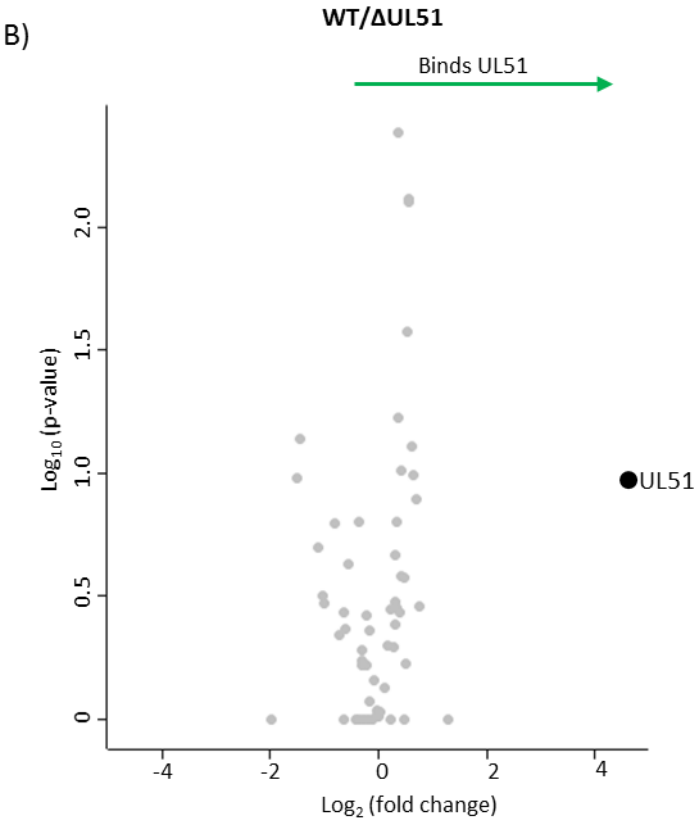
B)
WT/ΔUL51
Binds UL51
UL51
Log10 (p-value)
Log2 (fold change)
0
0.5
1.0
1.5
2.0
-4
-2
0
2
4

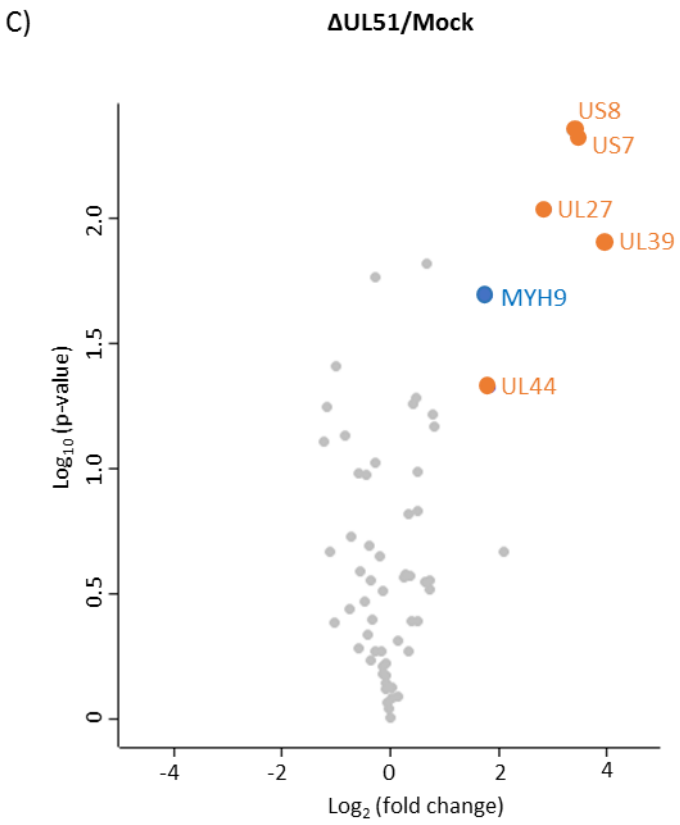

Figure 6.14 Potential UL51 interaction partners following analysis SILAC screen 3 data
A and B) Volcano plots showing the $\log_2$ fold-change for WT HSV-1 samples over mock or ΔUL51 HSV-1. (C) Volcano plot showing ΔUL51 HSV-1 sample over mock. Proteins with a fold-change > 2 and a $p < 0.05$ were deemed hits and are highlighted blue (cellular proteins) or orange (HSV-1 proteins).

6.5 Discussion

This chapter outlines the attempts to identify host-cell interaction partners for HSV-1 UL7/UL51 using SILAC-based quantitative proteomics. Three SILAC-immunoprecipitation screens were performed, the first used transiently expressed GFP-tagged UL7 and UL51 bait proteins in the absence of other viral proteins. In this screen chaperone and heat shock proteins were the predominant class of interaction partner identified for both bait proteins, which would suggest that GFP-UL7 and GFP-UL51 are unfolded/misfolded when transiently expressed in transfected cells. The second and third SILAC screens aimed to immunoprecipitate the UL7-UL51 complex from HSV-1-infected cells using the αUL51 (2B3) antibody at 16 and 7 h.p.i., respectively. Unexpectedly, UL7 was not detected in two of the three biological repeats in the second screen, nor was it detected in either biological repeat in the third screen. Mass spectrometers can fail to detect peptide and an immunoblot for UL7 would determine whether UL7 was co-immunoprecipitated with UL51 in the SILAC samples. Cellular proteins NIPSNAP 1 and 2 were identified as UL51 interaction partners but were ruled out after it was shown

that the αUL51 antibody could immunoprecipitate gE(-gI), which is known to interact with the NIPSNAP proteins. Furthermore, re-analysis of the SILAC screen 2 data using MaxQuant and Perseus did not identify NIPSNAP 1 and 2 as significantly enriched. Pontin and reptin were both enriched in SILAC screen 1 in samples with GFP-UL7 bait protein, and also in the SILAC screen 2 based on WT/Mock and Δ51/Mock ratios. The validation attempts demonstrated that the pontin-reptin complex was able to interact with purified GST-tagged UL7-UL51 complex. However, the pontin-reptin complex also bound GST-UL56 (1-207), which is known to be unfolded. In cells, pontin and reptin recognise aggregated and misfolded proteins at aggresomes [377] and may act as chaperone proteins for disaggregation. There is also evidence that pontin and reptin may assist in the assembly of large cellular complexes [391,392]. HSV-1 infection induces the formation of inclusions close to the nucleus to which many viral proteins localise, these inclusions resemble cellular aggresomes. It was hypothesised that HSV-1 may usurp aggresomal pathways to concentrate viral and host-cell proteins, mitochondria and membranes to enhance viral replication efficiency [396], and that the interaction between UL51(-UL7) and pontin-reptin may play a role in this process. Alternatively, the interaction between pontin-reptin and UL51(-UL7) could be the result of an innate cellular stress response mechanism implemented to cope with high levels of 'foreign' viral proteins, particularly if these proteins are prone to aggregate or are misfolded. There was no evidence of pontin co-localisation with UL51(-UL7) at 15 h.p.i. in immunofluorescence microscopy images, and unfortunately the αreptin antibody was not suitable for this technique. There are caveats associated with immunofluorescence microscopy such as epitope masking and inefficient fixing and cell permeabilisation, that might prevent the detection of pontin-UL51(-UL7) co-localisation. However, it was concluded that the interaction between UL51(-UL7) is most likely to be non-specific, occurring as a result of high levels of potentially aggregated and/or misfolded protein in the cell at 16 h.p.i.

Despite, several SILAC-co-immunoprecipitation attempts no high-confidence UL51(-UL7) interaction partners were identified. Problems with the experimental design of SILAC screen 1 explain the failure to detect protein hits. With the benefit of hindsight a better experiment would have been to co-transfect cells with UL7 and UL51, where one partner is GFP-tagged and the other untagged, then to co-immunoprecipitate the complex. The late infection time-point at which the immunoprecipitation experiment for SILAC screen 2 was performed is likely to explain the identification of pontin-reptin complex in the sample, and the failure to detect interaction partners in the third screen could be attributed to the low efficiency of the UL51 immunoprecipitation, although UL51 was enriched in these samples. It may be worth repeating the third SILAC screen in an attempt to improve the efficiency of UL51 capture. Caveats associated with immunoprecipitation experiments may prevent the detection of UL7-UL51 interaction partners, such as interactions being impinged upon by affinity tags or the antibody used for capture. Weak and/or transient interactions may not be detected if they are unstable in the lysis buffer or do not withstand the washes. Perhaps a better approach would be to perform

BioID, this technique uses biotinylation to identify interaction partners based on their proximity to the bait protein, which is expressed as a fusion protein with the active domain of biotin ligase [401]. Biotin affinity resin is then used to capture biotinylated proteins that can then be identified by mass spectrometry. This technique is more successful at identifying weak interactions because it does not depend on interactions remaining intact during the incubation and wash steps, and is an appropriate next step in the aim to identify UL7/UL51 interaction partners.

7 Conclusions and future directions

This study aimed to elucidate the molecular function of HSV-1 tegument proteins UL7 and UL51 during infection. Deletion of either UL7 or UL51 from HSV-1 is associated with a decrease in viral titre, a small plaque phenotype and the accumulation of unenveloped cytoplasmic capsids, which suggests a possible role for these proteins in virus assembly and egress. Both genes are conserved throughout the *Herpesviridae* family, and the phenotype observed upon deletion of homologous proteins from other herpesviruses (PrV, VZV and HCMV) resembles that of the UL7 and UL51 deletion viruses, suggesting a conserved role for these proteins. Thus, any insights gained into the function of the proteins at the molecular level may me applicable to other herpesviruses. An understanding of HSV-1 assembly pathways could contribute to the development of antiviral treatments that target this stage of the herpesvirus lifecycle.

7.1 UL7-UL51 form a complex during infection

Unpublished Y2H screen data from the lab of Dr Colin Crump suggested that UL7 and UL51 could interact to form a complex. This was supported by the finding that single (ΔUL7 or ΔUL51) and double-deletion (ΔUL7+ΔUL51) viruses exhibit comparable growth kinetics. This thesis presents evidence that UL7 and UL51 do form a complex during infection (Figure 3.19, page 85). The UL7-UL51 interaction was shown to be direct in pull-down experiments using recombinant UL7 and UL51 protein expressed in *E. coli,* and was mapped to within the first 170 residues of UL51. The UL7 and UL51 homologues from MHV (ORF42 and ORF55, respectively) also form a complex via a direct interaction, demonstrating that the complex is conserved in at least one other herpesvirus from a different subfamily (Figure 3.18, page 83). Expression levels of UL7 and UL51 during infection are interdependent, with UL7 no longer detectable by immunoblot in lysates of cells infected with ΔUL51 virus and UL51 levels are greatly reduced when UL7 is absent. The UL7 and UL51 proteins exhibited low solubility when individually expressed and purified from *E. coli*, and co-purification of chaperonin 60 with UL7 is an indication of protein misfolding. Chaperone proteins were also the major class of interaction partner identified in SILAC experiments when GFP-tagged UL7 and UL51 were transfected independently into cells.

Immunofluorescence microscopy experiments performed by Dr Anna Albecka provides further evidence that UL7 and UL51 function as a complex in cells. These experiments show UL7 and UL51 co-localisation to focal adhesions in transfected and infected cells, and that this was dependent on the expression of both proteins [277]. Cells infected with UL7/UL51 single or double-deletion virus became visibly more rounded and detached from the tissue culture dish earlier that those infected with the wild-type virus. A similar phenotype has been reported for cells infected with VZV deficient in the UL51

homologue, ORF7 [307]. Focal adhesions are necessary for lamellipodium and filopodium extension and also for maintaining contacts to the extracellular matrix [308]. HSV-1-infected cells have been shown to form filopodium-like projections that are thought to aid the transfer of virions to neighbouring cells [309]. This lead to the hypothesis that UL7 and UL51 might facilitate CCS by helping to maintain contacts between the infected cell and the extracellular matrix and/or neighbouring cells by stabilising focal adhesions. This hypothesis could, in part, explain the small plaque phenotype observed for the UL7/UL51 deletion viruses, which would be characteristic of defective CCS [277]. As mentioned in section 3.2.3, the UL51 homologues from MHV, KSHV and EBV are predicted to share structural homology with the small polypeptide Brk1/HSPC300, which is a component of the actin nucleating Scar/WAVE complex [402]. The homologous region is within the conserved core U44-domain so the fold may be conserved in the alphaherpesvirus homologues although the sequence is not. The Scar/WAVE complex bridges upstream signalling events with Arp2/3-mediated actin nucleation and assembly in lamellipodia during cell migration [403]. Such homology raises the question of whether UL51 could mimic the Brk1 protein in infected cells [403-407], though this is highly speculative given that the homologous region spans only 31 residues of the UL51 homologues. It was reasonable to predict that focal adhesions proteins might be identified in the SILAC-immunoprecipitation experiments performed as part of this thesis. The failure to identify such proteins in these experiments may be due to the formation of weak and/or transient interactions. Optimisation of the immunoprecipitation experiment, for example, by using chemical cross-linking to stabilise weak interactions or by enriching focal adhesions in the sample before performing the immunoprecipitation [408], could yet lead to the identification of UL7-UL51 interaction partners that explain their role at focal adhesions.

7.2 Co-expression and co-purification of UL7 and UL51 improves solubility

Co-expression and co-purification of UL7 and UL51 from *E. coli* cells greatly enhanced protein yield and solubility compared to expressing the proteins individually. Large-scale expression and purification of the UL7-UL51 complex was achieved, obtaining full-length UL7 and truncated UL51 (either aa. 1-170, 29-170 or 8-142). Based on analysis by SEC-MALS the purified complex has a propensity to self-associate meaning that it was not possibly to determine the precise stoichiometry of the complex and also rendering the sample unsuitable for SAXS experiments. In the virus UL7 and UL51 are located within the protein-dense tegument layer where they are likely to form interactions with other tegument and glycoproteins, e.g. UL14 and gE [168,229]. In the context of the virus, the 'sticky' nature of the UL7-UL51 complex might contribute to tegumentation. However, the absence of UL14 and gE (and possibly other viral or cellular proteins) in the purified UL7-UL51 sample could result in exposed hydrophobic patches on the surface of the complex, which may explain the propensity for self-association as observed in the SEC-MALS experiments. Co-expression of the complex with UL14

might prevent self-association and produce a monodisperse sample suitable for SAXS. Screening different buffer conditions and/or additives could also help to limit self-association.

Knowledge of the crystal structure of UL7-UL51 could provide insight into the molecular role of the complex, e.g. if the structure resembles proteins known to function at focal adhesions, in vesicular transport or possibly the Brk1/HSPC300 polypeptide mentioned above. Knowledge of the structure of the UL7-UL51 interaction interface would inform the design of point-mutations that could abolish the interaction, which would open the possibility to study any separate function(s) that the UL7 and UL51 proteins may have outside the function of the complex. The purified UL7-UL51 complexes were entered into crystallisation trials with varying degrees of success. Very fine crystalline needles were obtained for the UL7-UL51 C9S 1-170 complex but proved to be irreproducible. Sparse-matrix screening with the UL7-UL51 C9S 8-142 complex did yield reproducible crystals. However, these crystals are thin and fragile, preventing their analysis by X-ray diffraction. More robust crystals may be obtained by optimising the crystallisation conditions (e.g. grid and additive screening). Other options available include micro-seeding [409], reductive methylation [410], surface entropy reduction and/or *in situ* X-ray diffraction measurements. In the first instance, *in situ* diffraction experiments would be useful to determine if the crystals are proteinaceous. If they are found to be protein crystals, then grid and additive screening in conjunction with micro-seeding would be the easiest rescue strategy and should be attempted first, followed by reductive methylation and/or surface entropy reduction if necessary.

7.3 Screening for UL7/UL51 host-cell interaction partners

Two independent screening techniques were used in this study, Y2H screening and SILAC-based quantitative proteomics. The aim was to elucidate the function of UL7 and UL51 by identifying host-cell interaction partners to give an indication of the metabolic processes or cellular pathways within which these proteins function. Given the hypothesis that UL7 and UL51 are involved in virus assembly and egress, it was anticipated that they would interact with proteins involved in intracellular vesicular transport, or proteins that regulate cell morphology and/or the cytoskeleton. Y2H screening using UL51 identified numerous putative interaction partners, of which only the centriolar scaffold protein CPAP was shown to interact with UL51 in pull-down experiments using purified GST-tagged UL51 and the CPAP G-box domain expressed in wheat germ cell extract. It was also possible to co-immunoprecipitate CPAP G-box domain from cells co-transfected with myc-CPAP and either GFP-UL51 or GFP-UL7 + untagged UL51 (Figure 5.5, page 126), and to capture the UL7-UL51 complex from infected cell lysates using a purified GST-tagged CPAP G-box domain (Figure 5.7, page 128). It seemed plausible that HSV-1 protein(s) could interact with CPAP early during infection since HSV-1 has been shown to trigger the reorganisation of the microtubule network [324]. Furthermore, the MTOC may be lost by 6 h post HSV-1 infection based on staining for gamma tubulin, a MTOC marker and CPAP-

binding protein, raising the question of whether UL51 would be able to mediate the disassembly of the MTOC [333]. Several attempts were made to monitor CPAP expression levels during HSV-1 infection by immunoblotting whole-cell lysates. However, it was not possible to detect any change in CPAP level during infection, although these experiments were confounded by the poor quality of the αCPAP antibody, which made it difficult to unambiguously identify a band(s) corresponding to endogenous CPAP. Interestingly, CPAP levels were shown to decrease from 2 h.p.i. in a whole cell proteomic analysis experiment (Personal communication from Dr Tim Soh), which may be coincident with increasing UL51 expression in HSV-1-infected cells. However, there is a general decrease in the rate of host-cell protein synthesis in infected cells, as host mRNAs are degraded by the HSV-1 virion host shutoff (VHS) protein, which would also explain the decrease in CPAP expression [411].The CPAP binding region in UL51 was mapped and shown to resemble a known CPAP-binding motif present in the centriolar protein STIL. Specific point mutations in this motif abolished the CPAP-UL51 interaction, but no effect on HSV-1 replication in cell culture was evident when these mutations were introduced into the virus. Fluorescence polarisation experiments using purified *D. melanogaster* CPAP and fluorescently-labelled UL51 peptide demonstrated a weak interaction between CPAP and the motif in UL51. The weak nature of the association was supported by the SEC-MALS experiments in which the UL7-UL51 complex did not co-elute with purified CPAP domain (Figure 5.18, page 148), and this may explain why it was not possible to co-crystallise CPAP with the UL51 peptides. Based on these findings it was deemed unlikely that the interaction between UL51 and CPAP is biologically relevant during infection. While Y2H screening can be an effective means to identify interaction partners, the technique often result in a high number of false positives partly due to the high sensitivity. Improper folding, localisation and a lack of post-translational modifications can prevent the identification of genuine binding partners by this method.

SILAC-based quantitative proteomics was also employed to identify host-cell interaction partners for UL7 and UL51 proteins. Unlike Y2H screening, SILAC utilises labelled mammalian cells, which facilitates post-translational modifications and correct cellular localisation of bait and prey proteins, and can lead to the identification of whole protein complexes. The first SILAC screen was based on the immunoprecipitation of GFP-tagged UL7 and UL51 protein from transfected cells. In hindsight, the cellular localisation of the UL7 and UL51 bait proteins may have been disrupted by the presence of the GFP-tag, in particular, the ability of UL51 to associate with membranes via palmitoylation at cysteine 9 may have been disrupted by the N-terminal location of the tag. Over expression and/or improper cellular localisation of the bait proteins may explain the abundance of chaperone proteins in the list of putative interaction partners. The pontin-reptin complex was co-immunoprecipitated with GFP-UL7 in this screen and also in the second SILAC screen where UL51-(UL7) was immunoprecipitated from infected cells at 16 h.p.i., but not in the screen performed at 7 h.p.i. The pontin-reptin complex possess chaperone-like activity and recruits misfolded proteins to aggresomes

where it functions to dissemble aggregated proteins. The pontin-reptin complex did bind purified GST-tagged UL7-UL51 complex in a pull-down experiment, but it also bound purified GST-UL56 protein that is known to be intrinsically disordered. Immunofluorescence microscopy showed no evidence of pontin co-localisation with UL51 at assembly compartments or focal adhesions at 15 h.p.i.. Thus, it was concluded that the interaction between UL51(-UL7) is most likely to be non-specific, occurring as a result of high levels of potentially aggregated and/or misfolded protein in the cell at 16 h.p.i. Despite multiple attempts, it was not possible to identify genuine host-cell interaction partners for the UL7-UL51 complex using SILAC. This might be due to the formation of weak interactions with host-cell proteins that are not able to withstand the immunoprecipitation process, a problem that may be overcome through chemical cross-linking or the use of BioID [401]. Alternatively, UL51(-UL7) may not interact with host-cell proteins but function via interactions with other tegument proteins or glycoproteins.

7.4 Structural features of UL51 might promote secondary envelopment

While a possible role for UL51 and UL7 in CCS is becoming apparent, the molecular mechanisms underlying the assembly defect (i.e. the accumulation of unenveloped capsids in the cytoplasm) observed upon deletion of UL7 and UL51 remains unclear. It is possible that destabilisation of focal adhesion in the absence of UL7-UL51 could disrupt the cellular cytoskeleton and result in inefficient trafficking of the glycoprotein-laden vesicle required for secondary envelopment. Or the putative YXXϕ motif in UL51 and the cytoplasmic tail of gE could recruit AP adaptor proteins to mediate clathrin-coated vesicle formation [168]. Interestingly, residues 1-22 of UL51 are predicted to form an amphipathic alpha-helix (AH) (Figure 7.1). Amphipathic helices embed their hydrophobic face into lipid bilayers by inserting hydrophobic amino acid side-chains between acyl-chains in an entropy-driven process that releases water molecules [412,413]. Amphipathic helices have recently been shown to act as a signal for palmitoylation [303,304], thus the predicted AH in UL51 may signal for the palmitoylation of cysteine 9, which is positioned at the edge of the hydrophobic face (Figure 7.1). The proposed YXXϕ motif in UL51 resides within the hydrophobic face of the predicted AH encompassing residues 1-20, the question is whether UL51 membrane association would promote or preclude AP adaptor protein binding.

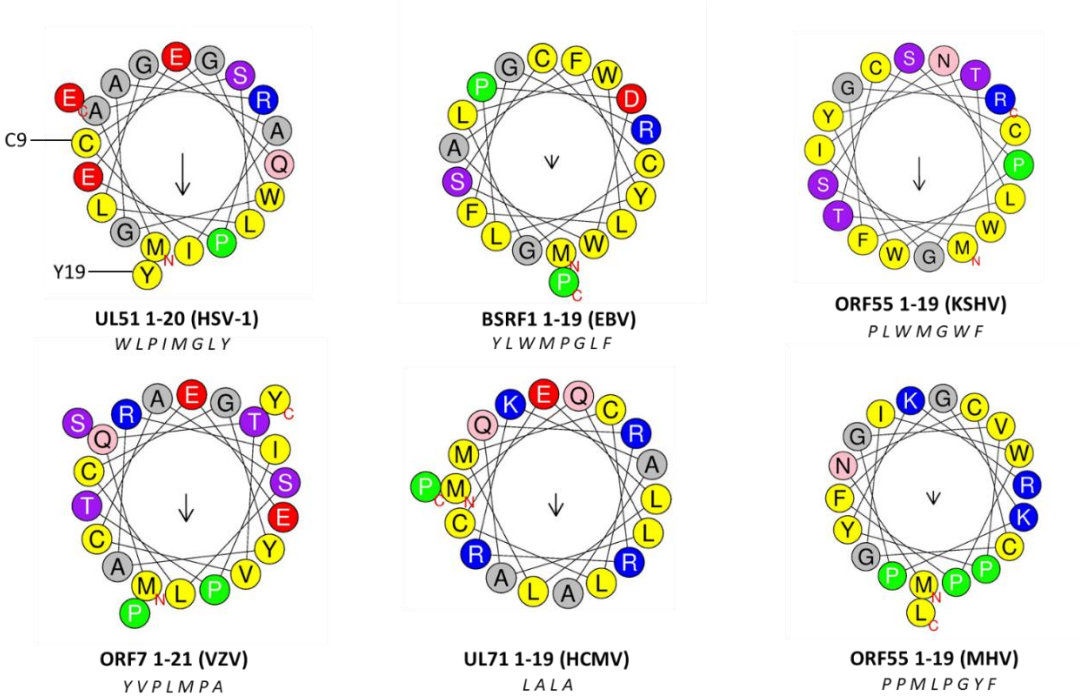

Figure 7.1 Amphipathic helix prediction for UL51 and homologues
The N-terminal 1-20 residues of UL51 are predicted to form an amphipathic helix, which may signal for palmitoylation at cysteine 9 and also contribute to membrane association. Homologues from VZV and KSHV are also predicted to form amphipathic helices. The homologues from EBV, HCMV and MHV are predicted to have hydrophobic faces but the hydrophobic moment prediction (denoted by the length of the arrow) is not as high as for the homologues from UL51 and the homologues from VZV and KSHV, suggesting that these would not be classed as amphipathic helices. Prediction by HeliQuest server [305]. Colour code for residues: yellow, hydrophobic; purple, serine and threonine; blue, basic; red, acidic; pink, asparagine and glutamine; grey, alanine and glycine; green, proline; light blue, histidine. Residues contributing to the formation of a hydrophobic face are shown in italics. The arrow in the wheel corresponds to the hydrophobic moment.

Multiple AHs embedded in a bilayer can induce membrane curvature through a 'wedge-effect', whereby embedded helices increase the surface area of the associated membrane leaflet, if the area of the opposite membrane leaflet is not increased equally then the membrane can curve [412]. For example, the AH in epsin contributes to membrane curvature and the formation for clathrin-coated vesicles at the plasma membrane [414,415]. Proteins containing large regions of disorder have also be shown to drive membrane curvature. Steric pressure generated by collisions between highly crowded membrane-embedded proteins can cause the expansion of the membrane surface, which is sufficient to drive membrane curving in a manner similar to AHs [416-418]. Proteins with a large hydrodynamic radius can occupy a large area on the surface of a membrane and so theoretically could contribute considerably to membrane crowding. Disordered proteins have significantly higher hydrodynamic radii than globular proteins of equivalent molecular mass and may act as drivers of membrane curvature by crowding the membrane surface. This hypothesis has been cited to explain membrane bending during coated vesicle assembly [419-422]. On this basis, membrane-associated UL51 may be able to induce

membrane curvature though the predicted amphipathic helix and disordered C-terminal region. The recruitment of other tegument proteins to the membrane via UL51, e.g. UL7 and UL14 or UL7-UL51 self-association, may further contribute to membrane crowding. Membrane curvature induced by UL51 could contribute to secondary envelopment if UL51 is present on the cytoplasmic surface of vesicles that form the viral envelope during secondary envelopment, or at the leading edges of the enveloping membrane (Figure 7.2). Disrupting the proposed amphipathic helix by introducing helix-breaking amino acids (e.g. proline) or substituting negatively charged residues in place of those that form the hydrophobic face could reveal whether the predicted AH is required for secondary envelopment. A role for palmitoylation in secondary envelopment could be investigated by mutating cysteine 9 of UL51 to block palmitoylation. This could be done in conjunction with the mutations intended to disrupt the predicted AH, to determine whether any effects of losing palmitoylation and the proposed AH are additive. While the amphipathic helix prediction looks convincing for UL51, it is less so for the other homologues, particularly those from EBV, MHV and HCMV (Figure 7.1). If the putative amphipathic helix does have a role in secondary envelopment, this role may not be conserved in all of the homologues.

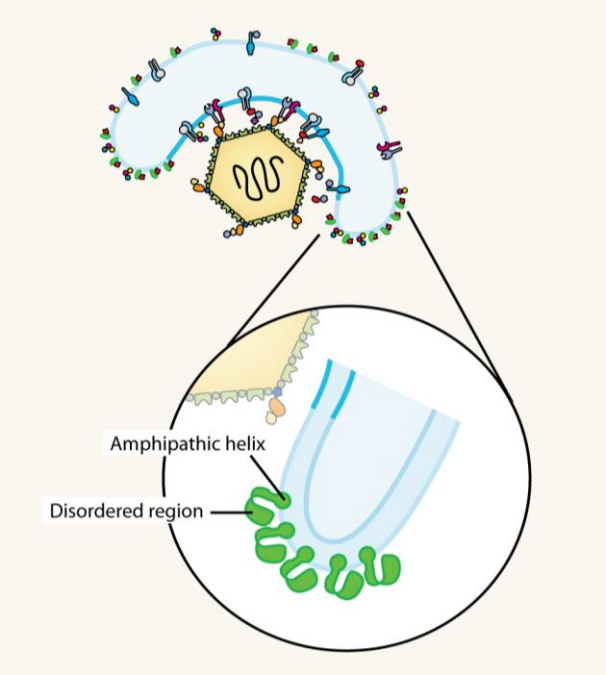

Figure 7.2 UL51 structure may contribute to membrane curvature
UL51 associates with membranes via a palmitoyl anchor at cysteine 9. Residues 1-20 of UL51 are predicted to form an amphipathic helix, which could act as a signal for palmitoylation and also contribute to membrane association. Amphipathic helices can induce membrane curvature, as can large disordered regions, such as residues 170-244 of UL51. During secondary envelopment, these features of UL51 may contribute to membrane curvature particularly at the leading edges of the enveloping membrane.

7.5 Future directions

This study has provided evidence for the formation of a direct interaction between HSV-1 proteins UL7 and UL51, and also between the homologous proteins from MHV. Immunofluorescence experiments, performed by Dr Anna Albecka, show localisation of the UL7-UL51 complex at focal adhesions in transfected and infected cells. Furthermore, cells infected with ΔUL7 or ΔUL51 HSV-1 round up and detach from the culture dish faster than wild-type infected cells, which would be consistent with the UL7-UL51 complex functioning to stabilise focal adhesions during infection. There is evidence in the literature to suggest a role for UL7 and UL51 in secondary envelopment and viral egress, based on the accumulation of unenveloped capsids in the cytoplasm that is observed when either of these proteins is not expressed. Thus, it was predicted that UL7 and UL51 might interact with host-cell proteins involved in membrane trafficking, however, no such interactions were identified in the yeast-two-hybrid screen (UL51) or SILAC (UL7 and UL51) experiments presented in this thesis, nor were any focal adhesion proteins detected, the reasons why this may have been the case are discussed in the previous section. It is plausible that the loss of focal adhesion stability in ΔUL7 and/or ΔUL51 HSV-1 infected cells could have an impact on the organisation and stability of the cellular cytoskeleton, which could in turn have a detrimental effect on membrane trafficking and subsequently secondary envelopment and viral egress. However, there is still potential to identify host-cell proteins that could elucidate a more specific role for UL7 and UL51 in secondary envelopment and egress. The following comprises a list of further experiments that should be performed:

- Optimisation of the co-IP experiments from infected cells for SILAC by using chemical cross-linking to stabilise weak interactions. Another approach that can facilitate the identification of weak/transient interacts is Bio-ID. These experiments should be performed at earlier time-points during infection e.g. 7 h.p.i.
- Continue with the optimisation of the UL7-UL51 C9S 8-142 crystals, using grid and additive screening in conjunction with micro-seeding, followed by reductive methylation and/or surface entropy reduction if necessary. Also, attempt to co-purify UL14 with the UL7-UL51 complex, which may result in a monodisperse sample suitable for SAXS.
- Further investigate the role of UL7 and UL51 at focal adhesions using functional *in vitro* assays. Since both proteins are required for the localisation of either protein at focal adhesions it is assumed that it is the UL7-UL51 complex that functions at these sites. Specific mutations that block the interaction would then help to dissect the role the complex may have versus the role these proteins have independently or in complex with other viral or host proteins.
- It would be interesting to test the hypothesis presented in section 7.4 that the AH in UL51 may have a role in secondary envelopment. This could be tested by disrupting the AH by introducing

the helix-breaking amino acid proline or by substituting negatively charged residues into the hydrophobic face and investigating the effect this has, if any, in the context of viral infection. These experiments could also be performed in the context of a cysteine 9 mutant that blocks palmitoylation.

8 Appendix 1: General Buffers

Buffer	Composition
5x SDS-PAGE loading buffer	250 mM Tris pH 6.8 10% w/v SDS 25% v/v glycerol 10 mM DTT 0.05% Bromophenol blue
10x DNA loading buffer	0.4% w/v Orange G 1 mM EDTA pH 8.0 50% v/v glycerol
Tris-borate EDTA (TBE) buffer	45 mM Tris base 45 mM Boric acid 1 mM EDTA
1x Immunoblot transfer buffer	25 mM Tris base 192 mM Glycine 20% v/v Methanol
Ponceau stain	2% w/v Ponceau S 30% w/v Trichloroacetic acid

9 Appendix 2: NetSurfP and RONN output

The predicted secondary structure and disorder profiles for UL7 and UL51 homologues from VZV, KSHV and MHV are shown. Secondary structure and disorder prediction was performed using NetSurfP [292] and RONN [293]. A RONN probability score (blue line) greater than 0.5 is classed as disordered.

9.1 UL7 homologues

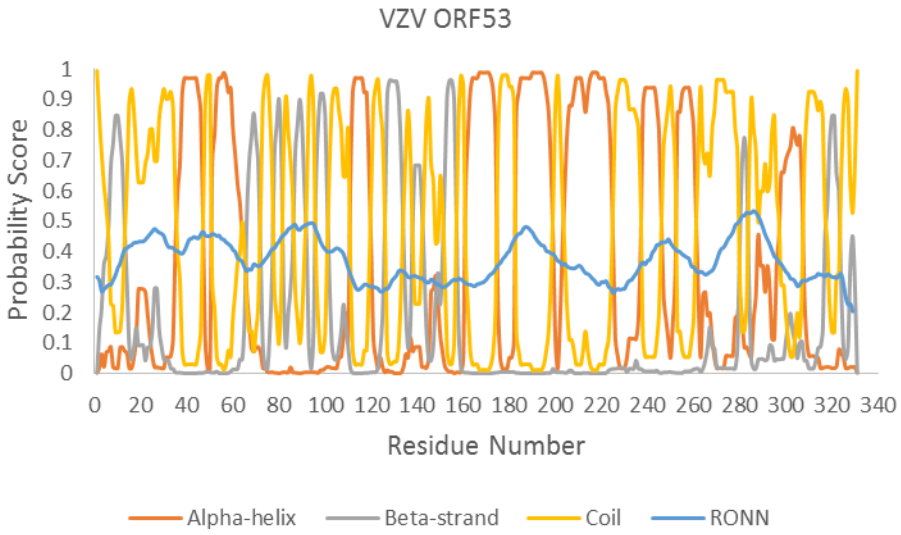

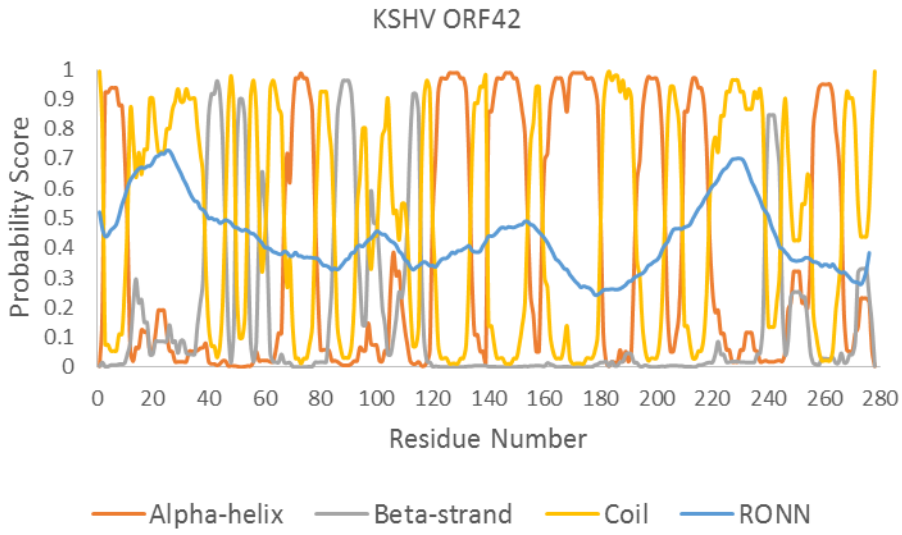

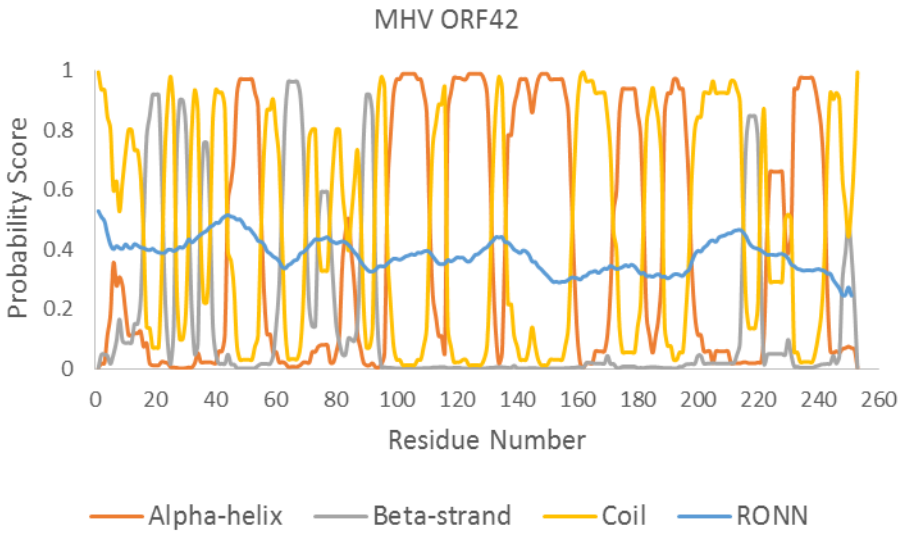

9.2 UL51 homologues

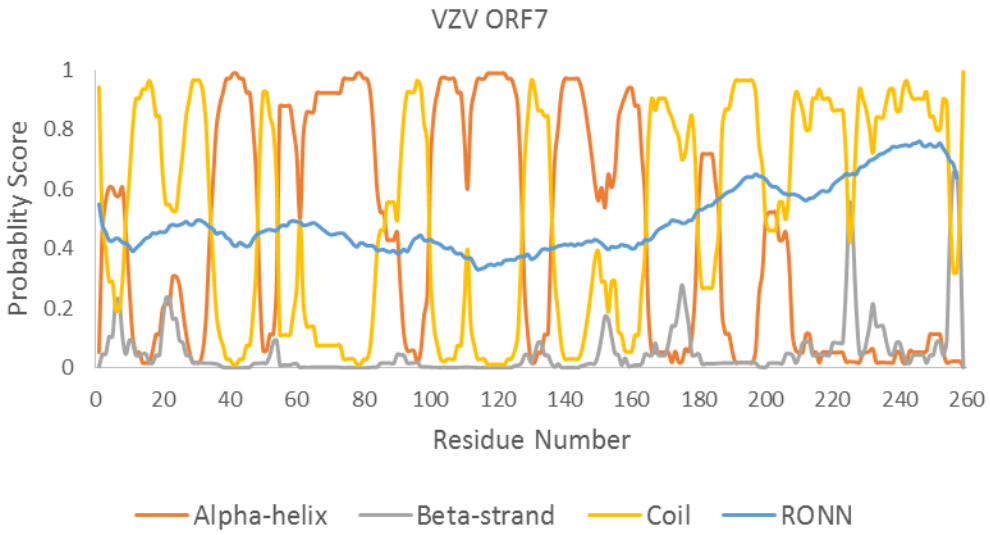

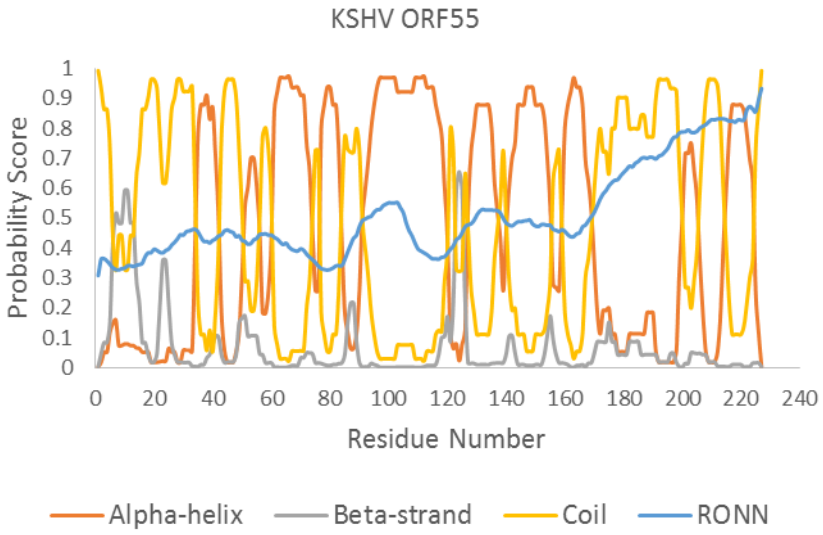

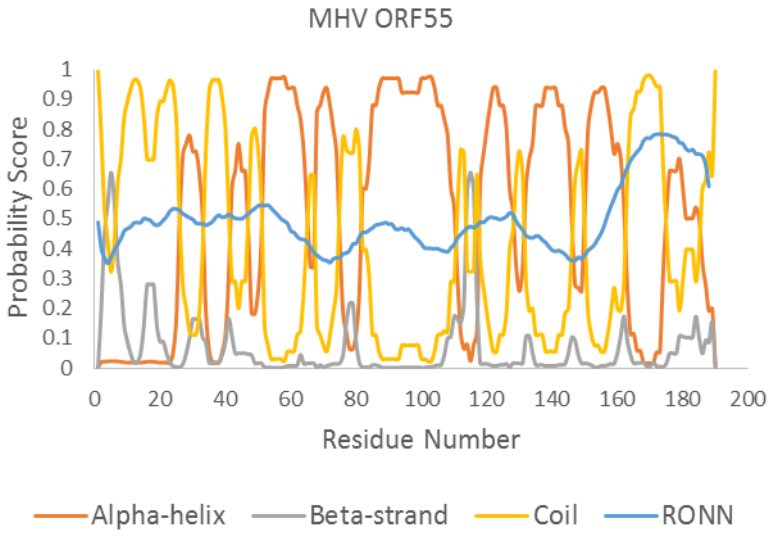
MHV ORF55
Probability Score
1
0.9
0.8
0.7
0.6
0.5
0.4
0.3
0.2
0.1
0
0
20
40
60
80
100
120
140
160
180
200
Residue Number
Alpha-helix
Beta-strand
Coil
RONN

1. Davison, A.J.; Eberle, R.; Ehlers, B.; Hayward, G.S.; McGeoch, D.J.; Minson, A.C.; Pellett, P.E.; Roizman, B.; Studdert, M.J.; Thiry, E. The order Herpesvirales. *Archives of virology* **2009**, *154*, 171-177.
2. McGeoch, D.J.; Gatherer, D. Integrating reptilian herpesviruses into the family herpesviridae. *Journal of Virology* **2005**, *79*, 725-731.
3. Roizman, B.; Carmichael, L.E.; Deinhardt, F.; de-The, G.; Nahmias, A.J.; Plowright, W.; Rapp, F.; Sheldrick, P.; Takahashi, M.; Wolf, K. Herpesviridae. Definition, provisional nomenclature, and taxonomy. The Herpesvirus Study Group, the International Committee on Taxonomy of Viruses. *Intervirology* **1981**, *16*, 201-217.
4. Mocarski, E.S., Jr. Comparative analysis of herpesvirus-common proteins. In *Human Herpesviruses: Biology, Therapy, and Immunoprophylaxis*, Arvin, A.; Campadelli-Fiume, G.; Mocarski, E.; Moore, P.S.; Roizman, B.; Whitley, R.; Yamanishi, K., Eds. Cambridge University Press: Cambridge, UK, 2007; pp 44-58.
5. Mettenleiter, T.C.; Klupp, B.G.; Granzow, H. Herpesvirus assembly: An update. *Virus research* **2009**, *143*, 222-234.
6. Mettenleiter, T.C. Herpesvirus assembly and egress. *Journal of virology* **2002**, *76*, 1537-1547.
7. Roizman, B.; Knipe, D.M.; Whitley, R.J. Herpes simplex viruses. In *Fields virology*, 5th ed.; Fields, B.N.; Knipe, D.M.; Howley, P.M., Eds. Wolters Kluwer Health/Lippincott Williams & Wilkins: Philadelphia: London, UK, 2007; pp 2501-2601.
8. Nicoll, M.P.; Proença, J.T.; Efstathiou, S. The molecular basis of herpes simplex virus latency. *FEMS microbiology reviews* **2012**, *36*, 684-705.
9. White, D.W.; Beard, R.S.; Barton, E.S. Immune Modulation During Latent Herpesvirus Infection. *Immunological reviews* **2012**, *245*, 189-208.
10. Sylwester, A.W.; Mitchell, B.L.; Edgar, J.B.; Taormina, C.; Pelte, C.; Ruchti, F.; Sleath, P.R.; Grabstein, K.H.; Hosken, N.A.; Kern, F.*, et al.* Broadly targeted human cytomegalovirus-specific CD4+ and CD8+ T cells dominate the memory compartments of exposed subjects. *The Journal of experimental medicine* **2005**, *202*, 673-685.
11. Hislop, A.D.; Annels, N.E.; Gudgeon, N.H.; Leese, A.M.; Rickinson, A.B. Epitope-specific evolution of human CD8(+) T cell responses from primary to persistent phases of Epstein-Barr virus infection. *The Journal of experimental medicine* **2002**, *195*, 893-905.
12. Hislop, A.D.; Kuo, M.; Drake-Lee, A.B.; Akbar, A.N.; Bergler, W.; Hammerschmitt, N.; Khan, N.; Palendira, U.; Leese, A.M.; Timms, J.M.*, et al.* Tonsillar homing of Epstein-Barr virus-specific CD8+ T cells and the virus-host balance. *The Journal of clinical investigation* **2005**, *115*, 2546-2555.
13. Tan, L.C.; Gudgeon, N.; Annels, N.E.; Hansasuta, P.; O'Callaghan, C.A.; Rowland-Jones, S.; McMichael, A.J.; Rickinson, A.B.; Callan, M.F. A re-evaluation of the frequency of CD8+ T cells specific for EBV in healthy virus carriers. *Journal of Immunology* **1999**, *162*, 1827-1835.
14. Verjans, G.M.; Hintzen, R.Q.; van Dun, J.M.; Poot, A.; Milikan, J.C.; Laman, J.D.; Langerak, A.W.; Kinchington, P.R.; Osterhaus, A.D. Selective retention of herpes simplex virus-specific T cells in latently infected human trigeminal ganglia. *Proceedings of the National Academy of Sciences of the United States of America* **2007**, *104*, 3496-3501.
15. Theil, D.; Derfuss, T.; Paripovic, I.; Herberger, S.; Meinl, E.; Schueler, O.; Strupp, M.; Arbusow, V.; Brandt, T. Latent herpesvirus infection in human trigeminal ganglia causes chronic immune response. *The American journal of pathology* **2003**, *163*, 2179-2184.
16. Khanna, K.M.; Bonneau, R.H.; Kinchington, P.R.; Hendricks, R.L. Herpes simplex virus-specific memory CD8+ T cells are selectively activated and retained in latently infected sensory ganglia. *Immunity* **2003**, *18*, 593-603.
17. St Leger, A.J.; Jeon, S.; Hendricks, R.L. Broadening the repertoire of functional herpes simplex virus type 1-specific CD8+ T cells reduces viral reactivation from latency in sensory ganglia. *Journal of Immunology* **2013**, *191*, 2258-2265.

18. Sandalova, E.; Laccabue, D.; Boni, C.; Tan, A.T.; Fink, K.; Ooi, E.E.; Chua, R.; Shafaeddin Schreve, B.; Ferrari, C.; Bertoletti, A. Contribution of herpesvirus specific CD8 T cells to anti-viral T cell response in humans. *PLoS Pathog* **2010**, *6*, e1001051.
19. Doisne, J.M.; Urrutia, A.; Lacabaratz-Porret, C.; Goujard, C.; Meyer, L.; Chaix, M.L.; Sinet, M.; Venet, A. CD8+ T cells specific for EBV, cytomegalovirus, and influenza virus are activated during primary HIV infection. *Journal of Immunology* **2004**, *173*, 2410-2418.
20. Pomeranz, L.E.; Reynolds, A.E.; Hengartner, C.J. Molecular biology of pseudorabies virus: Impact on neurovirology and veterinary medicine. *Microbiology and Molecular Biology Reviews* **2005**, *69*, 462-500.
21. Azwa, A.; Barton, S.E. Aspects of herpes simplex virus: a clinical review. *The journal of family planning and reproductive health care* **2009**, *35*, 237-242.
22. Dodding, M.P.; Way, M. Coupling viruses to dynein and kinesin-1. *EMBO journal* **2011**, *30*, 3527-3539.
23. Smith, G. Herpesvirus transport to the nervous system and back again. *Annual Review of Microbiology* **2012**, *66*, 153-176.
24. Kramer, T.; Enquist, L.W. Directional spread of alphaherpesviruses in the nervous system. *Viruses* **2013**, *5*, 678-707.
25. Luker, K.E.; Schultz, T.; Romine, J.; Leib, D.A.; Luker, G.D. Transgenic reporter mouse for bioluminescence imaging of herpes simplex virus 1 infection in living mice. *Virology* **2006**, *347*, 286-295.
26. Luxton, G.W.; Haverlock, S.; Coller, K.E.; Antinone, S.E.; Pincetic, A.; Smith, G.A. Targeting of herpesvirus capsid transport in axons is coupled to association with specific sets of tegument proteins. *Proceedings of the National Academy of Sciences of the United States of America* **2005**, *102*, 5832-5837.
27. Antinone, S.E.; Smith, G.A. Retrograde axon transport of herpes simplex virus and pseudorabies virus: a live-cell comparative analysis. *Journal of Virology* **2010**, *84*, 1504-1512.
28. Antinone, S.E.; Zaichick, S.V.; Smith, G.A. Resolving the assembly state of herpes simplex virus during axon transport by live-cell imaging. *J Virol* **2010**, *84*, 13019-13030.
29. Smith, G.A.; Pomeranz, L.; Gross, S.P.; Enquist, L.W. Local modulation of plus-end transport targets herpesvirus entry and egress in sensory axons. *Proceedings of the National Academy of Sciences, USA* **2004**, *101*, 16034-16039.
30. Liu, W.W.; Goodhouse, J.; Jeon, N.L.; Enquist, L.W. A microfluidic chamber for analysis of neuron-to-cell spread and axonal transport of an alpha-herpesvirus. *PLoS One* **2008**, *3*, e2382.
31. Wagner, E.K.; Guzowski, J.F.; Singh, J. Transcription of the herpes simplex virus genome during productive and latent infection. *Progress in nucleic acid research and molecular biology* **1995**, *51*, 123-165.
32. Weir, J.P. Regulation of herpes simplex virus gene expression. *Gene* **2001**, *271*, 117-130.
33. Flint, J.; Shenk, T. Viral transactivating proteins. *Annual review of genetics* **1997**, *31*, 177-212.
34. Suk, H.; Knipe, D.M. Proteomic analysis of the herpes simplex virus 1 virion protein 16 transactivator protein in infected cells. *Proteomics* **2015**, *15*, 1957-1967.
35. Batterson, W.; Roizman, B. Characterization of the herpes simplex virion-associated factor responsible for the induction of alpha genes. *J Virol* **1983**, *46*, 371-377.
36. Honess, R.W.; Roizman, B. Regulation of herpesvirus macromolecular synthesis. I. Cascade regulation of the synthesis of three groups of viral proteins. *Journal of Virology* **1974**, *14*, 8-19.
37. Honess, R.W.; Roizman, B. Regulation of herpesvirus macromolecular synthesis: sequential transition of polypeptide synthesis requires functional viral polypeptides. *Proceedings of the National Academy of Sciences of the United States of America* **1975**, *72*, 1276-1280.
38. Newcomb, W.W.; Trus, B.L.; Booy, F.P.; Steven, A.C.; Wall, J.S.; Brown, J.C. Structure of the herpes simplex virus capsid. Molecular composition of the pentons and the triplexes. *Journal of Molecular Biology* **1993**, *232*, 499-511.

39. Homa, F.L.; Huffman, J.B.; Toropova, K.; Lopez, H.R.; Makhov, A.M.; Conway, J.F. Structure of the pseudorabies virus capsid: Comparison with herpes simplex virus type 1 and differential binding of essential minor proteins. *Journal of Molecular Biology* **2013**, *425*, 3415-3428.
40. Schrag, J.D.; Prasad, B.V.; Rixon, F.J.; Chiu, W. Three-dimensional structure of the HSV1 nucleocapsid. *Cell* **1989**, *56*, 651-660.
41. Zhou, Z.H.; Dougherty, M.; Jakana, J.; He, J.; Rixon, F.J.; Chiu, W. Seeing the herpesvirus capsid at 8.5 A. *Science* **2000**, *288*, 877-880.
42. Newcomb, W.W.; Juhas, R.M.; Thomsen, D.R.; Homa, F.L.; Burch, A.D.; Weller, S.K.; Brown, J.C. The UL6 gene product forms the portal for entry of DNA into the herpes simplex virus capsid. *Journal of virology* **2001**, *75*, 10923-10932.
43. Trus, B.L.; Newcomb, W.W.; Cheng, N.; Cardone, G.; Marekov, L.; Homa, F.L.; Brown, J.C.; Steven, A.C. Allosteric signaling and a nuclear exit strategy: Binding of UL25/UL17 heterodimers to DNA-filled HSV-1 capsids. *Molecular Cell* **2007**, *26*, 479-489.
44. Cockrell, S.K.; Huffman, J.B.; Toropova, K.; Conway, J.F.; Homa, F.L. Residues of the UL25 protein of herpes simplex virus that are required for its stable interaction with capsids. *Journal of Virology* **2011**, *85*, 4875-4887.
45. Klupp, B.G.; Granzow, H.; Keil, G.M.; Mettenleiter, T.C. The capsid-associated UL25 protein of the alphaherpesvirus pseudorabies virus is nonessential for cleavage and encapsidation of genomic DNA but is required for nuclear egress of capsids. *Journal of Virology* **2006**, *80*, 6235-6246.
46. Leelawong, M.; Lee, J.I.; Smith, G.A. Nuclear egress of pseudorabies virus capsids is enhanced by a subspecies of the large tegument protein that is lost upon cytoplasmic maturation. *Journal of Virology* **2012**, *86*, 6303-6314.
47. Booy, F.P.; Newcomb, W.W.; Trus, B.L.; Brown, J.C.; Baker, T.S.; Steven, A.C. Liquid-crystalline, phage-like packing of encapsidated DNA in herpes simplex virus. *Cell* **1991**, *64*, 1007-1015.
48. Liu, T.; Sae-Ueng, U.; Li, D.; Lander, G.C.; Zuo, X.; Jonsson, B.; Rau, D.; Shefer, I.; Evilevitch, A. Solid-to-fluid-like DNA transition in viruses facilitates infection. *Proceedings of the National Academy of Sciences of the United States of America* **2014**, *111*, 14675-14680.
49. Sae-Ueng, U.; Li, D.; Zuo, X.; Huffman, J.B.; Homa, F.L.; Rau, D.; Evilevitch, A. Solid-to-fluid DNA transition inside HSV-1 capsid close to the temperature of infection. *Nature chemical biology* **2014**, *10*, 861-867.
50. Fan, W.H.; Roberts, A.P.E.; McElwee, M.; Bhella, D.; Rixon, F.J.; Lauder, R. The large tegument protein pUL36 is essential for formation of the capsid vertex-specific component at the capsid-tegument interface of herpes simplex virus 1. *Journal of Virology* **2015**, *89*, 1502-1511.
51. Dai, X.; Gong, D.; Wu, T.-T.; Sun, R.; Zhou, Z.H. Organization of capsid-associated tegument components in Kaposi's sarcoma-associated herpesvirus. *Journal of Virology* **2014**, *88*, 12694-12702.
52. Trus, B.L.; Booy, F.P.; Newcomb, W.W.; Brown, J.C.; Homa, F.L.; Thomsen, D.R.; Steven, A.C. The herpes simplex virus procapsid: structure, conformational changes upon maturation, and roles of the triplex proteins VP19c and VP23 in assembly. *J Mol Biol* **1996**, *263*, 447-462.
53. Zhou, Z.H.; Chen, D.H.; Jakana, J.; Rixon, F.J.; Chiu, W. Visualization of tegument-capsid interactions and DNA in intact herpes simplex virus type 1 virions. *Journal of Virology* **1999**, *73*, 3210-3218.
54. Newcomb, W.W.; Brown, J.C. Structure and capsid association of the herpesvirus large tegument protein UL36. *Journal of Virology* **2010**, *84*, 9408-9414.
55. Toropova, K.; Huffman, J.B.; Homa, F.L.; Conway, J.F. The herpes simplex virus 1 UL17 protein is the second constituent of the capsid vertex-specific component required for DNA packaging and retention. *Journal of Virology* **2011**, *85*, 7513-7522.
56. Newcomb, W.W.; Jones, L.M.; Dee, A.; Chaudhry, F.; Brown, J.C. Role of a reducing environment in disassembly of the herpesvirus tegument. *Virology* **2012**, *431*, 71-79.
57. McLauchlan, J.; Rixon, F.J. Characterization of enveloped tegument structures (L particles) produced by alphaherpesviruses: Integrity of the tegument does not depend on the presence of capsid or envelope. *Journal of General Virology* **1992**, *73*, 269-276.

58. Loret, S.; Guay, G.; Lippé, R. Comprehensive characterization of extracellular herpes simplex virus type 1 virions. *Journal of Virology* **2008**, *82*, 8605-8618.
59. Radtke, K.; Kieneke, D.; Wolfstein, A.; Michael, K.; Steffen, W.; Scholz, T.; Karger, A.; Sodeik, B. Plus- and minus-end directed microtubule motors bind simultaneously to herpes simplex virus capsids using different inner tegument structures. *PLoS pathogens* **2010**, *6*, e1000991.
60. Wolfstein, A.; Nagel, C.H.; Radtke, K.; Döhner, K.; Allan, V.J.; Sodeik, B. The inner tegument promotes herpes simplex virus capsid motility along microtubules in vitro. *Traffic* **2006**, *7*, 227-237.
61. Grünewald, K.; Desai, P.; Winkler, D.C.; Heymann, J.B.; Belnap, D.M.; Baumeister, W.; Steven, A.C. Three-dimensional structure of herpes simplex virus from cryo-electron tomography. *Science* **2003**, *302*, 1396-1398.
62. Laine, R.F.; Albecka, A.; van de Linde, S.; Rees, E.J.; Crump, C.M.; Kaminski, C.F. Structural analysis of herpes simplex virus by optical super-resolution imaging. *Nature Communications* **2015**, *6*, 5980.
63. Bohannon, K.P.; Jun, Y.; Gross, S.P.; Smith, G.A. Differential protein partitioning within the herpesvirus tegument and envelope underlies a complex and variable virion architecture. *Proceedings of the National Academy of Sciences, USA* **2013**, *110*, E1613-1620.
64. Kelly, B.J.; Fraefel, C.; Cunningham, A.L.; Diefenbach, R.J. Functional roles of the tegument proteins of herpes simplex virus type 1. *Virus Research* **2009**, *145*, 173-186.
65. Lam, Q.; Smibert, C.A.; Koop, K.E.; Lavery, C.; Capone, J.P.; Weinheimer, S.P.; Smiley, J.R. Herpes simplex virus VP16 rescues viral mRNA from destruction by the virion host shutoff function. *EMBO Journal* **1996**, *15*, 2575-2581.
66. Matis, J.; Kudelova, M. Early shutoff of host protein synthesis in cells infected with herpes simplex viruses. *Acta virologica* **2001**, *45*, 269-277.
67. Smiley, J.R. Herpes simplex virus virion host shutoff protein: Immune evasion mediated by a viral RNase? *Journal of Virology* **2004**, *78*, 1063-1068.
68. Mingo, R.M.; Han, J.; Newcomb, W.W.; Brown, J.C. Replication of herpes simplex virus: egress of progeny virus at specialized cell membrane sites. *Journal of Virology* **2012**, *86*, 7084-7097.
69. Connolly, S.A.; Jackson, J.O.; Jardetzky, T.S.; Longnecker, R. Fusing structure and function: a structural view of the herpesvirus entry machinery. *Nature Reviews: Microbiology* **2011**, *9*, 369-381.
70. Sathiyamoorthy, K.; Chen, J.; Longnecker, R.; Jardetzky, T.S. The COMPLEXity in herpesvirus entry. *Current Opinion in Virology* **2017**, *24*, 97-104.
71. Eisenberg, R.J.; Atanasiu, D.; Cairns, T.M.; Gallagher, J.R.; Krummenacher, C.; Cohen, G.H. Herpes virus fusion and entry: a story with many characters. *Viruses* **2012**, *4*, 800-832.
72. Turner, A.; Bruun, B.; Minson, T.; Browne, H. Glycoproteins gB, gD, and gHgL of Herpes Simplex Virus Type 1 Are Necessary and Sufficient To Mediate Membrane Fusion in a Cos Cell Transfection System. In *Journal of Virology*, 1998; Vol. 72, pp 873-875.
73. Heldwein, E.E.; Krummenacher, C. Entry of herpesviruses into mammalian cells. *Cellular and Molecular Life Sciences* **2008**, *65*, 1653-1668.
74. Heldwein, E.E.; Lou, H.; Bender, F.C.; Cohen, G.H.; Eisenberg, R.J.; Harrison, S.C. Crystal structure of glycoprotein B from herpes simplex virus 1. *Science* **2006**, *313*, 217-220.
75. Laquerre, S.; Argnani, R.; Anderson, D.B.; Zucchini, S.; Manservigi, R.; Glorioso, J.C. Heparan sulfate proteoglycan binding by herpes simplex virus type 1 glycoproteins B and C, which differ in their contributions to virus attachment, penetration, and cell-to-cell spread. *Journal of Virology* **1998**, *72*, 6119-6130.
76. Connolly, S.A.; Landsburg, D.J.; Carfi, A.; Whitbeck, J.C.; Zuo, Y.; Wiley, D.C.; Cohen, G.H.; Eisenberg, R.J. Potential nectin-1 binding site on herpes simplex virus glycoprotein d. *Journal of Virology* **2005**, *79*, 1282-1295.
77. Montgomery, R.I.; Warner, M.S.; Lum, B.J.; Spear, P.G. Herpes simplex virus-1 entry into cells mediated by a novel member of the TNF/NGF receptor family. *Cell* **1996**, *87*, 427-436.
78. Yoon, M.; Zago, A.; Shukla, D.; Spear, P.G. Mutations in the N termini of herpes simplex virus type 1 and 2 gDs alter functional interactions with the entry/fusion receptors HVEM, nectin-

2, and 3-O-sulfated heparan sulfate but not with nectin-1. *Journal of Virology* **2003**, *77*, 9221-9231.
79. Shukla, D.; Liu, J.; Blaiklock, P.; Shworak, N.W.; Bai, X.; Esko, J.D.; Cohen, G.H.; Eisenberg, R.J.; Rosenberg, R.D.; Spear, P.G. A novel role for 3-O-sulfated heparan sulfate in herpes simplex virus 1 entry. *Cell* **1999**, *99*, 13-22.
80. Lazear, E.; Whitbeck, J.C.; Zuo, Y.; Carfi, A.; Cohen, G.H.; Eisenberg, R.J.; Krummenacher, C. Induction of conformational changes at the N-terminus of herpes simplex virus glycoprotein D upon binding to HVEM and nectin-1. *Virology* **2014**, *448*, 185-195.
81. Maurer, U.E.; Sodeik, B.; Grünewald, K. Native 3D intermediates of membrane fusion in herpes simplex virus 1 entry. *Proceedings of the National Academy of Sciences, USA* **2008**, *105*, 10559-10564.
82. Sodeik, B.; Ebersold, M.W.; Helenius, A. Microtubule-mediated transport of incoming herpes simplex virus 1 capsids to the nucleus. *The Journal of Cell Biology* **1997**, *136*, 1007-1021.
83. Luxton, G.W.; Haverlock, S.; Coller, K.E.; Antinone, S.E.; Pincetic, A.; Smith, G.A. Targeting of herpesvirus capsid transport in axons is coupled to association with specific sets of tegument proteins. *Proceedings of the National Academy of Sciences, USA* **2005**, *102*, 5832-5837.
84. Aggarwal, A.; Miranda-Saksena, M.; Boadle, R.A.; Kelly, B.J.; Diefenbach, R.J.; Alam, W.; Cunningham, A.L. Ultrastructural visualization of individual tegument protein dissociation during entry of herpes simplex virus 1 into human and rat dorsal root ganglion neurons. *Journal of Virology* **2012**, *86*, 6123-6137.
85. Antinone, S.E.; Shubeita, G.T.; Coller, K.E.; Lee, J.I.; Haverlock-Moyns, S.; Gross, S.P.; Smith, G.A. The herpesvirus capsid surface protein, VP26, and the majority of the tegument proteins are dispensable for capsid transport toward the nucleus. *J Virol* **2006**, *80*, 5494-5498.
86. Schipke, J.; Pohlmann, A.; Diestel, R.; Binz, A.; Rudolph, K.; Nagel, C.-H.; Bauerfeind, R.; Sodeik, B. The C terminus of the large tegument protein pUL36 contains multiple capsid binding sites that function differently during assembly and cell entry of herpes simplex virus. *Journal of Virology* **2012**, *86*, 3682-3700.
87. Copeland, A.M.; Newcomb, W.W.; Brown, J.C. Herpes simplex virus replication: Roles of viral proteins and nucleoporins in capsid-nucleus attachment. *Journal of Virology* **2009**, *83*, 1660-1668.
88. Abaitua, F.; Daikoku, T.; Crump, C.M.; Bolstad, M.; O'Hare, P. A single mutation responsible for temperature-sensitive entry and assembly defects in the VP1-2 protein of herpes simplex virus. *Journal of Virology* **2011**, *85*, 2024-2036.
89. Batterson, W.; Furlong, D.; Roizman, B. Molecular genetics of herpes simplex virus. VIII. Further characterization of a temperature-sensitive mutant defective in release of viral DNA and in other stages of the viral reproductive cycle. *Journal of Virology* **1983**, *45*, 397-407.
90. Knipe, D.M.; Batterson, W.; Nosal, C.; Roizman, B.; Buchan, A. Molecular genetics of herpes simplex virus. VI. Characterization of a temperature-sensitive mutant defective in the expression of all early viral gene products. *Journal of Virology* **1981**, *38*, 539-547.
91. Pasdeloup, D.; Blondel, D.; Isidro, A.L.; Rixon, F.J. Herpesvirus capsid association with the nuclear pore complex and viral DNA release involve the nucleoporin CAN/Nup214 and the capsid protein pUL25. *Journal of Virology* **2009**, *83*, 6610-6623.
92. Garber, D.A.; Beverley, S.M.; Coen, D.M. Demonstration of circularization of herpes simplex virus DNA following infection using pulsed field gel electrophoresis. *Virology* **1993**, *197*, 459-462.
93. Strang, B.L.; Stow, N.D. Circularization of the herpes simplex virus type 1 genome upon lytic infection. *Journal of Virology* **2005**, *79*, 12487-12494.
94. Brown, J.C.; Newcomb, W.W. Herpesvirus capsid assembly: insights from structural analysis. *Current Opinion in Virology* **2011**, *1*, 142-149.
95. Newcomb, W.W.; Homa, F.L.; Thomsen, D.R.; Booy, F.P.; Trus, B.L.; Steven, A.C.; Spencer, J.V.; Brown, J.C. Assembly of the herpes simplex virus capsid: characterization of intermediates observed during cell-free capsid formation. *Journal of Molecular Biology* **1996**, *263*, 432-446.

96. Newcomb, W.W.; Homa, F.L.; Thomsen, D.R.; Ye, Z.; Brown, J.C. Cell-free assembly of the herpes simplex virus capsid. *Journal of Virology* **1994**, *68*, 6059-6063.
97. Tatman, J.D.; Preston, V.G.; Nicholson, P.; Elliott, R.M.; Rixon, F.J. Assembly of herpes simplex virus type 1 capsids using a panel of recombinant baculoviruses. *Journal of General Virology* **1994**, *75 (Pt 5)*, 1101-1113.
98. Thomsen, D.R.; Roof, L.L.; Homa, F.L. Assembly of herpes simplex virus (HSV) intermediate capsids in insect cells infected with recombinant baculoviruses expressing HSV capsid proteins. *Journal of Virology* **1994**, *68*, 2442-2457.
99. Aksyuk, A.A.; Newcomb, W.W.; Cheng, N.; Winkler, D.C.; Fontana, J.; Heymann, J.B.; Steven, A.C. Subassemblies and asymmetry in assembly of herpes simplex virus procapsid. *MBio* **2015**, *6*, e01525-01515.
100. Heming, J.D.; Conway, J.F.; Homa, F.L. Herpesvirus Capsid Assembly and DNA Packaging. *Advances in anatomy, embryology, and cell biology* **2017**, *223*, 119-142.
101. Heymann, J.B.; Cheng, N.; Newcomb, W.W.; Trus, B.L.; Brown, J.C.; Steven, A.C. Dynamics of herpes simplex virus capsid maturation visualized by time-lapse cryo-electron microscopy. *Nature structural biology* **2003**, *10*, 334-341.
102. Church, G.A.; Wilson, D.W. Study of herpes simplex virus maturation during a synchronous wave of assembly. *Journal of Virology* **1997**, *71*, 3603-3612.
103. Sheaffer, A.K.; Newcomb, W.W.; Gao, M.; Yu, D.; Weller, S.K.; Brown, J.C.; Tenney, D.J. Herpes simplex virus DNA cleavage and packaging proteins associate with the procapsid prior to its maturation. *Journal of Virology* **2001**, *75*, 687-698.
104. Thurlow, J.K.; Murphy, M.; Stow, N.D.; Preston, V.G. Herpes simplex virus type 1 DNA-packaging protein UL17 is required for efficient binding of UL25 to capsids. *Journal of Virology* **2006**, *80*, 2118-2126.
105. Huet, A.; Makhov, A.M.; Huffman, J.B.; Vos, M.; Homa, F.L.; Conway, J.F. Extensive subunit contacts underpin herpesvirus capsid stability and interior-to-exterior allostery. *Nature structural & molecular biology* **2016**, *23*, 531-539.
106. Jacob, R.J.; Morse, L.S.; Roizman, B. Anatomy of herpes simplex virus DNA. XII. Accumulation of head-to-tail concatemers in nuclei of infected cells and their role in the generation of the four isomeric arrangements of viral DNA. *Journal of Virology* **1979**, *29*, 448-457.
107. Boehmer, P.E.; Lehman, I.R. Herpes simplex virus DNA replication. *Annual review of biochemistry* **1997**, *66*, 347-384.
108. Jacobson, J.G.; Yang, K.; Baines, J.D.; Homa, F.L. Linker insertion mutations in the herpes simplex virus type 1 UL28 gene: effects on UL28 interaction with UL15 and UL33 and identification of a second-site mutation in the UL15 gene that suppresses a lethal UL28 mutation. *Journal of Virology* **2006**, *80*, 12312-12323.
109. Yang, K.; Baines, J.D. The putative terminase subunit of herpes simplex virus 1 encoded by UL28 is necessary and sufficient to mediate interaction between pUL15 and pUL33. *Journal of Virology* **2006**, *80*, 5733-5739.
110. Higgs, M.R.; Preston, V.G.; Stow, N.D. The UL15 protein of herpes simplex virus type 1 is necessary for the localization of the UL28 and UL33 proteins to viral DNA replication centres. *Journal of General Virology* **2008**, *89*, 1709-1715.
111. Bubeck, A.; Wagner, M.; Ruzsics, Z.; Lötzerich, M.; Iglesias, M.; Singh, I.R.; Koszinowski, U.H. Comprehensive Mutational Analysis of a Herpesvirus Gene in the Viral Genome Context Reveals a Region Essential for Virus Replication. In *Journal of Virology*, 2004; Vol. 78, pp 8026-8035.
112. Chang, Y.E.; Roizman, B. The product of the UL31 gene of herpes simplex virus 1 is a nuclear phosphoprotein which partitions with the nuclear matrix. *Journal of Virology* **1993**, *67*, 6348-6356.
113. Farina, A.; Feederle, R.; Raffa, S.; Gonnella, R.; Santarelli, R.; Frati, L.; Angeloni, A.; Torrisi, M.R.; Faggioni, A.; Delecluse, H.J. BFRF1 of Epstein-Barr virus is essential for efficient primary viral envelopment and egress. *Journal of Virology* **2005**, *79*, 3703-3712.
114. Roller, R.J.; Zhou, Y.; Schnetzer, R.; Ferguson, J.; DeSalvo, D. Herpes simplex virus type 1 U(L)34 gene product is required for viral envelopment. *Journal of Virology* **2000**, *74*, 117-129.

115. Bigalke, J.M.; Heuser, T.; Nicastro, D.; Heldwein, E.E. Membrane deformation and scission by the HSV-1 nuclear egress complex. *Nature Communications* **2014**, *5*, 4131.
116. Lorenz, M.; Vollmer, B.; Unsay, J.D.; Klupp, B.G.; Garcia-Saez, A.J.; Mettenleiter, T.C.; Antonin, W. A single herpesvirus protein can mediate vesicle formation in the nuclear envelope. *The Journal of biological chemistry* **2015**, *290*, 6962-6974.
117. Bigalke, J.M.; Heldwein, E.E. Structural basis of membrane budding by the nuclear egress complex of herpesviruses. *The EMBO journal* **2015**, *34*, 2921-2936.
118. Hagen, C.; Dent, K.C.; Zeev-Ben-Mordehai, T.; Grange, M.; Bosse, J.B.; Whittle, C.; Klupp, B.G.; Siebert, C.A.; Vasishtan, D.; Bauerlein, F.J.*, et al.* Structural basis of vesicle formation at the inner nuclear membrane. *Cell* **2015**, *163*, 1692-1701.
119. Bigalke, J.M.; Heldwein, E.E. Have NEC coat, will travel: structural basis of membrane budding during nuclear egress in herpesviruses. *Advances in virus research* **2017**, *97*, 107-141.
120. Newcomb, W.W.; Fontana, J.; Winkler, D.C.; Cheng, N.; Heymann, J.B.; Steven, A.C. The Primary Enveloped Virion of Herpes Simplex Virus 1: Its Role in Nuclear Egress. *MBio* **2017**, *8*.
121. Mou, F.; Wills, E.; Baines, J.D. Phosphorylation of the U(L)31 protein of herpes simplex virus 1 by the U(S)3-encoded kinase regulates localization of the nuclear envelopment complex and egress of nucleocapsids. *Journal of Virology* **2009**, *83*, 5181-5191.
122. Reynolds, A.E.; Wills, E.G.; Roller, R.J.; Ryckman, B.J.; Baines, J.D. Ultrastructural Localization of the Herpes Simplex Virus Type 1 U(L)31, U(L)34, and U(S)3 Proteins Suggests Specific Roles in Primary Envelopment and Egress of Nucleocapsids. In *Journal of Virology*, 2002; Vol. 76, pp 8939-8952.
123. Farnsworth, A.; Wisner, T.W.; Webb, M.; Roller, R.; Cohen, G.; Eisenberg, R.; Johnson, D.C. Herpes simplex virus glycoproteins gB and gH function in fusion between the virion envelope and the outer nuclear membrane. In *Proceedings of the National Academy of Sciences of the United States of America*, 2007; Vol. 104, pp 10187-10192.
124. Wisner, T.W.; Wright, C.C.; Kato, A.; Kawaguchi, Y.; Mou, F.; Baines, J.D.; Roller, R.J.; Johnson, D.C. Herpesvirus gB-induced fusion between the virion envelope and outer nuclear membrane during virus egress is regulated by the viral US3 kinase. *J Virol* **2009**, *83*, 3115-3126.
125. Kato, A.; Arii, J.; Shiratori, I.; Akashi, H.; Arase, H.; Kawaguchi, Y. Herpes simplex virus 1 protein kinase Us3 phosphorylates viral envelope glycoprotein B and regulates its expression on the cell surface. *J Virol* **2009**, *83*, 250-261.
126. Stackpole, C.W. Herpes-Type Virus of the Frog Renal Adenocarcinoma: I. Virus Development in Tumor Transplants Maintained at Low Temperature. *J Virol* **1969**, *4*, 75-93.
127. Browne, H.; Bell, S.; Minson, T.; Wilson, D.W. An endoplasmic reticulum-retained herpes simplex virus glycoprotein H is absent from secreted virions: evidence for reenvelopment during egress. *Journal of virology* **1996**, *70*, 4311-4316.
128. Granzow, H.; Weiland, F.; Jons, A.; Klupp, B.G.; Karger, A.; Mettenleiter, T.C. Ultrastructural analysis of the replication cycle of pseudorabies virus in cell culture: a reassessment. *J Virol* **1997**, *71*, 2072-2082.
129. Granzow, H.; Klupp, B.G.; Fuchs, W.; Veits, J.; Osterrieder, N.; Mettenleiter, T.C. Egress of alphaherpesviruses: comparative ultrastructural study. *J Virol* **2001**, *75*, 3675-3684.
130. Skepper, J.N.; Whiteley, A.; Browne, H.; Minson, A. Herpes simplex virus nucleocapsids mature to progeny virions by an envelopment --> deenvelopment --> reenvelopment pathway. *J Virol* **2001**, *75*, 5697-5702.
131. Reynolds, A.E.; Wills, E.G.; Roller, R.J.; Ryckman, B.J.; Baines, J.D. Ultrastructural localization of the herpes simplex virus type 1 UL31, UL34, and US3 proteins suggests specific roles in primary envelopment and egress of nucleocapsids. *J Virol* **2002**, *76*, 8939-8952.
132. Fuchs, W.; Klupp, B.G.; Granzow, H.; Osterrieder, N.; Mettenleiter, T.C. The interacting UL31 and UL34 gene products of pseudorabies virus are involved in egress from the host-cell nucleus and represent components of primary enveloped but not mature virions. *J Virol* **2002**, *76*, 364-378.

133. Lee, J.H.; Vittone, V.; Diefenbach, E.; Cunningham, A.L.; Diefenbach, R.J. Identification of structural protein-protein interactions of herpes simplex virus type 1. *Virology* **2008**, *378*, 347-354.
134. Mettenleiter, T.C. Intriguing interplay between viral proteins during herpesvirus assembly or: The herpesvirus assembly puzzle. *Veterinary Microbiology* **2006**, *113*, 163-169.
135. Vittone, V.; Diefenbach, E.; Triffett, D.; Douglas, M.W.; Cunningham, A.L.; Diefenbach, R.J. Determination of interactions between tegument proteins of herpes simplex virus type 1. *Journal of virology* **2005**, *79*, 9566-9571.
136. del Rio, T.; DeCoste, C.J.; Enquist, L.W. Actin is a component of the compensation mechanism in pseudorabies virus virions lacking the major tegument protein VP22. *Journal of Virology* **2005**, *79*, 8614-8619.
137. Michael, K.; Böttcher, S.; Klupp, B.G.; Karger, A.; Mettenleiter, T.C. Pseudorabies virus particles lacking tegument proteins pUL11 or pUL16 incorporate less full-length pUL36 than wild-type virus, but specifically accumulate a pUL36 N-terminal fragment. *Journal of General Virology* **2006**, *87*, 3503-3507.
138. Michael, K.; Klupp, B.G.; Mettenleiter, T.C.; Karger, A. Composition of pseudorabies virus particles lacking tegument protein US3, UL47, or UL49 or envelope glycoprotein E. *Journal of Virology* **2006**, *80*, 1332-1339.
139. Roller, R.J.; Fetters, R. The herpes simplex virus 1 UL51 protein interacts with the UL7 protein and plays a role in its recruitment into the virion. *Journal of Virology* **2015**, *89*, 3112-3122.
140. Yeh, P.-C.; Han, J.; Chadha, P.; Meckes, D.G.; Ward, M.D.; Semmes, O.J.; Wills, J.W. Direct and specific binding of the UL16 tegument protein of herpes simplex virus to the cytoplasmic tail of glycoprotein E. *Journal of Virology* **2011**, *85*, 9425-9436.
141. Yeh, P.-C.; Meckes, D.G.; Wills, J.W. Analysis of the interaction between the UL11 and UL16 tegument proteins of herpes simplex virus. *Journal of Virology* **2008**, *82*, 10693-10700.
142. Harper, A.L.; Meckes, D.G.; Marsh, J.A.; Ward, M.D.; Yeh, P.-C.; Baird, N.L.; Wilson, C.B.; Semmes, O.J.; Wills, J.W. Interaction domains of the UL16 and UL21 tegument proteins of herpes simplex virus. *Journal of Virology* **2010**, *84*, 2963-2971.
143. Starkey, J.L.; Han, J.; Chadha, P.; Marsh, J.A.; Wills, J.W. Elucidation of the block to herpes simplex virus egress in the absence of tegument protein UL16 reveals a novel interaction with VP22. *Journal of Virology* **2014**, *88*, 110-119.
144. Farnsworth, A.; Wisner, T.W.; Johnson, D.C. Cytoplasmic residues of herpes simplex virus glycoprotein gE required for secondary envelopment and binding of tegument proteins VP22 and UL11 to gE and gD. *Journal of Virology* **2007**, *81*, 319-331.
145. Han, J.; Chadha, P.; Starkey, J.L.; Wills, J.W. Function of glycoprotein E of herpes simplex virus requires coordinated assembly of three tegument proteins on its cytoplasmic tail. *Proceedings of the National Academy of Sciences, USA* **2012**, *109*, 19798-19803.
146. Cardone, G.; Newcomb, W.W.; Cheng, N.; Wingfield, P.T.; Trus, B.L.; Brown, J.C.; Steven, A.C. The UL36 tegument protein of herpes simplex virus 1 has a composite binding site at the capsid vertices. *Journal of Virology* **2012**, *86*, 4058-4064.
147. Coller, K.E.; Lee, J.I.-H.; Ueda, A.; Smith, G.A. The capsid and tegument of the alphaherpesviruses are linked by an interaction between the UL25 and VP1/2 proteins. *Journal of Virology* **2007**, *81*, 11790-11797.
148. Mijatov, B.; Cunningham, A.L.; Diefenbach, R.J. Residues F593 and E596 of HSV-1 tegument protein pUL36 (VP1/2) mediate binding of tegument protein pUL37. *Virology* **2007**, *368*, 26-31.
149. Bucks, M.A.; Murphy, M.A.; O'Regan, K.J.; Courtney, R.J. Identification of interaction domains within the UL37 tegument protein of herpes simplex virus type 1. *Virology* **2011**, *416*, 42-53.
150. Bucks, M.A.; O'Regan, K.J.; Murphy, M.A.; Wills, J.W.; Courtney, R.J. Herpes simplex virus type 1 tegument proteins VP1/2 and UL37 are associated with intranuclear capsids. *Virology* **2007**, *361*, 316-324.
151. Svobodova, S.; Bell, S.; Crump, C.M. Analysis of the interaction between the essential herpes simplex virus 1 tegument proteins VP16 and VP1/2. *Journal of Virology* **2012**, *86*, 473-483.

152. Ko, D.H.; Cunningham, A.L.; Diefenbach, R.J. The major determinant for addition of tegument protein pUL48 (VP16) to capsids in herpes simplex virus type 1 is the presence of the major tegument protein pUL36 (VP1/2). *Journal of Virology* **2009**, *84*, 1397-1405.
153. Apcarian, A.; Cunningham, A.L.; Diefenbach, R.J. Identification of binding domains in the herpes simplex virus type 1 small capsid protein pUL35 (VP26). *Journal of General Virology* **2010**, *91*, 2659-2663.
154. Jambunathan, N.; Chouljenko, D.; Desai, P.; Charles, A.-S.; Subramanian, R.; Chouljenko, V.N.; Kousoulas, K.G. Herpes simplex virus 1 protein UL37 interacts with viral glycoprotein gK and membrane protein UL20 and functions in cytoplasmic virion envelopment. *Journal of Virology* **2014**, *88*, 5927-5935.
155. Kato, K.; Daikoku, T.; Goshima, F.; Kume, H.; Yamaki, K.; Nishiyama, Y. Synthesis, subcellular localization and VP16 interaction of the herpes simplex virus type 2 UL46 gene product. *Archives of Virology* **2000**, *145*, 2149-2162.
156. Lin, A.E.; Greco, T.M.; Dohner, K.; Sodeik, B.; Cristea, I.M. A proteomic perspective of inbuilt viral protein regulation: pUL46 tegument protein is targeted for degradation by ICP0 during herpes simplex virus type 1 infection. *Molecular and Cellular Proteomics* **2013**, *12*, 3237-3252.
157. Zhang, Y.; Sirko, D.A.; McKnight, J.L. Role of herpes simplex virus type 1 UL46 and UL47 in alpha TIF-mediated transcriptional induction: Characterization of three viral deletion mutants. *Journal of Virology* **1991**, *65*, 829-841.
158. Smibert, C.A.; Popova, B.; Xiao, P.; Capone, J.P.; Smiley, J.R. Herpes simplex virus VP16 forms a complex with the virion host shutoff protein vhs. *Journal of Virology* **1994**, *68*, 2339-2346.
159. Schmelter, J.; Knez, J.; Smiley, J.R.; Capone, J.P. Identification and characterization of a small modular domain in the herpes simplex virus host shutoff protein sufficient for interaction with VP16. *Journal of Virology* **1996**, *70*, 2124-2131.
160. Knez, J.; Bilan, P.T.; Capone, J.P. A single amino acid substitution in herpes simplex virus type 1 VP16 inhibits binding to the virion host shutoff protein and is incompatible with virus growth. *Journal of Virology* **2003**, *77*, 2892-2902.
161. Elliott, G.; Mouzakitis, G.; O'Hare, P. VP16 interacts via its activation domain with VP22, a tegument protein of herpes simplex virus, and is relocated to a novel macromolecular assembly in coexpressing cells. *Journal of Virology* **1995**, *69*, 7932-7941.
162. Gross, S.T.; Harley, C.A.; Wilson, D.W. The cytoplasmic tail of herpes simplex virus glycoprotein H binds to the tegument protein VP16 in vitro and in vivo. *Virology* **2003**, *317*, 1-12.
163. Maringer, K.; Stylianou, J.; Elliott, G. A network of protein interactions around the herpes simplex virus tegument protein VP22. *Journal of Virology* **2012**, *86*, 12971-12982.
164. Hafezi, W.; Bernard, E.; Cook, R.; Elliott, G. Herpes Simplex Virus Tegument Protein VP22 Contains an Internal VP16 Interaction Domain and a C-Terminal Domain That Are Both Required for VP22 Assembly into the Virus Particle. *Journal of Virology* **2005**, *79*, 13082-13093.
165. Elliott, G.; Hafezi, W.; Whiteley, A.; Bernard, E. Deletion of the herpes simplex virus VP22-encoding gene (UL49) alters the expression, localization, and virion incorporation of ICP0. *Journal of Virology* **2005**, *79*, 9735-9745.
166. Maringer, K.; Elliott, G. Recruitment of herpes simplex virus type 1 immediate-early protein ICP0 to the virus particle. *Journal of Virology* **2010**, *84*, 4682-4696.
167. Oda, S.; Arii, J.; Koyanagi, N.; Kato, A.; Kawaguchi, Y. The Interaction between Herpes Simplex Virus 1 Tegument Proteins UL51 and UL14 and Its Role in Virion Morphogenesis. In *Journal of Virology*, Sandri-Goldin, R.M., Ed. 1752 N St., N.W., Washington, DC, 2016; Vol. 90, pp 8754-8767.
168. Roller, R.J.; Haugo, A.C.; Yang, K.; Baines, J.D. The herpes simplex virus 1 UL51 gene product has cell type-specific functions in cell-to-cell spread. *Journal of Virology* **2014**, *88*, 4058-4068.
169. Johnson, D.C.; Feenstra, V. Identification of a novel herpes simplex virus type 1-induced glycoprotein which complexes with gE and binds immunoglobulin. *Journal of Virology* **1987**, *61*, 2208-2216.

170. Johnson, D.C.; Frame, M.C.; Ligas, M.W.; Cross, A.M.; Stow, N.D. Herpes simplex virus immunoglobulin G Fc receptor activity depends on a complex of two viral glycoproteins, gE and gI. *Journal of Virology* **1988**, *62*, 1347-1354.
171. Chowdary, T.K.; Cairns, T.M.; Atanasiu, D.; Cohen, G.H.; Eisenberg, R.J.; Heldwein, E.E. Crystal structure of the conserved herpesvirus fusion regulator complex gH-gL. *Nature structural & molecular biology* **2010**, *17*, 882-888.
172. Hutchinson, L.; Browne, H.; Wargent, V.; Davis-Poynter, N.; Primorac, S.; Goldsmith, K.; Minson, A.C.; Johnson, D.C. A novel herpes simplex virus glycoprotein, gL, forms a complex with glycoprotein H (gH) and affects normal folding and surface expression of gH. *J Virol* **1992**, *66*, 2240-2250.
173. Handler, C.G.; Cohen, G.H.; Eisenberg, R.J. Cross-linking of glycoprotein oligomers during herpes simplex virus type 1 entry. *J Virol* **1996**, *70*, 6076-6082.
174. Desai, P.J. A null mutation in the UL36 gene of herpes simplex virus type 1 results in accumulation of unenveloped DNA-filled capsids in the cytoplasm of infected cells. *Journal of Virology* **2000**, *74*, 11608-11618.
175. Fuchs, W.; Klupp, B.G.; Granzow, H.; Mettenleiter, T.C. Essential function of the pseudorabies virus UL36 gene product is independent of its interaction with the UL37 protein. *Journal of Virology* **2004**, *78*, 11879-11889.
176. Roberts, A.P.E.; Abaitua, F.; O'Hare, P.; McNab, D.; Rixon, F.J.; Pasdeloup, D. Differing roles of inner tegument proteins pUL36 and pUL37 during entry of herpes simplex virus type 1. *Journal of Virology* **2009**, *83*, 105-116.
177. Desai, P.; Sexton, G.L.; McCaffery, J.M.; Person, S. A null mutation in the gene encoding the herpes simplex virus type 1 UL37 polypeptide abrogates virus maturation. *Journal of Virology* **2001**, *75*, 10259-10271.
178. Bechtel, J.T.; Shenk, T. Human cytomegalovirus UL47 tegument protein functions after entry and before immediate-early gene expression. *Journal of Virology* **2002**, *76*, 1043-1050.
179. Rozen, R.; Sathish, N.; Li, Y.; Yuan, Y. Virion-wide protein interactions of Kaposi's sarcoma-associated herpesvirus. *Journal of Virology* **2008**, *82*, 4742-4750.
180. Cappadona, I.; Villinger, C.; Schutzius, G.; Mertens, T.; von Einem, J. Human cytomegalovirus pUL47 modulates tegumentation and capsid accumulation at the viral assembly complex. *Journal of Virology* **2015**, *89*, 7314-7328.
181. Klupp, B.G.; Fuchs, W.; Granzow, H.; Nixdorf, R.; Mettenleiter, T.C. Pseudorabies virus UL36 tegument protein physically interacts with the UL37 protein. *Journal of Virology* **2002**, *76*, 3065-3071.
182. Kelly, B.J.; Bauerfeind, R.; Binz, A.; Sodeik, B.; Laimbacher, A.S.; Fraefel, C.; Diefenbach, R.J. The interaction of the HSV-1 tegument proteins pUL36 and pUL37 is essential for secondary envelopment during viral egress. *Virology* **2014**, *454-455*, 67-77.
183. Sandbaumhüter, M.; Döhner, K.; Schipke, J.; Binz, A.; Pohlmann, A.; Sodeik, B.; Bauerfeind, R. Cytosolic herpes simplex virus capsids not only require binding inner tegument protein pUL36 but also pUL37 for active transport prior to secondary envelopment. *Cellular Microbiology* **2013**, *15*, 248-269.
184. McLauchlan, J. The abundance of the herpes simplex virus type 1 UL37 tegument protein in virus particles is closely controlled. *Journal of General Virology* **1997**, *78*, 189-194.
185. McNabb, D.S.; Courtney, R.J. Characterization of the large tegument protein (ICP1/2) of herpes simplex virus type 1. *Virology* **1992**, *190*, 221-232.
186. Scrima, N.; Lepault, J.; Boulard, Y.; Pasdeloup, D.; Bressanelli, S.; Roche, S. Insights into herpesvirus tegument organization from structural analyses of the 970 central residues of HSV-1 UL36 protein. *The Journal of biological chemistry* **2015**, *290*, 8820-8833.
187. Tullman, J.A.; Harmon, M.E.; Delannoy, M.; Gibson, W. Recovery of an HMWP/hmwBP (pUL48/pUL47) complex from virions of human cytomegalovirus: subunit interactions, oligomer composition, and deubiquitylase activity. *Journal of Virology* **2014**, *88*, 8256-8267.
188. Baines, J.D.; Ward, P.L.; Campadelli-Fiume, G.; Roizman, B. The UL20 gene of herpes simplex virus 1 encodes a function necessary for viral egress. *J Virol* **1991**, *65*, 6414-6424.

189. Fuchs, W.; Klupp, B.; Granzow, H.; Mettenleiter, T. The UL20 gene product of pseudorabies virus functions in virus egress. *Journal of Virology* **1997**, *71*, 5639-5646.
190. Foster, T.P.; Melancon, J.M.; Baines, J.D.; Kousoulas, K.G. The herpes simplex virus type 1 UL20 protein modulates membrane fusion events during cytoplasmic virion morphogenesis and virus-induced cell fusion. *Journal of Virology* **2004**, *78*, 5347-5357.
191. Foster, T.P.; Melancon, J.M.; Olivier, T.L.; Kousoulas, K.G. Herpes simplex virus type 1 glycoprotein K and the UL20 protein are interdependent for intracellular trafficking and trans-Golgi network localization. *Journal of Virology* **2004**, *78*, 13262-13277.
192. Lau, S.Y.; Crump, C.M. HSV-1 gM and the gK/pUL20 complex are important for the localization of gD and gH/L to viral assembly sites. *Viruses* **2015**, *7*, 915-938.
193. Desai, P.; Sexton, G.L.; Huang, E.; Person, S. Localization of herpes simplex virus type 1 UL37 in the Golgi complex requires UL36 but not capsid structures. *Journal of Virology* **2008**, *82*, 11354-11361.
194. Mossman, K.L.; Sherburne, R.; Lavery, C.; Duncan, J.; Smiley, J.R. Evidence that herpes simplex virus VP16 is required for viral egress downstream of the initial envelopment event. *Journal of Virology* **2000**, *74*, 6287-6299.
195. Weinheimer, S.P.; Boyd, B.A.; Durham, S.K.; Resnick, J.L.; O'Boyle, D.R. Deletion of the VP16 open reading frame of herpes simplex virus type 1. *Journal of Virology* **1992**, *66*, 258-269.
196. Zhang, Y.; McKnight, J.L. Herpes simplex virus type 1 UL46 and UL47 deletion mutants lack VP11 and VP12 or VP13 and VP14, respectively, and exhibit altered viral thymidine kinase expression. *Journal of Virology* **1993**, *67*, 1482-1492.
197. Pomeranz, L.E.; Blaho, J.A. Assembly of infectious herpes simplex virus type 1 virions in the absence of full-length VP22. *Journal of Virology* **2000**, *74*, 10041-10054.
198. Fuchs, W.; Granzow, H.; Klupp, B.G.; Kopp, M.; Mettenleiter, T.C. The UL48 tegument protein of pseudorabies virus is critical for intracytoplasmic assembly of infectious virions. *Journal of Virology* **2002**, *76*, 6729-6742.
199. Bortz, E.; Wang, L.; Jia, Q.; Wu, T.T.; Whitelegge, J.P.; Deng, H.; Zhou, Z.H.; Sun, R. Murine gammaherpesvirus 68 ORF52 encodes a tegument protein required for virion morphogenesis in the cytoplasm. *J Virol.* **2007**, *81*, 10137-10150. doi: 10110.11128/JVI.01233-10106. Epub 12007 Jul 10118.
200. Hew, K.; Dahlroth, S.L.; Pan, L.X.; Cornvik, T.; Nordlund, P. VP22 core domain from Herpes simplex virus 1 reveals a surprising structural conservation in both the Alpha- and Gammaherpesvirinae subfamilies. *Journal of General Virology* **2015**, *96*, 1436-1445.
201. Kamen, D.E.; Gross, S.T.; Girvin, M.E.; Wilson, D.W. Structural basis for the physiological temperature dependence of the association of VP16 with the cytoplasmic tail of herpes simplex virus glycoprotein H. *Journal of Virology* **2005**, *79*, 6134-6141.
202. Zhu, Q.; Courtney, R.J. Chemical cross-linking of virion envelope and tegument proteins of herpes simplex virus type 1. *Virology* **1994**, *204*, 590-599.
203. Duffy, C.; Lavail, J.H.; Tauscher, A.N.; Wills, E.G.; Blaho, J.A.; Baines, J.D. Characterization of a UL49-null mutant: VP22 of herpes simplex virus type 1 facilitates viral spread in cultured cells and the mouse cornea. *Journal of Virology* **2006**, *80*, 8664-8675.
204. Stylianou, J.; Maringer, K.; Cook, R.; Bernard, E.; Elliott, G. Virion incorporation of the herpes simplex virus type 1 tegument protein VP22 occurs via glycoprotein E-specific recruitment to the late secretory pathway. *Journal of Virology* **2009**, *83*, 5204-5218.
205. Taddeo, B.; Sciortino, M.T.; Zhang, W.; Roizman, B. Interaction of herpes simplex virus RNase with VP16 and VP22 is required for the accumulation of the protein but not for accumulation of mRNA. *Proceedings of the National Academy of Sciences of the United States of America* **2007**, *104*, 12163-12168.
206. Kopp, M.; Klupp, B.G.; Granzow, H.; Fuchs, W.; Mettenleiter, T.C. Identification and characterization of the pseudorabies virus tegument proteins UL46 and UL47: Role for UL47 in virion morphogenesis in the cytoplasm. *Journal of Virology* **2002**, *76*, 8820-8833.
207. Fossum, E.; Friedel, C.C.; Rajagopala, S.V.; Titz, B.; Baiker, A.; Schmidt, T.; Kraus, T.; Stellberger, T.; Rutenberg, C.; Suthram, S.*, et al.* Evolutionarily conserved herpesviral protein interaction networks. *PLoS Pathogens* **2009**, *5*, e1000570.

208. Scholtes, L.D.; Yang, K.; Li, L.X.; Baines, J.D. The capsid protein encoded by U(L)17 of herpes simplex virus 1 interacts with tegument protein VP13/14. *Journal of Virology* **2010**, *84*, 7642-7650.
209. Baines, J.D.; Jacob, R.J.; Simmerman, L.; Roizman, B. The herpes simplex virus 1 UL11 proteins are associated with cytoplasmic and nuclear membranes and with nuclear bodies of infected cells. *Journal of Virology* **1995**, *69*, 825-833.
210. Loomis, J.S.; Bowzard, J.B.; Courtney, R.J.; Wills, J.W. Intracellular trafficking of the UL11 tegument protein of herpes simplex virus type 1. *Journal of Virology* **2001**, *75*, 12209-12219.
211. MacLean, C.A.; Dolan, A.; Jamieson, F.E.; McGeoch, D.J. The myristylated virion proteins of herpes simplex virus type 1: Investigation of their role in the virus life cycle. *Journal of General Virology* **1992**, *73*, 539-547.
212. Han, J.; Chadha, P.; Meckes, D.G.; Baird, N.L.; Wills, J.W. Interaction and interdependent packaging of tegument protein UL11 and glycoprotein e of herpes simplex virus. *Journal of virology* **2011**, *85*, 9437-9446.
213. Baines, J.D.; Roizman, B. The UL11 gene of herpes simplex virus 1 encodes a function that facilitates nucleocapsid envelopment and egress from cells. *Journal of Virology* **1992**, *66*, 5168-5174.
214. Fulmer, P.A.; Melancon, J.M.; Baines, J.D.; Kousoulas, K.G. UL20 protein functions precede and are required for the UL11 functions of herpes simplex virus type 1 cytoplasmic virion envelopment. *Journal of Virology* **2007**, *81*, 3097-3108.
215. Kopp, M.; Granzow, H.; Fuchs, W.; Klupp, B.G.; Mundt, E.; Karger, A.; Mettenleiter, T.C. The pseudorabies virus UL11 protein is a virion component involved in secondary envelopment in the cytoplasm. *Journal of Virology* **2003**, *77*, 5339-5351.
216. Seo, J.-Y.; Britt, W.J. Multimerization of tegument protein pp28 within the assembly compartment is required for cytoplasmic envelopment of human cytomegalovirus. *Journal of Virology* **2008**, *82*, 6272-6287.
217. Silva, M.C.; Yu, Q.-C.; Enquist, L.; Shenk, T. Human cytomegalovirus UL99-encoded pp28 is required for the cytoplasmic envelopment of tegument-associated capsids. *Journal of Virology* **2003**, *77*, 10594-10605.
218. Leege, T.; Fuchs, W.; Granzow, H.; Kopp, M.; Klupp, B.G.; Mettenleiter, T.C. Effects of simultaneous deletion of pUL11 and glycoprotein M on virion maturation of herpes simplex virus type 1. *Journal of Virology* **2009**, *83*, 896-907.
219. Baird, N.L.; Starkey, J.L.; Hughes, D.J.; Wills, J.W. Myristylation and palmitylation of HSV-1 UL11 are not essential for its function. *Virology* **2010**, *397*, 80-88.
220. Loomis, J.S.; Courtney, R.J.; Wills, J.W. Binding partners for the UL11 tegument protein of herpes simplex virus type 1. *Journal of Virology* **2003**, *77*, 11417-11424.
221. Meckes, D.G.; Marsh, J.A.; Wills, J.W. Complex mechanisms for the packaging of the UL16 tegument protein into herpes simplex virus. *Virology* **2010**, *398*, 208-213.
222. Meckes, D.G.; Wills, J.W. Dynamic interactions of the UL16 tegument protein with the capsid of herpes simplex virus. *Journal of Virology* **2007**, *81*, 13028-13036.
223. Johnson, D.C.; Baines, J.D. Herpesviruses remodel host membranes for virus egress. *Nature Reviews: Microbiology* **2011**, *9*, 382-394.
224. Kopp, M.; Granzow, H.; Fuchs, W.; Klupp, B.; Mettenleiter, T.C. Simultaneous deletion of pseudorabies virus tegument protein UL11 and glycoprotein M severely impairs secondary envelopment. *Journal of Virology* **2004**, *78*, 3024-3034.
225. Owen, D.J.; Crump, C.M.; Graham, S.C. Tegument Assembly and Secondary Envelopment of Alphaherpesviruses. *Viruses* **2015**, *7*, 5084-5114.
226. Klupp, B.G.; Böttcher, S.; Granzow, H.; Kopp, M.; Mettenleiter, T.C. Complex formation between the UL16 and UL21 tegument proteins of pseudorabies virus. *Journal of Virology* **2005**, *79*, 1510-1522.
227. Zaichick, S.V.; Bohannon, K.P.; Hughes, A.; Sollars, P.J.; Pickard, G.E.; Smith, G.A. The herpesvirus VP1/2 protein is an effector of dynein-mediated capsid transport and neuroinvasion. *Cell Host & Microbe* **2013**, *13*, 193-203.

228. Fuchs, W.; Klupp, B.G.; Granzow, H.; Hengartner, C.; Brack, A.; Mundt, A.; Enquist, L.W.; Mettenleiter, T.C. Physical interaction between envelope glycoproteins E and M of pseudorabies virus and the major tegument protein UL49. *Journal of Virology* **2002**, *76*, 8208-8217.
229. Oda, S.; Arii, J.; Koyanagi, N.; Kato, A.; Kawaguchi, Y. The Interaction between Herpes Simplex Virus 1 Tegument Proteins UL51 and UL14 and Its Role in Virion Morphogenesis. *Journal of Virology* **2016**, *90*, 8754-8767.
230. Ibiricu, I.; Maurer, U.; Grünewald, K. Characterization of herpes simplex virus type 1 L-particle assembly and egress in hippocampal neurones by electron cryo-tomography. *Cellular Microbiology* **2013**, *15*, 285-291.
231. Dargan, D.J.; Subak-Sharpe, J.H. The effect of herpes simplex virus type 1 L-particles on virus entry, replication, and the infectivity of naked herpesvirus DNA. *Virology* **1997**, *239*, 378-388.
232. Beitia Ortiz de Zarate, I.; Cantero-Aguilar, L.; Longo, M.; Berlioz-Torrent, C.; Rozenberg, F. Contribution of endocytic motifs in the cytoplasmic tail of herpes simplex virus type 1 glycoprotein B to virus replication and cell-cell fusion. *Journal of Virology* **2007**, *81*, 13889-13903.
233. Alconada, A.; Bauer, U.; Sodeik, B.; Hoflack, B. Intracellular traffic of herpes simplex virus glycoprotein gE: Characterization of the sorting signals required for its trans-Golgi network localization. *Journal of Virology* **1999**, *73*, 377-387.
234. Nixdorf, R.; Klupp, B.G.; Mettenleiter, T.C. Role of the cytoplasmic tails of pseudorabies virus glycoproteins B, E and M in intracellular localization and virion incorporation. *J Gen Virol* **2001**, *82*, 215-226.
235. Van Minnebruggen, G.; Favoreel, H.W.; Nauwynck, H.J. Internalization of pseudorabies virus glycoprotein B is mediated by an interaction between the YQRL motif in its cytoplasmic domain and the clathrin-associated AP-2 adaptor complex. *J Virol* **2004**, *78*, 8852-8859.
236. McMillan, T.N.; Johnson, D.C. Cytoplasmic domain of herpes simplex virus gE causes accumulation in the trans-Golgi network, a site of virus envelopment and sorting of virions to cell junctions. *Journal of Virology* **2001**, *75*, 1928-1940.
237. Crump, C.M.; Bruun, B.; Bell, S.; Pomeranz, L.E.; Minson, T.; Browne, H.M. Alphaherpesvirus glycoprotein M causes the relocalization of plasma membrane proteins. *J Gen Virol* **2004**, *85*, 3517-3527.
238. Ren, Y.; Bell, S.; Zenner, H.L.; Lau, S.Y.; Crump, C.M. Glycoprotein M is important for the efficient incorporation of glycoprotein H-L into herpes simplex virus type 1 particles. *J Gen Virol* **2012**, *93*, 319-329.
239. Sugimoto, K.; Uema, M.; Sagara, H.; Tanaka, M.; Sata, T.; Hashimoto, Y.; Kawaguchi, Y. Simultaneous tracking of capsid, tegument, and envelope protein localization in living cells infected with triply fluorescent herpes simplex virus 1. *J Virol* **2008**, *82*, 5198-5211.
240. Turcotte, S.; Letellier, J.; Lippe, R. Herpes simplex virus type 1 capsids transit by the trans-Golgi network, where viral glycoproteins accumulate independently of capsid egress. *J Virol* **2005**, *79*, 8847-8860.
241. Hollinshead, M.; Johns, H.L.; Sayers, C.L.; Gonzalez-Lopez, C.; Smith, G.L.; Elliott, G. Endocytic tubules regulated by Rab GTPases 5 and 11 are used for envelopment of herpes simplex virus. *EMBO journal* **2012**, *31*, 4204-4220.
242. Johns, H.L.; Gonzalez-Lopez, C.; Sayers, C.L.; Hollinshead, M.; Elliott, G. Rab6 dependent post-Golgi trafficking of HSV1 envelope proteins to sites of virus envelopment. *Traffic* **2014**, *15*, 157-178.
243. Henne, W.M.; Buchkovich, N.J.; Emr, S.D. The ESCRT pathway. *Dev Cell* **2011**, *21*, 77-91.
244. Votteler, J.; Sundquist, W.I. Virus budding and the ESCRT pathway. *Cell Host Microbe* **2013**, *14*, 232-241.
245. Scourfield, E.J.; Martin-Serrano, J. Growing functions of the ESCRT machinery in cell biology and viral replication. *Biochem Soc Trans* **2017**, *45*, 613-634.
246. Weiss, E.R.; Gottlinger, H. The role of cellular factors in promoting HIV budding. *J Mol Biol* **2011**, *410*, 525-533.

247. Van Engelenburg, S.B.; Shtengel, G.; Sengupta, P.; Waki, K.; Jarnik, M.; Ablan, S.D.; Freed, E.O.; Hess, H.F.; Lippincott-Schwartz, J. Distribution of ESCRT machinery at HIV assembly sites reveals virus scaffolding of ESCRT subunits. *Science* **2014**, *343*, 653-656.
248. Calistri, A.; Sette, P.; Salata, C.; Cancellotti, E.; Forghieri, C.; Comin, A.; Gottlinger, H.; Campadelli-Fiume, G.; Palu, G.; Parolin, C. Intracellular trafficking and maturation of herpes simplex virus type 1 gB and virus egress require functional biogenesis of multivesicular bodies. *J Virol* **2007**, *81*, 11468-11478.
249. Crump, C.M.; Yates, C.; Minson, T. Herpes simplex virus type 1 cytoplasmic envelopment requires functional Vps4. *J Virol* **2007**, *81*, 7380-7387.
250. Pawliczek, T.; Crump, C.M. Herpes simplex virus type 1 production requires a functional ESCRT-III complex but is independent of TSG101 and ALIX expression. *J Virol* **2009**, *83*, 11254-11264.
251. Kharkwal, H.; Smith, C.G.; Wilson, D.W. Blocking ESCRT-mediated envelopment inhibits microtubule-dependent trafficking of alphaherpesviruses in vitro. *J Virol* **2014**, *88*, 14467-14478.
252. Tandon, R.; AuCoin, D.P.; Mocarski, E.S. Human cytomegalovirus exploits ESCRT machinery in the process of virion maturation. *J Virol* **2009**, *83*, 10797-10807.
253. Calistri, A.; Munegato, D.; Toffoletto, M.; Celestino, M.; Franchin, E.; Comin, A.; Sartori, E.; Salata, C.; Parolin, C.; Palu, G. Functional interaction between the ESCRT-I component TSG101 and the HSV-1 tegument ubiquitin specific protease. *J Cell Physiol* **2015**, *230*, 1794-1806.
254. Hogue, I.B.; Bosse, J.B.; Hu, J.-R.; Thiberge, S.Y.; Enquist, L.W. Cellular mechanisms of alpha herpesvirus egress: Live cell fluorescence microscopy of pseudorabies virus exocytosis. *PLoS pathogens* **2014**, *10*, e1004535.
255. Miranda-Saksena, M.; Boadle, R.A.; Aggarwal, A.; Tijono, B.; Rixon, F.J.; Diefenbach, R.J.; Cunningham, A.L. Herpes simplex virus utilizes the large secretory vesicle pathway for anterograde transport of tegument and envelope proteins and for viral exocytosis from growth cones of human fetal axons. *Journal of virology* **2009**, *83*, 3187-3199.
256. Roberts, K.L.; Baines, J.D. Myosin Va enhances secretion of herpes simplex virus 1 virions and cell surface expression of viral glycoproteins. *Journal of Virology* **2010**, *84*, 9889-9896.
257. Rudolf, R.; Kogel, T.; Kuznetsov, S.A.; Salm, T.; Schlicker, O.; Hellwig, A.; Hammer, J.A., 3rd; Gerdes, H.H. Myosin Va facilitates the distribution of secretory granules in the F-actin rich cortex of PC12 cells. *Journal of cell science* **2003**, *116*, 1339-1348.
258. Wu, X.; Bowers, B.; Rao, K.; Wei, Q.; Hammer, J.A., 3rd. Visualization of melanosome dynamics within wild-type and dilute melanocytes suggests a paradigm for myosin V function In vivo. *Journal of Cell Biology* **1998**, *143*, 1899-1918.
259. Akhtar, J.; Shukla, D. Viral entry mechanisms: cellular and viral mediators of herpes simplex virus entry. *The FEBS journal* **2009**, *276*, 7228-7236.
260. Karasneh, G.A.; Ali, M.; Shukla, D. An Important Role for Syndecan-1 in Herpes Simplex Virus Type-1 Induced Cell-to-Cell Fusion and Virus Spread. In *PLoS One*, Badley, A.D., Ed. San Francisco, USA, 2011; Vol. 6.
261. Johnson, D.C.; Webb, M.; Wisner, T.W.; Brunetti, C. Herpes simplex virus gE/gI sorts nascent virions to epithelial cell junctions, promoting virus spread. *Journal of Virology* **2001**, *75*, 821-833.
262. Farnsworth, A.; Johnson, D.C. Herpes Simplex Virus gE/gI Must Accumulate in the trans-Golgi Network at Early Times and Then Redistribute to Cell Junctions To Promote Cell-Cell Spread. In *Journal of Virology*, 2006; Vol. 80, pp 3167-3179.
263. Wisner, T.; Brunetti, C.; Dingwell, K.; Johnson, D.C. The extracellular domain of herpes simplex virus gE is sufficient for accumulation at cell junctions but not for cell-to-cell spread. *Journal of Virology* **2000**, *74*, 2278-2287.
264. Richart, S.M.; Simpson, S.A.; Krummenacher, C.; Whitbeck, J.C.; Pizer, L.I.; Cohen, G.H.; Eisenberg, R.J.; Wilcox, C.L. Entry of herpes simplex virus type 1 into primary sensory neurons in vitro is mediated by Nectin-1/HveC. *Journal of Virology* **2003**, *77*, 3307-3311.

265. Krummenacher, C.; Baribaud, I.; Eisenberg, R.J.; Cohen, G.H. Cellular localization of nectin-1 and glycoprotein D during herpes simplex virus infection. *Journal of Virology* **2003**, *77*, 8985-8999.
266. Nozawa, N.; Kawaguchi, Y.; Tanaka, M.; Kato, A.; Kato, A.; Kimura, H.; Nishiyama, Y. Herpes simplex virus type 1 UL51 protein is involved in maturation and egress of virus particles. *Journal of Virology* **2005**, *79*, 6947-6956.
267. Tanaka, M.; Sata, T.; Kawaguchi, Y. The product of the herpes simplex virus 1 UL7 gene interacts with a mitochondrial protein, adenine nucleotide translocator 2. *Virology Journal* **2008**, *5*, 125.
268. Nozawa, N.; Daikoku, T.; Yamauchi, Y.; Takakuwa, H.; Goshima, F.; Yoshikawa, T.; Nishiyama, Y. Identification and characterization of the UL7 gene product of herpes simplex virus type 2. *Virus Genes* **2002**, *24*, 257-266.
269. Klupp, B.G.; Granzow, H.; Klopfleisch, R.; Fuchs, W.; Kopp, M.; Lenk, M.; Mettenleiter, T.C. Functional analysis of the pseudorabies virus UL51 protein. *Journal of Virology* **2005**, *79*, 3831-3840.
270. Fuchs, W.; Granzow, H.; Klopfleisch, R.; Klupp, B.G.; Rosenkranz, D.; Mettenleiter, T.C. The UL7 gene of pseudorabies virus encodes a nonessential structural protein which is involved in virion formation and egress. *Journal of Virology* **2005**, *79*, 11291-11299.
271. Jiang, H.F.; Wang, W.; Jiang, X.; Zeng, W.B.; Shen, Z.Z.; Song, Y.G.; Yang, H.; Liu, X.J.; Dong, X.; Zhou, J.*, et al.* ORF7 of Varicella-Zoster Virus Is Required for Viral Cytoplasmic Envelopment in Differentiated Neuronal Cells. *Journal of Virology* **2017**, *91*.
272. Schauflinger, M.; Fischer, D.; Schreiber, A.; Chevillotte, M.; Walther, P.; Mertens, T.; von Einem, J. The tegument protein UL71 of human cytomegalovirus is involved in late envelopment and affects multivesicular bodies. *Journal of Virology* **2011**, *85*, 3821-3832.
273. Das, S.; Ortiz, D.A.; Gurczynski, S.J.; Khan, F.; Pellett, P.E. Identification of human cytomegalovirus genes important for biogenesis of the cytoplasmic virion assembly complex. *Journal of Virology* **2014**, *88*, 9086-9099.
274. Womack, A.; Shenk, T. Human cytomegalovirus tegument protein pUL71 is required for efficient virion egress. *MBio* **2010**, *1*.
275. Tanaka, M.; Sata, T.; Kawaguchi, Y. The product of the Herpes simplex virus 1 UL7 gene interacts with a mitochondrial protein, adenine nucleotide translocator 2. *Virology Journal* **2008**, *5*, 125.
276. Daikoku, T.; Ikenoya, K.; Yamada, H.; Goshima, F.; Nishiyama, Y. Identification and characterization of the herpes simplex virus type 1 UL51 gene product. *Journal of General Virology* **1998**, *79 (Pt 12)*, 3027-3031.
277. Albecka, A.; Owen, D.J.; Ivanova, L.; Brun, J.; Liman, R.; Davies, L.; Ahmed, M.F.; Colaco, S.; Hollinshead, M.; Graham, S.C.*, et al.* Dual Function of the pUL7-pUL51 Tegument Protein Complex in Herpes Simplex Virus 1 Infection. *Journal of Virology* **2017**, *91*.
278. Nozawa, N.; Daikoku, T.; Koshizuka, T.; Yamauchi, Y.; Yoshikawa, T.; Nishiyama, Y. Subcellular localization of herpes simplex virus type 1 UL51 protein and role of palmitoylation in Golgi apparatus targeting. *Journal of Virology* **2003**, *77*, 3204-3216.
279. Guan, X.; Fierke, C.A. Understanding Protein Palmitoylation: Biological Significance and Enzymology. *Science China. Chemistry* **2011**, *54*, 1888-1897.
280. Ohno, H.; Stewart, J.; Fournier, M.C.; Bosshart, H.; Rhee, I.; Miyatake, S.; Saito, T.; Gallusser, A.; Kirchhausen, T.; Bonifacino, J.S. Interaction of tyrosine-based sorting signals with clathrin-associated proteins. *Science* **1995**, *269*, 1872-1875.
281. Pearse, B.M.; Smith, C.J.; Owen, D.J. Clathrin coat construction in endocytosis. *Current opinion in structural biology* **2000**, *10*, 220-228.
282. Tan, S. A modular polycistronic expression system for overexpressing protein complexes in Escherichia coli. *Protein expression and purification* **2001**, *21*, 224-234.
283. Cooray, S.; Bahar, M.W.; Abrescia, N.G.; McVey, C.E.; Bartlett, N.W.; Chen, R.A.; Stuart, D.I.; Grimes, J.M.; Smith, G.L. Functional and structural studies of the vaccinia virus virulence factor N1 reveal a Bcl-2-like anti-apoptotic protein. *Journal of General Virology* **2007**, *88*, 1656-1666.

284. Niesen, F.H.; Berglund, H.; Vedadi, M. The use of differential scanning fluorimetry to detect ligand interactions that promote protein stability. *Nature protocols* **2007**, *2*, 2212-2221.
285. Winter, G. xia2: an expert system for macromolecular crystallography data reduction. *Journal of Applied Crystallography* **2010**, *43*, 186-190.
286. Hatzopoulos, G.N.; Erat, M.C.; Cutts, E.; Rogala, K.B.; Slater, L.M.; Stansfeld, P.J.; Vakonakis, I. Structural analysis of the G-box domain of the microcephaly protein CPAP suggests a role in centriole architecture. *Structure (London, England : 1993)* **2013**, *21*, 2069-2077.
287. Kampinga, H.H.; Van Waarde-Verhagen, M.A.; Van Assen-Bolt, A.J.; Nieuwenhuis, B.; Rodemann, H.P.; Prowse, K.R.; Linskens, M.H. Reconstitution of active telomerase in primary human foreskin fibroblasts: effects on proliferative characteristics and response to ionizing radiation. *International journal of radiation biology* **2004**, *80*, 377-388.
288. Boukamp, P.; Petrussevska, R.T.; Breitkreutz, D.; Hornung, J.; Markham, A.; Fusenig, N.E. Normal keratinization in a spontaneously immortalized aneuploid human keratinocyte cell line. *Journal of Cell Biology* **1988**, *106*, 761-771.
289. Wallace, I.M.; O'Sullivan, O.; Higgins, D.G.; Notredame, C. M-Coffee: combining multiple sequence alignment methods with T-Coffee. *Nucleic acids research* **2006**, *34*, 1692-1699.
290. Moretti, S.; Armougom, F.; Wallace, I.M.; Higgins, D.G.; Jongeneel, C.V.; Notredame, C. The M-Coffee web server: a meta-method for computing multiple sequence alignments by combining alternative alignment methods. *Nucleic acids research* **2007**, *35*, W645-648.
291. Waterhouse, A.M.; Procter, J.B.; Martin, D.M.; Clamp, M.; Barton, G.J. Jalview Version 2--a multiple sequence alignment editor and analysis workbench. *Bioinformatics (Oxford, England)* **2009**, *25*, 1189-1191.
292. Jones, D.T. Protein secondary structure prediction based on position-specific scoring matrices. *Journal of Molecular Biology* **1999**, *292*, 195-202.
293. Yang, Z.R.; Thomson, R.; McNeil, P.; Esnouf, R.M. RONN: the bio-basis function neural network technique applied to the detection of natively disordered regions in proteins. *Bioinformatics (Oxford, England)* **2005**, *21*, 3369-3376.
294. Morgan, A.A.; Rubenstein, E. Proline: the distribution, frequency, positioning, and common functional roles of proline and polyproline sequences in the human proteome. *PLoS One* **2013**, *8*, e53785.
295. Williamson, M.P. The structure and function of proline-rich regions in proteins. *Biochemical Journal* **1994**, *297 (Pt 2)*, 249-260.
296. MacArthur, M.W.; Thornton, J.M. Influence of proline residues on protein conformation. *Journal of Molecular Biology* **1991**, *218*, 397-412.
297. Babu, M.M.; van der Lee, R.; de Groot, N.S.; Gsponer, J. Intrinsically disordered proteins: regulation and disease. *Current opinion in structural biology* **2011**, *21*, 432-440.
298. Dyson, H.J.; Wright, P.E. Intrinsically unstructured proteins and their functions. *Nature reviews. Molecular cell biology* **2005**, *6*, 197-208.
299. Meissner, C.S.; Suffner, S.; Schauflinger, M.; von Einem, J.; Bogner, E. A leucine zipper motif of a tegument protein triggers final envelopment of human cytomegalovirus. *Journal of Virology* **2012**, *86*, 3370-3382.
300. Meier, A.; Soding, J. Automatic Prediction of Protein 3D Structures by Probabilistic Multi-template Homology Modeling. *PLoS Computational Biology* **2015**, *11*, e1004343.
301. Hildebrand, A.; Remmert, M.; Biegert, A.; Soding, J. Fast and accurate automatic structure prediction with HHpred. *Proteins* **2009**, *77 Suppl 9*, 128-132.
302. Alva, V.; Nam, S.Z.; Soding, J.; Lupas, A.N. The MPI bioinformatics Toolkit as an integrative platform for advanced protein sequence and structure analysis. *Nucleic acids research* **2016**, *44*, W410-415.
303. Plain, F.; Congreve, S.D.; Yee, R.S.Z.; Kennedy, J.; Howie, J.; Kuo, C.W.; Fraser, N.J.; Fuller, W. An amphipathic alpha-helix directs palmitoylation of the large intracellular loop of the sodium/calcium exchanger. *The Journal of biological chemistry* **2017**, *292*, 10745-10752.
304. Khananshvili, D. How a helix imposes palmitoylation of a membrane protein: What one can learn from NCX. *Journal of Biological Chemistry* **2017**, *292*, 10753-10754.

305. Gautier, R.; Douguet, D.; Antonny, B.; Drin, G. HELIQUEST: a web server to screen sequences with specific alpha-helical properties. *Bioinformatics (Oxford, England)* **2008**, *24*, 2101-2102.
306. Huang, Q.; Hong, X.; Hao, Q. SNAP-25 is also an iron-sulfur protein. *FEBS letters* **2008**, *582*, 1431-1436.
307. Selariu, A.; Cheng, T.; Tang, Q.; Silver, B.; Yang, L.; Liu, C.; Ye, X.; Markus, A.; Goldstein, R.S.; Cruz-Cosme, R.S.*, et al.* ORF7 of varicella-zoster virus is a neurotropic factor. *Journal of Virology* **2012**, *86*, 8614-8624.
308. Kaverina, I.; Krylyshkina, O.; Small, J.V. Regulation of substrate adhesion dynamics during cell motility. *The international journal of biochemistry & cell biology* **2002**, *34*, 746-761.
309. Dixit, R.; Tiwari, V.; Shukla, D. Herpes simplex virus type 1 induces filopodia in differentiated P19 neural cells to facilitate viral spread. *Neuroscience letters* **2008**, *440*, 113-118.
310. Wilkins, M.R.; Gasteiger, E.; Bairoch, A.; Sanchez, J.C.; Williams, K.L.; Appel, R.D.; Hochstrasser, D.F. Protein identification and analysis tools in the ExPASy server. *Methods in Molecular Biology* **1999**, *112*, 531-552.
311. Fontana, A.; de Laureto, P.P.; Spolaore, B.; Frare, E.; Picotti, P.; Zambonin, M. Probing protein structure by limited proteolysis. *Acta biochimica Polonica* **2004**, *51*, 299-321.
312. Walter, T.S.; Meier, C.; Assenberg, R.; Au, K.F.; Ren, J.; Verma, A.; Nettleship, J.E.; Owens, R.J.; Stuart, D.I.; Grimes, J.M. Lysine methylation as a routine rescue strategy for protein crystallization. *Structure (London, England : 1993)* **2006**, *14*, 1617-1622.
313. Boivin, S.; Kozak, S.; Meijers, R. Optimization of protein purification and characterization using Thermofluor screens. *Protein expression and purification* **2013**, *91*, 192-206.
314. Seroussi, E.; Pan, H.Q.; Kedra, D.; Roe, B.A.; Dumanski, J.P. Characterization of the human NIPSNAP1 gene from 22q12: a member of a novel gene family. *Gene* **1998**, *212*, 13-20.
315. Buechler, C.; Bodzioch, M.; Bared, S.M.; Sigruener, A.; Boettcher, A.; Lapicka-Bodzioch, K.; Aslanidis, C.; Duong, C.Q.; Grandl, M.; Langmann, T.*, et al.* Expression pattern and raft association of NIPSNAP3 and NIPSNAP4, highly homologous proteins encoded by genes in close proximity to the ATP-binding cassette transporter A1. *Genomics* **2004**, *83*, 1116-1124.
316. Lee, A.H.; Zareei, M.P.; Daefler, S. Identification of a NIPSNAP homologue as host cell target for Salmonella virulence protein SpiC. *Cell Microbiology* **2002**, *4*, 739-750.
317. Creutz, C.E.; Pazoles, C.J.; Pollard, H.B. Self-association of synexin in the presence of calcium. Correlation with synexin-induced membrane fusion and examination of the structure of synexin aggregates. *Journal of Biological Chemistry* **1979**, *254*, 553-558.
318. Brownawell, A.M.; Creutz, C.E. Calcium-dependent binding of sorcin to the N-terminal domain of synexin (annexin VII). *Journal of Biological Chemistry* **1997**, *272*, 22182-22190.
319. Pollard, H.B.; Rojas, E.; Pastor, R.W.; Rojas, E.M.; Guy, H.R.; Burns, A.L. Synexin: molecular mechanism of calcium-dependent membrane fusion and voltage-dependent calcium-channel activity. Evidence in support of the "hydrophobic bridge hypothesis" for exocytotic membrane fusion. *Annals of the New York Academy of Sciences* **1991**, *635*, 328-351.
320. Burns, A.L.; Magendzo, K.; Shirvan, A.; Srivastava, M.; Rojas, E.; Alijani, M.R.; Pollard, H.B. Calcium channel activity of purified human synexin and structure of the human synexin gene. *Proceedings of the National Academy of Sciences of the United States of America* **1989**, *86*, 3798-3802.
321. Hung, L.Y.; Tang, C.J.; Tang, T.K. Protein 4.1 R-135 interacts with a novel centrosomal protein (CPAP) which is associated with the gamma-tubulin complex. *Molecular and cellular biology* **2000**, *20*, 7813-7825.
322. Raynaud-Messina, B.; Merdes, A. Gamma-tubulin complexes and microtubule organization. *Current opinion in cell biology* **2007**, *19*, 24-30.
323. Döhner, K.; Wolfstein, A.; Prank, U.; Echeverri, C.; Dujardin, D.; Vallee, R.; Sodeik, B. Function of dynein and dynactin in herpes simplex virus capsid transport. *Molecular Biology of the Cell* **2002**, *13*, 2795-2809.
324. Avitabile, E.; Di Gaeta, S.; Torrisi, M.R.; Ward, P.L.; Roizman, B.; Campadelli-Fiume, G. Redistribution of microtubules and Golgi apparatus in herpes simplex virus-infected cells and their role in viral exocytosis. *Journal of Virology* **1995**, *69*, 7472-7482.

325. Kotsakis, A.; Pomeranz, L.E.; Blouin, A.; Blaho, J.A. Microtubule reorganization during herpes simplex virus type 1 infection facilitates the nuclear localization of VP22, a major virion tegument protein. *Journal of Virology* **2001**, *75*, 8697-8711.
326. Arakawa, Y.; Cordeiro, J.V.; Way, M. F11L-mediated inhibition of RhoA-mDia signaling stimulates microtubule dynamics during vaccinia virus infection. *Cell Host & Microbe* **2007**, *1*, 213-226.
327. Ploubidou, A.; Moreau, V.; Ashman, K.; Reckmann, I.; Gonzalez, C.; Way, M. Vaccinia virus infection disrupts microtubule organization and centrosome function. *The EMBO journal* **2000**, *19*, 3932-3944.
328. Warren, J.C.; Rutkowski, A.; Cassimeris, L. Infection with replication-deficient adenovirus induces changes in the dynamic instability of host cell microtubules. *Molecular biology of the Cell* **2006**, *17*, 3557-3568.
329. Brunet, J.P.; Jourdan, N.; Cotte-Laffitte, J.; Linxe, C.; Geniteau-Legendre, M.; Servin, A.; Quero, A.M. Rotavirus infection induces cytoskeleton disorganization in human intestinal epithelial cells: implication of an increase in intracellular calcium concentration. *Journal of Virology* **2000**, *74*, 10801-10806.
330. Zambrano, J.L.; Sorondo, O.; Alcala, A.; Vizzi, E.; Diaz, Y.; Ruiz, M.C.; Michelangeli, F.; Liprandi, F.; Ludert, J.E. Rotavirus infection of cells in culture induces activation of RhoA and changes in the actin and tubulin cytoskeleton. *PLoS One* **2012**, *7*, e47612.
331. Jouvenet, N.; Wileman, T. African swine fever virus infection disrupts centrosome assembly and function. *Journal of General Virology* **2005**, *86*, 589-594.
332. Campadelli, G.; Brandimarti, R.; Di Lazzaro, C.; Ward, P.L.; Roizman, B.; Torrisi, M.R. Fragmentation and dispersal of Golgi proteins and redistribution of glycoproteins and glycolipids processed through the Golgi apparatus after infection with herpes simplex virus 1. *Proceedings of the National Academy of Sciences, USA* **1993**, *90*, 2798-2802.
333. Pasdeloup, D.; Labetoulle, M.; Rixon, F.J. Differing effects of herpes simplex virus 1 and pseudorabies virus infections on centrosomal function. *Journal of Virology* **2013**, *87*, 7102-7112.
334. Griffiths, S.J.; Koegl, M.; Boutell, C.; Zenner, H.L.; Crump, C.M.; Pica, F.; Gonzalez, O.; Friedel, C.C.; Barry, G.; Martin, K*., et al.* A systematic analysis of host factors reveals a Med23-interferon-λ regulatory axis against herpes simplex virus type 1 replication. *PLoS pathogens* **2013**, *9*, e1003514.
335. Jourdain, L.; Curmi, P.; Sobel, A.; Pantaloni, D.; Carlier, M.F. Stathmin: a tubulin-sequestering protein which forms a ternary T2S complex with two tubulin molecules. *Biochemistry* **1997**, *36*, 10817-10821.
336. Cassimeris, L. The oncoprotein 18/stathmin family of microtubule destabilizers. *Current opinion in cell biology* **2002**, *14*, 18-24.
337. Rubin, C.I.; Atweh, G.F. The role of stathmin in the regulation of the cell cycle. *Journal of Cellular Biochemistry* **2004**, *93*, 242-250.
338. Antrobus, R.; Grant, K.; Gangadharan, B.; Chittenden, D.; Everett, R.D.; Zitzmann, N.; Boutell, C. Proteomic analysis of cells in the early stages of herpes simplex virus type-1 infection reveals widespread changes in the host cell proteome. *Proteomics* **2009**, *9*, 3913-3927.
339. Zheng, X.; Gooi, L.M.; Wason, A.; Gabriel, E.; Mehrjardi, N.Z.; Yang, Q.; Zhang, X.; Debec, A.; Basiri, M.L.; Avidor-Reiss, T*., et al.* Conserved TCP domain of Sas-4/CPAP is essential for pericentriolar material tethering during centrosome biogenesis. *Proceedings of the National Academy of Sciences of the United States of America* **2014**, *111*, E354-363.
340. Cottee, M.A.; Muschalik, N.; Wong, Y.L.; Johnson, C.M.; Johnson, S.; Andreeva, A.; Oegema, K.; Lea, S.M.; Raff, J.W.; van Breugel, M. Crystal structures of the CPAP/STIL complex reveal its role in centriole assembly and human microcephaly. *Elife* **2013**, *2*, e01071.
341. Tang, C.J.; Fu, R.H.; Wu, K.S.; Hsu, W.B.; Tang, T.K. CPAP is a cell-cycle regulated protein that controls centriole length. *Nature cell biology* **2009**, *11*, 825-831.
342. Brito, D.A.; Gouveia, S.M.; Bettencourt-Dias, M. Deconstructing the centriole: structure and number control. *Current opinion in cell biology* **2012**, *24*, 4-13.

343. Delattre, M.; Gonczy, P. The arithmetic of centrosome biogenesis. *Journal of cell science* **2004**, *117*, 1619-1630.
344. Conduit, P.T.; Wainman, A.; Raff, J.W. Centrosome function and assembly in animal cells. *Natature Reviews. Molecular Cell Biology* **2015**, *16*, 611-624.
345. Gonczy, P. Towards a molecular architecture of centriole assembly. *Nature reviews. Molecular cell biology* **2012**, *13*, 425-435.
346. Comartin, D.; Gupta, G.D.; Fussner, E.; Coyaud, E.; Hasegan, M.; Archinti, M.; Cheung, S.W.; Pinchev, D.; Lawo, S.; Raught, B*., et al.* CEP120 and SPICE1 cooperate with CPAP in centriole elongation. *Current Biology* **2013**, *23*, 1360-1366.
347. Lin, Y.C.; Chang, C.W.; Hsu, W.B.; Tang, C.J.; Lin, Y.N.; Chou, E.J.; Wu, C.T.; Tang, T.K. Human microcephaly protein CEP135 binds to hSAS-6 and CPAP, and is required for centriole assembly. *The EMBO journal* **2013**, *32*, 1141-1154.
348. Tang, C.J.; Lin, S.Y.; Hsu, W.B.; Lin, Y.N.; Wu, C.T.; Lin, Y.C.; Chang, C.W.; Wu, K.S.; Tang, T.K. The human microcephaly protein STIL interacts with CPAP and is required for procentriole formation. *The EMBO journal* **2011**, *30*, 4790-4804.
349. Kuriyama, R.; Borisy, G.G. Centriole cycle in Chinese hamster ovary cells as determined by whole-mount electron microscopy. *Journal of Cell Biology* **1981**, *91*, 814-821.
350. Chretien, D.; Buendia, B.; Fuller, S.D.; Karsenti, E. Reconstruction of the centrosome cycle from cryoelectron micrographs. *Journal of structural biology* **1997**, *120*, 117-133.
351. Kinoshita, K.; Arnal, I.; Desai, A.; Drechsel, D.N.; Hyman, A.A. Reconstitution of physiological microtubule dynamics using purified components. *Science* **2001**, *294*, 1340-1343.
352. Sharma, A.; Aher, A.; Dynes, N.J.; Frey, D.; Katrukha, E.A.; Jaussi, R.; Grigoriev, I.; Croisier, M.; Kammerer, R.A.; Akhmanova, A*., et al.* Centriolar CPAP/SAS-4 Imparts Slow Processive Microtubule Growth. *Developmental cell* **2016**, *37*, 362-376.
353. Hung, L.Y.; Chen, H.L.; Chang, C.W.; Li, B.R.; Tang, T.K. Identification of a Novel Microtubule-destabilizing Motif in CPAP That Binds to Tubulin Heterodimers and Inhibits Microtubule Assembly. In *Mol Biol Cell*, Stearns, T., Ed. 2004; Vol. 15, pp 2697-2706.
354. Kohlmaier, G.; Loncarek, J.; Meng, X.; McEwen, B.F.; Mogensen, M.M.; Spektor, A.; Dynlacht, B.D.; Khodjakov, A.; Gonczy, P. Overly long centrioles and defective cell division upon excess of the SAS-4-related protein CPAP. *Current Biology* **2009**, *19*, 1012-1018.
355. Schmidt, T.I.; Kleylein-Sohn, J.; Westendorf, J.; Le Clech, M.; Lavoie, S.B.; Stierhof, Y.D.; Nigg, E.A. Control of centriole length by CPAP and CP110. *Current Biology* **2009**, *19*, 1005-1011.
356. Gudi, R.; Zou, C.; Dhar, J.; Gao, Q.; Vasu, C. Centrobin-centrosomal protein 4.1-associated protein (CPAP) interaction promotes CPAP localization to the centrioles during centriole duplication. *Journal of Biological Chemistry* **2014**, *289*, 15166-15178.
357. Cutts, E.E.; Inglis, A.; Stansfeld, P.J.; Vakonakis, I.; Hatzopoulos, G.N. The centriolar protein CPAP G-box: an amyloid fibril in a single domain. *Biochemical Society transactions* **2015**, *43*, 838-843.
358. Vulprecht, J.; David, A.; Tibelius, A.; Castiel, A.; Konotop, G.; Liu, F.; Bestvater, F.; Raab, M.S.; Zentgraf, H.; Izraeli, S*., et al.* STIL is required for centriole duplication in human cells. *Journal of cell science* **2012**, *125*, 1353-1362.
359. Arquint, C.; Sonnen, K.F.; Stierhof, Y.D.; Nigg, E.A. Cell-cycle-regulated expression of STIL controls centriole number in human cells. *Journal of cell science* **2012**, *125*, 1342-1352.
360. Arquint, C.; Gabryjonczyk, A.M.; Imseng, S.; Bohm, R.; Sauer, E.; Hiller, S.; Nigg, E.A.; Maier, T. STIL binding to Polo-box 3 of PLK4 regulates centriole duplication. *Elife* **2015**, *4*.
361. Arquint, C.; Nigg, E.A. The PLK4-STIL-SAS-6 module at the core of centriole duplication. *Biochemical Society transactions* **2016**, *44*, 1253-1263.
362. Emsley, P.; Lohkamp, B.; Scott, W.G.; Cowtan, K. Features and development of Coot. *Acta crystallographica. Section D, Biological crystallography* **2010**, *66*, 486-501.
363. Emmott, E.; Goodfellow, I. Identification of protein interaction partners in mammalian cells using SILAC-immunoprecipitation quantitative proteomics. *Journal of visualized experiments : JoVE* **2014**.

364. Tsaneva, I.R.; Muller, B.; West, S.C. RuvA and RuvB proteins of Escherichia coli exhibit DNA helicase activity in vitro. *Proceedings of the National Academy of Sciences of the United States of America* **1993**, *90*, 1315-1319.
365. Putnam, C.D.; Clancy, S.B.; Tsuruta, H.; Gonzalez, S.; Wetmur, J.G.; Tainer, J.A. Structure and mechanism of the RuvB Holliday junction branch migration motor. *Journal of Molecular Biology* **2001**, *311*, 297-310.
366. Yamada, K.; Kunishima, N.; Mayanagi, K.; Ohnishi, T.; Nishino, T.; Iwasaki, H.; Shinagawa, H.; Morikawa, K. Crystal structure of the Holliday junction migration motor protein RuvB from Thermus thermophilus HB8. *Proceedings of the National Academy of Sciences of the United States of America* **2001**, *98*, 1442-1447.
367. Gorynia, S.; Bandeiras, T.M.; Pinho, F.G.; McVey, C.E.; Vonrhein, C.; Round, A.; Svergun, D.I.; Donner, P.; Matias, P.M.; Carrondo, M.A. Structural and functional insights into a dodecameric molecular machine - the RuvBL1/RuvBL2 complex. *Journal of structural biology* **2011**, *176*, 279-291.
368. Makino, Y.; Kanemaki, M.; Kurokawa, Y.; Koji, T.; Tamura, T. A rat RuvB-like protein, TIP49a, is a germ cell-enriched novel DNA helicase. *Journal of Biological Chemistry* **1999**, *274*, 15329-15335.
369. Kanemaki, M.; Kurokawa, Y.; Matsu-ura, T.; Makino, Y.; Masani, A.; Okazaki, K.; Morishita, T.; Tamura, T.A. TIP49b, a new RuvB-like DNA helicase, is included in a complex together with another RuvB-like DNA helicase, TIP49a. *Journal of Biological Chemistry* **1999**, *274*, 22437-22444.
370. Matias, P.M.; Gorynia, S.; Donner, P.; Carrondo, M.A. Crystal structure of the human AAA+ protein RuvBL1. *Journal of Biological Chemistry* **2006**, *281*, 38918-38929.
371. Shen, X.; Mizuguchi, G.; Hamiche, A.; Wu, C. A chromatin remodelling complex involved in transcription and DNA processing. *Nature* **2000**, *406*, 541-544.
372. Jonsson, Z.O.; Dhar, S.K.; Narlikar, G.J.; Auty, R.; Wagle, N.; Pellman, D.; Pratt, R.E.; Kingston, R.; Dutta, A. Rvb1p and Rvb2p are essential components of a chromatin remodeling complex that regulates transcription of over 5% of yeast genes. *Journal of Biological Chemistry* **2001**, *276*, 16279-16288.
373. Choi, J.; Heo, K.; An, W. Cooperative action of TIP48 and TIP49 in H2A.Z exchange catalyzed by acetylation of nucleosomal H2A. *Nucleic acids research* **2009**, *37*, 5993-6007.
374. Ohdate, H.; Lim, C.R.; Kokubo, T.; Matsubara, K.; Kimata, Y.; Kohno, K. Impairment of the DNA binding activity of the TATA-binding protein renders the transcriptional function of Rvb2p/Tih2p, the yeast RuvB-like protein, essential for cell growth. *Journal of Biological Chemistry* **2003**, *278*, 14647-14656.
375. Petukhov, M.; Dagkessamanskaja, A.; Bommer, M.; Barrett, T.; Tsaneva, I.; Yakimov, A.; Queval, R.; Shvetsov, A.; Khodorkovskiy, M.; Kas, E.*, et al.* Large-scale conformational flexibility determines the properties of AAA+ TIP49 ATPases. *Structure (London, England : 1993)* **2012**, *20*, 1321-1331.
376. Cvackova, Z.; Albring, K.F.; Koberna, K.; Ligasova, A.; Huber, O.; Raska, I.; Stanek, D. Pontin is localized in nucleolar fibrillar centers. *Chromosoma* **2008**, *117*, 487-497.
377. Zaarur, N.; Xu, X.; Lestienne, P.; Meriin, A.B.; McComb, M.; Costello, C.E.; Newnam, G.P.; Ganti, R.; Romanova, N.V.; Shanmugasundaram, M.*, et al.* RuvbL1 and RuvbL2 enhance aggresome formation and disaggregate amyloid fibrils. *The EMBO journal* **2015**, *34*, 2363-2382.
378. Johnston, J.A.; Ward, C.L.; Kopito, R.R. Aggresomes: a cellular response to misfolded proteins. *Journal of Cell Biology* **1998**, *143*, 1883-1898.
379. Chung, K.K.; Zhang, Y.; Lim, K.L.; Tanaka, Y.; Huang, H.; Gao, J.; Ross, C.A.; Dawson, V.L.; Dawson, T.M. Parkin ubiquitinates the alpha-synuclein-interacting protein, synphilin-1: implications for Lewy-body formation in Parkinson disease. *Nature medicine* **2001**, *7*, 1144-1150.
380. Webb, J.L.; Ravikumar, B.; Rubinsztein, D.C. Microtubule disruption inhibits autophagosome-lysosome fusion: implications for studying the roles of aggresomes in polyglutamine diseases. *The international journal of biochemistry & cell biology* **2004**, *36*, 2541-2550.

381. Corboy, M.J.; Thomas, P.J.; Wigley, W.C. Aggresome formation. *Methods In Molecular Biology* **2005**, *301*, 305-327.
382. Garcia-Mata, R.; Bebok, Z.; Sorscher, E.J.; Sztul, E.S. Characterization and dynamics of aggresome formation by a cytosolic GFP-chimera. *Journal of Cell Biology* **1999**, *146*, 1239-1254.
383. Garcia-Mata, R.; Gao, Y.S.; Sztul, E. Hassles with taking out the garbage: aggravating aggresomes. *Traffic* **2002**, *3*, 388-396.
384. Johnston, J.A.; Illing, M.E.; Kopito, R.R. Cytoplasmic dynein/dynactin mediates the assembly of aggresomes. *Cell motility and the cytoskeleton* **2002**, *53*, 26-38.
385. Anton, L.C.; Schubert, U.; Bacik, I.; Princiotta, M.F.; Wearsch, P.A.; Gibbs, J.; Day, P.M.; Realini, C.; Rechsteiner, M.C.; Bennink, J.R.*, et al.* Intracellular localization of proteasomal degradation of a viral antigen. *Journal of Cell Biology* **1999**, *146*, 113-124.
386. Fabunmi, R.P.; Wigley, W.C.; Thomas, P.J.; DeMartino, G.N. Activity and regulation of the centrosome-associated proteasome. *Journal of Biological Chemistry* **2000**, *275*, 409-413.
387. Wigley, W.C.; Fabunmi, R.P.; Lee, M.G.; Marino, C.R.; Muallem, S.; DeMartino, G.N.; Thomas, P.J. Dynamic association of proteasomal machinery with the centrosome. *Journal of Cell Biology* **1999**, *145*, 481-490.
388. Doyle, S.M.; Wickner, S. Hsp104 and ClpB: protein disaggregating machines. *Trends in Biochemical Sciences* **2009**, *34*, 40-48.
389. Clare, D.K.; Saibil, H.R. ATP-driven molecular chaperone machines. *Biopolymers* **2013**, *99*, 846-859.
390. Winkler, J.; Tyedmers, J.; Bukau, B.; Mogk, A. Chaperone networks in protein disaggregation and prion propagation. *Journal of structural biology* **2012**, *179*, 152-160.
391. Nano, N.; Houry, W.A. Chaperone-like activity of the AAA+ proteins Rvb1 and Rvb2 in the assembly of various complexes. *Philosophical transactions of the Royal Society of London. Series B, Biological sciences* **2013**, *368*, 20110399.
392. Machado-Pinilla, R.; Liger, D.; Leulliot, N.; Meier, U.T. Mechanism of the AAA+ ATPases pontin and reptin in the biogenesis of H/ACA RNPs. *RNA (New York, N.Y.)* **2012**, *18*, 1833-1845.
393. Heath, C.M.; Windsor, M.; Wileman, T. Aggresomes resemble sites specialized for virus assembly. *Journal of Cell Biology* **2001**, *153*, 449-455.
394. Novoa, R.R.; Calderita, G.; Arranz, R.; Fontana, J.; Granzow, H.; Risco, C. Virus factories: associations of cell organelles for viral replication and morphogenesis. *Biology of the cell* **2005**, *97*, 147-172.
395. Wileman, T. Aggresomes and autophagy generate sites for virus replication. *Science* **2006**, *312*, 875-878.
396. Wileman, T. Aggresomes and pericentriolar sites of virus assembly: cellular defense or viral design? *Annual Review of Microbiology* **2007**, *61*, 149-167.
397. Orvedahl, A.; Alexander, D.; Talloczy, Z.; Sun, Q.; Wei, Y.; Zhang, W.; Burns, D.; Leib, D.A.; Levine, B. HSV-1 ICP34.5 confers neurovirulence by targeting the Beclin 1 autophagy protein. *Cell Host & Microbe* **2007**, *1*, 23-35.
398. Cox, J.; Mann, M. MaxQuant enables high peptide identification rates, individualized p.p.b.-range mass accuracies and proteome-wide protein quantification. *Nature biotechnology* **2008**, *26*, 1367-1372.
399. Tyanova, S.; Mann, M.; Cox, J. MaxQuant for in-depth analysis of large SILAC datasets. *Methods in Molecular Biology* **2014**, *1188*, 351-364.
400. Mellacheruvu, D.; Wright, Z.; Couzens, A.L.; Lambert, J.P.; St-Denis, N.A.; Li, T.; Miteva, Y.V.; Hauri, S.; Sardiu, M.E.; Low, T.Y.*, et al.* The CRAPome: a contaminant repository for affinity purification-mass spectrometry data. *Nature methods* **2013**, *10*, 730-736.
401. Roux, K.J.; Kim, D.I.; Burke, B. BioID: a screen for protein-protein interactions. *Current protocols in protein science* **2013**, *74*, Unit 19.23.
402. Linkner, J.; Witte, G.; Stradal, T.; Curth, U.; Faix, J. High-resolution X-ray structure of the trimeric Scar/WAVE-complex precursor Brk1. *PLoS One* **2011**, *6*, e21327.

403. Steffen, A.; Faix, J.; Resch, G.P.; Linkner, J.; Wehland, J.; Small, J.V.; Rottner, K.; Stradal, T.E. Filopodia formation in the absence of functional WAVE- and Arp2/3-complexes. *Molecular Biology of the Cell* **2006**, *17*, 2581-2591.
404. Takenawa, T.; Suetsugu, S. The WASP-WAVE protein network: connecting the membrane to the cytoskeleton. *Nature reviews. Molecular cell biology* **2007**, *8*, 37-48.
405. Mullins, R.D.; Pollard, T.D. Structure and function of the Arp2/3 complex. *Current opinion in structural biology* **1999**, *9*, 244-249.
406. Lai, F.P.; Szczodrak, M.; Block, J.; Faix, J.; Breitsprecher, D.; Mannherz, H.G.; Stradal, T.E.; Dunn, G.A.; Small, J.V.; Rottner, K. Arp2/3 complex interactions and actin network turnover in lamellipodia. *The EMBO journal* **2008**, *27*, 982-992.
407. Pollard, T.D.; Beltzner, C.C. Structure and function of the Arp2/3 complex. *Current opinion in structural biology* **2002**, *12*, 768-774.
408. Kuo, J.C.; Han, X.; Yates, J.R., 3rd; Waterman, C.M. Isolation of focal adhesion proteins for biochemical and proteomic analysis. *Methods in Molecular Biology* **2012**, *757*, 297-323.
409. Shang, G.; Feng, D.; Lu, F.; Zhang, H.; Cang, H.; Gao, W.; Bi, R. Purification, crystallization and preliminary crystallographic analysis of a ribosome-recycling factor from Thermoanaerobacter tengcongensis (TteRRF). *Acta crystallographica. Section F, Structural biology communications* **2014**, *70*, 588-591.
410. Tan, K.; Kim, Y.; Hatzos-Skintges, C.; Chang, C.; Cuff, M.; Chhor, G.; Osipiuk, J.; Michalska, K.; Nocek, B.; An, H.*, et al.* Salvage of failed protein targets by reductive alkylation. *Methods in Molecular Biology* **2014**, *1140*, 189-200.
411. Zelus, B.D.; Stewart, R.S.; Ross, J. The virion host shutoff protein of herpes simplex virus type 1: messenger ribonucleolytic activity in vitro. *J Virol* **1996**, *70*, 2411-2419.
412. Drin, G.; Antonny, B. Amphipathic helices and membrane curvature. *FEBS letters* **2010**, *584*, 1840-1847.
413. Cui, H.; Lyman, E.; Voth, G.A. Mechanism of Membrane Curvature Sensing by Amphipathic Helix Containing Proteins. In *Biophysics Journal*, 2011; Vol. 100, pp 1271-1279.
414. Ford, M.G.; Mills, I.G.; Peter, B.J.; Vallis, Y.; Praefcke, G.J.; Evans, P.R.; McMahon, H.T. Curvature of clathrin-coated pits driven by epsin. *Nature* **2002**, *419*, 361-366.
415. Horvath, C.A.; Vanden Broeck, D.; Boulet, G.A.; Bogers, J.; De Wolf, M.J. Epsin: inducing membrane curvature. *The international journal of biochemistry & cell biology* **2007**, *39*, 1765-1770.
416. Stachowiak, J.C.; Hayden, C.C.; Sasaki, D.Y. Steric confinement of proteins on lipid membranes can drive curvature and tubulation. *Proceedings of the National Academy of Sciences of the United States of America* **2010**, *107*, 7781-7786.
417. Stachowiak, J.C.; Schmid, E.M.; Ryan, C.J.; Ann, H.S.; Sasaki, D.Y.; Sherman, M.B.; Geissler, P.L.; Fletcher, D.A.; Hayden, C.C. Membrane bending by protein-protein crowding. *Nature cell biology* **2012**, *14*, 944-949.
418. Snead, W.T.; Hayden, C.C.; Gadok, A.K.; Zhao, C.; Lafer, E.M.; Rangamani, P.; Stachowiak, J.C. Membrane fission by protein crowding. *Proceedings of the National Academy of Sciences of the United States of America* **2017**, *114*, E3258-e3267.
419. Copic, A.; Latham, C.F.; Horlbeck, M.A.; D'Arcangelo, J.G.; Miller, E.A. ER cargo properties specify a requirement for COPII coat rigidity mediated by Sec13p. *Science* **2012**, *335*, 1359-1362.
420. Vanlandingham, P.A.; Barmchi, M.P.; Royer, S.; Green, R.; Bao, H.; Reist, N.; Zhang, B. AP180 couples protein retrieval to clathrin-mediated endocytosis of synaptic vesicles. *Traffic* **2014**, *15*, 433-450.
421. Goh, S.L.; Wang, Q.; Byrnes, L.J.; Sondermann, H. Versatile membrane deformation potential of activated pacsin. *PLoS One* **2012**, *7*, e51628.
422. Busch, D.J.; Houser, J.R.; Hayden, C.C.; Sherman, M.B.; Lafer, E.M.; Stachowiak, J.C. Intrinsically disordered proteins drive membrane curvature. *Nature Communications* **2015**, *6*, 7875.